WEST Search History

Hide Items | Restore | Clear | Cancel

DATE: Tuesday, January 16, 2007

Hide?	Set Name	Query	Hit Count
		DB=PGPB,USPT; PLUR=NO; OP=ADJ	
☐	L17	L16 and l14	5
☐	L16	L9[ti,ab]	5
☐	L15	L14 with l9	10
☐	L14	L13 or l12	1807420
☐	L13	stag$3 or grad$3	1308915
☐	L12	prognos$3 or spread$3 or invasiv$5 or aggressiv$5 or surviv$3 or predict$3	825467
☐	L11	L9 same l10	5
☐	L10	(nuclear or nucleus of cytosol$2 or cytoplasm$2) near5 (stain$3 or express$3 or localiz$5 or enrichment)	23662
☐	L9	L6 or l4 or l3 or l2 or l1	158
☐	L8	humGKLF or humKLF4 or humEZF or (humKLF adj (4 or IV))	0
☐	L7	huGKLF or huKLF4 or huEZF or (huKLF adj (4 or IV))	0
☐	L6	hGKLF or hKLF4 or hEZF or (hKLF adj (4 or IV))	10
☐	L5	kruppel adj like adj (4 or iv)	0
☐	L4	epithelial adj zinc adj finger	6
☐	L3	endothelial adj kruppel adj like	1
☐	L2	gut adj2 kruppel adj like	19
☐	L1	GKLF or KLF4 or EZF or (KLF adj (4 or IV))	149

END OF SEARCH HISTORY

Krueppel (?)

```
display history full
ENTER (L1-), L#, OR ?:l1-166

     (FILE 'MEDLINE, BIOSIS, LIFESCI, BIOTECHDS, SCISEARCH, HCAPLUS' ENTERED
     AT 18:04:01 ON 16 JAN 2007)
L1           507 SEA ABB=ON  (RUPPERT, J?)/AU
L2           159 SEA ABB=ON  (RUPPERT, M?)/AU
L3          1060 SEA ABB=ON  (ENGLER, J?)/AU
L4          1715 SEA ABB=ON  L1 OR L2 OR L3
L5           905 SEA ABB=ON  GKLF OR EZF OR KLF4 OR (KLF(W) 4)
L6           307 SEA ABB=ON  (KRUPPEL(W) LIKE(2W)(4 OR IV))
L7             1 SEA ABB=ON  ENDOTHELIAL(W) KRUPPEL(W) LIKE
L8           385 SEA ABB=ON  GUT(2W) KRUPPEL(W) LIKE
L9            11 SEA ABB=ON  EPITHELIAL(W) ZINC(W) FINGER
L10          982 SEA ABB=ON  L5 OR L6 OR L7 OR L8 OR L9
L11           29 SEA ABB=ON  L4 AND L10
L12           10 DUP REM L11 (19 DUPLICATES REMOVED)
                 D IBIB ABS TOT
L13            5 SEA ABB=ON  HGKLF OR HEZF OR HKLF4 OR (HKLF(W)(4 OR IV)) OR
                 ((HKLF OR KLF)(W) IV)
L14            0 SEA ABB=ON  HUGLKF OR HUEZF OR HUKLF4 OR (HUKLF(W)(4 OR IV))
L15            0 SEA ABB=ON  L13 AND L4
L16           44 SEA ABB=ON  L4 AND (MAMMARY OR BREAST OR DCIS OR (DUCTAL(W)
                 CARCINOMA#))
L17           31 SEA ABB=ON  L16 NOT L11
L18           13 DUP REM L17 (18 DUPLICATES REMOVED)
                 D IBIB ABS TOT
L19          982 SEA ABB=ON  L10 OR L13
L*** DEL     132 S L4 AND (MAMMARY OR BREAST OR DCIS OR SCC OR CARCINOMA# OR AD
L20           34 SEA ABB=ON  L4 AND (SCC OR (SQUAMOUS(W) CELL))
L21           14 DUP REM L20 (20 DUPLICATES REMOVED)
L22            7 SEA ABB=ON  L21 NOT L12
L23            6 SEA ABB=ON  L22 NOT L18
                 D IBIB ABS TOT
L24           89 SEA ABB=ON  L19 AND (MAMMARY OR BREAST OR DCIS OR (DUCTAL(W)
                 CARCINOMA#) OR SCC OR (SQUAMOUS(W) CELL(W) CARCINOMA#))
L25           25 SEA ABB=ON  L24 AND PY<2003
L26           15 SEA ABB=ON  L25 NOT L11
L27           15 SEA ABB=ON  L26 NOT L16
L28           15 SEA ABB=ON  L27 NOT L20
L29            9 DUP REM L26 (6 DUPLICATES REMOVED)
                 D IBIB ABS TOT
L30          216 SEA ABB=ON  L19 AND (PROGNOS? OR SPREAD? OR INVASIV? OR
                 METASTAT? OR SURVIV? OR STAGE# OR STAGING OR GRADE# OR GRADING
                 OR AGGRESS? OR PROGRESS?)
L31          185 SEA ABB=ON  L19 AND (TREATMENT# OR THERAP?)
L32          317 SEA ABB=ON  L30 OR L31
L33          336 SEA ABB=ON  L30 OR L31
L34           94 SEA ABB=ON  L33 AND PY<2003
L35           37 DUP REM L34 (57 DUPLICATES REMOVED)
                 D IBIB ABS TOT
L36         1670 SEA ABB=ON  IE5 OR IE2
L37            3 SEA ABB=ON  L4 AND L36
L38            3 DUP REM L37 (0 DUPLICATES REMOVED)
                 D IBIB ABS TOT
L39            9 SEA ABB=ON  L36 AND (MAMMARY OR BREAST OR DCIS OR (DUCTAL(W)
                 CARCINOMA#) OR SCC OR (SQUAMOUS(W) CELL(W) CARCINOMA#))
L40            9 DUP REM L39 (0 DUPLICATES REMOVED)
                 D IBIB ABS TOT

     FILE 'PCTFULL' ENTERED AT 20:09:24 ON 16 JAN 2007
L41          128 SEA ABB=ON  GKLF OR EZF OR KLF4 OR (KLF(W)(4 OR IV))
L42           63 SEA ABB=ON  KRUPPEL(W)LIKE(2W)(4 OR IV)
L43            1 SEA ABB=ON  ENDOTHELIAL(W)KRUPPEL(W)LIKE
```

```
L44           12 SEA ABB=ON  GUT(2W)KRUPPEL(W)LIKE
L45            5 SEA ABB=ON  EPITHELIAL(W)ZINC(W)FINGER
L46            4 SEA ABB=ON  HGKLF OR HKLF4 OR (HKLF(W)(4 OR IV)) OR HEZF
L47            0 SEA ABB=ON  HUGKLF OR HUKLF4 OR (HUKLF(W)(4 OR IV)) OR HUEZF
L48            0 SEA ABB=ON  HUMGKLF OR HUMKLF4 OR (HUMKLF(W)(4 OR IV)) OR
                             HUMEZF
L49          164 SEA ABB=ON  L41 OR L42 OR L43 OR L44 OR L45 OR L46
L50        65573 SEA ABB=ON  (RESPON? OR RESULT?)(5A)(TREATMENT# OR THERAP? OR
                             CHEMOTHERAP? OR ANTITUMOR OR ANTITUMOR OR ANTICANCER OR
                             ANTINEOPLASTIC)
L51            7 SEA ABB=ON  L49(5A)L50
L52            0 SEA ABB=ON  L51 AND AD<20000517
L53            9 SEA ABB=ON  L49(S)L50
L54            0 SEA ABB=ON  L53 AND AD<20000517
L55           83 SEA ABB=ON  L49 AND L50
L56            5 SEA ABB=ON  L55 AND AD<20000517
L57           11 SEA ABB=ON  (RUPPERT, J?)/IN
L58            5 SEA ABB=ON  (ENGLER, J?)/IN
                  D L56 IBIB TOT
L59            1 SEA ABB=ON  (WO2000022093)/PN
L60            1 SEA ABB=ON  (WO9304076)/PN
L61            1 SEA ABB=ON  L49 AND L59
                  D KWIC
L*** DEL      83 S L49 AND L50
L62            1 SEA ABB=ON  L59 AND L50
                  D KWIC
L63            1 SEA ABB=ON  L60 AND L49
                  D KWIC
L64            9 SEA ABB=ON  L49(5A)(MAMMARY OR BREAST OR DCIS OR (DUCTAL(W)CARC
                             INOMA#))
L65            2 SEA ABB=ON  L64 AND AD<20020712
                  D KWIC 2
                  D KWIC 1
                  D IBIB 1
L66            1 SEA ABB=ON  (WO2001077373)/PN
```

```
(FILE 'MEDLINE, BIOSIS, LIFESCI, BIOTECHDS, SCISEARCH, HCAPLUS' ENTERED
     AT 23:27:41 ON 16 JAN 2007)
L1          905 SEA ABB=ON  GKLF OR KLF4 OR EZF OR (KLF(W)(4 OR IV))
L2            5 SEA ABB=ON  HGKLF OR HKLF4 OR HEZF OR (HKLF(W)(4 OR IV))
L3          307 SEA ABB=ON  KRUPPEL(W) LIKE(2W)(4 OR IV)
L4            1 SEA ABB=ON  ENDOTHELIAL(W) KRUPPEL(W) LIKE
L5          385 SEA ABB=ON  GUT(2W) KRUPPEL(W) LIKE
L6           11 SEA ABB=ON  EPITHELIAL(W) ZINC(W) FINGER
L7          982 SEA ABB=ON  L1 OR L2 OR L3 OR L4 OR L5 OR L6
L8           89 SEA ABB=ON  L7 AND (MAMMARY OR BREAST OR DCIS OR SCC OR
                ((DUCTAL OR (SQUAMOUS(W) CELL))(W) CARCINOMA#))
L9          201 SEA ABB=ON  L7 AND (TREATMENT# OR THERAP? OR ANTICANCER OR
                ANTITUMOR OR ANTITUMOUR OR ANTINEOPLASTIC OR CHEMOTHERAP?)
L10         552 SEA ABB=ON  L7 AND (LOCAL? OR ENRICH? OR SUBCELLULAR? OR
                (SUB(W) CELLULAR?) OR NUCLEAR OR NUCLEUS OR CYTOSOL? OR
                CYTOPLASM?)
L11          37 SEA ABB=ON  L8 NOT PY>2004
L12         102 SEA ABB=ON  L9 NOT PY>2004
L13         375 SEA ABB=ON  L10 NOT PY>2004
L14         133 SEA ABB=ON  L11 OR L12
L15          57 DUP REM L14 (76 DUPLICATES REMOVED)
L16         171 DUP REM L13 (204 DUPLICATES REMOVED)
L17         196 SEA ABB=ON  L15 OR L16
                D IBIB ABS TOT
```

2736–2741 Nucleic Acids Research, 2002, Vc

Opposing effects of ctor 4 (gut-enriched Krüppel-like factor) e factor 5 (intestinal-enriched ctor) on the promoter of the *Krüppel-like factor 4* gene

Duyen T. Dang, Weidong Zhao[1], Channing S. Mahatan, Deborah E. Geiman and Vincent W. Yang[1,2,*]

Division of Gastroenterology, Department of Medicine, The Johns Hopkins University School of Medicine, Baltimore, MD 21205, USA, [1]Division of Digestive Diseases, Department of Medicine and [2]Winship Cancer Institute, Emory University School of Medicine, Atlanta, GA 30322, USA

Received as resubmission April 22, 2002; Revised and Accepted May 1, 2002

ABSTRACT

KLF4 (Krüppel-like factor 4 or gut-enriched Krüppel-like factor, GKLF) and KLF5 (Krüppel-like factor 5 or intestinal-enriched Krüppel-like factor, IKLF) are two closely related members of the zinc finger-containing Krüppel-like factor family of transcription factors. Although both genes are expressed in the intestinal epithelium, their distributions are different: *Klf4* is primarily expressed in the terminally differentiated villus cells while *Klf5* is primarily in the proliferating crypt cells. Previous studies show that Klf4 is a negative regulator of cell proliferation and Klf5 is a positive regulator of cell proliferation. In this study, we demonstrate that Klf5 binds to a number of *cis*-DNA elements that have previously been shown to bind to Klf4. However, while Klf4 activates the promoter of its own gene, Klf5 suppresses the *Klf4* promoter. Moreover, Klf5 abrogates the activating effect of Klf4 on the *Klf4* promoter and Klf4 abrogates the inhibitory effect of Klf5 on the same promoter. An explanation of this competing effect is due to physical competition of the two proteins for binding to cognate DNA sequence. The complementary tissue localization of expression of *Klf4* and *Klf5* and the opposing effect of the two Klfs on the *Klf4* promoter activity may provide a basis for the coordinated regulation of expression of the *Klf4* gene in the intestinal epithelium.

INTRODUCTION

Krüppel-like factors (KLFs) are zinc finger-containing transcription factors that exhibit homology to the *Drosophila melanogaster* segmentation gene product Krüppel (1). A subfamily of mammalian KLFs highly related to the erythroid Krüppel-like factor (EKLF/KLF1) has recently been described (2). This rapidly expanding subfamily currently has 12 members, which have been given numerical designations by the Human Gene Nomenclature Committee (3). KLFs can be transcriptional activators or repressors (4) and they bind to a similar DNA sequence that has either a CACCC homology or is rich in GC content (5). It is therefore not surprising that KLFs may interact with the same *cis*-element in the same gene. For example, both KLF12/AP2-rep and KLF9/BTEB1 bind to the CACCC element in the *AP2α* promoter (6). But, while KLF12 acts as a repressor, KLF9 acts as a strong activator of the *AP2α* promoter (6). In another example, both KLF6/Zf9 and KLF4/GKLF activate the human *keratin 4* promoter through the CACCC motif and the two factors physically interact (7). Finally, both KLF4/GKLF and KLF5/IKLF bind to the CACCC element in the *α-smooth muscle* and *SM22α* promoters (8). In this case, KLF4 represses while KLF5 activates the induction of these two promoters by TGFβ (8).

The reciprocal effect of KLF4 and KLF5 in regulating gene expression merits additional consideration. Aside from their opposing biochemical effects on several smooth muscle gene promoters as described above, the cellular distribution and regulatory functions of KLF4 and KLF5 also exhibit an opposite pattern. For example, while *Klf4* is mainly expressed in the post-mitotic differentiated villus epithelial cells of the intestinal tract (9), *Klf5* is found primarily in the proliferating crypt cells (10). The cellular distribution of the two genes in the epidermis of the skin also mirrors that in the intestinal epithelium (11–13). *In vitro*, expression of *Klf4* is associated with a process of growth arrest (9), while that of *Klf5* mainly accompanies cellular proliferation (14). Moreover, forced expression of *Klf4* leads to a G_1/S cell cycle arrest (15,16) but that of *Klf5* causes a transformed phenotype (14).

Because of the relatively restricted pattern of tissue expression of *Klf4*, we have been characterizing factors that regulate its expression. One such factor, Cdx2, previously shown to drive differentiation of intestinal epithelial cells (17), is shown to be a transactivator of the *Klf4* promoter (18,19). In addition, Klf4 is capable of transactivating the promoter of its own gene

*To whom correspondence should be addressed at: Emory University School of Medicine, Department of Medicine, Division of Digestive Diseases, 201 Whitehead Biomedical Research Building, 615 Michael Street, Atlanta, GA 30322, USA. Tel: +1 404 7275638; Fax: +1 404 727 5767; Email: vyang@emory.edu

through three closely spaced GC-boxes within the promoter (18). The present study demonstrates that Klf5 binds to the same DNA *cis*-elements as Klf4, including those within the *Klf4* promoter. However, while Klf4 activates, Klf5 represses *Klf4* promoter activity. Furthermore, the two factors can abrogate each other's effect on the *Klf4* promoter. Lastly, the two factors compete with each other for binding to the same *cis*-element. The results of these studies suggest that Klf4 and Klf5 have opposing biochemical functions in regulating expression of the *Klf4* gene and may potentially be involved in a coordinated effort to orchestrate the proliferative and differentiated phenotype of the intestinal epithelium.

MATERIALS AND METHODS

Plasmid constructs

The eukaryotic expression construct containing full-length Klf4 (PMT3–Klf4) and the luciferase reporter construct containing 1.0 kb of the 5′ flanking promoter region of the *Klf4* gene (*Klf4*–pGL2–Luciferase) were previously described (18). The expression construct containing full-length Klf5, pBK CMV–Klf5, was generously provided by J. Lingrel (University of Cincinnati, College of Medicine) (10). An *Eco*RI–*Kpn*I fragment of the full-length *Klf5* cDNA from pBK CMV–Klf5 was subcloned into the PMT3 vector to create PMT3–Klf5. The two PMT3 constructs were digested with appropriate restriction endonucleases to release the zinc finger portions of Klf4 and Klf5, which were then subcloned back into the PMT3 vector to create PMT3–Klf4–ZF and PMT3–Klf5–ZF, respectively. The internal control for transfection, pRL–CMV, was purchased from Promega Corporation (Madison, WI).

The prokaryotic expression vector pET–16b containing the zinc finger portion of Klf4 (amino acids 350–483) has previously been described (20). The C-terminal portion of Klf5 between amino acids 242 and 446 was cloned into the prokaryotic expression vector pET101/D. Both recombinant proteins contained a 10-histidine tag at the N-terminus and were purified by nickel affinity chromatography as described before (20). The apparent molecular weight for the resultant recombinant protein was 18 and 26 kDa, respectively, for Klf4 and Klf5.

Preparation of nuclear extracts

Nuclear extracts containing full-length Klf4 or full-length Klf5 were prepared from COS-1 cells transfected with PMT3–Klf4 or PMT3–Klf5. Nuclear extracts from cells transfected with PMT3 alone were used as controls. Extracts from transfected cells were prepared as previously described (18). Briefly, transfected cells were rinsed with ice-cold phospate-buffered saline, scraped, harvested and pelleted. The pellets were washed with 4 pack cell volume (p.c.v.) of solution containing 10 mM Tris–HCl pH 7.8, 1.5 mM $MgCl_2$, 10 mM KCl, 0.5 mM DTT and a Complete Protease Inhibitor Cocktail Tablet (Roche, Indianapolis, IN). Following 10 min incubation on ice, the cells were lysed by 10 strokes of a Dounce homogenizer. Nuclei were collected by centrifugation (Sorvall Microspin) and resuspended in 2 p.c.v. of a lysis solution containing 420 mM KCl, 20 mM Tris–HCl pH 7.8, 1.5 mM $MgCl_2$, 0.5 mM DTT, 20% glycerol and a Complete Protease Inhibitor Tablet (Roche). After incubation for 1 h at 4°C with gentle agitation, the solution was centrifuged and the supernatant dialyzed twice against 500 ml of 20 mM Tris–HCl pH 7.8, 100 mM KCl, 0.2 mM EDTA, 0.5 mM DTT, 20% glycerol and a Complete Protease Inhibitor Tablet (Roche). Extracts were divided into small aliquots and immediately cryopreserved.

Electrophoretic mobility shift assays (EMSAs)

EMSAs were performed according to previously published protocols (9,20). The basic transcription element (BTE) probe contained a sequence in the promoter of the cytochrome *P4501A1* gene that had previously been shown to bind to Klf4 (21). The target detection assay (TDA) probe was a previously selected consensus-binding site for KLF4 (20) and closely resembled the three GC-boxes in the promoter of the *Klf4* gene (18). The GC-2 probe refers to the GC-box 2 sequence in the *Klf4* promoter between nucleotide −108 and −86 that has previously been shown to bind Klf4 (18). Probes were labeled with [γ-^{32}P]ATP using T4 polynucleotide kinase. In each reaction, 0.5 pmol of labeled probe was used. Nuclear extracts from PMT3-, PMT3–Klf4- or PMT3–Klf5-transfected cells, or purified recombinant Klf4 or Klf5 were incubated in a volume of 30 µl containing 20 mM Tris–HCl pH 7.2, 10 mM $MgCl_2$, 150 mM NaCl, 20 mM KCl, 5 µM $ZnCl_2$, 0.5 mM DTT, 5% glycerol and 2 µg poly(dI•dC) on ice for 30 min. The labeled probe was then added to the reaction and the incubation continued for another 15 min at room temperature. The DNA and DNA–protein complexes were resolved from one another by native 6.0% polyacrylamide gel electrophoresis and visualized by autoradiography.

Transfection and reporter assays

Transient transfection by lipofection of Chinese hamster ovary (CHO) cells with various DNA constructs (*Klf4*–pGL2–Luciferase, PMT3–Klf4, PMT3–Klf5, PMT3–Klf4–ZF and PMT3–Klf5–ZF) were performed as previously described (9,18,20). Transfections were performed in 6-well tissue culture dishes at 37°C for 16 h. All transfections included the internal standard pRL–CMV (Promega) to normalize for transfection efficiency. Luciferase and *Renilla* assays were performed using the Dual-Luciferase Assay (Promega).

RESULTS

Klf4 and Klf5 bind to similar *cis*-DNA elements

We first examined whether Klf4 and Klf5 bound to similar sequences by EMSAs using radiolabeled oligonucleotides containing either an established consensus sequence for Klf4 (TDA) (20) or the BTE (21). As shown in Figure 1A, two common DNA–protein complexes were formed when the TDA probe was incubated with nuclear extracts from PMT3-, PMT3–Klf4- and PMT3–Klf5-transfected cells. However, an additional complex was formed in the reaction that contained either PMT3–Klf4- or PMT3–Klf5-transfected cells. The Klf4–TDA complex is identified by * and the Klf5–TDA complex is identified by +. The specificities of all the DNA–protein complexes were demonstrated by their gradual disappearance upon addition of increasing amounts of unlabeled probe (Fig. 1A). A similar pattern was observed when BTE was used as a probe except that the intensities of the two common bands were stronger when compared with the TDA probe (Fig. 1B). The results suggest that Klf4 and Klf5 bind to

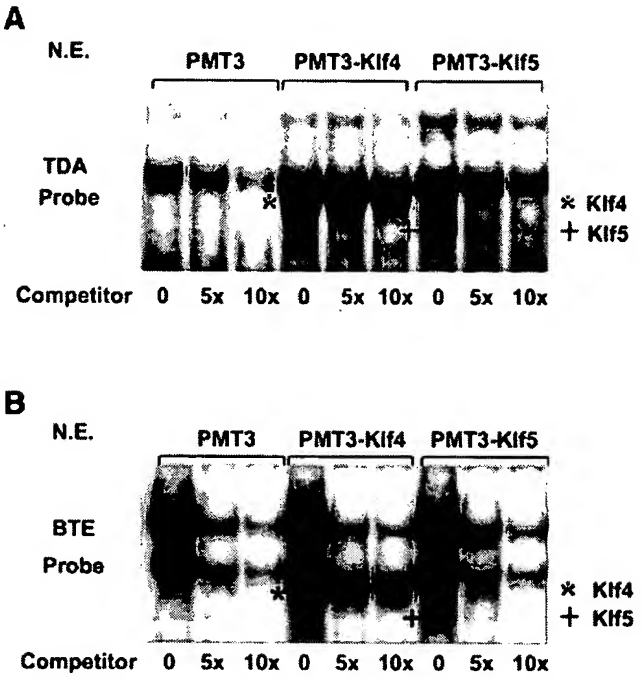

Figure 1. EMSAs of Klf4 and Klf5 on two *cis*-elements, TDA and BTE. EMSAs were performed using 10 μg nuclear extracts prepared from COS-1 cells transfected with an expression construct containing vector alone (PMT3), full-length Klf4 (PMT3–Klf4), or full-length Klf5 (PMT3–Klf5) and two radiolabeled oligonucleotide probes containing established *cis*-elements for Klf4: TDA (**A**) and BTE (**B**). Where indicated, an unlabeled cognate oligonucleotide was used as a competitor at 5× and 10× molar excess of the labeled probe. * represents the shifted Klf4–probe complex and + represents the shifted Klf5–probe complex. N.E., nuclear extracts.

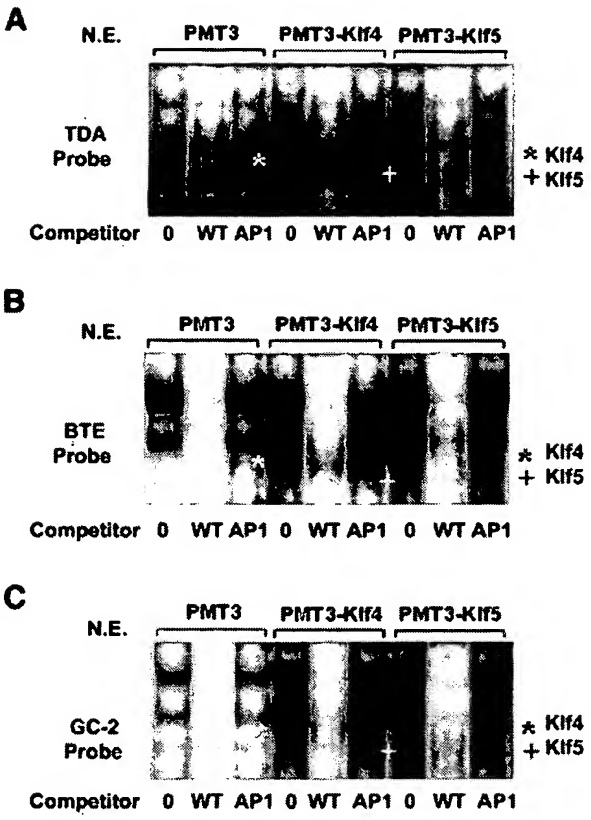

Figure 2. EMSAs of Klf4 and Klf5 on an additional *cis*-element, GC-2, that is present in the Klf4 promoter. EMSAs were performed with 10 μg nuclear extracts (N.E.) prepared from cells transfected with PMT3, PMT3–Klf4 or PMT3–Klf5 in the absence of any competitors (0), or in the presence of 25× molar excess of a cognate competitor (WT) or an unrelated competitor (AP1). Probes used include TDA (**A**), BTE (**B**) and GC-2 (**C**). * represents the shifted Klf4–probe complex and + represents the shifted Klf5–probe complex.

similar DNA elements. Furthermore, both Klf4 and Klf5 bound to the GC-2 probe (Fig. 2C) which represents one of three GC-box sequences in the *Klf4* promoter, all of which have been shown to bind Klf4 (18). The specificities of DNA–protein interaction with all three probes were further demonstrated by the failure of an unrelated AP1 probe to compete for the formation of the complexes (Fig. 2A–C).

Klf4 activates and Klf5 represses the *Klf4* promoter

Recent work from our laboratory showed that Klf4 activates the promoter of its own gene by interacting with the GC-boxes in the proximal promoter (18). To determine whether Klf5 also influences the promoter activity of the *Klf4* gene, we performed co-transfection studies using the *Klf4*–pGL2–Luciferase reporter and a eukaryotic expression construct containing either Klf4 or Klf5. As depicted in Figure 3, PMT3–Klf4 significantly activated the *Klf4* promoter when compared with PMT3 alone, confirming previous findings. In contrast, PMT3–Klf5 significantly suppressed *Klf4* promoter activity when compared with PMT3 alone. Thus, Klf4 and Klf5 have opposite effects on the activity of the *Klf4* promoter.

Klf4 and Klf5 compete to regulate the *Klf4* promoter

To further determine a possible interaction between Klf4 and Klf5 on the *Klf4* promoter, we performed co-transfection experiments using the *Klf4*–pGL2–Luciferase reporter, a constant amount of PMT3–Klf5 and increasing amounts of PMT3–Klf4 or PMT3–Klf4–ZF. As seen in Figure 4A, in the absence of any competing Klf4, Klf5 suppressed the reporter activity, as in Figure 3. The addition of Klf4 removed this inhibitory effect in a dose-dependent fashion (solid line). In contrast, a construct including only the zinc finger portion of Klf4 failed to reverse the inhibitory effect on the *Klf4* promoter (dashed line). Similarly, in a converse experiment with PMT3–Klf4 as the primary effector and Klf5 as the competing effector (Fig. 4B), Klf5 (solid line) but not Klf5–ZF (dashed line) abrogated the stimulatory effect of Klf4 on the *Klf4* promoter activity. These results indicate that Klf4 and Klf5 not only exhibit an opposite effect on the *Klf4* promoter, they actively compete with each other. Moreover, this competitive effect requires the full-length protein. The zinc fingers alone are not sufficient.

Klf4 and Klf5 compete with each other for DNA binding

One possibility that may explain the competing effects of Klf4 and Klf5 on the *Klf4* promoter is that the two proteins may compete with each other for binding to DNA. To address this possibility, we produced purified partial-length recombinant proteins that contained the zinc finger region of Klf4 and Klf5 (Fig. 5A). When incubated individually with a labeled GC-2 probe, each protein interacted avidly with the probe (Fig. 5B). We next performed EMSA of GC-2 using a constant amount of recombinant Klf4 and increasing amounts of Klf5. As seen,

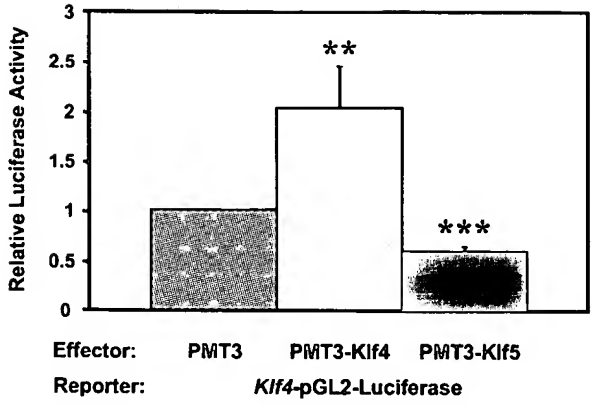

Figure 3. The opposite effects of Klf4 or Klf5 on the Klf4 promoter. Five micrograms each of the *Klf4*–pGL2–Luciferase reporter and PMT3, PMT3–Klf4 or PMT3–Klf5 and 2 μg pCMV–RL were co-transfected into CHO cells using Lipofectamine reagent (Promega). Firefly and *Renilla* luciferase assays were determined 24 h after transfection. Shown are the means of three independent experiments (n = 3) performed in triplicate. Relative luciferase activity was standardized with the internal control *Renilla* luciferase activity. Bars represent standard deviations. ** = $P < 0.01$, *** = $P < 0.001$ by Student's t-test compared with PMT3 vector control.

Klf5 reduced the binding of Klf4 to the probe in a dose-dependent fashion (Fig. 5C). Similarly, if an increasing amount of Klf4 was incubated with a constant amount of Klf5, the binding of Klf5 to the probe also gradually diminished (Fig. 5D). These results indicate that Klf4 and Klf5 compete with each other in binding to DNA.

DISCUSSION

The present study demonstrates how two closely related Klfs exert their effects on transcription of a target gene in an opposing manner. We show that Klf5 binds to several *cis*-elements previously established to be the binding sites for Klf4, including TDA, BTE and GC-2, the last a native *cis*-element in the *Klf4* promoter. However, while Klf4 activates the promoter activity of its own gene, Klf5 has exactly the opposite effect. Moreover, when present together, the two Klfs interfere with each other in modulating the *Klf4* promoter activity. We also show that a possible explanation for this interfering effect is due to competition of the two proteins for binding to DNA.

Opposing effects of other KLFs on the promoters of several other genes have previously been described. For example, Klf4 suppresses the activity of the cytochrome *p4501A1* (*CYP1A1*) promoter while Sp1 activates it in a BTE-dependent fashion (21). Also, similar to the present study, Klf4 abrogates the stimulatory effect of Sp1 on the *CYP1A1* gene in a dose-dependent manner. In this case, it was shown that the zinc fingers of Klf4 compete for binding to BTE with Sp1 (21). It is of interest to note that KLF5, also known as BTEB2 (10), is a strong activator of the *CYP1A1* promoter (22). The findings on the *CYP1A1* promoter would then be the first example in which KLF4 and KLF5 antagonize each other in regulating promoter activity. In another example, KLF4 and KLF5 bind to the same CACCC element present in the promoters of two smooth muscle genes, α-*smooth muscle actin* and *SM22α* (8). Here, KLF4 inhibits TGFβ-dependent stimulation of the *SM22α* promoter while KLF5 further activates TGFβ-dependent stimulation of the same promoter (8). Thus, evidence from literature to date indicates that KLF4 and KLF5 exert opposite effects on the promoters of the genes studied.

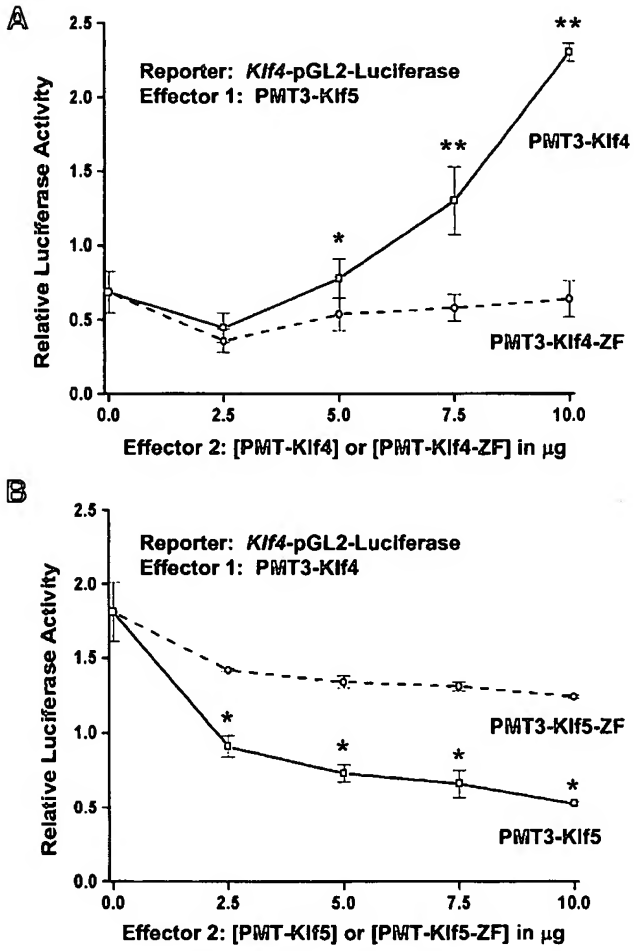

Figure 4. The competing effects of Klf4 and Klf5 on the Klf4 promoter. (A) Five micrograms each of *Klf4*–pGL2–Luciferase reporter and effector 1 (PMT3–Klf5) were co-transfected into CHO cells in presence of increasing amounts of effector 2: either PMT3–Klf4 (solid line) or PMT–Klf4–ZF (dashed line). (B) Five micrograms each of *Klf4*–pGL2–Luciferase reporter and effector 1 (PMT3–Klf4) were co-transfected into CHO cells with increasing amounts of effector 2: either PMT3–Klf5 (solid line) or PMT3–Klf5–ZF (dashed line). The total amount of DNA transfected was kept constant at 25 μg by the addition of PMT3 DNA. Firefly and *Renilla* luciferase assays were determined 24 h after transfection. Shown are the means of four independent experiments (n = 4) performed in triplicate. The relative activity was determined from dividing the reporter activity of effector 1-transfected cells by that of PMT3-transfected cells. Bars represent standard deviations. * = $P < 0.05$, ** = $P < 0.01$ by Student's t-test comparing full-length with zinc finger only-containing constructs.

It should be noted that the biochemical behavior of KLF4 and KLF5 described above is a reflection of their biological behavior. For example, the cellular distribution of the two Klfs in several epithelial tissues is complementary, rather than redundant, to each other. Thus, *Klf4* is mainly expressed in the post-mitotic villus epithelial cells of the intestine (9) and the suprabasal epidermal cells of the skin (11), while *Klf5* is expressed mostly in the proliferating cells of the crypt in the intestine (10) and the basal epidermal cells of the skin (13). Moreover, the pattern of expression of the two genes *in vitro*

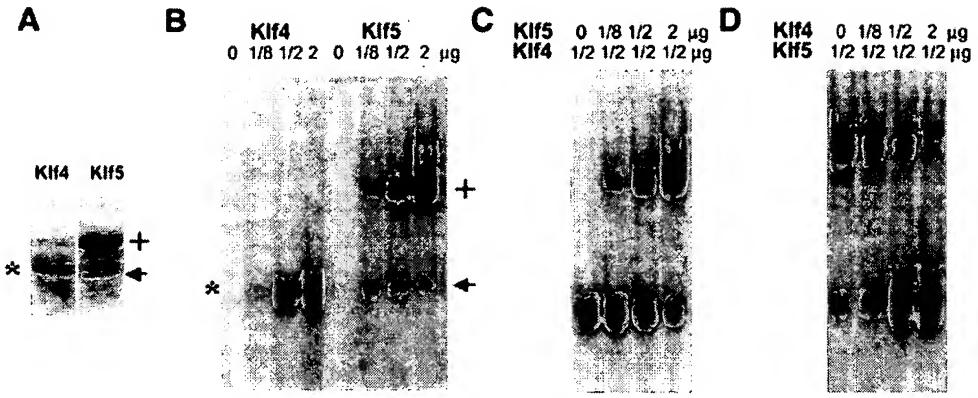

Figure 5. The competing effects of Klf4 and Klf5 on binding to DNA. **(A)** Purified recombinant proteins containing the zinc finger portion of Klf4 (*) and Klf5 (+) are shown in this Commassie blue-stained gel. The apparent molecular weight for Klf4 is 18 kDa and that for Klf5 is 26 kDa. The arrow points to a degradation product of Klf5, which apparently binds to DNA (B). **(B)** EMSAs of recombinant Klf4 and Klf5 on the GC-2 probes. Increasing amounts of purified recombinant Klf4 or Klf5 were used in the experiment. **(C)** EMSAs were performed using a constant amount of recombinant Klf4 and increasing amounts of Klf5. **(D)** EMSAs were performed with a constant amount of recombinant Klf5 and increasing amounts of Klf4.

contrasts each other. *Klf4* is mainly expressed in the growth-arrested cells due to serum deprivation (9), contact inhibition (9) or DNA damage (21). Expression of *Klf5*, on the contrary, is associated with a proliferative state as seen during serum or mitogenic stimulation (14). Based on the results of current and past studies, one may speculate that the lack of crypt expression of *Klf4* in the intestinal crypt epithelium may, in part, be due to the presence of Klf5 in this compartment.

A potential mechanism that may explain how Klf4 and Klf5 compete with each other to regulate the activity of the *Klf4* promoter appears to be exerted at the level of DNA–protein interaction. As demonstrated in Figure 5, Klf5 actively inhibits the binding of Klf4 to the GC-2 probe, and vice versa. However, the zinc finger portion of one Klf is not sufficient in reversing the effect of the other Klf on the activity of the *Klf4* promoter (Fig. 4). These results indicate that amino acid sequence outside the zinc fingers of both proteins is required for the full regulation of the *Klf4* promoter. Klf4 has previously been shown to be a pleiotropic transcription factor, with activating and repressing effects (23). Mutational studies have also located the activating and repressive domains to regions outside the zinc fingers in the Klf4 polypeptide (24). KLF5, although known to be a transcription activator in most studies (10,22), can act as a repressor (25). One might therefore expect that some of these domains involved in transcriptional regulation by the two proteins are responsible for the interplay noted in the current study.

The opposing effects of Klf4 and Klf5 are reminiscent of the opposing effects of Cdx1 and Cdx2 along the crypt–villus axis of the intestinal epithelium. CDX1 and CDX2 are homeodomain transcription factors with sequence homology to the *caudal* gene of *D.melanogaster*, which in mammals are specifically expressed in the epithelium of small intestine and colon (26–29). *Cdx1* is expressed in the proliferating crypt cells (27,30,31) while *Cdx2* is expressed predominantly in the differentiated villus cells (28,32). Several studies have shown that CDX1 regulates cell proliferation (33,34) and CDX2 regulates cell differentiation and growth arrest (17,35).

Of interest, we have recently reported that the intestinal gatekeeper adenomatous polyposis coli (APC) induces *Klf4* expression via Cdx2 (19). APC is a cytoplasmic protein that modulates the oncogenic Wnt signal transduction cascade by binding to β-catenin and promoting its phosphorylation by glycogen synthase kinase 3 β (GSK3β), for subsequent degradation (36). Our previous data, which showed that APC activation of *Klf4* via Cdx2 occurred through a β-catenin independent pathway, have led to our proposal that these three proteins form a part of an enterocyte-specific tumor suppressor pathway in the sequence of APC → CDX2 → KLF4 → growth arrest (19). This pathway may become active as epithelial cells migrate up the intestinal villus and undergo differentiation with the simultaneous loss of proliferative potential. Interestingly, Wnt, which is the product of a proto-oncogene with opposing effects to APC, can up-regulate *CDX1* but not *CDX2* expression (37). Moreover, Wnt has recently been reported to induce mouse *KLF5/BTEB2* through a β-catenin independent, protein kinase C dependent pathway (38). A search of the mouse *Klf5* promoter (DDBJ/EMBL/GenBank accession no. AF285184) reveals several potential CDX1 binding sites (39). We may postulate that *KLF5* is regulated by Wnt via CDX1 in the proliferating intestinal crypt cells while *KLF4* is regulated by APC via CDX2 in the differentiating intestinal villus cells. Crosstalk and negative regulation between these opposing pathways, at the level of KLF4 and KLF5 as shown in this paper, as well as possibly higher levels involving CDX1, CDX2, Wnt and APC, tightly coordinate the intestinal epithelial cells as they proliferate, migrate and differentiate. Current studies are underway to address these interactions.

ACKNOWLEDGEMENTS

We thank Dr Jerry Lingrel for providing reagents. This work was supported in part by grants from the National Institutes of Health (DK52230 and CA84197 to V.W.Y. and DK59970 to D.T.D.). D.T.D. is a recipient of an American Digestive Health Foundation/American Gastroenterological Association Research Scholar Award and a Glaxo Institute for Digestive Health Basic Research Award.

REFERENCES

1. Schuh,R., Aicher,W., Gaul,U., Cote,S., Preiss,A., Maier,D., Seifert,E., Nauber,U., Schroder,C. and Kemler,R. (1986) A conserved family of nuclear

proteins containing structural elements of the finger protein encoded by Krüppel, a *Drosophila* segmentation gene. *Cell*, **47**, 1025–1032.
2. Turner,J. and Crossley,M. (1999) Mammalian Krüppel-like transcription factors: more than just a pretty finger. *Trends Biochem. Sci.*, **24**, 236–240.
3. White,J.A., McAlpine,P.J., Antonarakis,S., Cann,H., Eppig,J.T., Frazer,K., Frezal,J., Lancet,D., Nahmias,J., Pearson,P., Peters,J., Scott,A., Scott,H., Spurr,N., Talbot,C.,Jr. and Povey,S. (1997) Guidelines for human gene nomenclature. HUGO nomenclature committee. *Genomics*, **45**, 468–471.
4. Bieker,J.J. (2001) Krüppel-like factors: three fingers in many pies. *J. Biol. Chem.*, **276**, 34355–34358.
5. Dang,D.T., Pevsner,J. and Yang,V.W. (2000) The biology of mammalian Krüppel-like factors. *Int. J. Biochem. Cell Biol.*, **32**, 1103–1121.
6. Imhof,A., Schuierer,M., Werner,O., Moser,M., Roth,C., Bauer,R. and Buettner,R. (1999) Transcriptional regulation of the AP-2alpha promoter by BTEB-1 and AP-2rep, a novel wt-1/egr-related zinc finger repressor. *Mol. Cell. Biol.*, **19**, 194–204.
7. Okano,J., Opitz,O.G., Nakagawa,H., Jenkins,T.D., Friedman,S.L. and Rustgi,A.K. (2000) The Krüppel-like transcriptional factors Zf9 and GKLF coactivate the human keratin 4 promoter and physically interact. *FEBS Lett.*, **473**, 95–100.
8. Adam,P.J., Regan,C.P., Hautmann,M.B. and Owens,G.K. (2000) Positive- and negative-acting Krüppel-like transcription factors bind a transforming growth factor beta control element required for expression of the smooth muscle cell differentiation marker SM22α *in vivo*. *J. Biol. Chem.*, **275**, 37798–37806.
9. Shields,J.M., Christy,R.J. and Yang,V.W. (1997) Identification and characterization of a gene encoding a gut-enriched Krüppel-like factor expressed during growth arrest. *J. Biol. Chem.*, **271**, 20009–20017.
10. Conkright,M.D., Wani,M.A., Anderson,K.P. and Lingrel,J.B. (1999) A gene encoding an intestinal-enriched member of the Krüppel-like factor family expressed in intestinal epithelial cells. *Nucleic Acids Res.*, **27**, 1263–1270.
11. Garrett-Sinha,L.A., Eberspaecher,H., Seldin,M.F. and de Crombrugghe,B. (1996) A gene for a novel zinc-finger protein expressed in differentiated epithelial cells and transiently in certain mesenchymal cells. *J. Biol. Chem.*, **271**, 31384–31390.
12. Segre,J.A., Bauer,C. and Fuchs,E. (1999) Klf4 is a transcription factor required for establishing the barrier function of the skin. *Nature Genet.*, **22**, 356–360.
13. Ohnishi,S., Laub,F., Matsumoto,N., Asaka,M., Ramirez,F., Yoshida,T. and Terada,M. (2000) Developmental expression of the mouse gene coding for the Krüppel-like transcription factor KLF5. *Dev. Dyn.*, **217**, 421–429.
14. Sun,R., Chen,X.M. and Yang,V.W. (2001) Intestinal-enriched Krüppel-like factor (Krüppel-like factor 5) is a positive regulator of cellular proliferation. *J. Biol. Chem.*, **276**, 6897–6900.
15. Chen,X.M., Johns,D.C., Geiman,D.E., Marban,E., Dang,D.T., Hamlin,G., Sun,R. and Yang,V.W. (2001) Gut-enriched Krüppel-like factor (Krüppel-like factor 4) inhibits cell proliferation by blocking G1/S progression of the cell cycle. *J. Biol. Chem.*, **276**, 30423–30428.
16. Shie,J.L., Chen,Z.Y., O'Brien,M.J., Pestell,R.G., Lee,M.E. and Tseng,C.C. (2000) Role of gut-enriched Krüppel-like factor in colonic cell growth and differentiation. *Am. J. Physiol. Gastrointest. Liver Physiol.*, **279**, G806–G814.
17. Suh,E. and Traber,P.G. (1996) An intestine-specific homeobox gene regulates proliferation and differentiation. *Mol. Cell. Biol.*, **16**, 619–625.
18. Mahatan,C.S., Kaestner,K.H., Geiman,D.E. and Yang,V.W. (1999) Characterization of the structure and regulation of the murine gene encoding gut-enriched Krüppel-like factor (Krüppel-like factor 4). *Nucleic Acids Res.*, **27**, 4562–4569.
19. Dang,D.T., Mahatan,C.S., Dang,L.H., Agboola,I.A. and Yang,V.W. (2001) Expression of the gut-enriched Krüppel-like factor (Krüppel-like factor 4) gene in the human colon cancer cell line RKO is dependent on *CDX2*. *Oncogene*, **20**, 4884–4890.
20. Shields,J.M. and Yang,V.W. (1998) Identification of the DNA sequence that interacts with the gut-enriched Krüppel-like factor. *Nucleic Acids Res.*, **26**, 796–802.
21. Zhang,W., Shields,J.M., Sogawa,K., Fujii-Kuriyama,Y. and Yang,V.W. (1998) The gut-enriched Krüppel-like factor suppresses the activity of the CYP1A1 promoter in an Sp1-dependent fashion. *J. Biol. Chem.*, **273**, 17917–17925.
22. Sogawa,K., Imataka,H., Yamasaki,Y., Kusume,H., Abe,H. and Fujii-Kuriyama,Y. (1993) cDNA cloning and transcriptional properties of a novel GC box-binding protein, BTEB2. *Nucleic Acids Res.*, **21**, 1527–1532.
23. Zhang,W., Geiman,D.E., Shields,J.M., Dang,D.T., Mahatan,C., Kaestner,K.H., Biggs,J.R., Kraft,A.S. and Yang,V.W. (2000) The gut-enriched Krüppel-like factor (Krüppel-like factor 4) mediates the transactivating effect of p53 on the p21WAF1/Cip1 promoter. *J. Biol. Chem.*, **275**, 18391–18398.
24. Yet,S.F., Folta,S.C., Jain,M.K., Hsieh,C.M., Maemura,K., Layne,M.D., Zhang,D., Marria,P.B., Yoshizumi,M., Chin,M.T., Perrella,M.A. and Lee,M.E. (1998) Human EZF, a Krüppel-like zinc finger protein, is expressed in vascular endothelial cells and contains transcriptional activation and repression domains. *J. Biol. Chem.*, **273**, 1026–1031.
25. Shi,H., Zhang,Z., Wang,X., Liu,S. and Teng,C.T. (1999) Isolation and characterization of a gene encoding human Krüppel-like factor 5 (IKLF): binding to the CAAT/GT box of the mouse lactoferrin gene promoter. *Nucleic Acids Res.*, **27**, 4807–4815.
26. Duprey,P., Chowdhury,K., Dressler,G.R., Balling,R., Simon,D., Guenet,J.L. and Gruss,P. (1988) A mouse gene homologous to the *Drosophila* gene caudal is expressed in epithelial cells from the embryonic intestine. *Genes Dev.*, **2**, 1647–1654.
27. James,R. and Kazenwadel,J. (1991) Homeobox gene expression in the intestinal epithelium of adult mice. *J. Biol. Chem.*, **266**, 3246–3251.
28. James,R., Erler,T. and Kazenwadel,J. (1994) Structure of the murine homeobox gene cdx-2. Expression in embryonic and adult intestinal epithelium. *J. Biol. Chem.*, **269**, 15229–15237.
29. Freund,J.N., Domon-Dell,C., Kedinger,M. and Duluc,I. (1998) The Cdx-1 and Cdx-2 homeobox genes in the intestine. *Biochem. Cell Biol.*, **76**, 957–969.
30. Silberg,D.G., Furth,E.E., Taylor,J.K., Schuck,T., Chiou,T. and Traber,P.G. (1997) CDX1 protein expression in normal, metaplastic and neoplastic human alimentary tract epithelium. *Gastroenterology*, **113**, 478–486.
31. Subramanian,V., Meyer,B. and Evans,G.S. (1998) The murine Cdx1 gene product localises to the proliferative compartment in the developing and regenerating intestinal epithelium. *Differentiation*, **64**, 11–18.
32. Silberg,D.G., Swain,G.P., Suh,E.R. and Traber,P.G. (2000) Cdx1 and cdx2 expression during intestinal development. *Gastroenterology*, **119**, 961–971.
33. Maulbecker,C.C. and Gruss,P. (1993) The oncogenic potential of deregulated homeobox genes. *Cell Growth Differ.*, **4**, 431–441.
34. Soubeyran,P., Haglund,K., Garcia,S., Barth,B.U., Iovanna,J. and Dikic,I. (2001) Homeobox gene Cdx1 regulates Ras, Rho and PI3 kinase pathways leading to transformation and tumorigenesis of intestinal epithelial cells. *Oncogene*, **20**, 4180–4187.
35. Suh,E., Chen,L., Taylor,J. and Traber,P.G. (1994) A homeodomain protein related to caudal regulates intestine-specific gene transcription. *Mol. Cell. Biol.*, **14**, 7340–7351.
36. Polakis,P. (2000) Wnt signaling and cancer. *Genes Dev.*, **14**, 1837–1851.
37. Lickert,H., Domon,C., Huls,G., Wehrle,C., Duluc,I., Clevers,H., Meyer,B.I., Freund,J.N. and Kemler,R. (2000) Wnt/β-catenin signaling regulates the expression of the homeobox gene Cdx1 in embryonic intestine. *Development*, **127**, 3805–3813.
38. Ziemer,L.T., Pennica,D. and Levine,A.J. (2001) Identification of a mouse homolog of the human BTEB2 transcription factor as a β-catenin-independent Wnt-1-responsive gene. *Mol. Cell. Biol.*, **21**, 562–574.
39. Schug,J. and Overton,G.C. (1997) TESS: Transcription Element Search Software on the WWW, Technical Report CBIL-TR-1997-1001-v0.0. Computational Biology and Informatics Laboratory, School of Medicine, University of Pennsylvania. http://www.cbil.upenn.edu/tess/index.html.

Redox-sensitive vascular smooth muscle cell proliferation is mediated by GKLF and Id3 in vitro and in vivo

GEORG NICKENIG,[1,2] STEPHANIE BAUDLER,[2] CORNELIUS MÜLLER, CHRISTIAN WERNER, NIKOS WERNER, HILKE WELZEL, KERSTIN STREHLOW, AND MICHAEL BÖHM

Universitätskliniken des Saarlandes, Medizinische Klinik und Poliklinik, Innere Medizin III, 66424 Homburg/Saar, Germany

ABSTRACT. **Reactive oxygen species such as superoxide and hydroxyl radicals have been implicated in the pathogenic growth of various cell types. The molecular mechanisms involved in redox-sensitive cell growth control are poorly understood. Stimulation of cultured vascular smooth muscle cells (VSMC) with xanthin/xanthin oxidase (X/XO) increases proliferation, whereas stimulation with hydrogen peroxide and Fe^{3+}NTA (H-Fe) causes growth arrest of VSMC. Differential Display led to the identification of two novel, differentially regulated redox-sensitive genes. The dominant negative helix-loop-helix protein Id3 is induced by X/XO and down-regulated by H-Fe. The transcription factor gut-enriched Kruppel-like factor (GKLF) is induced by H-Fe but not by X/XO. Induction of GKLF and inhibition of Id3 via transfection experiments leads to growth arrest, whereas overexpression of Id3 and inhibition of GKLF cause cell growth. Id3 down-regulation is induced via binding of GKLF to the Id3 promotor and concomitantly reduced Id3 gene transcription rate. GKLF induction by H-Fe is mediated through hydroxyl radicals, p38MAP kinase-, calcium-, and protein synthesis-dependent pathways. Id3 is induced by X/XO via superoxide, calcium, p38, and p42/44 MAP kinase. GKLF induces and Id3 depresses expression of $p21^{WAF1/Cip1}$, $p27^{KIP1}$, p53. Induction of Id3 is accomplished by angiotensin II via superoxide release. A vascular injury mouse model revealed that Id3 is overexpressed in proliferating vascular tissue in vivo. These findings reveal novel mechanisms of redox-controlled cellular proliferation involving GKLF and Id3 that may have general implications for our understanding of vascular and nonvascular growth control.—Nickenig, G., Baudler, S., Müller, C., Werner, N., Welzel, H., Strehlow, K., Böhm, M. redox-sensitive vascular smooth muscle cell proliferation is mediated by GKLF and Id3 in vitro and in vivo. *FASEB J.* 16, 1077–1086 (2002)**

Key Words: reactive oxygen species · VSMC · proliferation · gene expression

REACTIVE OXYGEN SPECIES (ROS) such as superoxide ($O_2^{\cdot}$), hydrogen peroxide, and hydroxyl anions ($OH^{\cdot}$) are involved in a multiplicity of pathological settings such as inflammation, cancer development, and vascular lesions (1–3). ROS exert direct cellular damage and mitogenicity, serve as intracellular second messengers, and scavenge vasoprotective nitric oxide (1–5). Among other factors, the induction of cellular growth in tumor cells and vascular smooth muscle cells (VSMC) by ROS is of fundamental relevance. $O_2^{\cdot}$ induces a wide array of second messengers typical of mitogens (3, 6, 7). In contrast, data concerning the role of $OH^{\cdot}$ in cell proliferation are conflicting. Hypertrophic as well as apoptotic effects have been ascribed to $OH^{\cdot}$, for example, in VSMC (8–10). Proliferation, growth arrest, and apoptosis are key steps in various states of atherogenesis and tumor progression; therefore, it is crucial to dissect not only the potentially differential influence of various ROS on cell growth but to clarify the molecular events that govern ROS-induced regulation of proliferation. We investigated potential differential effects of radicals on VSMC growth and monitored its influence on genes such as cyclin-dependent kinase inhibitors (11–13), which are involved in control of cell proliferation. To identify currently unknown gene expression alterations devoted to VSMC growth, we chose an unbiased gene hunting approach, the differential display technique. The latter enabled identification of two redox-sensitive genes engaged in proliferation pathways.

MATERIALS AND METHODS

Cellular proliferation

The rate of cellular proliferation was determined using cell proliferation ELISA (Roche Molecular Biochemicals, Mannheim, Germany) via BrdU incorporation into new synthesized DNA according to the manufacturer's protocol. Each experiment was performed in triplicate. VSMC were plated on microtiter plates at 10^4 cells per well. After 12 h, cells were serum starved for 24 h and treated with ROS for 24 h. BrdU

[1] Correspondence: Klinik und Poliklinik Innere Medizin III;, Universität des Saarlandes, 66424 Homburg, Germany. E-mail: nickenig@med-in.uni-sb.de

[2] G.N. and S. B. contributed equally.

was added at a final concentration of 10 μM and cells were reincubated an additional 12 h at 37°C. Cells were fixed with fixation solution for 30 min at room temperature and incubated with 100 μL anti-BrdU peroxidase-labeled antibody for 90 min. After three washings, the substrate solution for the colorimetric quantification was added at a final concentration of 100 μL/mL and left at room temperature for 5–30 min until color development was sufficient for photometric detection.

For cell counting, cells were treated with ROS for 12 h, removed from the culture dish by addition of trypsin, and pelleted. The pellet was resuspended in 1 mL DMEM and cells were counted in a Neubauer chamber.

Apoptosis

The rate of apoptosis in ROS-treated cells was assessed using the Cell Death Detection ELISA^{PLUS} System (Roche Molecular Biochemicals). The test principle is based on determination of the amount of nucleosomes generated during the apoptotic fragmentation of cellular DNA. Cells were scraped and collected by centrifugation for 5 min at 1500 rpm (Heraeus Megafuge 1.0) and washed in 1 mL DMEM. The pellet was resuspended in 0.5 mL incubation buffer and left at 4°C for 30 min. After centrifugation for 10 min at 15,000 rpm and 4°C in a microcentrifuge, 200 μL of supernatant was diluted in 1.8 mL of incubation buffer and 100 μL of each sample was incubated in anti-histone-coated microtiter plate wells for 90 min, the wells were washed three times with incubation buffer and 100 μL of anti-DNA peroxidase-linked antibody was added, followed by further incubation for 90 min. After three washing steps with incubation buffer, 100 μL of ABTS® substrate solution for the peroxidase was added; after 10–20 min, the rate of apoptosis was determined by photometric measurement at 492 nm.

RNA isolation

Total RNA from ROS-treated and control cells was isolated using PEQGold RNAPure (PeqLab, Erlangen, Germany) according to the manufacturer's protocol. To eliminate false positives generated from genomic DNA, RNA was treated with 10 U RNase-free DNaseI (Roche Molecular Biochemicals) for 30 min at 37°C and extracted with phenol/chloroform.

Differential display

Differential display of mRNA was carried out using the RNA image mRNA Differential Display System (GenHunter Corporation, Nashville). Two micrograms of purified total RNA was reverse transcribed using one of the three provided H-T_{11}-M-Primers (M: A, T, or G) and cDNA representing 200 ng of RNA was submitted to the Differential Display PCR using the respective H-T_{11}-M primer and one of eight arbitrary primers provided, 1 U of AmpliTaq DNA polymerase (Perkin-Elmer Corp., Ueberlingen, Germany) and 2 μCi α-[^{33}P]dATP (ICN Biomedicals, Eschwege, Germany) per reaction. PCR was carried out using 40 cycles of 94°C for 30 s, 42°C for 2 min, 72°C for 30 s, followed by a final extension step at 72°C for 5 min. PCR products were resolved on a 6% denaturing polyacrylamide gel in 1× TBE, followed by autoradiography. Reproducibly differentially expressed bands were cut out of the gel and the cDNA was eluted by boiling for 15 min. The gel debris was pelleted by centrifugation and the supernatant was transferred to a fresh microcentrifuge tube. The DNA was precipitated by addition of 100% ethanol, incubation on dry ice for 30 min, and centrifugation at 4°C in an Eppendorf microcentrifuge. The pellet was washed with 85% v/v ethanol, dried, and resuspended in ddH_2O. Reamplification of the purified cDNA was performed using the same primer set and PCR conditions used for the differential display PCR. Reamplified cDNAs were either directly sequenced using the respective arbitrary primer or after cloning into the pCR2.2 vector (Invitrogen BV, Groningen, Netherlands) via the TA cloning method.

Northern blot and PCR

Fifteen micrograms of total RNA were electrophoresed on an 1.2% agarose/0.67% formaldehyde gel. After electrophoresis, RNA was transferred on Hybond N nylon membrane (Amersham Pharmacia Biotech, Freiburg, Germany). PCR fragments of 897 bp (ID3) and 1456 bp gut-enriched Kruppel-like factor (GKLF) were radiolabeled with α-[^{32}P]-dCTP (ICN Biomedicals, Eschwege, Germany) using the Prime-It® II Random Primer Labeling Kit (Stratagene, La Jolla, CA). Membranes were prehybridized in a solution containing 50% formamide, 6× SSC (standard saline citrate), 0.5% SDS, 5× Denhard's solution, and 100 μg/mL salmon testes DNA (Sigma-Aldrich GmbH, Taufkirchen, Germany) for at least 30 min at 42°C. Hybridization was carried out in hybridization solution containing 50% formamide, 6× SSC, 0.5% SDS, 100 μg/mL salmon testes DNA, and the denatured radiolabeled probe in an overnight incubation at 42°C. Membranes were washed twice with 2× SSC and two to four times with 2× SSC/0.1% SDS at 50–65°C, sealed in a plastic bag, and submitted to autoradiography.

For semiquantitative RT-PCR, 2 μg of total RNA from ROS-treated and control cells was reverse transcribed using 100 pmol of p(dN_6)-oligonucleotide-Primer (Roche Molecular Biochemicals) and 200 U of MMLV Reverse Transcriptase (Gibco BRL, Karlsruhe, Germany) in the supplied buffer for reverse transcription and 10 U RNasin (Promega, Heidelberg, Germany). One microliter of each reaction was used for PCR with 50 pmol each of the respective primers for amplification of Id3 (sense: 5′-CGACATGAACCACTGCTACTC-3′, antisense: 5′-GGTCAGTGGCAAAAACTCCTC-3′) or GKLF (sense: 5′-CAACGACCTCCTGGACCTAGA-3′, antisense: 5′-TTCCTCGGGACTCAGTGTAGG-3′) in red *Taq* PCR buffer, dNTP mix and 1.25 U of red *Taq* DNA polymerase (Sigma-Aldrich GmbH). PCR conditions were one 5 min cycle of 95°C, followed by 25 cycles (GAPDH: 23 cycles) of 94°C for 30 s, 57°C (Id3), or 60°C (GAPDH) for 45 s, 72°C for 45 s, and a final extension for 10 min at 72°C. 20–40 μL of each PCR reaction were analyzed on a 1% agarose-TAE gel, visualized by ethidium bromide-staining, and optical densities of the cDNA bands were quantified. The same cDNA samples were used for the amplification of a 452 nt fragment of glyceraldehyde-3-phosphate dehydrogenase (GAPDH) (sense: 5′-ACCACAGTCCATGCCATCAC-3′, antisense: 5′-TCCACCACCCTGTTGCTGTA-3′) to confirm that equal amounts of RNA were reverse transcribed.

Western blot

ROS-treated and control cells were washed twice with ice-cold PBS, scraped in 1 mL of ice-cold lysis buffer (100 mM TRIS pH6.8, 4% SDS, 20% glycerol, 0.1 mM PMSF, 1 μg/mL leupeptin, 1 μg/mL aprotinin), heated to 95°C for 5 min, and stored at −20°C until use. Aliquots (40 μg) of the cellular lysate were electrophoresed through an 0.1% SDS/10% polyacrylamide gel. Proteins were blotted to nitrocellulose membranes in a semidry blotting chamber (Pharmacia Biotech, Uppsala, Sweden). Blot membranes were stained with Ponceau red to verify appropriate protein transfer and equal

loading for each lane. Immunoblotting was performed overnight at 4°C for all antibodies used. Antibody dilutions were p53 (Pab 240 mouse monoclonal IgG, sc-99, Santa Cruz Biotechnology Inc., Santa Cruz, CA) ,1:300; p27 (F-8 mouse monoclonal IgG, sc-1641, Santa Cruz), 1:300; p21 (mouse mixed monoclonal IgG, #05–345, Upstate Biotechnology, Biomol, Hamburg, Germany), 1:600; Rb (M-153 rabbit polyclonal, sc-7905, Santa Cruz), 1:100; Id3 (C-20 rabbit polyclonal, sc-490, Santa Cruz), 1:100. Immunodetection was accomplished using the appropriate secondary antibody for 1 h at room temperature (1:20,000 dilution, Sigma Chemical, Deisenhofen, Germany) and the enhanced chemiluminescence kit (Amersham, Braunschweig, Germany). Autoradiography was performed at room temperature.

Transfection

Full-length cDNAs of Id3 were generated by PCR amplification of reverse transcribed RNA derived from VSMC (see above). Primers were for Id3: sense: 5′-CTCCAACCTCCAACATGAAGG-3′, antisense: 5′-GTTAAAAATGGTTTATTATGCAAAATGTT-3′. PCR products were checked on a 1% TAE agarose gel and cloned into the pCR2.2 vector (Invitrogen BV, Groningen, Netherlands) via TA cloning. Orientation and validity of the insert was determined by automated sequencing, and Id3 sense and antisense constructs for electroporation were generated by cloning *Hin*dIII/*Not*I fragments into the pcDNA3 vector. For electroporation, VSMC grown at a confluent monolayer were removed from the culture dish by addition of trypsin and pelleted. The pellet was resuspended in 200 μL of Optimem 1 (Gibco BRL, Karlsruhe, Germany) and cells were counted. 10^6 cells per sample were incubated with 20 μg of the respective DNA in precooled cuvettes (Promega, Heidelberg, Germany) for 30 min on ice. After warming the cuvette to 37°C for 30 s in a water bath, electroporation was performed for 16 ms at 0.3 kV and 500 μF. After an additional incubation for 30 min at room temperature, cells were plated on the appropriate culture dishes or microtiter plates.

Luciferase assays

Binding of GKLF to putative binding sites within the Id3 promotor was investigated using a promotor-reporter construct with the luciferase gene driven by the Id3 promotor (luciferase assay system, Promega GmbH, Mannheim Germany). VSMC were cotransfected with GKLF, pGL2-Id3 (promotor-reporter construct) +pcDNA3, pGL2+pcDNA3, pGL2-Id3+GKLF, and pcDNA3 by electroporation. Afterward cells were plated on 10 cm plates and incubated for 24 h at 37°C until cell density was sufficient for the assessment of luciferase activity. After two washes with PBS, cells were lysed with 900 μL of the provided lysis buffer per plate, scraped, and transferred to a microcentrifuge tube. After vortexing for 10 s, the debris was pelleted by centrifugation for 2 min at 16,000 *g* and the supernatant was transferred to a new tube. For measurement of luciferase activity, an automatic luminometer (MicroLumat plus LB 96 V) was used. 20 μL of cellular lysate were incubated with 100 μL of luciferase-Assay-Reagent by automatic injection, luminescence was measured over a time course of 30 s

Electrophoretic mobility shift assay

Oligonucleotides containing the known binding site for GKLF (5′-$^{G}/_{A}{}^{G}/_{A}GG^{C}/_{T}G^{C}/_{T}$-3′) 5′-ATGCAGGAGAAAGAAGGGCGTAGTATCTACTAG-3′) (K-I) and oligonucleotide derived from the human Id3 promotor region in which a GKLF binding site putatively is localized, KII: 5′-ACTCCCCAGCATGAAGGCGCTGAGCCCGGTGCG-3′, (Id3 promotor sequence 730bp-766bp) were purchased as single-stranded oligonucleotides (MWG Biotech, Ebersberg, Gemany) and annealed. The GKLF oligonucleotide was end-labeled with γ[^{32}P]-ATP.

Nuclear extracts (2 μg) from VSMC were incubated in 10 μL binding buffer (20 mM HEPES, pH7.9 with KOH, 20% v/v glycerol, 100 mM KCl, 0.2 mM EDTA, 0.2 mM PMSF, 1 mM DTT) and 2 μL EMSA buffer (150 mM HEPES, pH7.6 with KOH, 100 mM KCL, 2.5 mM DTT, 2 mg/mL bovine serum albumin, 20 mM $MgCl_2$) containing 0.1 mM $ZnCl_2$ and 1 μg POLY(dA-dT)·POLY(dA-dT) (Amersham Pharmacia Biotech) for 10 min at room temperature before addition of 50 fmol of ^{32}P-end-labeled, double-stranded oligonucleotide specific for binding of GKLF. After incubation for 15 min, proteins were resolved on a nondenaturing 5% polyacrylamide gel. The gel was submitted to autoradiography. In experiments that contained competitor DNA, a 2- to 50-fold molar excess of unlabeled oligonucleotide over the labeled probe was included.

Vascular injury model

Carotid artery injury was performed in adult male C57Bl/6 mice. Using a dissecting microscope (MZ6, Leica, Heerbrugg, Switzerland), bifurcation of the left carotid artery was exposed via a midline incision of the ventral side of the neck. Two ligatures were placed proximally and distally around the external carotid artery. The distal ligature was tied off. After temporary occlusion of the internal and common carotid artery with ligatures, a transverse arteriotomy was performed between the ligatures of the external carotid artery to introduce a curved flexible wire (0.13 mm in diameter). The wire was passed along the common carotid artery in a rotating manner three times. After removal of the wire, the proximal ligature of the external carotid artery was tied off. Normal blood flow was reassured and the skin was closed with single sutures using 6/0 silk. Animals were allowed to recover and carotid arteries were harvested at various times.

Perfusion-fixed carotid arteries were embedded in Tissue Tek O.C.T. embedding medium (Miles Inc., Niles, MI), snap frozen, and stored at −80°C. Samples were sectioned on a Leica cryostat and placed on poly-L-lysine (Sigma) coated slides for immunohistochemical analysis.

Cryosections were assessed for endothelial cell markers (von Willebrand factor, Dako), MC (alpha smooth muscle actin, Sigma), or the Id3 antigen with a indirect immunoenzymatic method. Tissue cryosections were postfixed in 4% formaldehyde for 2 min. Slides were preincubated with 0.5% Igpal and 5% normal goat serum (Sigma) for 30 min each. The primary antibody (Id3 C20, Santa Cruz) was applied for 2–3 h at room temperature or at 4°C overnight, followed by application of the appropriate horseradish peroxidase-conjugated secondary antibody (Sigma) for 30 min. Id3 expression was visualized with a DAB chromogen substrate (Sigma). Sections were rinsed and mounted with Kaiser's glycerin (Merck) for light microscopic analysis (Nikon E600).

RESULTS

ROS-induced growth regulation in VSMC

Cultured rat VSMC were incubated with either xanthin, 100 μM, xanthin oxidase 1.6 10^{-3} U/mL (100

μM X/XO) to induce production of $O_2^{\cdot}$ or H_2O_2, 100 μM, Fe^{3+}NTA, 10 μM (100 μM H_2O_2-Fe) to release OH. After a 24 h incubation, DNA synthesis and cell proliferation were assessed. **Figure 1*A*** shows that X/XO caused a significant increase in DNA synthesis and cell proliferation whereas H_2O_2-Fe exerted a growth-arresting and proliferation-inhibiting effect. X/XO-induced mitogenicity (maximal at 100 μM) and H_2O_2-Fe-caused growth arrest (maximal at 100 μM) were concentration dependent (Fig. 1*B*). In the absence of the Fenton reagent, H_2O_2 revealed no influence on cellular growth. Apoptosis in VSMC at concentrations of 100 μM X/XO or H_2O_2-Fe was excluded (Fig. 1*C*).

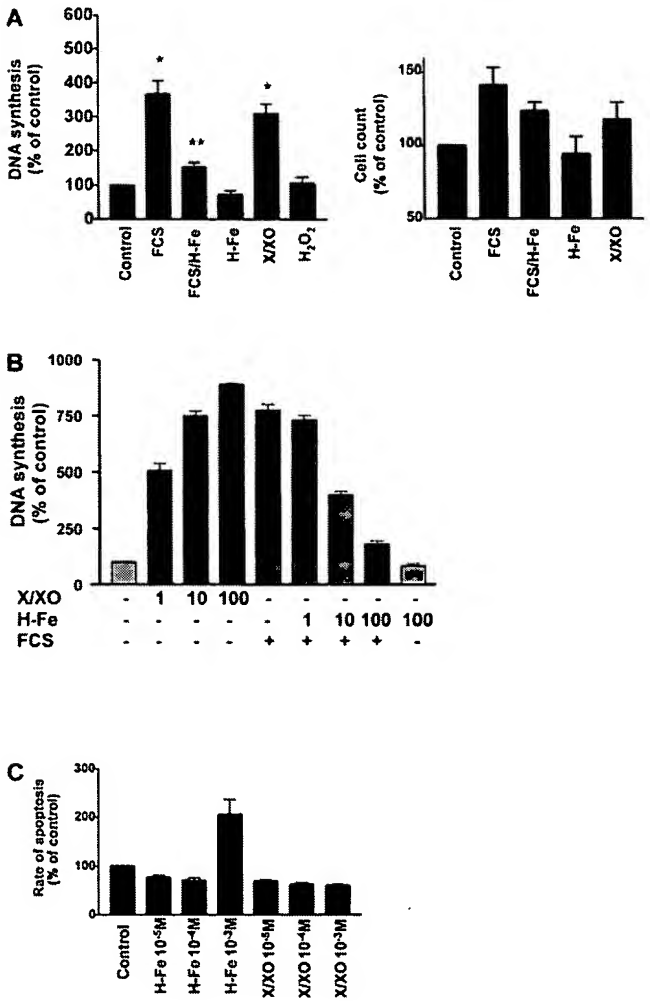

Figure 1. X/XO causes cellular proliferation whereas H_2O_2-Fe induces growth arrest. VSMC were incubated with either vehicle (control), 100 μM X/XO, 100 μM H_2O_2-Fe (H-Fe), 10% FCS, or 100 μM H_2O_2 for 24 h incubation. H-Fe effects were measured in the presence of FCS. DNA synthesis was assessed by BRDU labeling; proliferation was quantified by cell counting (*A*). Concentration dependency of ROS effects on DNA synthesis is shown in VMC after a 24 h incubation (*B*). Apoptosis was detected after a 24 h incubation with 10 μM–1 mM of either X/XO or H-Fe (12) (*C*). n = 3–6. *$P < 0.05$ FCS or X/XO vs. control, **$P < 0.05$ FCS vs. FCS+OH.

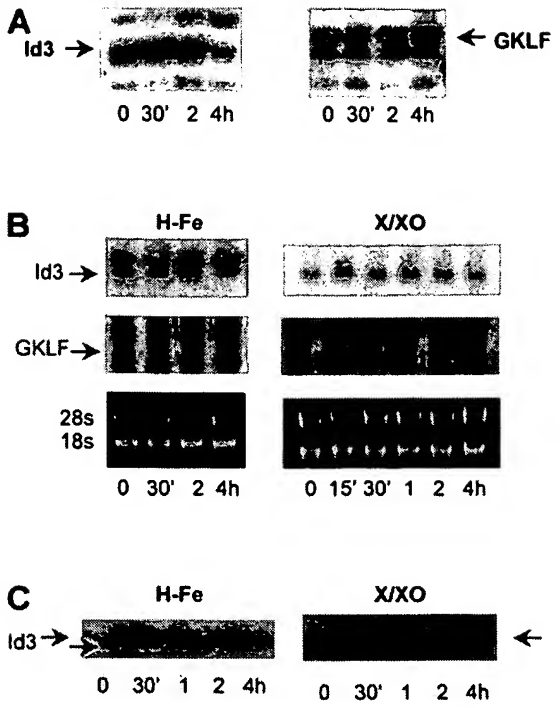

Figure 2. Differential display analysis led to the identification of novel redox-sensitive genes GKLF and Id3. VSMC were incubated with 100 μM X/XO or H_2O_2-Fe (H-Fe) for 0, 0.5, 2, and 4 h. Two differentially regulated genes were reproducibly detected (*A*). Cloning and sequencing revealed 100% homology with GKLF and Id3, respectively. For confirmation of differential display results, VSMC were incubated with either 100 μM X/XO or H-Fe for 0, 0.5, 2, and 4 h. Total RNA was isolated and Northern blotting was performed and hybridized with either radiolabeled Id3 or GKLF cDNA probes (*B*). Western blot analysis of proteins isolated from VSMC incubated with either vehicle (control), 100 μM X/XO, or H-Fe for the indicated times confirmed that Id3 was up-regulated by X/XO and depressed by H-Fe (*C*). Autoradiographs are representative of at least three separate experiments.

Gene expression analysis during oxidative stress

To identify concomitant changes in gene expression patterns, differential display was performed in VSMC incubated with either 100 μM X/XO or H_2O_2-Fe for 0, 0.5, 2, and 4 h. Serial analysis led to identification of two differentially regulated genes (**Fig. 2*A***). Reference methods such as Northern blotting and semiquantitative PCR demonstrated that the transcription factor GKLF was induced by H_2O_2-Fe and not by X/XO. Densitometric analysis of five separate experiments revealed that H_2O_2-Fe increased GKLF mRNA expression after a 2 h incubation to 177 ± 14% of control levels, $P < 0.05$. X/XO had no significant effect on GKLF expression (95±5%, 1 h incubation, n=4, p=ns), The dominant negative helix-loop-helix protein Id3 was induced by X/XO (maximal after 30 min to 170±6%, n=5, P<0.05) and decreased by H_2O_2-Fe (maximal after 4 h to 31±4, n=5, P<0.05) (Fig. 2*B*). Western blot analysis confirmed that Id3 was up-regulated by X/XO and depressed by H_2O_2-Fe (Fig. 2*C*).

Influence of GKLF and Id3 on cell growth

To clarify if GKLF and Id3 mediate redox-sensitive growth processes, VSMC were transfected with sense/antisense GKLF and Id3 cDNAs were inserted in the expression vector pcDNA3. Overexpression or inhibition was confirmed by Western analysis (Id3 sense 204±12% of control, Id3 antisense 31±5% of control) (**Fig. 3*A***). VSMC were stimulated with 10% fetal calf serum (FCS), 100 μM X/XO, 100 μM H_2O_2-Fe, or H_2O_2-Fe and FCS. Control experiments were performed with an insertless vector. Overexpression of sense GKLF and antisense Id3 abrogated growth induction by FCS or X/XO (Fig. 3*B*). Overexpression of antisense GKLF or sense Id3 increased X/XO-induced cell growth and diminished H_2O_2-Fe-caused growth arrest (Fig. 3*B*). These findings demonstrate that induction of GKLF and depression of Id3 are decisively involved in H_2O_2-Fe-induced growth arrest, whereas induction of Id3 governs X/XO-caused VSMC proliferation.

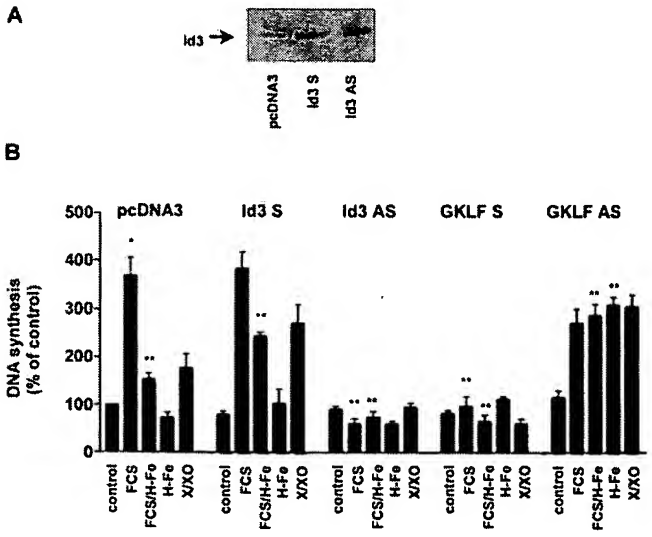

Figure 3. GKLF and Id3 mediate X/XO -and H_2O_2-Fe induced growth regulation. Full-length Id3 and GKLF cDNAs were obtained by PCR. Nucleotide sequence was confirmed by automated sequencing. cDNAs were cloned in sense and antisense orientation in the expression vector pcDNA3. VSMC were transfected by electroporation (16). *A)* Representative Western blot detecting Id3 protein after transfection with Id3 cDNAs and confirming successful overexpression and inhibition of Id3 protein. VSMC were stimulated with vehicle (control), 10% FCS, 100 μM X/XO, or H_2O_2-Fe (H-Fe), or H-Fe and FCS. Control experiments were performed with an insertless vector (pcDNA3) (*B*). n = 3–5. Id3 S/AS = Id3 sense/antisense cDNA. GKLF S/AS = GKLF sense/antisense cDNA. pcDNA3: $*P < 0.05$ FCS or X/XO vs. control, $**P < 0.05$ FCS vs. FCS+H-Fe; Id3 sense (Id3S): $**P < 0.05$ pcDNA3-FCS+H-Fe vs. Id3 S-FCS+H-Fe; Id3 antisense (Id3 AS): $**P < 0.05$ pcDNA3-FCS+H-Fe vs. Id3 AS-FCS+H-Fe, pcDNA3-FCS vs. Id3 AS-FCS; GKLF sense (GKLF S): $**P < 0.05$ pcDNA3-FCS+H-Fe vs. GKLF S-FCS+H-Fe, pcDNA3-FCS vs. GKLF S-FCS; GKLF antisense (GKLF AS): $**P < 0.05$ pcDNA3-FCS+H-Fe vs. GKLF AS-FCS+H-Fe, pcDNA3-$OH^{\cdot}$ vs. GKLF AS-H-Fe.

Effect of ROS, GKLF, and Id3 on $p21^{WAF1/Cip1}$, $p27^{KIP1}$, p53, and Rb

Cyclin-dependent kinase inhibitors are essential modulators of cellular proliferation (11–13). Therefore, VSMC were incubated for the indicated periods with X/XO or H_2O_2-Fe and protein expression of $p21^{WAF1/Cip1}$, $p27^{KIP1}$, and p53 was assessed by Western blotting. X/XO down-regulated expression of $p21^{WAF1/Cip1}$ (23±7% of control level, n=3, P<0.05, 24 h incubation) and p53 (31±7% of control level, n=3, P<0.05, 24 h incubation), whereas H_2O_2-Fe led to the up-regulation of $p21^{WAF1/Cip1}$ (421±123% of control level, n=3, P<0.05, 12 h incubation) and p53 (264±71% of control level, n=3, P<0.05, 24 h incubation). $p27^{Kip1}$ expression was depressed by X/XO (75±9% of control level, n=3, P<0.05, 24 h incubation) and enhanced by H_2O_2-Fe (291±81% of control level, n=3, P<0.05, 24 h incubation). Hyperphosphorylation of the retinoblastoma gene product Rb is closely involved in the execution of mitogenic signals. Rb hyperphosphorylation was propagated by X/XO, whereas FCS-induced Rb hyperphosphorylation was diminished by H_2O_2-Fe (**Fig. 4*A***). Consistently, overexpression of sense GKLF and antisense Id3 caused an enhanced expression of $p21^{WAF1/Cip1}$, $p27^{Kip1}$, and p53 and hypophosphorylation of Rb (Fig. 4*B*), suggesting that the cyclin-kinase inhibitors $p21^{WAF1/Cip1}$ and $p27^{Kip1}$, the tumor suppressor gene p53, and hypophosphorylation of Rb are induced by H_2O_2-Fe via induction of GKLF and depression of Id3. In contrast, overexpression of sense Id3 and antisense GKLF induces hyperphosphorylation of Rb. Therefore, GKLF as well as Id3 act upstream of these established growth-regulating genes.

Interaction of GKLF and Id3

GKLF is up-regulated by $OH^{\cdot}$ within 30 min; Id3 is down-regulated after 2–4 h. The Id3 promotor contains GKLF binding sites. To test whether GKLF regulation is a prerequisite of Id3 modulation, we incubated nuclear proteins isolated from VSMC, which were stimulated with 100 μM H_2O_2-Fe for 0–4 h with radioactively labeled oligonucleotides representing the GKLF binding site. **Figure 5*A*** (left panel) shows the autoradiography of a gel shift experiment revealing that GKLF binding to its consensus sequence is profoundly induced by H_2O_2-Fe. Figure 5*A* (right panel) shows that unlabeled oligonucleotides derived from regions of the Id3 promotor that contain a putative GKLF binding site inhibit the protein–DNA interaction demonstrating the specificity of the reaction. Therefore, GKLF binds to the Id3 promotor and this binding is increased by stimulation with H_2O_2-Fe. To clarify the functional relevance, VSMC were cotransfected with expression vectors harboring either the GKLF cDNA or/and a luciferase reporter gene fused to the Id3 promotor. Figure 5*B* summarizes the data of four separate experiments. Transcription of the luciferase reporter gene is low without inserted promotor (pGL2). Activity is

greatly enhanced on fusion to the Id3 promotor (Id3-pGL2). Cotransfection with GKLF as well as stimulation of cells with 100 μM H_2O_2-Fe for 2 h reduces significantly the luciferase activity, demonstrating that GKLF represses Id3 promotor activity and thereby Id3 gene transcription rate.

Second messengers involved in GKLF and Id3 induction

Cells were incubated with 100 μM H_2O_2-Fe or 100 μM X/XO for 30 min with or without the following pharmacological inhibitors: 20 μmol/L PD98059 (p42/44 MAP kinase inhibitor), 1 μmol/L SB203580 (p38 MAP kinase inhibitor), 10 μmol/L genistein (tyrosin kinase inhibitor), 10 μmol/L wortmannin (PI-3 kinase inhibitor), 10 μmol/L N_ω-nitro-L-arginin (nitric oxide inhibitor), 20 μmol/L Bis-(2-amino-5-methylphenoxy)ethane-N, N, N', N'-tetraacetic acid tetraacetoxymethyl ester (MAPTAM, calcium chelator), 20 mmol/L mannitol (hydroxyl scavenger), 10 μg/mL cycloheximide (protein synthesis inhibitor), 200 U/mL PEG-catalase (CAT, H_2O_2 scavenger), and 100 U/mL PEG-superoxide dismutase (SOD, O_2^- scavenger), followed by RNA isolation and GKLF mRNA quantification by Northern blotting and PCR. The data show that GKLF induction by H_2O_2-Fe is dependent on OH^- release, intracellular calcium, p38 MAP kinase, and protein synthesis (**Fig. 6A**), whereas Id3 induction by X/XO is dependent on superoxide release, p38, as well as p42/44 MAP kinase and intracellular calcium.

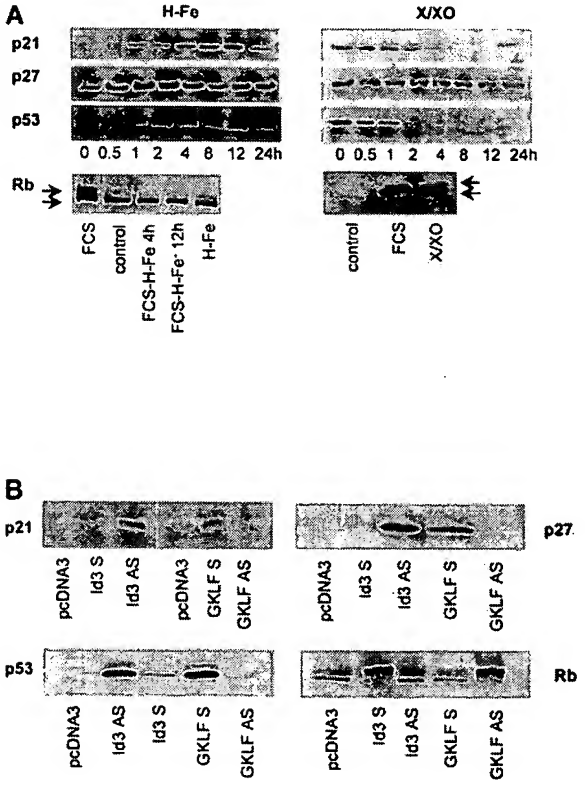

Figure 4. $p21^{WAF1/Cip1}$, p27, and p53 are depressed by X/XO and induced by H_2O_2-Fe. VSMC were incubated for the indicated periods with 100 μM X/XO or 100 μM H_2O_2-Fe (H-Fe), cellular proteins were isolated, and expression of $p21^{WAF1/Cip1}$, p27, and p53 and Rb was assessed by Western blotting. For Rb detection, cells were stimulated with 10% FCS as indicated. *A)* The effects of X/XO and OH. Overexpression of sense GKLF and antisense Id3 was achieved by electroporation-guided transfection. Protein expression of $p21^{WAF1/Cip1}$, p27, and p53 was assessed by Western blotting 48 h after transfection (*B*). Autoradiographs are representative of at least 3 separate experiments. Id3 S/AS = Id3 sense/antisense cDNA. GKLF S/AS = GKLF sense/antisense cDNA.

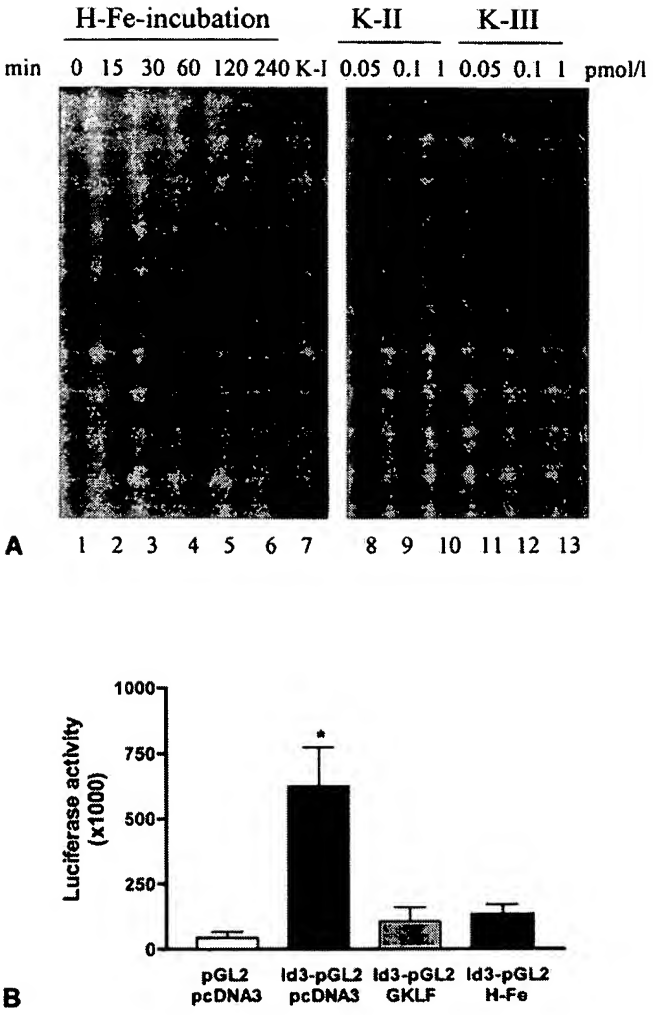

Figure 5. *A)* GKLF binding to its consensus sequence is time-dependently enhanced. Electrophoretic mobility shift assay with nuclear proteins from VSMC stimulated with 100 μmol/L H_2O_2-Fe (H-Fe) for 0–240 min bound to the GKLF-consensus oligonucleotide (lanes 1–6). Binding was competed with unlabeled GKLF oligonucleotide (K-I, lane 7) and increasing concentrations of K-II that represent a putative binding site of the Id3 promotor (bp 730–766) and a unspecific competitor K-III (Nf_{kappaB}-motif). *B)* GKLF reduces ID3 promotor activity. VSMC were transfected with a luciferase-harboring promotorless construct (pGL2) or a luciferase-harboring-ID3 promotor construct (Id3-pGL2) in the presence of an insertless expression vector (pcDNA3, bar 2) or a pcDNA3-GKLF cDNA construct (bar 3). Some cells were stimulated with 100 μmol/L H_2O_2-Fe (H-Fe) (bar 4). Promotor activity was assessed by luciferase assays. $^*P < 0.05$ pGL2 vs. ID3-pGL2.

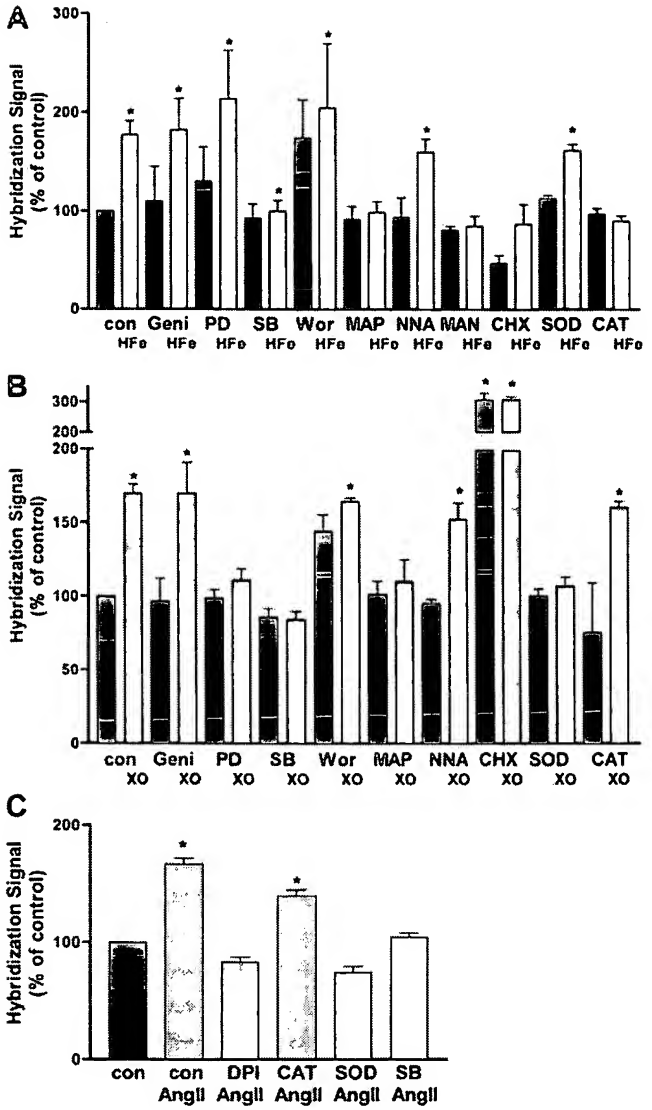

Figure 6. *A)* Second messengers. Cells were incubated with 100 μM H_2O_2-Fe (H-Fe) for 30 min with or without 20 μmol/L PD98059 (PD), 1 μmol/L SB203580 (SB), 10 μmol/L genistein (Geni), 10 μmol/L wortmannin (Wor), 10 μmol/L N_ω-nitro-L-arginin (NNLA), 20 μmol/L Bis-(2-amino-5-methylphenoxy)-ethane-N,N,N′,N′-tetraacetic acid tetraacetoxymethyl ester (MAPTAM), 20 mmol/L mannitol (Man), 10 μg/mL cycloheximide (CHX), 200 U/mL PEG-catalase (CAT), and 100 U/mL PEG-superoxide dismutase (SOD), followed by RNA isolation and GKLF mRNA quantification by Northern blotting and PCR. Densitometric analysis of 3–5 separate experiments. *B)* Cells were incubated with 100 μM xanthin/xanthin oxidase (X/XO) for 30 min with or without 20 μmol/L PD98059 (PD), 1 μmol/L SB203580 (SB), 10 μmol/L genistein (Geni), 10 μmol/L wortmannin (Wor), 10 μmol/L N_ω-nitro-L-arginin (NNLA), 20 μmol/L Bis-(2-amino-5-methylphenoxy)ethane-N,N,N′,N′-tetraacetic acid tetraacetoxymethyl ester (MAPTAM), 10 μg/mL cycloheximide (CHX), 200 U/mL PEG catalase (CAT), and 100 U/mL PEG-superoxide dismutase (SOD), followed by RNA isolation and Id3 mRNA quantification by Northern blotting and PCR. Densitometric analysis of 3–5 separate experiments. *C)* Effect of angiotensin II on Id3. VSMC were stimulated with 100 nmol/L angiotensin II for 2 h. Id3 mRNA was quantified by Northern analysis. Some cells were coincubated with 10 μmol/L of diphenylene iodonium (DPI), 1 μmol/L SB203580 (SB), 200 U/mL PEG-catalase (CAT), and 100 U/mL PEG-superoxide dismutase (SOD).

Effect of angiotensin II on Id3 and GKLF

Angiotensin II is known to release intracellular $O_2^{\cdot}$ and hydrogen peroxide upon activation of AT1 receptors. To test whether intracellular release of $O_2^{\cdot}$ and hydrogen peroxide could influence Id3 expression, cells were stimulated with 100 nmol/L angiotensin II for 0–2 h. Id3 mRNA was quantified by Northern analysis. Figure 6*B* demonstrates that angiotensin II up-regulates Id3 expression within 1 h. This was completely inhibited in the presence of 10 μmol/L of the flavoprotein inhibitor diphenylene iodonium, which omits intracellular free radical release by angiotensin II. Superoxide dismutase, which specifically scavenges $O_2^{\cdot}$ but not catalase, a hydrogen peroxide scavenger, inhibited the effect of angiotensin II. GKLF expression was not influenced by angiotensin II (data not shown). Thus, angiotensin II, which acts as a VSMC mitogen via a membrane-bound receptor, modulates Id3 gene expression via intracellular superoxide release.

In vivo model

To extend our in vitro findings, we induced a vascular injury in arteria carotis of mice resulting in lesions characterized by neointima formation due to VSMC proliferation. The vessels were harvested and immunohistochemistry was performed in lesion segments. **Figure 7** shows visualization of Id3 protein and VSMC-specific alpha-smooth muscle actin protein. Id3 is predominately expressed in VSMC of the media and the neointima but in the endothelium. Of note, Id3 expression is profoundly enhanced in the neointima that contains proliferating VSMC in comparison to media composed of mainly quiescent VSMC.

DISCUSSION

ROS such as superoxide and hydroxyl radicals are generated in early as well as advanced atherosclerosis and have been strongly implicated in the pathogenesis of this disease (4). Despite numerous experimental studies and interventional trials, the definitive molecular actions of ROS are poorly defined. Proliferation, growth arrest, and apoptosis are key events in atherogenesis and are observed in endothelial cells, macrophages, and VSMC within the vessel wall (11). ROS act as extra- and intracellular signaling molecules involved in cellular growth, apoptosis, and survival (9, 10, 12, 13). Similar to growth factors and hormones, ROS interfere with various transduction pathways such as calcium, protein kinases, MAP kinase, and proto-oncogenes (3, 14–18). The response elicited by ROS intermediaries is in part determined by the intracellular targets and is dependent on the species of oxidants produced (6, 9, 18, 19).

Our data indicate that xanthin/xanthin oxidase and hydrogen peroxide/Fe exert differential effects on growth of VSMC. Concomitant application of specific

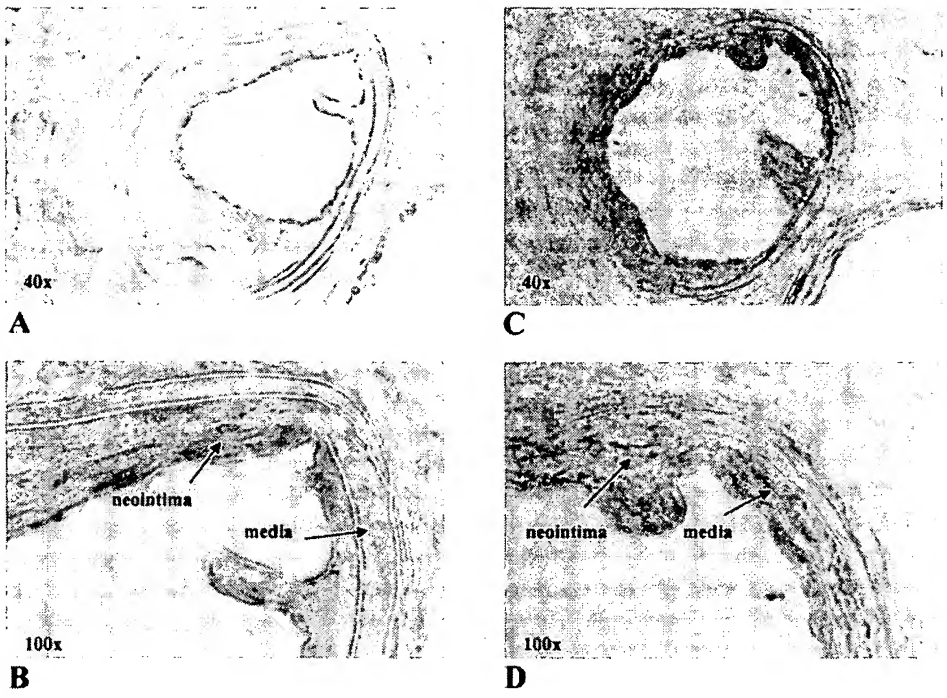

Figure 7. Vascular injury in arteria carotis of mice resulting in lesions characterized by neointima formation due to VSMC proliferation. Vessels were harvested and immunohistochemistry was performed in lesion segments. Visualization of Id3 protein (*A, C*) and VSMC-specific alpha-smooth muscle actin protein (*B, D*).

radical scavengers such as mannitol, catalase and superoxide dismutase suggest that the effects of xanthin/xanthin oxidase are mediated through release of superoxide, whereas hydroxyl radicals seem to transfer the effects of hydrogen peroxide/Fe. It is concluded based on these observations that superoxide induces VSMC proliferation and that hydroxyl radicals cause growth arrest in the absence of detectable apoptosis. It is well established that superoxide induces second messenger pathways typical of mitogens, such as the mitogen-activated kinase family (14–18). However, the cascade of participating genes is less defined.

According to the data presented, induction of Id3 is a prerequisite of superoxide-caused proliferation. Inhibition of Id3 by transfection of antisense constructs inhibits superoxide and serum-induced growth. Moreover, superoxide-associated mitogenesis is enhanced by transfection of sense Id3 cDNA. The Id proteins 1–4 antagonize the function of DNA binding basic helix-loop-helix transcription factors such as E2A. The latter defines cellular differentiation and increased proliferation (20). Id3 has been implicated in the apoptosis of fibroblasts (21). However, the redox-sensitive properties of Id3 and its decisive role in regulation of VSMC growth have not been elucidated. Id3 expression is increased via receptor-mediated processes as exemplified with angiotensin II. This peptide propagates intracellular radical release and causes proliferation of VSMC (22, 23). The fact that angiotensin II causes Id3 overexpression via radical release supports the concept of Id3-triggered growth events in VSMC. The second gene identified via differential display analysis, GKLF, acts in an opposite manner. GKLF expression is not altered by superoxide. Nevertheless, selective induction of GKLF abrogates completely superoxide- and serum-induced proliferation, whereas inhibition of GKLF enhances the mitogenic effects of superoxide.

GKLF has been shown to be expressed in epithelial cells of the gastrointestinal tract, skin, thymus, and endothelial cells (24–28). GKLF functions as transcription factor that interacts with a GC-rich consensus site residing in the promotor of various genes such as cytochrome P450IA1 and $p21^{WAF1/Cip1}$ (29, 30). In fibroblasts, induction of GKLF is associated with growth arrest potentially through interaction with p53 and $p21^{WAF1/Cip1}$ (30).

The data demonstrate a differential impact of superoxide and hydroxyl radicals on VSMC growth and connect these effects to the novel redox-sensitive target genes, GKLF and Id3. GKLF expression is increased by hydroxyl radicals. Functional data reveal that the hydroxyl-caused growth arrest is mediated by the induction of GKLF. Transfection of GKLF antisense vectors completely abolishes the growth-arresting potential of hydroxyl radicals.

GKLF or inhibition of Id3 diminishes serum-elicited proliferation, suggesting that serum-associated mitogenesis is mediated by ROS or that GKLF and Id3 are generally involved in growth regulation pathways in VSMC.

It is not known by which signal transduction cascades GKLF and Id3 are activated or inhibited. The data reported here indicate that ROS play a pivotal role in the expression regulation of these genes. However, it cannot be excluded that other signaling pathways may also be involved. Our data suggest that hydroxyl radicals induce GKLF via the p38 subunit of MAP, which is a principal intracellular target of reactive oxygen species (14–18). Furthermore, intracellular calcium seems to participate in the hydroxyl-induced GKLF regulation. This agrees with previous reports of calcium-

releasing properties of free radicals (31). Despite the rapid regulation of GKLF within 30 min, the process is protein synthesis dependent, suggesting that additional, so far unknown transcribed/translated factors mediate the hydroxyl effect on GKLF.

The time course of events of GKLF and Id3 regulation and the fact that the Id3 promotor contains putative GKLF binding sites led us to the hypothesis that GKLF my interact with the Id3 promotor and thereby influence Id3 gene transcription. According to the results presented, GKLF binds to its consensus sequence in the Id3 promotor. The cotransfection reporter assays clearly show that GKLF reduces Id3 promotor activity revealing a so far unknown interaction.

GKLF as well as Id3 have been associated with cell cycle factors such as p53 and $p21^{WAF1/Cip1}$ (22). Our results show that superoxide, Id3, and inhibition of GKLF down-regulate the expression of p53 and $p21^{WAF1/Cip1}$ and, to a lesser extent, the expression of $p27^{Kip1}$. In contrast, hydroxyl radicals, GKLF overexpression, and inhibition of Id3 induce p53, $p21^{WAF1/Cip1}$, and $p27^{Kip1}$. Consequently, hyperphosphorylation of Rb, which is a well-established measure for cell cycle progress, is either propagated or abolished. Therefore, GKLF and Id3 interfere effectively with cell cycle-associated factors. This partly clarifies the intracellular targets of GKLF and Id3 with respect to their growth-regulating properties.

Pathological growth of vascular smooth muscle cells occurs especially during atherosclerotic disease and restenosis after angioplasty (32). To validate in vitro findings and at least speculate about a transfer of the cell culture results to atherosclerosis in humans, it is essential to prove the concept in an in vivo setting. Therefore, we applied a carotid injury model in mice. The induced lesion, the neointima, is predominately composed of proliferating vascular smooth muscle cells. The histological analysis showed that Id3 is expressed in vascular smooth muscle cells in vivo. Id3 expression is enhanced in neointimal, proliferating cells. These data may serve as a first proof of the concept. Of course, these data do not ultimately prove a causal relationship between Id3 overexpression and neointima formation, which would have to be tested in an in vivo gene transfer experiment.

GKLF and Id3 are of central relevance for ROS-induced growth regulation in VSMC via interaction with cyclin-dependent kinase inhibitors, p53, and Rb. It is speculated that these findings reveal general mechanisms of growth control that could lead to new therapeutic strategies for the treatment of atherosclerosis, coronary restenosis, and cancer. FJ

This work was supported by the Deutsche Forschungsgemeinschaft.

REFERENCES

1. Babior, B. M. (2000) Phagocytes and oxidative stress. *Am. J. Med.* **109,** 33–44
2. Berk, B. C. (1999) Redox signals that regulate the vascular response to injury. *Thromb. Haemost.* **82,** 810–817
3. Greene, E. L., Velarde, V., and Jaffa, A. A. (2000) Role of reactive oxygen species in bradykinin-induced mitogen-activated protein kinase and c-fos induction in vascular cells. *Hypertension* **35,** 942–947
4. Dreher, D., and Junod, A. F. (1995) Differential effects of superoxide, hydrogen peroxide, and hydroxyl radical on intracellular calcium in human endothelial cells. *J. Cell. Physiol.* **162,** 147–153
5. Irani, K. (2000) Oxidant signaling in vascular cell growth, death, and survival : a review of the roles of reactive oxygen species in smooth muscle and endothelial cell mitogenic and apoptotic signaling. *Circ. Res.* **87,** 179–183
6. Griendling, K. K., and Harrison, D. G. (1999) Dual role of reactive oxygen species in vascular growth. *Circ. Res.* **85,** 562–563
7. Hensley, K., Robinson, K. A., Gabbita, S. P., Salsman, S., and Floyd, R. A. (2000) Reactive oxygen species, cell signaling, and cell injury. *Free Radic. Biol. Med.* **28,** 1456–1462
8. Kamata, H., and Hirata, H. (1999) Redox regulation of cellular signalling. *Cell Signal* **11,** 1–14
9. Kanoh, S., Kondo, M., Tamaoki, J., Kobayashi, H., Motoyoshi, K., and Nagai, A. (2000) Effects of reactive oxygen species on intracellular calcium in bovine tracheal epithelium: modulation by nitric oxide. *Exp. Lung Res.* **26,** 335–348
10. Kojda, G., and Harrison, D. (1999) Interactions between NO and reactive oxygen species: pathophysiological importance in atherosclerosis, hypertension, diabetes and heart failure. *Cardiovasc. Res.* **43,** 562–571
11. Kunsch, C., and Medford, R. M. (1999) Oxidative stress as a regulator of gene expression in the vasculature. *Circ. Res.* **85,** 753–766
12. Li, P. F., Dietz, R., and von Harsdorf, R. (1997) Differential effect of hydrogen peroxide and superoxide anion on apoptosis and proliferation of vascular smooth muscle cells. *Circulation* **96,** 3602–3609
13. Li, P. F., Dietz, R., and von Harsdorf, R. (1997) Reactive oxygen species induce apoptosis of vascular smooth muscle cell. *FEBS Lett.* **404,** 249–252
14. Li, P. F., Maasch, C., Haller, H., Dietz, R., and von Harsdorf, R. (1999) Requirement for protein kinase C in reactive oxygen species-induced apoptosis of vascular smooth muscle cells. *Circulation* **100,** 967–973
15. Loveys, D. A., Streiff, M. B., and Kato, G. J. (1996) E2A basic-helix-loop-helix transcription factors are negatively regulated by serum growth factors and by the Id3 protein. *Nucleic Acids Res.* **24,** 2813–2820
16. Morel, Y., and Barouki, R. (1999) Repression of gene expression by oxidative stress. *Biochem. J.* **342,** 481–496
17. Norton, J. D., and Atherton, G. T. (1998) Coupling of cell growth control and apoptosis functions of Id proteins. *Mol. Cell. Biol.* **18,** 2371–2381
18. Okano, J., Opitz, O. G., Nakagawa, H., Jenkins, T. D., Friedman, S. L., and Rustgi, A. K. (2000) The Kruppel-like transcriptional factors Zf9 and GKLF coactivate the human keratin 4 promoter and physically interact. *FEBS Lett.* **473,** 95–100
19. Panigada, M., Porcellini, S., Sutti, F., Doneda, L., Pozzoli, O., Consalez, G. G., Guttinger, M., and Grassi, F. (1999) GKLF in thymus epithelium as a developmentally regulated element of thymocyte-stroma cross-talk. *Mech. Dev.* **81,** 103–113
20. Patel, R. P., Moellering, D., Murphy-Ullrich, J., Jo, H., Beckman, J. S., and Darley-Usmar, V. M. (2000) Cell signaling by reactive nitrogen and oxygen species in atherosclerosis. *Free Radic. Biol. Med.* **28,** 1780–1794
21. Rao, G. N., and Berk, B. C. (1992) Active oxygen species stimulate vascular smooth muscle cell growth and proto-oncogene expression. *Circ. Res.* **70,** 593–599
22. Timmermans, P. B., Wong, P. C., Chiu, A. T., Herblin, W. F., Benfield, P., Carini, D. J., Lee, R. J., Wexler, R. R., Saye, J. A., and Smith, R. D. (1993) Angiotensin II receptors and angiotensin II receptor antagonists. *Pharmacol. Rev.* **45,** 205–251
23. Griendling, K. K., Minieri, C. A., Ollerenshaw, J. D., and Alexander, R. W. (1994) Angiotensin II stimulates NADH and NADPH oxidase activity in cultured vascular smooth muscle cells. *Circ. Res.* **74,** 1141–1148
24. Kawakami, M., and Okabe, E. (1998) Superoxide anion radical-triggered Ca^{2+} release from cardiac sarcoplasmic reticulum

through ryanodine receptor Ca^{2+} channel. *Mol. Pharmacol.* **53,** 497–503
25. Ross, R. (1999) Atherosclerosis—an inflammatory disease. *N. Engl. J. Med.* **340,** 115–126
26. Segre, J. A., Bauer, C., and Fuchs, E. (1999) Klf4 is a transcription factor required for establishing the barrier function of the skin. *Nat. Genet.* **22,** 356–360
27. Tanner, F. C., Boehm, M., Akyurek, L. M., San, H., Yang, Z. Y., Tashiro, J., Nabel, G. J., and Nabel, E. G. (2000) Differential effects of the cyclin-dependent kinase inhibitors p27(Kip1), p21(Cip1), and p16(Ink4) on vascular smooth muscle cell proliferation. *Circulation* **101,** 2022–2025
28. Ton-That, H., Kaestner, K. H., Shields, J. M., Mahatanankoon, C. S., and Yang, V. W. (1997) Expression of the gut-enriched Kruppel-like factor gene during development and intestinal tumorigenesis. *FEBS Lett.* **419,** 239–243
29. Yet, S. F., McA'Nulty, M. M., Folta, S. C., Yen, H. W., Yoshizumi, M., Hsieh, C. M., Layne, M. D., Chin, M. T., Wang, H., Perrella, M. A., Jain, M. K., and Lee, M. E. (1998) Human EZF, a Kruppel-like zinc finger protein, is expressed in vascular endothelial cells and contains transcriptional activation and repression domains. *J. Biol. Chem.* **273,** 1026–1031
30. Zafari, A. M., Ushio-Fukai, M., Akers, M., Yin, Q., Shah, A., Harrison, D. G., Taylor, W. R., and Griendling, K. K. (1998) Role of NADH/NADPH oxidase-derived H2O2 in angiotensin II-induced vascular hypertrophy. *Hypertension* **32,** 488–495
31. Zhang, W., Shields, J. M., Sogawa, K., Fujii-Kuriyama, Y., and Yang, V. W. (1998) The gut-enriched Kruppel-like factor suppresses the activity of the CYP1A1 promoter in an Sp1-dependent fashion. *J. Biol. Chem.* **273,** 17917–17925
32. Zhang, W., Geiman, D. E., Shields, J. M., Dang, D. T., Mahatan, C. S., Kaestner, K. H., Biggs, J. R., Kraft, A. S., and Yang, V. W. (2000) The gut-enriched Kruppel-like factor (Kruppel-like factor 4) mediates the transactivating effect of p53 on the p21WAF1/Cip1 promoter. *J. Biol. Chem.* **275,** 18391–18398

Received for publication October 25, 2001.
Revised for publication February 18, 2002.

34. S. L. Buchwald and S. M. King, *ibid.* 113, 258 (1991).
35. S. L. Buchwald, E. A. Lucas, J. C. Dewan, *ibid.* 109, 4396 (1987).
36. This value was calculated from standard heats of hydrogenation of an alkyne and the values calculated by L. Radom [*Pure Appl. Chem.* 58, 75 (1986)].
37. D. P. Hsu, E. A. Lucas, S. L. Buchwald, *Tetrahedron Lett.* 31, 5563 (1990).
38. S. L. Buchwald and R. B. Nielsen, *J. Am. Chem. Soc.* 110, 3171 (1988).
39. S. L. Buchwald, B. T. Watson, M. W. Wannamaker, J. C. Dewan, *ibid.* 111, 4486 (1989).
40. M. Jensen and T. Livinghouse, *ibid.*, p. 4495.
41. N. Coles, R. J. Whitby, J. Blagg, *Synlett.*, 271 (1990).
42. ———, *ibid.*, 143 (1992).
43. R. Halterman, *Chem. Rev.* 92, 965 (1992).
44. R. B. Grossman, W. M. Davis, S. L. Buchwald, *J. Am. Chem. Soc.* 113, 2321 (1991).
45. F. R. W. P. Wild, M. Wasiucionek, G. Huttner, H. H. Brintzinger, *J. Organomet. Chem.* 288, 63 (1985).
46. A. Schafer, E. Karl, L. Zsolnai, G. Huttner, H. H. Britziriger, *ibid.* 328, 87 (1987).
47. This method is based on the method described by Brintzinger for the analogous Ti compounds [F. R. W. P. Wild, L. Zsolnai, G. Hettner, H. H. Brintzinger, *ibid.* 232, 233 (1982)].
48. R. Noyori, *Science* 248, 1194 (1990).
49. W. A. Nugent, T. V. RajanBabu, M. J. Burk, *ibid.* 259, 479 (1993).
50. R. F. Jordan and D. F. Taylor, *J. Am. Chem. Soc.* 111, 778 (1989).
51. V. M. Dzhemilev *et al.*, *Izv. Akad. Nauk Kaz. SSR Ser. Khim.* 38, 207 (1989).
52. K. S. Knight and R. M. Waymouth, *J. Am. Chem. Soc.* 113, 6268 (1991).
53. U. Wischmeyer, K. S. Knight, R. M. Waymouth, *Tetrahedron Lett.* 33, 7735 (1992).
54. A. H. Hoveyda, J. P. Morken, A. F. Houri, Z. Xu, *J. Am. Chem. Soc.* 114, 6692 (1992).
55. T. Takahashi *et al.*, *ibid.* 113, 6266 (1991).
56. D. P. Lewis, P. M. Muller, R. J. Whitby, R. V. H. Jones, *Tetrahedron Lett.* 32, 6797 (1991).
57. S. C. Berk, R. B. Grossman, S. L. Buchwald, *J. Am. Chem. Soc.* 115, 4912 (1993).
58. Supported at MIT by the National Institutes of Health (GM 34917), the Petroleum Research Fund (administered by the American Chemical Society), National Cancer Institute training grant #CA 09112 (R.D.B.), and the Office of Naval Research; S.L.B. was supported as an Alfred P. Sloan Fellow and a Camille & Henry Dreyfus Teacher-Scholar. We thank our many co-workers whose efforts provide a partial basis for this article, whose names appear in the references; and J. Stubbe, R. Grossman, J. Tidwell, and B. Warner for useful comments on the manuscript.

RESEARCH ARTICLE

Crystal Structure of a Five-Finger GLI-DNA Complex: New Perspectives on Zinc Fingers

Nikola P. Pavletich* and Carl O. Pabo

Zinc finger proteins, of the type first discovered in transcription factor IIIA (TFIIIA), are one of the largest and most important families of DNA-binding proteins. The crystal structure of a complex containing the five Zn fingers from the human *GLI* oncogene and a high-affinity DNA binding site has been determined at 2.6 Å resolution. Finger one does not contact the DNA. Fingers two through five bind in the major groove and wrap around the DNA, but lack the simple, strictly periodic arrangement observed in the Zif268 complex. Fingers four and five of GLI make extensive base contacts in a conserved nine base-pair region, and this section of the DNA has a conformation intermediate between B-DNA and A-DNA. Analyzing the GLI complex and comparing it with Zif268 offers new perspectives on Zn finger-DNA recognition.

Zinc fingers, of the type found in TFIIIA (*1*), are one of the most common DNA-binding motifs in eukaryotic transcription factors. This family of zinc finger proteins is characterized by the consensus sequence X_3-Cys-X_{2-4}-Cys-X_{12}-His-X_{3-5}-His-X_4 (where X is any amino acid residue); more than a thousand such zinc finger sequences have been reported (*2*). The zinc finger forms a compact globular structure that contains a β sheet and an α helix held together by a central Zn ion (*3*). The two cysteines, which are in the β sheet region, and the two histidines, which are in the α helical region, are tetrahedrally coordinated to the Zn. Crystallographic studies of a complex containing the three Zn fingers from the Zif268 protein (*4*) revealed that the Zif fingers bind in the major groove and wrap partway around the double helix. Residues from the NH_2-terminal portion of each α helix contact the bases, and a conserved pattern of side chain-base interactions is observed in the Zif complex.

Although only a small number of the known Zn finger proteins have been characterized in detail, it is clear that this family of proteins can recognize a diverse set of DNA sequences. For example, the *Drosophila* Hunchback protein recognizes a site that includes the sequence AAAAA (*5*); the human Sp1 protein recognizes a site that includes the sequence GGGGGC (*6*); and the human glioblastoma (GLI) protein recognizes a site that includes the sequence TGGGTGGTC (*7*). Preliminary attempts to model other Zn finger complexes suggested that Zif might provide a reliable basis for modeling complexes formed by closely related proteins [such as Sp1 and WT1 (*8*)], but it did not appear that Zif would provide a satisfactory basis for modeling complexes formed by other, more distantly related Zn finger proteins.

To help understand how Zn fingers can recognize such a diverse set of binding sites, we have studied a complex that contains the five Zn fingers from the human *GLI* oncogene. The *GLI* gene was first discovered because it was amplified in human glioblastomas (*9*), and GLI was later found to be amplified in other tumors (*10*). In vitro studies have shown that the GLI protein, in conjunction with the adenovirus E1A protein, can transform primary rodent cells (*11*). GLI is a sequence-specific DNA-binding protein, and three high-affinity sites have been recovered from a pool of human genomic DNA (*7*). Our crystals contain the five Zn fingers of the human GLI protein (Fig. 1A) bound to a 21–base pair (bp) DNA fragment (Fig. 1B) that includes a high affinity DNA-binding site. We now describe the crystal structure of the GLI complex at 2.6 Å resolution, compare it with Zif, and consider the broader implications for our understanding of Zn finger–DNA interactions.

Overall structure of the GLI complex. The overall structure of the GLI-DNA complex shows that fingers 2 to 5 fit in the major groove and wrap around the DNA for a full helical turn (Fig. 2 and Table 1). Finger 1 surprisingly does not contact the DNA but instead makes extensive protein-protein contacts with finger 2. The overall arrangement of the other fingers is generally similar to that observed for the fingers in the Zif complex. The α helix of each finger fits into the major groove, and the NH_2-terminal portion of each of these α helices

The authors are in the Howard Hughes Medical Institute and Department of Biology, Massachusetts Institute of Technology, Cambridge, MA 02139.

*Present address: Memorial Sloan-Kettering Cancer Center, Cellular Biochemistry and Biophysics Program, 1275 York Avenue, New York, NY 10021.

is closest to the bases. Fingers 4 and 5 of GLI appear to be the most important for recognition. These fingers make extensive base contacts in a 9-bp region that is conserved in all of the known binding sites (7). Fingers 2 and 3 make a set of contacts with the DNA backbone, but a comparison of the high-affinity GLI binding sites (7) shows that the DNA sequence of this region can vary, and the only base contact in this region is a single hydrogen bond contributed by finger 2.

The DNA is most readily described by dividing it into three regions that have distinct conformations. The conserved region, recognized by fingers 4 and 5, has a structure that is intermediate between that expected for B-DNA and that expected for A-DNA. This region is underwound (relative to B-DNA), and has a deep major groove. The second region involves the

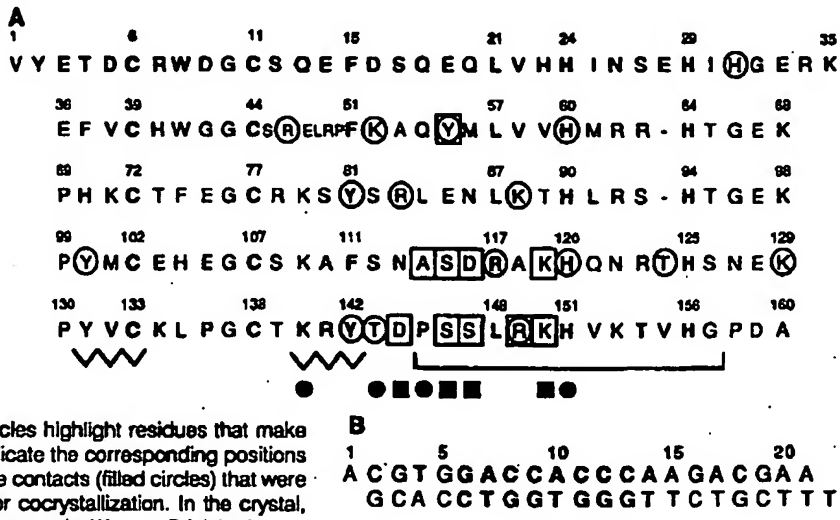

Fig. 1. Sequences of the GLI zinc finger domain and the DNA-binding site used for cocrystallization. (**A**) The peptide contains 160 residues [corresponding to amino acids 232 to 391 of the GLI protein (9)], and the current model includes residues 3 to 157 of this peptide. (The terminal residues are disordered in the crystal.) The GLI peptide (A) was cloned, expressed in *Escherichia coli*, and purified as described for Zif (4). The cloned gene was sequenced, and the identity of the purified peptide was confirmed by high-resolution mass spectroscopy (27). The five zinc fingers of GLI are aligned to show the conserved residues and secondary structures. The approximate position of the α helix is underlined, and that of the β sheet is indicated by zig-zag lines. In finger 2, the sheet region is perturbed by a three-residue insertion, and the second strand of the β sheet contains residues 49 to 51. Open boxes highlight residues that make base contacts in the crystal structure, and open circles highlight residues that make phosphate contacts. Symbols below the GLI sequence indicate the corresponding positions of side chain–base (filled boxes) and side chain–phosphate contacts (filled circles) that were observed in the Zif complex (4). (**B**) DNA duplex used for cocrystallization. In the crystal, these molecules stack head-to-tail, and the overhanging bases make Watson-Crick hydrogen bonds. Bold letters highlight the 9 base pairs that are conserved in the three high-affinity GLI binding sites (7). Binding studies were performed with the purified GLI peptide and a 45-bp DNA fragment that contained the site shown above. This complex has a dissociation constant of approximately 20 nM (in the presence of 200 mM NaCl and nonspecific DNA at 25 μg/ml. Abbreviations for the amino acid residues are: A, Ala; C, Cys; D, Asp; E, Glu; F, Phe; G, Gly; H, His; I, Ile; K, Lys; L, Leu; M, Met; N, Asn; P, Pro; Q, Gln; R, Arg; S, Ser; T, Thr; V, Val; W, Trp; and Y, Tyr.

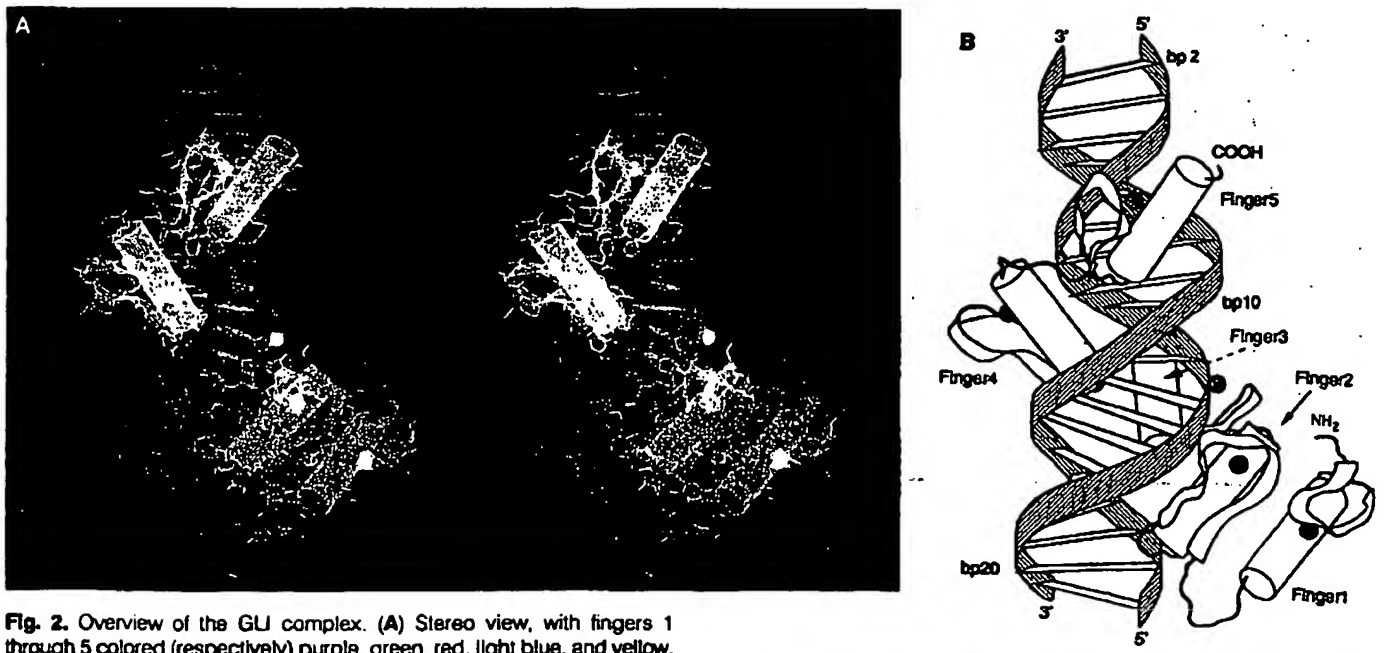

Fig. 2. Overview of the GLI complex. (**A**) Stereo view, with fingers 1 through 5 colored (respectively) purple, green, red, light blue, and yellow. The DNA is a darker blue. Cylinders and ribbons highlight the α helices and β sheets, and the cobalt ions are shown as light blue spheres. Note that finger 3 (in red) is directly behind the DNA in this view. (**B**) Sketch of the complex in a similar orientation. Samples were prepared for crystallization, by the addition of $CoCl_2$ to the purified peptide (2.0 molar equivalents of Co^{2+} per finger), adjusting the pH to 7.0 with 125 mM bis-tris-propane-HCl (BTP-HCl), and adding 1.2 molar equivalents of the DNA fragment (Fig. 1B) in 100 mM BTP-HCl pH 7.0. Crystals were grown in an anaerobic chamber by the hanging drop vapor diffusion method. The best crystals were obtained when hanging drops were prepared by mixing a solution of the complex (containing 0.5 mM protein and 0.6 mM DNA) with an equivalent volume of well buffer containing 60 to 100 mM $MgCl_2$, 20 to 25 percent PEG 400, and 50 mM BTP-HCl (pH 7.0). Crystals grew in 2 to 3 weeks. They form in space group $P2_12_12_1$, with a = 148.4 Å, b = 50.2 Å, and c = 45.4 Å; they have one complex in the asymmetric unit (28)].

subsites where fingers 2 and 3 bind, and here the structure is more characteristic of standard B-DNA. Finally, there is a region just beyond finger 5 where the DNA is overwound, with a narrow helical radius and a shallow major groove. The transition to this overwound region occurs just at the edge of the conserved recognition sequence, and thus is next to the bases that finger 5 contacts.

Protein-DNA interactions. Fingers 4 and 5 of GLI make most of the base contacts, and each of these fingers recognizes approximately half of a 9-bp conserved region (Fig. 1B). As observed with the Zif fingers, fingers 4 and 5 of GLI use residues from the NH_2-terminal portion of their α helices to contact the bases. Finger 4 has four residues—Ala^{114}, Ser^{115}, Asp^{116}, and Lys^{119}—that make base contacts (Figs. 3A and 4). These residues correspond to the first, second, third, and sixth residues of the α helix, and they make contacts over a 5-bp region of the GLI binding site. (Detailed contacts are listed in the legend to Fig. 4.) Finger 5 has five residues—Asp^{144}, Ser^{146}, Ser^{147}, Arg^{149}, and Lys^{150}—that make base contacts (Figs. 3A and 4). These residues correspond to the residue immediately preceding the α helix and to the second, third, fifth, and sixth residues of this helix. The contacts made by finger 5 are spread over a 4-bp region of the GLI binding site (Fig. 4). When the finger sequences are aligned (Fig. 1A), there is a clear correlation between the position of the GLI residues that make base contacts and the position of Zif residues that make base contacts. However, there are differences in the precise way that each finger docks against the DNA (Fig. 5), and there are corresponding differences in the detailed pattern of interactions between side chains and bases interactions (Fig. 6). Although these complexes are related (Fig. 5), the arrangements of the GLI fingers are different enough that these base contacts could not readily have been predicted from a knowledge of the Zif contacts.

Fingers 4 and 5 also make a number of contacts with the phosphodiester oxygens. Hydrogen bonds are made by the side chains of Tyr^{100}, Arg^{117}, His^{120}, and Thr^{124} in finger 4; by Lys^{129}, which is in the linker between fingers 4 and 5; and by the side chains of Tyr^{142} and Arg^{149} in finger 5 (Fig. 4). Finger 5 also makes one backbone-to-backbone contact. The peptide-NH of Thr^{143} hydrogen bonds to a phosphodiester oxygen. Comparison of the positions of these residues in the GLI sequence with the positions of Zif residues that make phosphate contacts (Fig. 1A) reveals only a weak correlation. Knowledge of the Zif contacts certainly would not have allowed us to predict the GLI contacts.

The docking arrangements for fingers 2 and 3 of GLI are generally similar to those observed with other fingers (Fig. 5), but these fingers only make a single base contact; Tyr^{55}, which is the second residue in the α helix of finger 2, accepts a hydrogen bond from the N4 of the cytosine at base pair 19 (Fig. 4). Fingers 2 and 3 make a number of contacts with the phosphodiester oxygens. Hydrogen bonds are made by the side chains of Arg^{46}, Lys^{52}, and His^{60} in finger 2, and by the side chains of Tyr^{81}, Arg^{83}, and Lys^{88} in finger 3. The peptide -NH of Tyr^{55} also contacts a phosphodiester oxygen. (The side chain of this residue makes the only base contact in this region.) An additional contact is provided by the side chain of His^{31}, which is in the linker region between fingers 1 and 2. Again, if we align fingers 2 and 3 of GLI with the Zif fingers, we find only a modest correlation in the positions of residues that make backbone contacts. Although the overall docking arrangements are similar in these two complexes, the fingers make significantly different contacts with the DNA backbone.

When considering the GLI complex, it is important to recognize that the binding site used in our study was obtained by in vitro selection from genomic DNA (7), and some caution must be exercised because the biologically relevant binding site is unknown. These concerns are relevant to fingers 1, 2, and 3 because the dearth of base contacts in this region raises the possibility that these fingers may represent a type of "nonspecific complex". We cannot

Table 1. Data collection and structure determination. Data were collected with a RAXIS-IIC area detector. At room temperature, the crystals deteriorated after x-ray exposure for 1 to 2 hours. Diffraction data were collected at −175°C to minimize radiation damage. Crystals were prepared for freezing by transferring them to a solution containing 15 percent isopropanol, 28 percent PEG 400, 50 mM $MgCl_2$, 50 mM BTP-HCl (pH 7.0), and 16 μM $CoCl_2$. Crystals were then placed in a thin wire loop and frozen in a stream of nitrogen at minus 175°C. Derivatives were prepared by substituting 5-iodouracil for thymine at bp 15, at bp 20, and at bp 21 (giving derivatives IdU^{15}, IdU^{20}, and IdU^{21}). Not all of the frozen crystals were isomorphous, and it was necessary to collect several native and several derivative data sets before we could solve the structure. Heavy-atom parameters for the three derivatives were refined (with the program REFINE from the CCP4 package) (*29*), and multiple isomorphous replacement (MIR) phases were calculated to 3.0 Å resolution with the program PHARE. Initial phases were improved by solvent flattening (*30*), and a model containing the DNA and fingers 2 through 4 was built into the MIR map by means of the program FRODO (*31*). This partial model was refined by simulated annealing with the program X-PLOR (*32*), and fingers 1 and were located in $2|F_o| - |F_c|$ maps. After several cycles of refinement with the full model, X-PLOR omit maps were used to systematically check and rebuild every part of the complex. About 2 to 5 percent of the structure was deleted in each calculation, and simulated annealing was used to reduce model bias in the omit maps. The only region of the complex that consistently had poor electron density was the linker connecting fingers 1 and 2 (residues 32 to 35), and we presume that this region is disordered in the crystal. The TNT package (*33*) was used in the final stages of refinement. To correct for anisotropic diffraction and for absorption problems during data collection, a local scaling program was used (*34*); this program scales the observed and calculated structure factor amplitudes. After several additional cycles of refinement, 44 water molecules were gradually added and individual (correlated) temperature factors were included.

	Native 2	Native 1	IdU^{15}	IdU^{20}	IdU^{21}
Resolution (Å)	2.6	2.9	3.0	2.9	3.0
Measured reflections	28039	18499	17690	13389	7517
Unique reflections	10856	6738	5879	6811	4451
Data coverage (%)	97.9	88.3	85.2	89.3	64.5
R_{sym}*	6.72	9.35	8.16	5.90	8.70
MIR analysis (Native 1)					
Resolution limits (Å)			20.0–3.0	20.0–3.0	20.0–3.5
Mean isomorphous difference			0.15	0.14	0.12
Phasing power			1.60	1.48	1.26
Cullis *R* factor			0.74	0.73	0.89
Refinement: (Native 2)					
Resolution limits	7.0–2.6				
R factor	0.228				
Reflections with $F > 2\sigma$	9187				
Total number of atoms	2130				
Water molecules	44				
Rms in B values (Å²)	2.50†				
Rms in bond lengths (Å)	0.015‡				
Rms in bond angles (deg.)	3.07‡				

*$R_{sym} = \Sigma_h\Sigma_i|I_{h,i} - I_h| / \Sigma_h\Sigma_i I_{h,i}$, where I_h is the mean intensity of the i observations of reflection h. Mean isomorphous difference = $\Sigma\,||F_{PH} - F_P|| / \Sigma\,F_{PH}$, where F_{PH} and F_P are the derivative and native structure factor amplitudes, respectively. Phasing power = $[(F_{H(calc)})^2/\langle(F_{PH(obs)} - F_{PH(calc)})^2\rangle]^{1/2}$. Cullis *R* factor = $\Sigma\,||F_{obs} \pm F_{calc}|| - F_{H(calc)}| / \Sigma|F_{obs} - F_{calc}|$ for centric reflections, where $F_{H(calc)}$ is the calculated heavy atom structure factor. *R* factor = $\Sigma\,||F_{obs}| - |F_{calc}|| / \Sigma F_{obs}$. †The rms in B values is the rms deviation in temperature factors between bonded atoms. ‡Rms in bond lengths and bond angles is the rms deviation of bond lengths and bond angles from ideal values.

exclude the possibility that these fingers might bind in a different way or might make additional contacts at some other binding site. Such concerns appear to be less relevant in regard to fingers 4 and 5, since these fingers clearly bind in a sequence-specific manner and since the sequence of this region was the same in each of the high-affinity sites that was isolated.

DNA structure. Examination of the DNA revealed three regions with distinct conformations, and structural parameters were calculated with a separate helical axis for each of these segments. The region containing base pairs 15 to 21, which corresponds to the nonconserved portion of the GLI binding site, has structural parameters characteristic of standard B-DNA. This section of the DNA (region III in Table 2) has an average helical twist of 34.7°, which corresponds to 10.4 bp per turn. There are small displacements of the bases from the helical axis, but the major groove is only slightly deeper than in canonical B-DNA.

Region II, which consists of base pairs 7 to 15 and thus is essentially coincident with the 9-bp consensus sequence, has a structure that is intermediate between that expected for B-DNA and that expected for A-DNA. This section of the DNA has an average helical twist of 30.7° (11.7 residues per turn) and a rise of 3.08 Å per base pair. Region II has an unusually deep major groove (the base pairs are displaced by about 3 Å) and a rather wide minor groove. The base pairs have a significant inclination (about 9°), and the backbone δ angles show a 50/50 mixture of values expected for B-DNA and values expected for A-DNA (*12*, *13*). It is interesting that this region contains the conserved part of the GLI binding site and includes almost all of the base contacts.

Region I, which consists of base pairs 2 to 7, has several features that are characteristic of C-DNA. This region is overwound, with an average helical twist of 37.5° (corresponding to 9.6 bp per turn). This section of the DNA also has a shallow major groove (the helical axis passes through the minor groove) and an unusually small helical radius. Although region I is not the primary binding site for any of the fingers, the transition between Regions I and II occurs near one end of the consensus sequence and seems to affect the position of a few bases that are contacted by finger 5.

Finger structure. As expected, the structures of the GLI fingers are very similar to those observed in other TFIIIA-like zinc fingers: Each finger contains a β sheet and an α helix that are held together by a central Zn ion. Superimposing fingers also shows that their tertiary structures are very similar. For example, residues 70 to 95 from finger 3 of GLI can be superimposed on finger 1 of Zif with a root-mean-square deviation of 0.79 Å for the Cα coordinates (*14*).

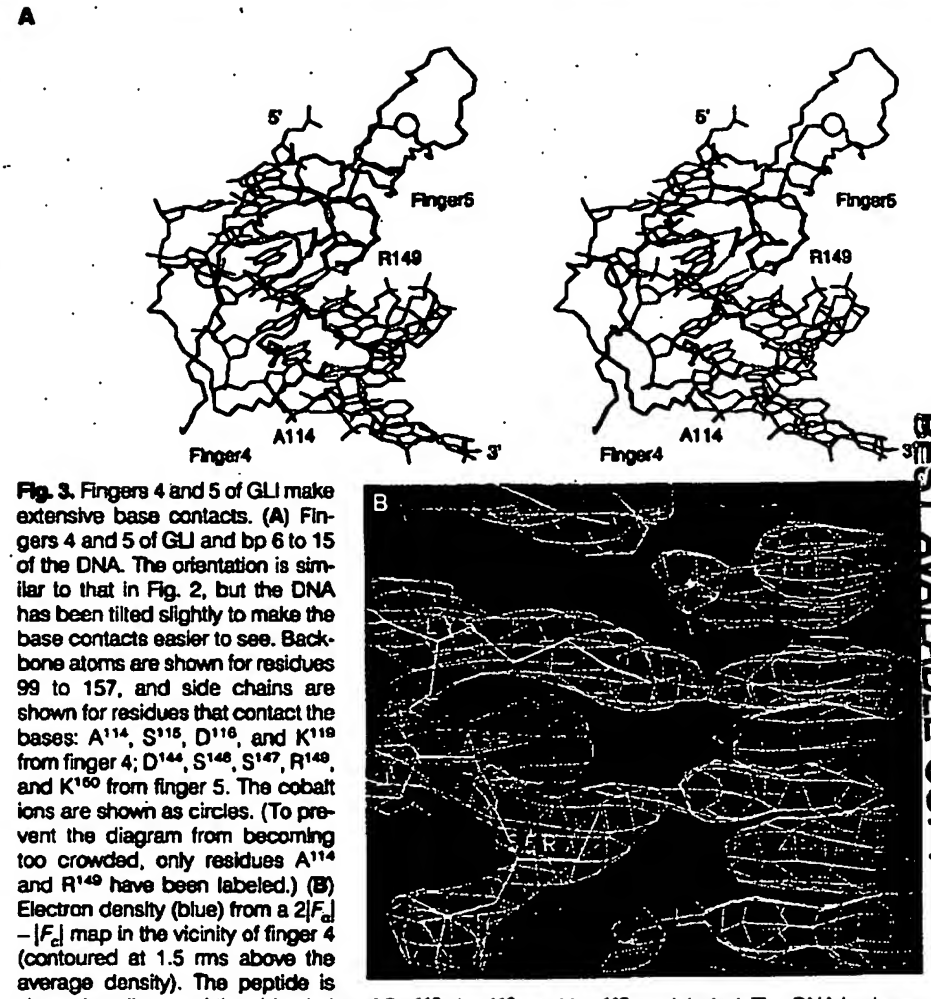

Fig. 3. Fingers 4 and 5 of GLI make extensive base contacts. (**A**) Fingers 4 and 5 of GLI and bp 6 to 15 of the DNA. The orientation is similar to that in Fig. 2, but the DNA has been tilted slightly to make the base contacts easier to see. Backbone atoms are shown for residues 99 to 157, and side chains are shown for residues that contact the bases: A^{114}, S^{115}, D^{116}, and K^{119} from finger 4; D^{144}, S^{146}, S^{147}, R^{149}, and K^{150} from finger 5. The cobalt ions are shown as circles. (To prevent the diagram from becoming too crowded, only residues A^{114} and R^{149} have been labeled.) (**B**) Electron density (blue) from a $2|F_o| - |F_c|$ map in the vicinity of finger 4 (contoured at 1.5 rms above the average density). The peptide is shown in yellow, and the side chains of Ser^{115}, Asp^{116}, and Lys^{119} are labeled. The DNA is shown in red. (The cytosine that is contacted by Asp^{116} is just beyond the block of density that is displayed in this figure.)

Some of the fingers in GLI have a His-X_3-His spacing in the α helical region while others have a His-X_4-His spacing. Thus fingers 2 and 3 of GLI have three residues between the histidines, and their α helices are similar to the Zif helices. Fingers 1, 4, and 5 of GLI have four residues between the conserved histidines. In these fingers, the regular α helix typically ends one residue before the second histidine, and the backbone continues with a wider turn. However, the second histidine is still constrained by the zinc ion, and the additional residue does not change the overall arrangement of the polypeptide chain as it comes out of the helical region. It is possible that structural differences in this COOH-terminal portion of the α helix affect the arrangement of the subsequent linker and finger (*15*) but the differences are complex enough that it is not possible to describe the His-X_3-His to His-X_4-His change in terms of a simple structural switch.

Finger 1, which does not contact the DNA, makes extensive protein-protein interactions with finger 2. Surprisingly, these fingers are related by a local twofold rotation axis, and they have a pair of hydrogen bonds connecting their polypeptide backbones. (The CO of residue 7 and the -NH of residue 9 are involved in hydrogen bonds with the -NH of residue 40 and the CO of residue 42.) These backbone hydrogen bonds flank tryptophans (Trp^8 and Trp^{41}) that make critical hydrophobic contacts at the interface of the two fingers. Many other residues contribute hydrophobic contacts or hydrogen bonds that stabilize this interaction (*16*).

There only are a few contacts between the other fingers, and these contacts are similar to ones seen in Zif (*17*). The conformations of the linker regions between these other fingers are generally similar to those seen in Zif. However, there are differences in the precise arrangements, and these modest differences may help to deter-

Fig. 4 (right). Sketch summarizing base and phosphate contacts made by the GLI peptide. The DNA is represented as a cylindrical projection that has been "unwrapped" to provide a continuous view of the major groove over a region containing about 1.5 helical turns. Solid arrows indicate base contacts and dotted arrows indicate phosphate contacts. (The contacted bases and phosphates are shaded for clarity.) Base contacts made by fingers 4 and 5 are as follows: Ala 114 makes van der Waals contact (3.5 Å) with the methyl group of the T; Ser^{115} donates a hydrogen bond to the O6 of the G while the C_β of this residue makes van der Waals contact (3.1 Å) with the methyl group of the T; Asp^{116} accepts a hydrogen bond from the N4 of the C; Lys^{119} hydrogen bonds to the O6 of the G at bp 12. (The amino group of Lys^{119} also comes within 3.4 Å of the O6 of the G at bp 13.) Asp^{144} accepts a hydrogen bond from the N4 of each C; Ser^{146} hydrogen bonds to the O6 of the G; Ser^{147} hydrogen bonds to the N7 of the A; Arg^{149} donates hydrogen bonds to (i) the N7 of the G, (ii) the hydroxyl of Ser^{146}, and (iii) a phosphodiester oxygen from the T at bp 10; Lys^{150} hydrogen bonds to the N7 and O6 positions of the G.

mine the precise spacing and orientation of the neighboring fingers.

Perspectives on Zn finger–DNA recognition. The crystal structure of the Zif268 complex gave an initial view of Zn finger–DNA interactions, but with only one structure available it was impossible to determine which features were peculiar to Zif (and its closest relatives) and which features were characteristic of Zn fingers in general. Comparing the Zif and GLI structures provides a broader perspective on many of the fundamental questions about Zn finger–DNA interactions.

The overall arrangement of fingers 2 through 5 in GLI is similar to the arrangement in Zif. The fingers bind in the major groove with the NH_2-terminal portion of their α helices closest to the bases, and successive fingers wrap around the double helix (Figs. 2 and 5). The Zif and GLI complexes also have related patterns of side chain–base interactions (Fig. 6). Specifically: (i) There are four bases in each subsite that are contacted most frequently. (ii) There are four positions on the α helix that usually provide the critical contacts. (iii) There is a clear correlation between the position of a residue on the α helix and the position (within the finger's subsite) of the base that it contacts. (The correlation of residue positions and base positions is most striking for Zif, but more than half of the GLI contacts involve alignment of analogous residues and bases.) However, there also are differences in the precise docking arrangements, such as: (i) The subsites for fingers 4 and 5 of GLI are somewhat farther apart than any of the Zif subsites. (ii) A majority of the Zif contacts involve one

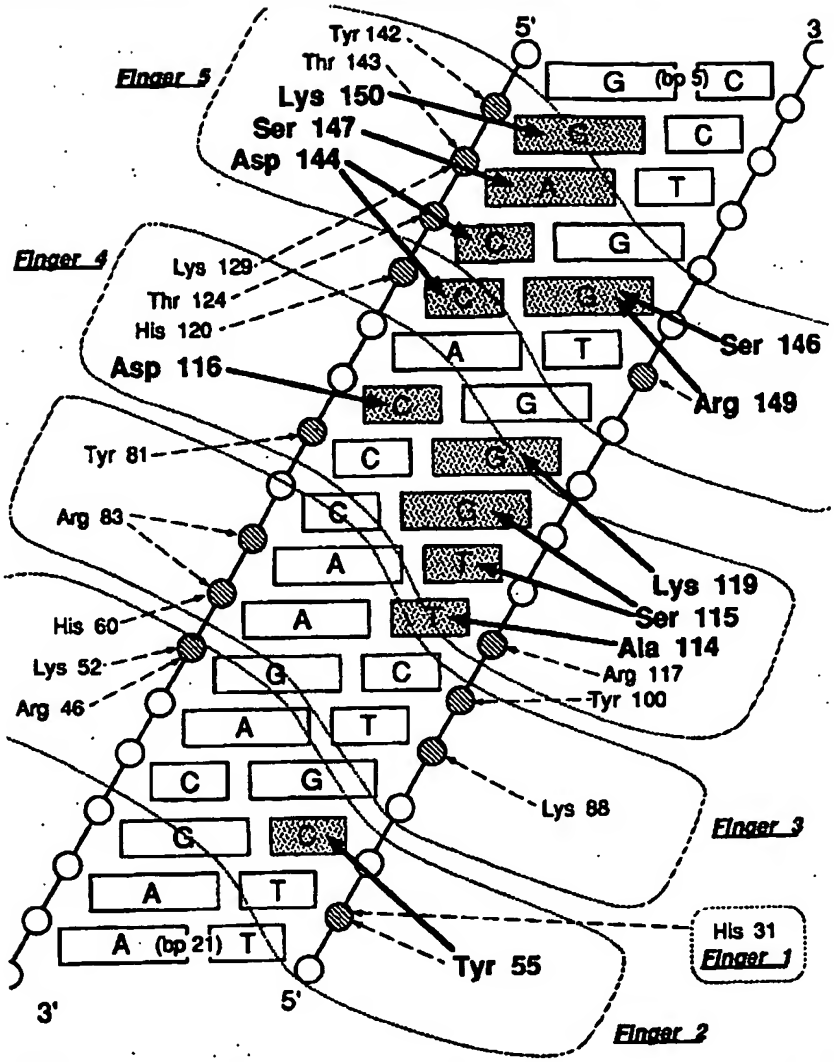

Fig. 5 (above). Comparison of docking arrangements in the GLI and Zif complexes. The complexes have been dissected to show the individual fingers and their subsites, and these "mini-complexes" have been aligned by superimposing the P atoms of the DNA backbone. Residues in the second β strand and residues in the α helix of each finger are shown as Cα traces. The three Zif fingers are purple; the GLI fingers are green (finger 2), red (finger 3), light blue (finger 4), and yellow (finger 5). The DNA subsites are blue, and the complexes are viewed looking down the DNA axes. The DNA subsites used in making these GLI mini-complexes have a simple 3-bp periodicity, and thus the subsites are centered on base pairs 7 to 9 (finger 5), 10 to 12 (finger 4), 13 to 15 (finger 3), and 16 to 18 (finger 2). All of the fingers have basically similar docking arrangements, but differences can involve translations as large as 5 Å and rotations as large as 25°, and these clearly are critical for recognition. (The Zif fingers are most similar to each other; docking arrangements in GLI are more variable.)

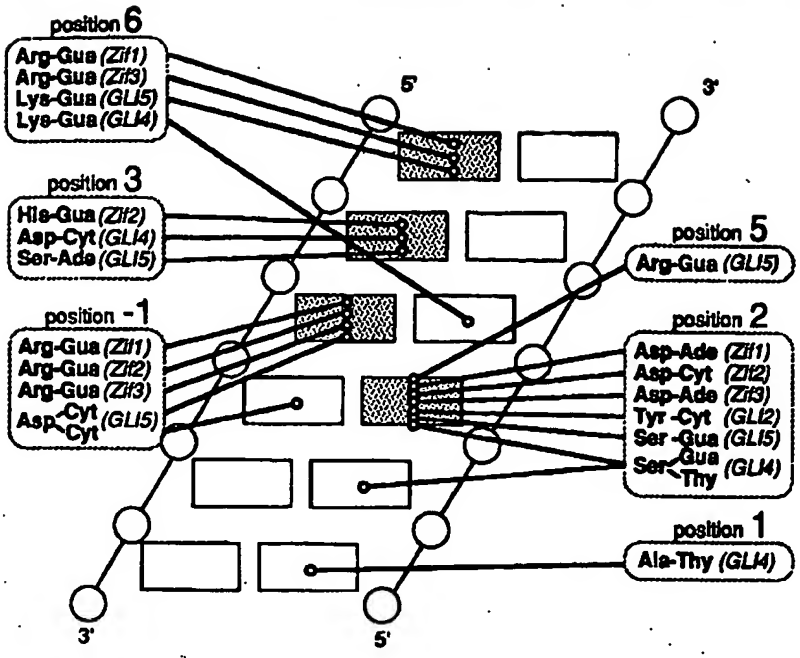

Fig. 6. Comparison of base contacts in the GLI and Zif complexes. Mapping base contacts with the subsites for individual fingers reveals similar patterns relating the position of a residue in the α helix and the position of the base that it contacts. The subsites used in Fig. 5 are used for the Zif fingers and for fingers 2, 3, and 4 of GLI. Finger 5 of GLI is aligned with the use of the side chain–base contacts to provide a frame of reference, and this gives a subsite centered on bp 6 to 8. (In this alignment, the subsites for fingers 4 and 5 are separated by an additional base pair.) Residue positions are numbered with respect to the start of the α helix (where −1 denotes the residue immediately preceding the helix). Rectangles represent the bases in a canonical subsite (viewing the major groove as in Fig. 4), and the three bases corresponding to the primary strand of the Zif subsites (*4*) have been highlighted to facilitate comparisons. This chart includes three hydrogen bonds—one made by each of the Asp residues at position 2 in the Zif helices—that were not emphasized in our original discussion of the Zif complex (*4*). Although their hydrogen bonding geometry is not ideal (*36*), these residues may contribute to specificity and are included here for completeness.

strand of the DNA, but the GLI contacts are more evenly distributed between the two strands. (iii) GLI makes a number of interactions between side chains and bases that were not seen with Zif. Comparing Zif and GLI makes it appear quite unlikely that there will be any simple, general "code" describing Zn finger–DNA interactions.

Comparison of the Zif and GLI complexes also reveals distinctive features of the DNA conformation. Although our original description of the Zif DNA (*4*) focused on features that were similar to those expected for B-DNA, further analysis shows that the Zif DNA is underwound and has a deeper major groove than would be expected for canonical B-DNA (*13, 18*). These features are much more pronounced in certain regions of the GLI complex. The conserved region recognized by fingers 4 and 5 of GLI has a DNA conformation that is intermediate between A-DNA and B-DNA, and this observation is consistent with reports indicating that the binding sites for other Zn fingers may have some features characteristic of A-DNA (*19*).

In the Zif complex, each of the fingers makes generally similar contributions to DNA-binding, but the GLI complex shows that different fingers can have very different roles in recognition. Some fingers will make base contacts; some will make phosphate contacts; others will not contact the DNA at all. Recent chemical and biochemical studies of TFIIIA (*20*) have emphasized the distinct roles played by different sets of fingers, and the GLI complex provides a new perspective for thinking about such polyfinger complexes. The critical roles that fingers 4 and 5 play in the GLI complex may have a parallel in TFIIIA, where it has been shown that a peptide containing fingers 1 through 3 binds almost as tightly as the intact nine-finger protein (*21*). It should not be surprising that adequate specificity can be provided by a few critical fingers and that different fingers can have very different roles in a polydactyl complex.

The differences between Zif and GLI also suggest that it is necessary to keep track of relationships within families and subfamilies when modeling other Zn finger-DNA

Table 2. DNA conformational parameters calculated with the program NEWHELIX (*35*). Twist and rise were calculated with the use of the C1′ atoms; slide, inclination, tip, and X dsp (X displacement) were calculated from the C_6 (pyrimidines) or C_8 (purines) atoms. The twist, rise, and slide values are measured with reference to the base pair shown in the next line of the table.

Base pairs	Twist (deg)	Rise (Å)	Slide (Å)	Inclination (deg)	Tip (deg)	X Dsp (Å)
			Region I			
2 C·G	45.18	3.26	2.17	−0.60	0.08	3.76
3 G·C	32.26	3.42	1.23	−0.25	3.24	3.08
4 T·A	46.89	2.89	1.98	−3.40	1.12	2.79
5 G·C	27.45	4.04	1.07	−4.06	−0.37	2.31
6 G·C	35.92	3.82	0.78	−4.67	7.62	3.03
7 A·T				−1.20	9.19	2.13
Mean	37.54	3.48	1.45	−2.37	3.48	2.85
			Region II			
7 A·T	35.59	3.10	−0.05	4.68	3.71	−2.49
8 C·G	26.87	3.06	−1.07	11.51	3.45	−1.91
9 C·G	38.34	3.11	−0.36	9.61	2.41	−2.62
10 A·T	31.22	3.43	−1.17	8.96	−3.38	−3.32
11 C·G	25.53	2.77	−2.40	5.98	3.23	−3.14
12 C·G	28.43	3.29	−0.57	1.63	4.12	−3.65
13 C·G	33.16	2.87	−1.14	11.67	14.13	−2.78
14 A·T	26.30	3.03	−1.09	13.48	12.72	−3.72
15 A·T				14.74	10.14	−4.06
Mean	30.68	3.08	−0.98	9.14	5.62	−3.08
			Region III			
15 A·T	40.33	2.50	−0.41	11.00	7.96	−0.63
16 G·C	35.02	3.51	−0.16	9.06	1.15	−0.77
17 A·T	22.46	3.82	0.01	5.65	1.38	−0.86
18 C·G	37.19	3.30	0.38	8.16	2.08	−1.01
19 G·C	42.47	2.66	−0.17	6.94	2.90	−0.26
20 A·T	30.85	2.69	−0.23	5.80	−6.27	−0.18
21 A·T				1.83	−14.42	−0.84
Mean	34.72	3.08	−0.10	6.92	−0.75	−0.65

interactions. Some proteins are siblings, while others are distant relatives. For example, Krox-20 (22), WT-1, and Sp1 have fingers homologous to the Zif fingers and appear to recognize related DNA sequences. GLI is a more distant relative of Zif, but has its own subfamily. Thus, GLI3 (23, 24), tra-1 (25), and ciD (26) have fingers homologous to those of GLI, and it has been shown that the GLI3 protein binds specifically to the GLI consensus binding site (24). Thus, modeling efforts should be far more reliable when the structure of a closely related complex is known.

Finally, the GLI structure has implications for attempts to design novel zinc finger proteins. It still appears that the Zn finger motif will provide an excellent framework for designing and selecting DNA-binding proteins with novel specificities. (The amazing diversity of TFIIIA-like fingers that are found in nature provides the clearest proof of principle for these design strategies.) However, the GLI structure shows that design strategies need not be constrained by rigid rules which assume that all fingers will dock in the same way. Seeing the variety of structural arrangements that occur in Zif and GLI helps us understand the versatility of this zinc finger motif. Screening and selection methods that can test millions of different arrangements should be inherently more powerful than rule-based design strategies. The possibilities for Zn finger–DNA interactions are richer and more complex than one may have assumed.

REFERENCES AND NOTES

1. J. Miller, A. D. McLachlan, A. Klug, *EMBO J* 4, 1609 (1985).
2. A. Klug and D. Rhodes, *Trends Biochem. Sci.* 12, 464 (1987); G. Jacobs and G. Michaels, *New Biol.* 2, 583 (1990); G. H. Jacobs, *EMBO J.* 11, 4507 (1992).
3. G. Párraga *et al.*, *Science* 241, 1489 (1988); M. S. Lee, G. P. Gippert, K. V. Soman, D. A. Case, P. E. Wright, *Science* 245, 635 (1989); R. E. Klevit, J. R. Herriott, S. J. Horvath, *Proteins* 7, 215 (1990); J. G. Omichinski, G. M. Clore, E. Appella, K. Sakaguchi, A. M. Gronenborn, *Biochemistry* 29, 9324 (1990).
4. N. P. Pavletich and C. O. Pabo, *Science* 252, 809 (1991).
5. D. Stanojevic, T. Hoey, M. Levine, *Nature* 341, 331 (1989); J. Treisman and C. Desplan, *Ibid.*, p. 335.
6. M. R. Briggs, J. T. Kadonaga, S. P. Bell, R. Tjian, *Science* 234, 47 (1986); J. T. Kadonaga, K. R. Carner, F. R. Masiarz, R. Tjian, *Cell* 51, 1079 (1987); R. W. Kriwacki, S. C. Schultz, T. A. Steitz, J. P. Caradonna, *Proc. Natl. Acad. Sci. U.S.A.* 89, 9759 (1992).
7. K. W. Kinzler and B. Vogelstein, *Mol. Cell Biol.* 10, 634 (1990).
8. K. M. Ceil *et al.*, *Cell* 60, 509 (1990); M. Gessler *et al.*, *Nature* 343, 774 (1990); F. J. Rauscher III, J. F. Morris, O. E. Tournay, D. M. Cook, T. Curran, *Science* 250, 1259 (1990).
9. K. W. Kinzler, J. M. Ruppert, S. H. Bigner, B. Vogelstein, *Nature* 332, 371 (1988).
10. W. M. Roberts, E. C. Douglass, S. C. Peiper, P. J. Houghton, A. T. Look, *Cancer Res.* 49, 5407 (1989).
11. J. M. Ruppert, B. Vogelstein, K. W. Kinzler, *Mol. Cell Biol.* 11, 1724 (1991).
12. W. Saenger, *Principles of Nucleic Acid Structure*, (Springer-Verlag, New York, 1984).
13. L. Nekludova and C. O. Pabo, unpublished data.
14. Finger 2 of GLI is distinctive in that the sheet region is perturbed by an "insertion" just before the second β strand (Fig. 1A), and there are two consecutive reverse turns in this region.
15. M. Kochoyan, H. T. Keutmann, M. A. Weiss, *Biochemistry* 30, 9396 (1991).
16. It is interesting that the linker between fingers 1 and 2 has two unusual features. (i) This linker is two residues longer than the consensus linker. (ii) Residues 33 to 36 may be relatively flexible, since they do not have clear electron density in our maps. (Other linkers have clear density and thus appear to have a fixed structure in the GLI complex.)
17. The side chain of Arg^{62} (in finger 2) hydrogen bonds to the backbone carbonyl of Ser^{82} (in finger 3), and there is an equivalent interaction between Arg^{82} (finger 3) and the carbonyl of Ser^{112} (finger 4). (Finger 4, which has an extra residue just before this arginine, does not make a corresponding contact with finger 5.)
18. A. A. Travers, *Curr. Opin. Struct. Biol.* 2, 71 (1992).
19. M. McCall, T. Brown, W. N. Hunter, O. Kennard, *Nature* 322, 661 (1986); L. Fairall, S. Martin, D. Rhodes, *EMBO J.* 8, 1809 (1989); P. W. Huber, G. C. Blobe, K. M. Hartmann, *J. Biol. Chem.* 268, 3278 (1991); P. W. Huber, T. Moril, H-Y. Mei, J. K. Barton, *Proc. Natl. Acad. Sci. U.S.A.* 88, 10801 (1991).
20. M. E. A. Churchill, T. D. Tullius, A. Klug, *Proc. Natl. Acad. Sci. U.S.A.* 87, 5528 (1990); J. J. Hayes and T. D. Tullius, *J. Mol. Biol.* 227, 407 (1992); J. J. Hayes and K. R. Clemens, *Biochemistry* 31, 11600 (1992); K. R. Clemens, X. Liao, V. Wolf, P. E. Wright, J. M. Gottesfeld, *Proc. Natl. Acad. Sci. U.S.A.* 89, 10822 (1992).
21. X. Liao, K. R. Clemens, L. Tennant, P. E. Wright, J. M. Gottesfeld, *J. Mol. Biol.* 223, 857 (1992).
22. P. Chavrier *et al.*, *Mol. Cell Biol.* 9, 787 (1989).
23. J. M. Ruppert *et al.*, *Ibid.* 8, 3104 (1988); A. Vortkamp, M. Gessler, K.-H. Grzeschik, *Nature* 352, 539 (1991).
24. J. M. Ruppert, B. Vogelstein, K. Arheden, K. W. Kinzler, *Mol. Cell Biol.* 10, 5408 (1990).
25. D. Zarkower and J. Hodgkin, *Cell* 70, 237 (1992).
26. T. V. Orenic, D. C. Slusarski, K. L. Kroll, R. A. Holmgren, *Genes Devel.* 4, 1053 (1990).
27. Mass was determined by the electrospray ionization method at the Harvard Microchemistry Facility, 16 Divinity Avenue, Cambridge, MA 02138.
28. Attempts to obtain GLI crystals with peptide reconstituted with $ZnCl_2$ have been unsuccessful. Comparative studies with Zif had shown that the Zn complex and the Co complex were virtually identical (4). It is possible that Zn interferes with the crystallization of GLI by interacting—at these high peptide concentrations—with the additional (nonconsensus) histidines that appear in fingers 1, 2, and 3 of GLI.
29. S.E.R.C. [U.K.] Collaborative Computing Project No. 4 (Daresbury Laboratory, Warrington, U.K., 1979).
30. B. C. Wang, *Methods Enzymol.* 115, 90 (1985).
31. T. A. Jones, *J. Appl. Cryst.* 11, 268 (1978).
32. A. T. Brünger, J. Kuriyan, M. Karplus, *Science* 235, 458 (1987); A. T. Brünger, *X-PLOR v2.1 Manual* (Yale Univ. Press, New Haven, CT, 1990).
33. D. E. Tronrud, L. F. Ten Eyck, B. W. Matthews, *Acta Crystallogr.* A43, 489 (1987).
34. Program DSCALEAD, M. R. Rould (1989).
35. Program NEWHELIX (May 1989 Version), R. E. Dickerson, Molecular Biology Institute, UCLA, Los Angeles, CA 90024.
36. Binding experiments with a variant operator site also suggested that these contacts are not critical for recognition (N. P. Pavletich and C. O. Pabo, unpublished data).

37. Supported by the Howard Hughes Medical Institute, by NIH grant GM-31471 (C.O.P.), and by equipment purchased with support from the PEW Charitable Trusts. We thank K. Kinzler and B. Vogelstein for providing us with the GLI cDNA clone; M. Rould, C. Kissinger, and L. Nekludova for help in structure determination and interpretation; H. Drew and A. Klug for comments on the Zif DNA structure; and the National Cancer Institute for use of the Cray during molecular dynamics refinement. Coordinates are being deposited with the Brookhaven Data Bank. While these are being processed and prepared for distribution, interested scientists may obtain a set of coordinates by sending an appropriate e-mail address to PABO@PABO1.MIT.EDU.

24 February 1993; accepted 17 August 1993

Gateway

Your Entrance to the Knowledge Resources of the National Library of Medicine

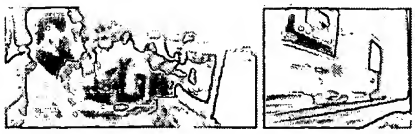

MeSH Term Information

Concept	GKLF protein
Name of Substance	GKLF protein
Entry Term	EZF protein
Entry Term	EZF protein, human
Entry Term	GKLF protein, human
Entry Term	GKLF protein, rat
Entry Term	Gklf protein, mouse
Entry Term	KLF4 protein, human
Entry Term	Klf4 protein
Entry Term	Klf4 protein, mouse
Entry Term	Klf4 protein, rat
Entry Term	Kruppel-like factor 4
Entry Term	Kruppel-like factor 4 (gut), human
Entry Term	Kruppel-like factor 4 (gut), mouse
Entry Term	Kruppel-like factor 4 (gut), rat
Entry Term	endothelial Kruppel-like zinc finger protein
Entry Term	endothelial Kruppel-like zinc finger protein, human
Entry Term	epithelial zinc finger protein
Entry Term	gut-enriched Kruppel-like factor
Heading Mapped to	*Kruppel-Like Transcription Factors
Indexing Information	Zinc Fingers
Source	J Biol Chem 1996 Aug 16;271(33):20009-17
Source	J Biol Chem 1996 Dec 6;271(49):31384-90
Pharm. Action	Growth Inhibitors
Frequency	99
Note	putative negative regulator of cell growth; RefSeq NM_004235 (human); NM_010637 (mouse); NM_053713 (rat)
Registry Number	0

THE JOURNAL OF BIOLOGICAL CHEMISTRY Vol. 276, No. 46, Issue of November 16, pp. 42863–42868, 2001
Printed in U.S.A.

Kruppel-like Factor 4 Regulates Laminin α3A Expression in Mammary Epithelial Cells*

Received for publication, August 23, 2001, and in revised form, September 5, 2001
Published, JBC Papers in Press, September 10, 2001, DOI 10.1074/jbc.M108130200

Kristi A. Miller‡, Elizabeth A. Eklund‡§, Marie L. Peddinghaus‡, Zhengjin Cao‡, Nisha Fernandes‡, Patrick W. Turk‡, Bayar Thimmapaya¶, and Sigmund A. Weitzman‡§‖

From the Departments of ‡Medicine, Division of Hematology/Oncology, and §Microbiology and Immunology, the Lurie Cancer Center, Northwestern University Medical School, and ¶Department of Medicine, Veterans Affairs Lakeside Medical Center, Chicago, Illinois 60611

Laminin-5, the major extracellular matrix protein produced by mammary epithelial cells, is composed of three chains (designated α3A, β3, and γ2), each encoded by a separate gene. Laminin-5 is markedly down-regulated in breast cancer cells. Little is known about the regulation of laminin gene transcription in normal breast cells, nor about the mechanism underlying the down-regulation seen in cancer. In the present study, we cloned the promoter of the gene for the human laminin α3A chain (*LAMA3A*) and investigated its regulation in functionally normal MCF10A breast epithelial cells and several breast cancer cell lines. Using site-directed mutagenesis of promoter-reporter constructs in transient transfection assays in MCF10A cells, we find that two binding sites for Kruppel-like factor 4 (KLF4/GKLF/EZF) are required for expression driven by the *LAMA3A* promoter. Electrophoretic mobility shift assays reveal absence of KLF4 binding activity in extracts from T47D, MDA-MB 231, ZR75-1, MDA-MB 436, and MCF7 breast cancer cells. Transient transfection of a plasmid expressing KLF4 activates transcription from the *LAMA3A* promoter in breast cancer cells. A reporter vector containing duplicate KLF4-binding sites in its promoter is expressed at high levels in MCF10A cells but at negligible levels in breast cancer cells. Thus, KLF4 is required for *LAMA3A* expression and absence of laminin α3A in breast cancer cells appears, at least in part, attributable to the lack of KLF4 activity.

The laminin family of extracellular matrix glycoproteins is heterotrimeric proteins consisting of three distinct subunits, designated α, β, and γ that are encoded by the *LAMA*, *LAMB*, and *LAMC* genes, respectively. To date there are five α chains, three β chains, and two γ chains that assemble into 12 laminins. Laminin-5 (α3A, β3, and γ2) is the major extracellular matrix protein produced in mammary epithelial cells. In these cells laminin-5 functions as a ligand for the $\alpha_3\beta_1$ and $\alpha_6\beta_4$ integrins to regulate adhesion, migration, and morphogenesis (1). Loss of laminin-5 has been found in breast cancer progression. Henning *et al.* (2) demonstrated a loss of laminin-5 protein expression by immunostaining in malignant lesions while benign ductal and lobular proliferations and fibroadenomas show continuous laminin-5 staining at the epithelial-stromal interface. Martin *et al.* (3) used a molecular approach to analyze mRNA expression of the laminin-5 subunits and found no expression in late stage tumors and decreased expression in early stage tumors compared with normal breast epithelial cells.

The murine *LAMA3A* promoter has been studied and found to contain three binding sites for the complex dimeric transcription factor, AP-1, one site of which is essential for basal expression of *LAMA3A* in keratinocytes (4). Mutation of this single key AP-1 site reduced promoter activity by ~90% while mutation of the other two sites had much less effect (4). In the present study we analyze the human *LAMA3A* promoter in the MCF10A mammary epithelial cell line and the T47D breast cancer cell line. We sought to find a mechanism that would explain the *LAMA3A* down-regulation in the nonexpressing cells. In doing this, we demonstrated a key role for the transcription factor Kruppel-like factor 4 (KLF4)[1] in regulating this gene.

KLF4, also known as gut-enriched Kruppel-like factor (GKLF) and epithelial zinc finger (EZF), is a member of the Kruppel-type zinc finger transcription factors (5–8). One of the best known members of this family is the erythroid Kruppel-like factor that is involved in the activation of the β-globin promoter in red blood cells (9). The family also includes LKLF (10), UKLF (11), IKLF (12), BTEB2 (13), and BKLF (14), many of which are tissue specific in their expression. Members of the Kruppel-type family are highly conserved in the carboxyl-terminal region that contains three zinc fingers and they bind similar GC-rich recognition sequences. KLF4 is a nuclear protein shown to contain both transcriptional activation and repression domains (8). In keratinocytes, KLF4 activates the keratin 4 promoter and may be important in the transition toward differentiation (7). KLF4 has also been shown to be involved in the regulation of the CYP1A1 gene (15). This report describes the novel role of this factor in the regulation of the *LAMA3A* promoter. Through transient transfections and EMSA we show that KLF4 activates expression of the *LAMA3A* gene in MCF10A cells and that loss of KLF4 activity is in part responsible for the loss of *LAMA3A* expression in breast cells.

EXPERIMENTAL PROCEDURES

Cell Culture and Transfections—MCF10A (a nontransformed, spontaneously immortalized human breast epithelial cell line) and M-H cells (a hygromycin resistant subclone of MCF10A cells) were maintained as previously described (16). T47D cells were cultured in RPMI 1640

* This work was supported by United States ARMY Grants DAMD17-94-J-4466 and DAMD17-94-J-4291 and National Institutes of Health Grant 5T32CA09560 and CA74403. The costs of publication of this article were defrayed in part by the payment of page charges. This article must therefore be hereby marked "*advertisement*" in accordance with 18 U.S.C. Section 1734 solely to indicate this fact.

The nucleotide sequence(s) reported in this paper has been submitted to the GenBank™/EBI Data Bank with accession number(s) AF279435.

‖ To whom correspondence should be addressed: Olson 8276, 303 E. Chicago Ave., Chicago, IL 60611. Tel.: 312-908-5284; Fax: 312-908-5717; E-mail: s-weitzman@northwestern.edu.

[1] The abbreviations used are: KLF4, Kruppel-like factor 4; GKLF, gut-enriched Kruppel-like factor; EZF, epithelial zinc finger; EMSA, electrophoretic mobility shift assay.

medium supplemented with 0.01 mg/ml insulin and 10% heat inactivated fetal bovine serum. MDA-MB 231, MCF7, and ZR75-1 cells were cultured in RPMI 1640 medium supplemented with 10% fetal bovine serum and 300 μg/ml glutamine. MDA-MB 436 cells were cultured in RPMI 1640 medium supplemented with 10% fetal bovine serum, 0.01 mg/ml insulin, and 16 μg/ml glutathione. MCF10A and T47D cells were transfected in log growth phase at a density of 1×10^5 cells per well in 6-well plates using the Superfect Transfection Reagent (Qiagen, Inc.) per the manufacturer's protocol. Quantities transfected of the respective vectors are indicated in the figure legends. Cells were harvested in Reporter Lysis Buffer (Promega Corp.) between 24 and 48 h. Luciferase activity was assayed by mixing aliquots of cell extracts with luciferin reaction mixture (Promega Luciferase Assay Kit) and emission of light was quantitated with a Microlumat luminometer. β-Galactosidase activity was determined using the β-Galactosidase Luminescence Kit (CLONTECH Laboratories, Inc., Palo Alto, CA) per the manufacturer's instruction. Transfections were normalized for efficiency by normalizing relative light units from the β-galactosidase assay to the luciferase light units for each individual sample.

Plasmids—The sequence for the intron between *LAMA3B* exon 1 and *LAMA3A* exon 1 which has been shown to constitute the *LAMA3A* promoter in mouse was kindly provided by Dr. Angela Christiano (Columbia University, New York). Based on this sequence, primers were designed to amplify 1410 base pairs of this intronal promoter. The 5′ primer 5′-CAGGTACCAAGTTTTCCCATCCGCAACATTTCC-3′ that has a *Kpn*I site engineered into the 5′ end and the 3′ primer 5′-CAGCTAGCAGGCTGACCGCCTCACTGCTGGAGG-3′ that has an *Nhe*I site engineered were used in polymerase chain reaction of genomic DNA from MCF10A cells. The polymerase chain reaction fragment was TA cloned into the pGEMT vector (Promega), then excised by *Kpn*I and *Nhe*I, and cloned into the pGL2 basic vector (Promega) that was digested with *Kpn*I and *Nhe*I. The resulting vector was transformed into XL1 Gold Supercompetent cells (Stratagene), named pL3A and contains the human *LAMA3A* promoter upstream of a luciferase reporter gene. Three separate colonies were sequenced and the consensus sequence was submitted to GenBank™ (accession number AF279435). Restriction sites were identified using MAP functions of GCG software. The adenine of the initiator ATG codon was designated base +1.

Dr. Mu-En Lee kindly provided the pcDNA3-hEZF vector containing the full-length cDNA for human KLF4 in the pcDNA3 mammalian expression vector (8). The TDA(WT)x2-pGL2-TATA-Luc and TDA(M6-Mut)x2-pGL2-TATA-Luc vectors were kindly provided by Dr. Vincent Yang (The Johns Hopkins University) (17). The cytomegalovirus-β-galactosidase vector was used as an internal control in transfections.

Site-directed Mutagenesis—The Quik-Change Mutagenesis kit from Stratagene was used to create site-directed mutants of the full-length pL3A vector. An oligonucleotide that changes overlapping KLF4-binding sites starting at base pair −412 from 5′-CTTCCCCTTCCTC-CAT-3′ to 5′-CTTCC**TTTTCAG**CCTCCAT-3′ created mutation pL3A-KLF4mut1. pL3A-KLFmut2 changes the KLF4 site at −367 from 5′-GAGGGAAAGAGAGGGACT-3′ to 5′-GAGGGAAAGAGA**TTG**ACT-3′. The pL3A-AP-1mut3 changes the AP-1 site at base pair −185 from 5′-GCTGACTCATG-3′ to 5′-GCTG**CCTTA**TG-3′. This corresponds to the AP-1B site described in the mouse promoter by Virolle *et al.* (4). The overlapping USF site found near the AP-1 site starting at base pair −179 was mutated from 5′-TCATGTGTGAAGTT-3′ to 5′-TCATG**CAT**-GAAGTTT-3′ to create pL3A-USFmut4. The KLF4 site at base pair −168 5′-GTTTAAAGGTGGGG-3′ was changed to 5′-GTTTAAAGGTG-G**TT**-3′ to create pL3A-KLF4mut5. Two overlapping KLF4-binding sites were mutated in pL3A-KLF4mut6 changing 5′-ATAAGAGGAA-GAGG-3′ to 5′-ATAAGA**TT**AAGA**TT**-3′ starting at position −87. All vectors were sequenced by the Northwestern Biotechnology Facility to verify the correct mutations were created.

EMSA—Nuclear extracts were prepared by collecting cells in cold Buffer A (10 mM HEPES pH 7.9, 1.5 mM $MgCl_2$, 10 mM KCl, 0.5 mM dithiothreitol, 0.2 mM phenylmethylsulfonyl fluoride) and incubated on ice for 10 min. Cells were then frozen and thawed once and vortexed for 10 s. Nuclei were pelleted by brief centrifugation and resuspended in cold Buffer C (20 mM HEPES pH 7.9, 25% glycerol, 420 mM NaCl, 1.5 mM $MgCl_2$, 0.2 mM EDTA, 0.5 mM dithiothreitol, 0.2 mM phenylmethylsulfonyl fluoride), incubated for 30 min, briefly centrifuged to remove debris, and the nuclear extract supernatant was collected and stored at −70 °C. Primers to the pL3A vector were used to amplify probe A, the 103-base pair fragment spanning bases −199 to −97, for gel shift analysis, 5′-CGCTCTGGCACAGG-3′ 5′-TTCCTGCTCAGTGCC-3′. Probe A was radiolabeled with [α-^{32}P]dCTP (Amersham Pharmacia Biotech) using T4 polynucleotide kinase. Probe B (−84 to −62) was created by annealing two oligonucleotides, 5′-AGAGGAAGAGGCA-GAGGTTC-3′ and 5′-CAGGAACCTCTGCCTCTTCCT-3′, that contain base pair overhangs that were radiolabeled using DNA polymerase in the presence of [α-^{32}P]dCTP (Amersham Pharmacia Biotech). The oligonucleotide containing the KLF4 consensus sequence designated TDA by Shields and Yang (15) and an oligonucleotide based on the TDA with 2 base pairs mutated that does not bind KLF4 designated TDAmut were created as described by Shields and Yang (17) and end labeled as Probe A. Labeled probes were then separated from free [α-^{32}P]dCTP using Sephadex ProbeQuant G-50 micro columns (Amersham Pharmacia Biotech). Binding reactions included: α-^{32}P-labeled DNA probes (1–5 ng, 100,000 cpm); 4 μg of poly(dI-dC); 10 μg of nuclear extract; 5 μg of bovine serum albumin; 6 μl of 5 × binding buffer (50 mM HEPES pH 7.9, 5 mM dithiothreitol, 0.5% Triton X-100, and 2.5% glycerol); and the appropriate volume of H_2O to a final volume of 30 μl. Binding reaction mixtures were then incubated at 30 °C for 30 min. Bound products were resolved by electrophoresis through a 7 or 8% native polyacrylamide gel in 1 × running buffer (50 mM Tris, 0.38 M glycine, 2.0 mM EDTA, pH 8.5). Gels were dried with a Bio-Rad Gel Dryer for 45 min at 85 °C, followed by exposure to Hyperfilm-MP (Amersham Pharmacia Biotech) at −70 °C. Film was then developed using an x-ray film processor (Fuji).

To deplete extracts of KLF4, 50 μl of nuclear extracts from an MCF10A subclone were incubated for 4 h at 4 °C with either 20 μl of rabbit preimmune serum or 10 μl each of KLF4 antibodies from Dr. Yang (6) and Dr. Tseng (18) and 40 μl of protein G-agarose beads (Life Technologies). Samples were briefly centrifuged, and supernatants were used in gel shifts as described above.

Competition experiments consisted of 150 × molar excess for the TDA, AP-1, and AP2 oligonucleotides that were preincubated with nuclear extracts for 30 min at room temperature before proceeding to the binding reactions with the 103-base pair DNA fragment. AP-1 and AP2 duplex oligonucleotides were obtained from Stratagene, the AP2 oligonucleotide serving as a nonspecific control. Competition of the labeled TDA probe consisted of 125 × molar excess of TDA(WT) and TDA(M6-mut) oligonucleotides in Fig. 6*A* and 250 × molar excess in Fig. 6*B*.

Western Analysis—Cells were lysed in RIPA buffer (50 mM Tris, pH 8.0, 150 mM NaCl, 1% Nonidet P-40, 0.5% deoxycholic acid, .1% SDS, 1 mM EDTA, 20 μg/ml phenylmethylsulfonyl fluoride, 1 μg/ml pepstatin, 1 μg/ml leupeptin, 1 μg/ml aprotinin). Protein concentrations were determined using the Bio-Rad protein reagent assay, 40 μg of protein were electrophoresed by SDS-polyacrylamide gel electrophoresis, transferred to nitrocellulose, and blotted using the rabbit polyclonal anti-KLF4 antibody (Santa Cruz Biotechnology, Santa Cruz, CA). Goat anti-rabbit HRP (Bio-Rad Laboratories) was used as a secondary antibody and detected using ECL reagent (Amersham Pharmacia Biotech).

RESULTS

The α3 Subunit of Laminin-5 Is Not Expressed in Breast Cancer Cell Lines—There is previous evidence that laminin-5 is down-regulated in breast cancer cell lines. Examination of mRNA in breast tumor cells showed that laminin α3 was greatly reduced or not present at all in breast tumor tissue and 15 breast cancer cell lines including T47D, MCF7, ZR75-1, MDA-MB 436, BT474, MDA-MB 361, and MDA-MB 231 (3). Long exposure of Northern blots revealed very low level expression in breast cancer cell lines, ruling out systematic deletion of this gene in breast cancer (3). The main transcript of the laminin-5 α3 subunit in mammary epithelia is the *LAMA3A* isoform (19). In the mouse the genetic structure of the *mLAMA3* gene consists of the *mLAMA3A* and *mLAMA3B* isoforms that each contain a unique exon 1 that is expressed using alternative promoters. Exon 1 of *mLAMA3B* is upstream of the *mLAMA3A* exon and the intron region between these exons contains the promoter for the *mLAMA3A* isoform. The genetic structure for the human *LAMA3* was previously described by Pulkinnen *et al.* (20) and is very similar to the mouse organization. We cloned the human intron region between the *LAMA3B* and *LAMA3A* exons into the pGL2 reporter vector and tested the transcriptional activity in MCF10A cells and T47D cells. We found that the resulting vector, pL3A, contained potent transcriptional activity when transfected into MCF10A cells but had no activity in T47D cells when compared with the activity of empty vector (Fig. 1*A*).

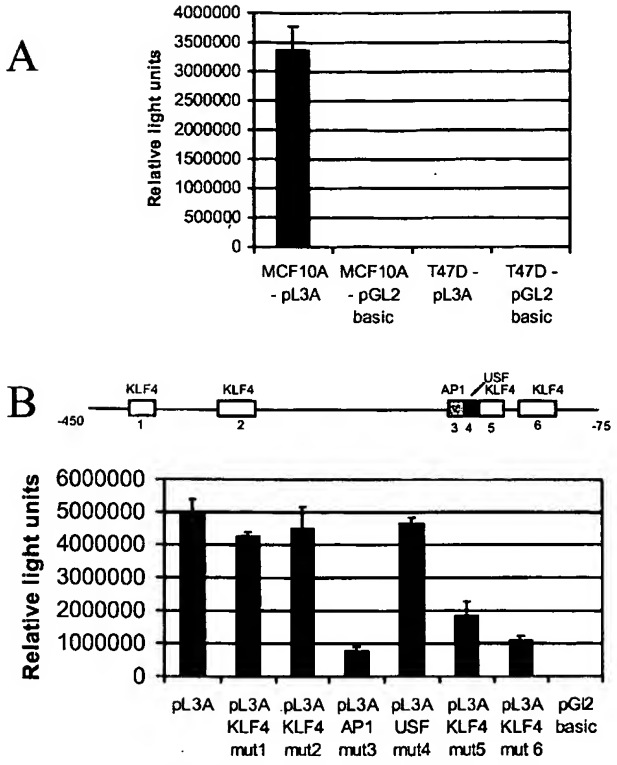

FIG. 1. **Control of *LAMA3A* by KLF4 and AP-1.** *A*, expression of *LAMA3A* is decreased in breast cancer cells. Transient transfection of 1 μg of the pL3A vector containing the human *LAMA3A* promoter in the pGL2 basic vector was compared with transfection of 1 μg of pGL2 basic vector in MCF10A and T47D cells. All wells were transfected with 200 ng of a cytomegalovirus-β-galactosidase vector. Transfections were normalized to β-galactosidase activity. MCF10A cells contain high *LAMA3A* promoter activity, while T47D cells have very low expression. Data represents at least two experiments performed in triplicate. *Error bars* represent standard error. *B*, transient transfection of pL3A mutant vectors in MCF10A cells. 1 μg of each vector was co-transfected with 200 ng of cytomegalovirus-β-gal. Luciferase counts were normalized to β-galactosidase activity to determine relative light units. A schematic diagram depicting locations of the binding sites that were mutated is shown directly above the graph. *White boxes* are KLF4-binding sites, the *gray box* is the mutated AP-1 site, and the *black box* is the USF site. Data represent at least two experiments performed in triplicate. *Error bars* represent standard error.

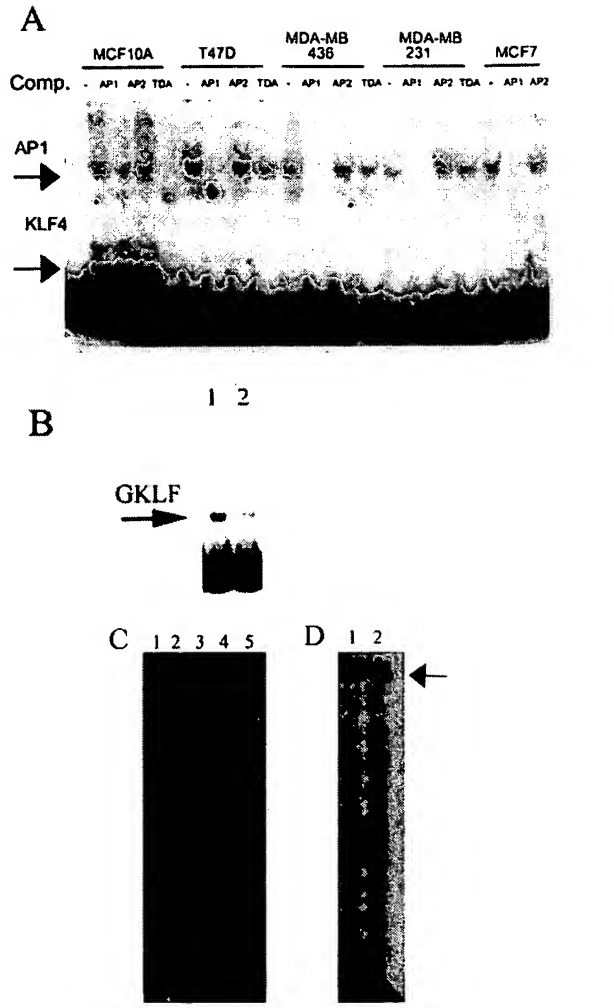

FIG. 2. **AP-1 and KLF4 bind the *LAMA3A* promoter sequence.** *A*, the 103-base pair oligonucleotide was polymerase chain reaction amplified, radiolabeled, and incubated with nuclear extracts from MCF10A, T47D, MDA-MB 436, MDA-MB 231, and MCF7 cells. The TDA (KLF4 consensus binding site), AP-1, and AP2 competitor oligonucleotides were added to 150 × molar excess. AP2 competitor oligonucleotide was used as a nonspecific competitor since there are no AP2 consensus sequence sites in this DNA fragment. Binding reactions were electrophoresed in a 7% native polyacrylamide gel. AP-1 specific binding indicated by an *arrow* is seen in all cell types (compare *lanes 3* and *4*, *7* and *8*, *11* and *12*, *15* and *16*, and *19* and *20*). The KLF4 specific complex indicated by an *arrow* was found only in the MCF10A cells were KLF4 specific oligonucleotide competed this complex (*lane 5*) where the AP-1 and AP2 oligonucleotides did not (*lane 3* and *4*, respectively). *Lane 1* shows free probe (*FP*). *B*, nuclear extracts from a MCF10A subclone were depleted of KLF4 by incubation with anti-KLF4 antibody and protein G-agarose beads for 4 h at 4 °C, centrifuged, and supernatants were used in gel shift assays. *Lane 1*, extracts cleared with rabbit preimmune serum. *Lane 2*, extracts cleared with anti-KLF4 antibody. *C*, purified KLF4 binds the *LAMA3A* promoter. Probe B spanning bases −84 to −62 is shifted with purified KLF4 (the generous gift of Dr. Anil Rustgi) (*lane 1*), and MCF10A extract (*lane 2*) but not MCF7 extract (*lane 3*), T47D extract (*lane 4*), or MDA-MB 231 extract (*lane 5*). *D*, supershift of KLF4 using a probe containing the KLF4-binding site at position −87. A 24-base pair probe was labeled and incubated with MCF10A nuclear extracts plus 4 μl of preimmune serum (*lane 1*) or MCF10A extracts plus 4 μl of anti-KLF4 antibody (the generous gift of Dr. Chi-Chuan Tseng) (*lane 2*). *Arrow* indicates the KLF band shift supershifted in the presence of the anti-KLF4 antibody.

KLF4 Regulates LAMA3A Promoter Activity—The murine *LAMA3A* promoter contains three AP-1 sites (AP-1A, AP-1B, and AP-1C) that are involved in the up-regulation of this gene by transforming growth factor-β in keratinocytes (4). One of these sites, designated AP-1-B is critical for basal expression as well (4). Computer analysis of the human *LAMA3A* promoter sequence using the Matinspector software (21) revealed several putative transcription factor-binding sites. As in the mouse promoter, there are three AP-1 sites identified in the human promoter at −387, −185, and −127. Ten putative KLF4-binding sites were noted throughout the 1410-base pair promoter and are located at positions −1327, −921, −892, −572, −412, −407, −367, −167, −87, and −81. KLF4 sites at −412 and −407 overlap as do the sites at −87 and −81. Bases upstream of position −589 lacked promoter activity (data not shown) and we further examined transcription factor-binding sites between bases −589 and −6. To analyze which specific transcription factors may be involved in the regulation of this promoter, site-directed mutations were created in the full-length pL3A vector. We found that mutation of the AP-1 site homologous to the key mouse AP-1B site (4) at position −185 in vector pL3A-AP-1mut3, nearly abolished transcription in MCF10A cells, while a mutation targeting a nearby putative USF1 site in vector pL3A-USFmut4 at position −180 had no effect (Fig. 1*B*). We were interested in the KLF4-binding sites and found that mutations in the KLF4-binding sites closest to the translational start site most dramatically decreased transcriptional activity in MCF10A cells (Fig. 1*B*). Mutation of the single KLF4 site at −167 in vector pL3A-KLF4mut5 abolished 63% of tran-

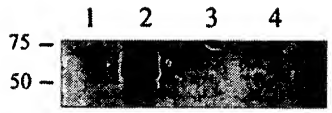

FIG. 3. **KLF4 is expressed in MCF10A but not MCF7, T47D, or MDA-MB 231 breast cancer cells.** Forty micrograms of whole cell extract from MCF-7 (*lane 1*), MCF10A (*lane 2*), T47D (*lane 3*), and MDA-MB 231 (*lane 4*) cells were electrophoresed by SDS-polyacrylamide gel electrophoresis, transferred to nitrocellulose and blotted with KLF4 antibody (Santa Cruz Biotechnology) at a dilution of 1:1000.

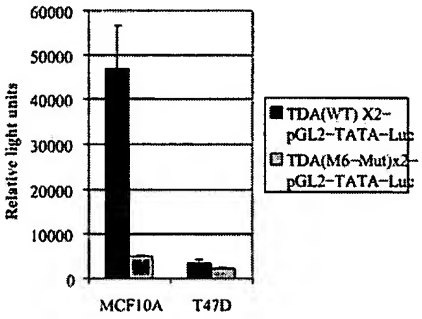

FIG. 4. **Tumor cell lines lack KLF4 transcriptional activity.** *LAMA3A* nonexpressing cells have less KLF4 transcriptional activity. Transient transfection of 5 μg of TDA(WT)x2-pGL2-TATA-Luc (*black bars*) or TDA(M6-Mut) x2-pGL2-TATA-Luc (*gray bars*) in MCF10A and T47D cells. Data represent two experiments performed in triplicate. *Error bars* show standard error.

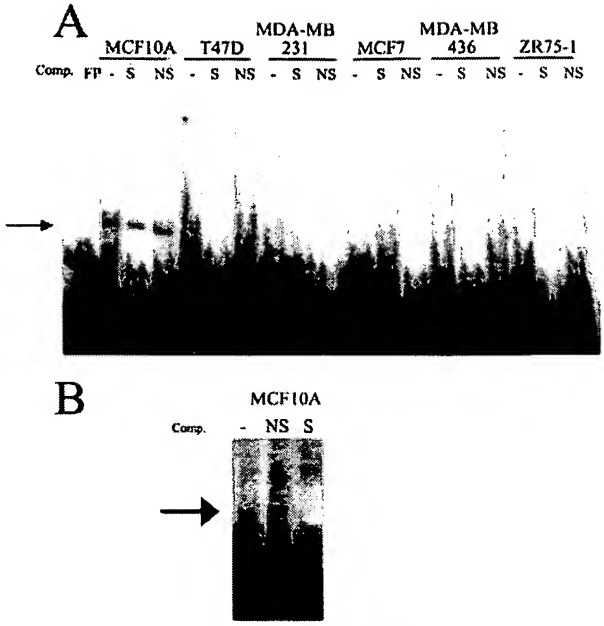

FIG. 5. **Tumor cell lines lack KLF4 DNA binding activity.** *A*, EMSA analysis of KLF4 DNA binding activity in MCF10A (*lanes 2–4*), T47D (*lanes 5–7*), MDA-MB 231 (*lanes 8–10*), MCF7 (*lanes 11–13*), MDA-MB 436 (*lanes 14–16*), and ZR75–1 (*lanes 17–19*) cells. An oligonucleotide containing the KLF4 consensus binding sequence was end labeled with T4 polynucleotide kinase, and binding reactions were electrophoresed in an 8% native polyacrylamide gel. The KLF4 specific complex was seen only in MCF10A cells (*lane 2*). The KLF4 binding complex was partially competed with 125 × cold specific (*S*) oligonucleotide (*lane 3*) but not a 125 × excess of mutated (*NS*) oligonucleotide that does not bind KLF4 (*lane 4*). None of the breast cancer cell lines tested had any KLF4 binding activity. *Lane 1* shows free probe (FP). *Arrow* points to the KLF4 specific complex. *B*, to better demonstrate the specific competition of the TDA oligonucleotide in MCF10A cells, competition with 250X molar excess of cold specific (*S*) and cold nonspecific (*NS*) oligonucleotide as in part A were used. Binding reactions were electrophoresed in a 7% native polyacrylamide gel. *Arrow* points to the KLF4 specific complex.

scriptional activity while vector pL3A-KLF4 mut6 with mutations in the two overlapping KLF4 sites at −87 and −81 abolished 79% of activity. Mutating the overlapping sites at −412 and −407, vector pL3A-KLF4mut1, as well as mutating the site at −367 in vector pL3A-KLF4mut2 had no significant effect on transcription (Fig. 1*B*). None of the site-directed mutations had any effect on the lack of transcription in T47D cells (data not shown).

The transfection results suggest that both AP-1 and KLF4 are important in the regulation of *LAMA3A*. A 103-base pair DNA fragment, Probe A, containing the key AP-1 site and the −167 KLF4 site was used for gel shift analysis. Extracts from MCF10A, T47D, MCF7, MDA-MB 231, and MDA-MB 436 cells all show AP-1 binding that is competed with an AP-1-specific oligonucleotide (Fig. 2*A*, *lanes 3, 7, 11, 15*, and *19*) but not a nonspecific competitor (Fig. 2A, *lanes 4, 8, 12, 16*, and *20*). This results confirms a previous report that AP-1 binds the human *LAMA3A* promoter (22). A complex near the free probe was noticed only in the MCF10A cell samples that was competed with a KLF4 consensus binding oligonucleotide (*lane 5*) designated TDA by Shields and Yang (15). To further prove that this shift was in fact KLF4, we show that depleting the nuclear extracts of KLF4 with anti-KLF4 antibody resulted in loss of the complex that was competed by the KLF4 consensus binding oligonucleotide (Fig. 2*B*). By transfection the KLF4 site at −81 was also important in *LAMA3A* transcription. Gel shift with Probe B, an oligonucleotide that spans bases −84 to −62, containing the −81 KL4-binding site showed a shift in MCF10A cells that was identical to a shift in a sample containing purified KLF4 (Fig. 2*C*). A band shift with Probe B was absent in breast cancer cells. To further prove that the shift seen with Probe B in MCF10A cells was in fact KLF4, a supershift experiment was performed with either preimmune serum or an anti-KLF4 antibody. The band shift of Probe B with MCF10A cell extract was specifically supershifted with the KLF4 antibody (Fig. 2*D*). One of the reasons that a band shift was not seen in the breast cancer cells with *LAMA3A* promoter sequence probes is that these cells do not express KLF4. In fact we found that to be the case by Western analysis. MCF10A cells clearly express KLF4 while no detectable KLF4 was found in whole cell extracts of MCF7, T47D, or MDA-MB 231 cells (Fig. 3).

KLF4 Activity Is Decreased in Breast Cancer Cells—To further confirm the lack of KLF4 protein in the breast cancer cells, we compared general KLF4 activity of MCF10A to the activity of T47D cells. Shields and Yang (17) have published a consensus binding sequence for KLF4. The vector TDA(WT)x2-pGL2-TATA-Luc basic contains two tandem copies of this consensus sequence upstream of a TATA element in the pGL2 basic vector. This vector has been shown to be activated by KLF4 (17). The TDA(M6-Mut)x2-pGL2-TATA-Luc vector has mutations in the KLF4 consensus and is not KLF4 responsive. We tested activity of the TDA(WT) vector compared with the TDA(M6-Mut) vector to analyze the overall KLF4 transcriptional activity in MCF10A and T47D cells. When the TDA vector was transfected in MCF10A cells, there was a 6-fold increase in transcriptional activity compared with the mutant vector that does not bind KLF4 (Fig. 4). Activation in the T47D cells, on the other hand was negligible (Fig. 4). We next analyzed KLF4 DNA binding activity by EMSA analysis in MCF10A and five different breast cancer cell lines. An oligonucleotide for EMSA analysis was created that contained the TDA consensus sequence as previously described (17). We found specific binding to the TDA-labeled oligonucleotide that was competed with cold TDA oligonucleotide but not the TDA mutant oligonucleotide in MCF10A cells (Fig. 5*A*). Specific binding was lacking in the five

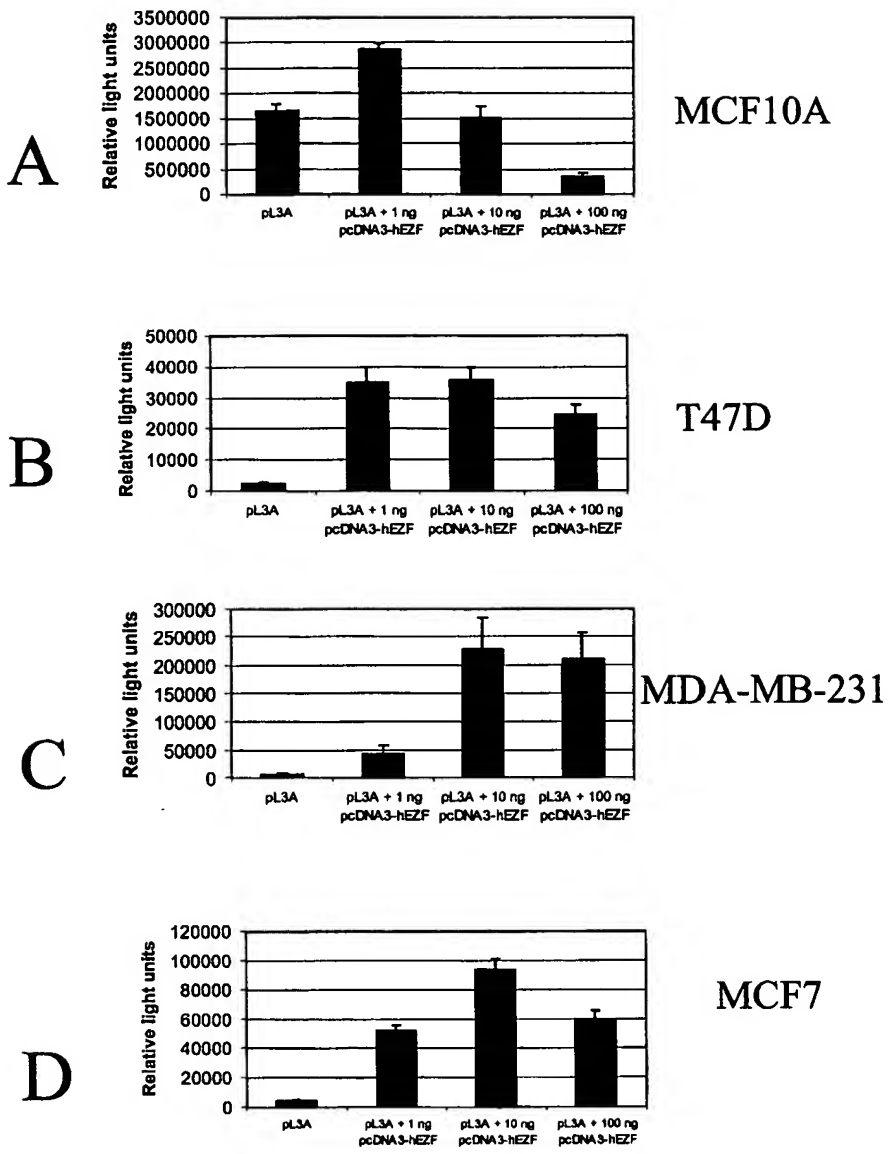

FIG. 6. **Transfection of KLF4 in MCF10A and T47D cells activates the *LAMA3A* promoter.** Transient transfections with 1 μg of pL3A alone (control) or with increasing amounts of pcDNA3-hEZF vector (1, 10, and 100 ng) in *A*, MCF10A cells; *B*, T47D cells; *C*, MDA-MB-231 cells; and *D*, MCF7 cells. Adding 10 ng of KLF4 vector gave the highest response in breast cancer cells. T47D cells had 15-fold activation over pL3A alone, MDA-MB-231 was activated 39-fold and MCF7 was activated 20-fold. MCF10A cells show modest activation. Data represent at least two experiments performed in triplicate. *Error bars* show standard error in *A* and *B* and standard deviation in *C* and *D*.

breast cancer cell lines tested (Fig. 5*A*). The competition in Fig. 5*A* was at 125 × molar excess that did not completely compete the TDA oligonucleotide. In Fig. 5*B* the competition was performed at 250 × molar excess that demonstrated complete complex inhibition with TDA(WT) but not TDA(Mut) oligonucleotides in MCF10A cells. The high level of competitor required for competition of binding to the labeled TDA oligonucleotide suggested a high level of KLF4 DNA binding activity in MCF10A cells. These data demonstrated that the KLF4 transcriptional activity and DNA binding activity was greater in the MCF10A cells than the breast cancer cells.

Expression of KLF4 in Breast Cancer Cells Stimulates LAMA3A Transcription—Lack of KLF4 protein expression and activity in breast cancer cells lead us to hypothesize that expressing KLF4 in the breast cancer cells would have a positive effect on pL3A activity in these cells. Expression of the pL3A vector was increased 15-fold in T47D cells when co-transfected with 10 ng of the pcDNA3-hEZF vector obtained from Dr. Mu-En Lee (8) (Fig. 6*B*). In MDA-MB-231 cells (Fig. 6*C*) the fold induction with 10 ng of pcDNA3-hEZF was 39-fold the basal expression of pL3A in these cells and in MCF7 cells (Fig. 6*D*) the induction was 20-fold. Thus, expression of KLF4 alone was sufficient to see promoter activity in *LAMA3A* nonexpressing cells. Transfection of the plasmids with mutated KLF4-binding sites into MCF7 cells (pL3A-Mut5 and pL3A-Mut6) showed no activation in the presence of co-transfected KLF4 (data not shown). We were unsure what the results would be of overexpressing KLF4 in the MCF10A cells that already express KLF4 protein. Co-transfection of pL3A with low doses of the pcDNA3-hEZF vector in MCF10A cells resulted in an increase in luciferase activity (Fig. 6*A*). On the other hand, a higher dose of KLF4 in MCF10A cells resulted in repression of the promoter by about 5-fold, suggesting that optimal levels of KLF4 are necessary for *LAMA3A* expression.

DISCUSSION

Laminin-5 is a highly tissue-specific gene with expression found only in epithelial cell populations. A recent study shows that the human *LAMA3A* promoter is also driven by AP-1 (22). Virolle *et al.* (22) suggest that the conformation of the AP-1 sites is critical in determining whether *LAMA3A* expression occurs or not. They suggest that under normal circumstances, a repressor binds AP-1 in the fibroblasts but this repressor is absent in keratinocytes which allows expression of *LAMA3A*. Our results confirm a role of AP-1 in the regulation of the human *LAMA3A* promoter. Mutation of the AP-1 site decreases transcriptional activity of pL3A in MCF10A cells. Unlike the previous report, our gel shift analysis does not suggest the

presence of a repressor complex that is unique to the breast cancer cells. Instead we find that the presence of KLF4 is involved. In MCF10A cells that contain KLF4, mutation of KLF4-binding sites also results in decreased transcription of pL3A. We show that breast cancer cells lack KLF4 expression and activity which likely results in the lack of *LAMA3A* expression in these cells. Expression of the *LAMA3A* promoter in the breast cancer cells by expression of KLF4 further supports this claim. This is not the first time that KLF4 has been shown to be involved in tissue specific expression. Presence of KLF4 has been shown to confer tissue specific expression of keratin 19 in pancreatic ductal cells (23). Acinar cells that do not express keratin 19 lack KLF4. We suggest that like keratin 19, *LAMA3A* expression relies on the presence of KLF4; cells that express KLF4 will express *LAMA3A* and those that do not express KLF4 will not express *LAMA3A*.

These studies do not address the mechanism of loss of KLF4 in the breast cancer cells. Further analysis is necessary to determine whether lack of KLF4 is due to gene loss, transcriptional repression, or protein instability. Studies in colon cells suggest that transcription of KLF4 is reduced in cancer cells. It has been shown that KLF4 mRNA is decreased in colon cancer cells and has an effect on the proliferation and differentiation of these cells (24, 25). Dang *et al.* (26) find that expression of KLF4 is decreased in patients with familial adenomatous polyposis. The actual regulation of KLF4 is not very well understood at this time. Several factors including Cdx2, Sp1, Sp3, and KLF4 itself may be involved in its regulation (27).

Higher doses of KLF4 results in declining *LAMA3A* promoter activation in both MCF10A and cancer cells. The mechanism for this is unknown. KLF4 has been shown to have both activation and repression domains (8). Also, the Cyclin D1 promoter has been shown to be repressed by KLF4 by competing away the positive acting transcription factor SP1 (18). Further studies will be necessary to determine the mechanism by which large amounts of KLF4 can result in inhibition of *LAMA3A* transcription.

It is unclear whether AP-1 and KLF4 form a complex in MCF10A cells. In the gel shift of Probe A that contains both AP-1- and KLF4-binding sites, we see that an AP-1 competitor competes only the AP-1 band while a KLF4 competitor competes both the AP-1 and KLF4 bands. However, there is no effect on AP-1 binding with the KLF4 oligo in the breast cancer cells. It is possible that the competition of AP-1 in the MCF10A cells with KLF4 is due to an interaction of the two transcription factors. Further studies would be necessary to confirm this finding.

In summary, this study clearly demonstrates a relationship between *LAMA3A* expression and KLF4. The MCF10A cells which express *LAMA3A* express KLF4 and have high levels of KLF4 binding activity while all the breast cancer cell lines tested lacked KLF4 expression and activity. Laminin-5 in conjunction with many other pathways mediates the differentiation of mammary epithelial cells. Therefore, lack of KLF4 may attribute to the undifferentiated phenotype of breast cancer cells.

Acknowledgments—We thank Dr. Vincent Yang for the TDA reporter vectors and KLF4 antibody, Dr. Mu-En Lee for the pcDNA3-hEZF expression vector, Dr. Chi-Chuan Tseng for KLF4 antibody, and Dr. Anil Rustgi for purified KLF4 protein.

REFERENCES

1. Stahl, S., Weitzman, S., and Jones, J. C. (1997) *J. Cell Sci.* **110,** 55–63
2. Henning, K., Berndt, A., Katenkamp, D., and Kosmehl, H. (1999) *Histopathology* **34,** 305–309
3. Martin, K. J., Kwan, C. P., Nagasaki, K., Zhang, X., O'Hare, M. J., Kaelin, C. M., Burgeson, R. E., Pardee, A. B., and Sager, R. (1998) *Mol. Med.* **4,** 602–613
4. Virolle, T., Monthouel, M. N., Djabari, Z., Ortonne, J. P., Meneguzzi, G., and Aberdam, D. (1998) *J. Biol. Chem.* **273,** 17318–17325
5. Garrett-Sinha, L. A., Eberspaecher, H., Seldin, M. F., and de Crombrugghe, B. (1996) *J. Biol. Chem.* **271,** 31384–31390
6. Shields, J. M., Christy, R. J., and Yang, V. W. (1996) *J. Biol. Chem.* **271,** 20009–20017
7. Jenkins, T. D., Opitz, O. G., Okano, J., and Rustgi, A. K. (1998) *J. Biol. Chem.* **273,** 10747–10754
8. Yet, S. F., McA'Nulty, M. M., Folta, S. C., Yen, H. W., Yoshizumi, M., Hsieh, C. M., Layne, M. D., Chin, M. T., Wang, H., Perrella, M. A., Jain, M. K., and Lee, M. E. (1998) *J. Biol. Chem.* **273,** 1026–1031
9. Tewari, R., Gillemans, N., Wijgerde, M., Nuez, B., von Lindern, M., Grosveld, F., and Philipsen, S. (1998) *EMBO J.* **17,** 2334–2341
10. Anderson, K. P., Kern, C. B., Crable, S. C., and Lingrel, J. B. (1995) *Mol. Cell. Biol.* **15,** 5957–5965
11. Matsumoto, N., Laub, F., Aldabe, R., Zhang, W., Ramirez, F., Yoshida, T., and Terada, M. (1998) *J. Biol. Chem.* **273,** 28229–28237
12. Shi, H., Zhang, Z., Wang, X., Liu, S., and Teng, C. T. (1999) *Nucleic Acids Res.* **27,** 4807–4815
13. Sogawa, K., Imataka, H., Yamasaki, Y., Kusume, H., Abe, H., and Fujii-Kuriyama, Y. (1993) *Nucleic Acids Res.* **21,** 1527–1532
14. Crossley, M., Whitelaw, E., Perkins, A., Williams, G., Fujiwara, Y., and Orkin, S. H. (1996) *Mol. Cell. Biol.* **16,** 1695–1705
15. Zhang, W., Shields, J. M., Sogawa, K., Fujii-Kuriyama, Y., and Yang, V. W. (1998) *J. Biol. Chem.* **273,** 17917–17925
16. Miller, K. A., Chung, J., Lo, D., Jones, J. C., Thimmapaya, B., and Weitzman, S. A. (2000) *J. Biol. Chem.* **275,** 8176–8182
17. Shields, J. M., and Yang, V. W. (1998) *Nucleic Acids Res.* **26,** 796–802
18. Shie, J. L., Chen, Z. Y., Fu, M., Pestell, R. G., and Tseng, C. C. (2000) *Nucleic Acids Res.* **28,** 2969–2976
19. Ferrigno, O., Virolle, T., Galliano, M. F., Chauvin, N., Ortonne, J. P., Meneguzzi, G., and Aberdam, D. (1997) *J. Biol. Chem.* **272,** 20502–20507
20. Pulkkinen, L., Cserhalmi-Friedman, P. B., Tang, M., Ryan, M. C., Uitto, J., and Christiano, A. M. (1998) *Lab. Invest.* **78,** 1067–1076
21. Quandt, K., Frech, K., Karas, H., Wingender, E., and Werner, T. (1995) *Nucleic Acids Res.* **23,** 4878–4884
22. Virolle, T., Djabari, Z., Ortonne, J., and Aberdam, D. (2000) *EMBO Rep.* **1,** 328–333
23. Brembeck, F. H., and Rustgi, A. K. (2000) *J. Biol. Chem.* **275,** 28230–28239
24. Shie, J. L., Chen, Z. Y., O'Brien, M. J., Pestell, R. G., Lee, M. E., and Tseng, C. C. (2000) *Am. J. Physiol. Gastrointest. Liver Physiol.* **279,** G806–814
25. Ton-That, H., Kaestner, K. H., Shields, J. M., Mahatanankoon, C. S., and Yang, V. W. (1997) *FEBS Lett.* **419,** 239–243
26. Dang, D. T., Bachman, K. E., Mahatan, C. S., Dang, L. H., Giardiello, F. M., and Yang, V. W. (2000) *FEBS Lett.* **476,** 203–207
27. Mahatan, C. S., Kaestner, K. H., Geiman, D. E., and Yang, V. W. (1999) *Nucleic Acids Res.* **27,** 4562–4569

THE JOURNAL OF BIOLOGICAL CHEMISTRY

Vol. 271, No. 33, Issue of August 16, pp. 20009–20017, 1996
Printed in U.S.A.

Identification and Characterization of a Gene Encoding a Gut-enriched Krüppel-like Factor Expressed during Growth Arrest*

(Received for publication, December 29, 1995, and in revised form, April 16, 1996)

Janiel M. Shields‡§, Robert J. Christy¶, and Vincent W. Yang‡‖**

From the Departments of ‡Medicine and ‖Biological Chemistry, The Johns Hopkins University School of Medicine, Baltimore, Maryland 21205 and the ¶Center for Molecular Medicine, Institute of Biotechnology, University of Texas Health Science Center, San Antonio, Texas 78250

A cDNA clone, named gut-enriched Krüppel-like factor (*GKLF*), was isolated from an NIH 3T3 library using a probe encoding the zinc finger region of the immediate-early transcription factor zif/268. The deduced GKLF amino acid sequence contains three tandem zinc fingers that are related to members of the Krüppel family of transcription factors. By indirect immunofluorescence, GKLF is localized to the cell nucleus. In cultured fibroblasts, *GKLF* mRNA is found in high levels in growth-arrested cells and is nearly undetectable in cells that are in the exponential phase of proliferation. The growth-arresting nature of GKLF is demonstrated by an inhibition of DNA synthesis in cells transfected with a *GKLF*-expressing plasmid construct. In the mouse, *GKLF* mRNA is present in select tissues and is most abundant in the colon, followed by the testis, lung, and small intestine. *In situ* hybridization experiments indicate that *GKLF* mRNA is enriched in epithelial cells located in the middle to upper crypt region of the colonic mucosa. Taken together, these results suggest that GKLF is potentially a negative regulator of cell growth in tissues such as the gut mucosa, where cell proliferation is intimately coupled to growth arrest and differentiation.

Eukaryotic transcription factors are classified according to the structural motif that contacts the DNA. The zinc finger motif is one such example, in which a zinc atom is tetrahedrally coordinated by 4 amino acid residues (usually cysteine or histidine) within a 30-amino acid sequence to form the DNA-binding domain. The biological importance of this structure is reflected by estimates that the human genome has between 300 and 700 genes containing the zinc finger motif (Klug and Schwabe, 1995; Hoovers *et al.*, 1992). A subset of the zinc finger transcription factors contain amino acid sequences that resemble those of the *Drosophila* segmentation gene product Krüppel (Schuh *et al.*, 1986). They are characterized by multiple zinc fingers containing the conserved sequence $\underline{C}X_2\underline{C}X_3FX_5LX_2\underline{H}X_3\underline{H}$ (X is any amino acid, and the underlined cysteine and histidine residues are involved in the coordination of zinc) that are separated from each other by a highly conserved 7-amino acid inter-finger spacer, TGEKP(Y/F)X, often referred to as the H/C link. These Krüppel-like proteins are involved in diverse aspects of eukaryotic gene regulation such as cell growth and/or differentiation (*e.g.* Egr-1 or zif/268 (Christy *et al.*, 1988; Sukhatme *et al.*, 1988) and the erythroid Krüppel-like factor (EKLF)[1] (Miller and Bieker, 1993)), general transcription (*e.g.* Sp1 (Kadonaga *et al.*, 1987)), oncogenesis (*e.g.* WT1 (Wilms' tumor gene) (Call *et al.*, 1990) and Gli (involved in gliomas) (Kinzler *et al.*, 1988)), and embryogenesis (*e.g.* Krüppel (Schuh *et al.*, 1986) and Hunchback (Stanojevic *et al.*, 1989)).

The eukaryotic cell cycle is a carefully controlled event that requires the participation of several zinc finger-containing transcription factors. It is divided into four major phases: G_1, S, G_2, and M (Hartwell and Weinert, 1989). Cells that do not divide are considered quiescent and reside in a special niche called the G_0 or growth-arrested state. When quiescent cells are given fresh medium containing serum, a cascade of cellular events occur that culminate in DNA synthesis and subsequent cell division. Genes that are induced shortly after quiescent cells are stimulated by serum or purified growth factors are often referred to as the "immediate-early" genes. Among these are several that encode zinc finger-containing transcription factors such as the Egr family of proteins (Sukhatme, 1992) (which includes zif/268 (Lau and Nathans, 1987) and nup475 (DuBois *et al.*, 1990)). The functions of many of these gene products are thought to induce the expression of subsequent "delayed-early" genes that are directly involved in DNA synthesis (Lanahan *et al.*, 1992).

A different facet of eukaryotic cell cycle regulation is manifested by proteins that exert negative impacts on cell growth. The tumor suppressor p53, for example, plays a prominent role in the arrest of cell growth induced by DNA damage (Hartwell and Kastan, 1994). Recently, a group of proteins have been identified and shown to inhibit the activities of the G_1 cyclins and their associated cyclin-dependent kinases, both of which are essential for the orderly progression of the cell cycle. The mechanisms by which these inhibitors act help explain how antiproliferative signals arrest cells in the G_1 phase in such diverse processes as the repair of DNA damage, terminal differentiation, and cell senescence (Sherr, 1993). Thus, expression of one such inhibitor, p21, is induced in response to DNA damage in a p53-dependent manner (Hartwell and Kastan, 1994). Similarly, the myogenic transcription factor MyoD causes terminal withdrawal of cells from the cell cycle by concomitantly inducing p21 expression and myocyte differentia-

* This work was supported in part by grants from the National Institutes of Health (to V. W. Y. and R. J. C.). The costs of publication of this article were defrayed in part by the payment of page charges. This article must therefore be hereby marked "*advertisement*" in accordance with 18 U.S.C. Section 1734 solely to indicate this fact.

§ Supported by a National Research Service Award from the National Institutes of Health.

** To whom correspondence should be addressed: Dept. of Medicine, Ross 918, The Johns Hopkins University School of Medicine, 720 Rutland Ave., Baltimore, MD 21205. Tel.: 410-955-9691; Fax: 410-955-9677; E-mail: vyang@welchlink.welch.jhu.edu.

[1] The abbreviations used are: EKLF, erythroid Krüppel-like factor; GKLF, gut-enriched Krüppel-like factor; LKLF, lung Krüppel-like factor; bp, base pair(s); ORF, open reading frame; PBS, phosphate-buffered saline; BrdUrd, bromodeoxyuridine; DMEM, Dulbecco's modified Eagle's medium; FCS, fetal calf serum; BTEB2, basic transcription element-binding protein 2.

tion (Halevy *et al.*, 1995). These findings suggest that depending on the signaling event, the mammalian cell cycle is regulated by both positive and negative control mechanisms.

In this study, we describe the identification and characterization of GKLF, a zinc finger-containing nuclear protein that is a member of the Krüppel family of transcription factors. Expression of *GKLF* in cultured fibroblasts is highest in growth-arrested cells and lowest in cells in the exponential phase of proliferation. Moreover, constitutive expression of *GKLF* in transfected cells results in the inhibition of DNA synthesis. *In vivo*, *GKLF* mRNA is very abundant in the crypt epithelium of the mouse colon. These findings suggest that GKLF may act as a negative regulator of proliferation of intestinal epithelial cells.

EXPERIMENTAL PROCEDURES

Materials—Restriction endonucleases and modifying enzymes were purchased from New England Biolabs Inc. (Beverly, MA). Sequenase was purchased from U. S. Biochemical Corp. Radioisotopes were purchased from DuPont NEN. Media and serum were purchased from Life Technologies, Inc. and Hyclone Laboratories (Logan, UT), respectively. Fluorescein isothiocyanate-, Texas Red-, and horseradish peroxidase-conjugated secondary antibodies were purchased from Amersham Corp. The prokaryotic expression vectors pET3d and pET16b (Studier *et al.*, 1990) were purchased from Novagen (Madison, WI). The constitutive eukaryotic expression vector PMT3 (Swick *et al.*, 1992), which utilizes the simian virus 40 enhancer and the adenovirus major late promoter for expression, was obtained with permission from the Genetics Institute (Cambridge, MA).

Library Screening and DNA Sequencing—An NIH 3T3 cDNA library in bacteriophage λgt10 (Lanahan *et al.*, 1992) was kindly provided by Dr. Ty Lanahan (The Johns Hopkins University). This library was screened under conditions of reduced stringency with a radioactively labeled DNA fragment containing the zinc finger portion of the immediate-early transcription factor zif/268 (Christy *et al.*, 1988). One of the positive clones, A14, contained a DNA insert of ~1900 base pairs (bp) and was selected for further investigation as it appeared to encode a novel gene based on partial sequence analysis. Radioactively labeled A14 cDNA was used to rescreen the same library under high stringency conditions, which yielded >50 positively hybridizing plaques. The plaque with the longest DNA insert, ~2800 bp in length, was amplified, and its insert was subcloned into the plasmid pBluescript (Stratagene, La Jolla, CA). Overlapping restriction endonuclease fragments of the cDNA with sizes of <400 bp were further subcloned and sequenced bidirectionally by the dideoxy chain termination method using the Sequenase kit (U. S. Biochemical Corp.). Sequence comparison was performed using the BLAST algorithm provided by the National Center for Biotechnology Information (Rockville, MD).

Production of GKLF in Bacteria and Generation of Anti-GKLF Serum—Complementary DNA containing the open reading frame (ORF) of *GKLF* was subcloned into pET3d and pET16b to generate pET3d-GKLF and pET16b-GKLF, respectively. The pET3d-GKLF construct was introduced into the BL21(DE3) strain of *Escherichia coli* cells, which were subsequently induced by the addition of 0.4 mM isopropyl-β-D-thiogalactopyranoside to produce GKLF. The protein, present largely in the form of inclusion bodies, was solubilized by the method of Fraser *et al.* (1993) and separated by SDS-polyacrylamide gel electrophoresis. GKLF was electroeluted from the gel and used to raise a rabbit polyclonal antiserum by HRP Inc. (Denver, PA).

Cell Transfection—Transient transfections were performed by the DEAE-dextran technique (Lopata *et al.*, 1984) or by lipofection (Felgner *et al.*, 1987) using the Lipofectin reagent as recommended by the manufacturer (Life Technologies, Inc.). The ORF of the *GKLF* cDNA was subcloned into the constitutive mammalian expression vector PMT3 to generate PMT3-GKLF. Transfections of the monkey kidney-derived cell line COS-1 (American Type Culture Collection, Rockville, MD) were accomplished with 1 μg/ml PMT3-GKLF DNA in 3.5- or 10-cm culture dishes. Two days following transfection, cells were examined for GKLF production by Western blot or immunocytochemical analysis (see below).

[^{3}H]Thymidine Incorporation—For [^{3}H]thymidine incorporation, proliferating COS-1 cells were transfected with 1 μg/ml PMT3-GKLF or control PMT3 DNA in 3.5-cm culture dishes. Twenty-four h following transfection, cells were incubated with 1 μCi/ml [^{3}H]thymidine (20 Ci/mmol) at 37 °C for 3 h. After washing twice with cold phosphate-buffered saline (PBS), cells were fixed with 10% trichloroacetic acid at 4 °C for 30 min, rinsed with 10% trichloroacetic acid, solubilized with 1 N NaOH, and neutralized with HCl. Aliquots equal to 0.1 volume of the solubilized material were counted in triplicate by liquid scintillation. Dishes that contained no cells were labeled and counted the same way to provide background counts.

Western Blot Analysis—SDS-polyacrylamide gel electrophoresis was performed according to Laemmli (1970) with the following modifications. The acrylamide concentrations of the stacking and running gels were 5 and 10%, respectively. Protein samples were dissolved in loading buffer (60 mM Tris-HCl, pH 6.8, 2% SDS, 100 mM dithiothreitol, and 0.01% bromphenol blue); heated to 100 °C for 3 min; and loaded onto the gel in electrophoresis buffer containing 25 mM Tris-HCl, pH 8.3, 250 mM glycine, and 0.1% SDS. At the completion of electrophoresis, proteins were transferred to nitrocellulose membranes according to the method of Towbin *et al.* (1979) and immunoblotted with rabbit anti-GKLF serum (1:1000 dilution) or preimmune serum. Following incubation with the secondary antibody (horseradish peroxidase-conjugated donkey anti-rabbit IgG), GKLF was visualized with enhanced chemiluminescence (Amersham Corp.).

Immunocytochemistry—Immunocytochemical studies of transiently transfected COS-1 cells grown on plastic coverslips were performed 2 days following transfection. Coverslips were washed with PBS and fixed in 3% paraformaldehyde in PBS for 20 min. Cells were then permeabilized with 0.1% Nonidet P-40 in PBS for 10 min, washed with PBS, blocked with 10% fetal calf serum at 37 °C for 15 min, and incubated with rabbit anti-GKLF serum (1:500 dilution) in PBS at room temperature for 1 h. After washing with PBS, the coverslips were incubated with fluorescein isothiocyanate-conjugated goat anti-rabbit IgG (1:200 dilution) at room temperature for 1 h, mounted in 25% glycerol with 1 mg/ml phenylenediamine, and visualized with a Zeiss Axioskop 20 microscope equipped for epifluorescence. For bromodeoxyuridine (BrdUrd) labeling, cells were first fed DMEM with 0.5% FCS for 24 h after transfection, followed by DMEM with 10% FCS and 100 μM BrdUrd (Sigma) for an additional 24 h. Coverslips bearing transfected cells were washed with PBS, fixed with 3% paraformaldehyde in PBS, permeabilized with 0.25% Triton X-100 in PBS for 10 min, and washed with PBS followed by water. Coverslips were then treated with 2 N HCl at room temperature for 30 min to denature the DNA, neutralized with 0.1 M sodium borate at room temperature for 5 min, and washed with PBS. A mouse monoclonal antibody raised against BrdUrd (1:5 dilution; Sigma B-2531) was then added to the coverslips at 37 °C for 2 h. Following washing with PBS, rabbit anti-GKLF serum (1:2000 dilution) was added to the coverslips at room temperature for 15 min, after which they were washed with PBS. Coverslips were subsequently incubated with a mixture of fluorescein isothiocyanate-conjugated goat anti-rabbit IgG (1:200) and Texas Red-conjugated sheep anti-mouse IgG (1:20) at 37 °C for 1 h, mounted, and visualized with a fluorescence microscope as described above.

RNA Isolation and Northern Blot Analysis—RNA was isolated from NIH 3T3 cells and from various mouse tissues by the guanidinium thiocyanate method (Chirgwin *et al.*, 1979). Twenty μg of total RNA were size-fractionated in 1.2% agarose gels containing 2.4 M formaldehyde (Ausubel *et al.*, 1991) and transblotted onto nylon membranes (Hybond-N, Amersham Corp.). Hybridizations and washings were performed under high stringency conditions as described by Oliva *et al.* (1993) using a radioactively labeled *GKLF* cDNA probe. To control for loading of RNA samples, all blots were stripped and reprobed with a radioactively labeled DNA fragment encoding the 18 S ribosomal RNA gene and, in some cases, with a cDNA fragment encoding the constitutively expressed glyceraldehyde-3-phosphate dehydrogenase gene (CLONTECH, Palo Alto, CA). When RNA from fractionated colonic tissue was used, the inner surface of an everted piece of freshly obtained mouse colon was gently scraped with a razor blade, and RNA was isolated as described above. This method yields a highly enriched population of cells of epithelial origin as noted before (Oliva *et al.*, 1993).

In Situ Hybridization—A 575-bp *Pf*MI-*Kpn*I restriction endonuclease fragment of the *GKLF* cDNA was subcloned into pBluescript, and the recombinant plasmid was used to generate ^{35}S-labeled antisense or sense RNA probe by *in vitro* transcription using T7 or T3 RNA polymerase, respectively. Freshly isolated mouse colon was fixed in 10% buffered Formalin solution, embedded in paraffin, sectioned into 5-μm slices, and layered onto microscope slides. Slides were processed for *in situ* hybridization as described previously (Tietjen *et al.*, 1994a, 1994b) and probed with either the antisense or control sense probe at high stringency. After washing, slides were submerged in Kodak NTB-2 liquid emulsion and stored in light-proof boxes. After development, slides were counterstained with hematoxylin and eosin and viewed under dark-field microscopy.

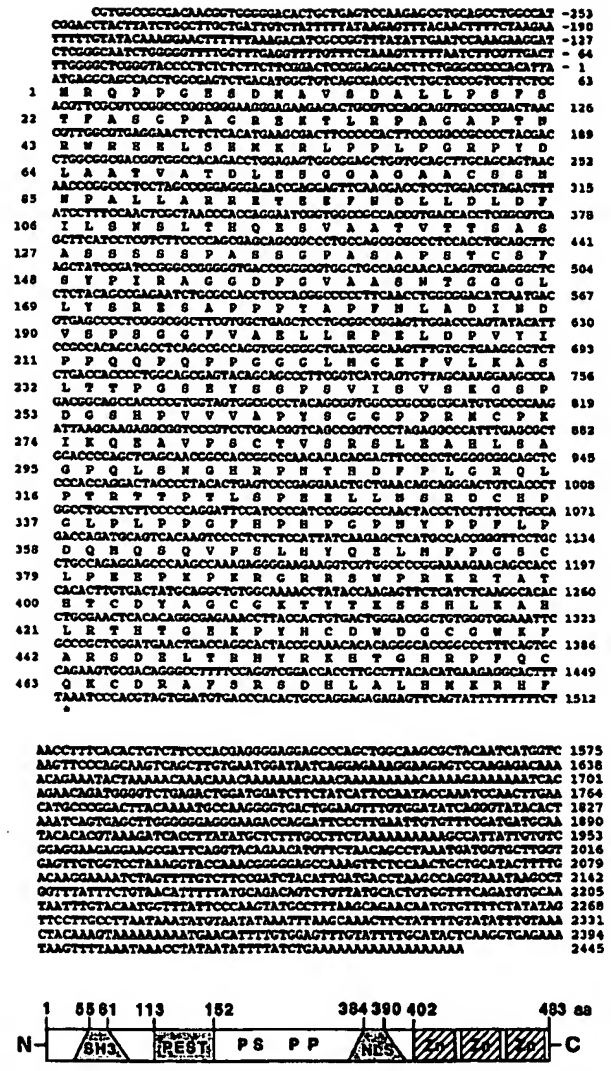

FIG. 1. **Complete nucleotide and deduced amino acid sequences of the *GKLF*.** *Numbers* on the left refer to the amino acid sequence, and those on the right refer to the nucleotide sequence. Diagrammed beneath the sequence is a schematic presentation of the GKLF open reading frame. *N*, amino terminus; *C*, carboxyl terminus. The *hatched areas* represent the three zinc fingers (*Zn*). The *three shaded areas* are (1) a putative sequence recognized by SH3 domain-containing proteins (SH3), (2), a PEST sequence (*PEST*), and (3) a potential nuclear localization signal (*NLS*). *P* and *S* depict the proline- and serine-rich regions. The nucleotide and amino acid sequences have been deposited in GenBank™ under the accession number U20344.

RESULTS

Cloning of Mouse GKLF cDNA—To identify transcription factors that are involved in growth regulation, a cDNA library generated with mRNA from NIH 3T3 cells that were rendered quiescent and stimulated with serum for 3 h (Lanahan *et al.*, 1992) was screened under reduced stringency conditions with a DNA probe containing the zinc finger region of the immediate-early transcription factor zif/268 (Christy *et al.*, 1988). Partial sequence analysis of the cDNA insert of a positive clone, A14, showed that it did not have any significant sequence identity to those stored in the GenBank™ DNA data base. The 1.9-kilobase insert of the A14 clone was used to rescreen the same library under high stringency hybridizing and washing conditions, which resulted in the identification of >50 positive clones. The clone with the longest insert, which we later named *GKLF*, was chosen for further analysis. Its complete nucleotide sequence was determined and is shown in Fig. 1.

Analysis of GKLF cDNA and Deduced Amino Acid Sequences—The *GKLF* cDNA contains a 311-bp 5′-untranslated region, a single ORF of 1449 bp, and a 977-bp 3′-untranslated region that is trailed by a poly(A) tail. The ORF potentially encodes a polypeptide of 483 amino acids with a predicted molecular mass of 53 kDa. Three potential methionine initiation codons are present in frame near the amino terminus (amino acids 1, 10, and 51), although nucleotide sequences surrounding the second methionine codon conform more closely to Kozak's rule for translation initiation (Kozak, 1987). A consensus sequence for polyadenylation, AATAAA (Proudfoot and Brownlee, 1976), is found 24 bp upstream of the poly(A) tail.

The deduced GKLF amino acid sequence contains three tandem zinc finger motifs at the carboxyl terminus. The three zinc fingers are closely related to the consensus sequence $CX_{2-4}CX_3FX_5LX_2HX_3H$ for zinc finger-containing transcription factors and are separated from each other by a 7-amino acid inter-finger spacer similar to the H/C link consensus sequence, TGEKP(Y/F)*X*. These features classify GKLF as a member of the Krüppel family of proteins (Chowdhury *et al.*, 1987; Morris *et al.*, 1994; Schuh *et al.*, 1986). GKLF is rich in proline and serine residues, which constitute 12.8 and 11.6% of the total amino acids, respectively. The clustering of these 2 amino acids is reminiscent of the transactivation domains of previously established transcription factors (Nakamura *et al.*, 1993). In addition, a potential nuclear localization signal (Boulikas, 1993) that is rich in arginine and lysine residues is found between amino acid residues 384 and 390. A "PEST" sequence, which is found in proteins with intracellular half-lives of <2 h (Rogers *et al.*, 1986), is present between amino acid residues 113 and 152. Finally, a 7-amino acid sequence, PPLPGRP, present between amino acid residues 55 and 61, is highly related to the consensus sequence to which proteins containing the SH3 domain bind (Alexandropoulos *et al.*, 1995; Ren *et al.*, 1993). Taken together, these features suggest that GKLF is a nuclear-localized transcription factor.

A search in the GenBank™ protein data base for amino acid sequences related to that of GKLF revealed many sequences similar to its zinc finger-containing region. In particular, the closest alignment was found with three recently identified eukaryotic transcription factors: 1) the lung Krüppel-like factor (LKLF) (Anderson *et al.*, 1995); 2) EKLF (Miller and Bieker, 1993); and 3) basic transcription element-binding protein 2 (BTEB2) (Sogawa *et al.*, 1993), expressed in the placenta and testis. The degree of sequence identity in the 82-amino acid zinc finger region of GKLF to these proteins is 92, 84, and 82%, respectively (Fig. 2). Other sequences that are related (but less conserved) to the zinc finger region of GKLF include WT1 (Call *et al.*, 1990) and Sp1 (Kadonaga *et al.*, 1987), showing 59 and 52% sequence identity, respectively. In contrast, the amino acid sequence outside the zinc finger region of GKLF bears no significant homology to any previously identified proteins with one notable exception: the 20 amino acids immediately preceding the first cysteine residue of the first zinc finger are 90% identical between GKLF and LKLF (Anderson *et al.*, 1995). These findings indicate that GKLF is a newly identified polypeptide.

When the nucleotide sequence of *GKLF* was compared with those stored in the GenBank™ nucleic acid data base, two additional cDNA clones with significant homology were identified. Both sequences correspond to the extreme 3′-end of the 3′-untranslated region of the *GKLF* cDNA. The first (GenBank™ accession number D25944) was obtained during a ran-

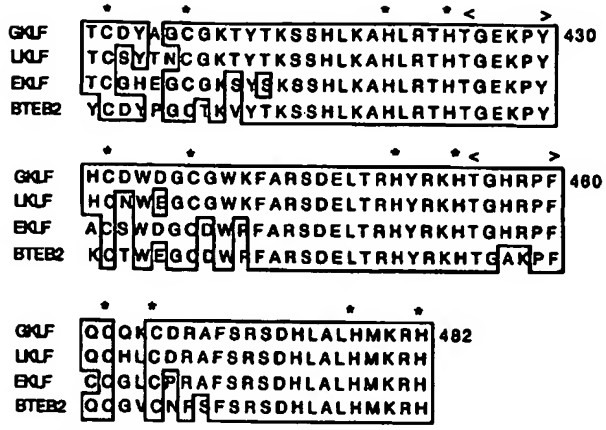

FIG. 2. **Amino acid sequence alignment between GKLF, LKLF, EKLF, and BTEB2.** The sequences presented are those from the zinc finger regions of the four proteins. The species from which the sequences are derived are as follows: GKLF, mouse (this study); LKLF, mouse (Anderson *et al.*, 1995); EKLF, mouse (Miller and Bieker, 1993); and BTEB2, human (Sogawa *et al.*, 1993). Identical sequences are *boxed*. *Numbers* on the right are the amino acid positions of the GKLF sequence. *Asterisks* indicate those amino acid residues involved in the coordination of the zinc atom, and the two inter-finger spacer regions that are highly conserved in the Krüppel family of transcription factors are bracketed (<>).

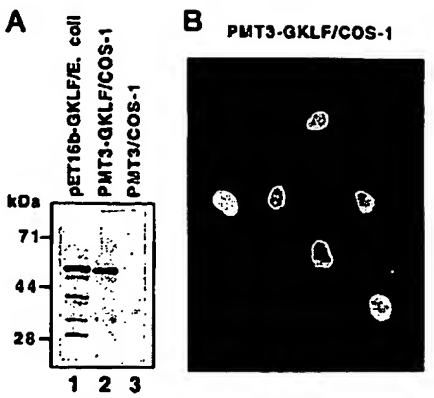

FIG. 3. **Immunodetection of GKLF.** *A*, Western blot analysis of protein extracts (20 μg) from the BL21(DE3) strain of *E. coli* cells transformed with pET16b-GKLF (*lane 1*) and induced with isopropyl-β-D-thiogalactopyranoside and from COS-1 cells transiently transfected with PMT3-GKLF (*lane 2*) or PMT3 (*lane 3*) using anti-GKLF serum. Molecular mass markers are shown on the left. GKLF was seen as a single prominent band in both *lanes 1* and *2*. The minor low molecular mass protein bands noted were variable among different experiments and probably represented degradation products. *B*, Indirect immunofluorescence of COS-1 cells transiently transfected with PMT3-GKLF and immunostained with anti-GKLF serum. Six cells were noted to express GKLF and exhibited intense nuclear staining. In contrast, the nonexpressing cells showed only a background level of cytoplasmic staining.

dom cDNA sequencing analysis of expressed genes in human colonic mucosa.[2] It contains 330 bp of sequence that exhibits 87% nucleotide identity to *GKLF*. The second cDNA, named clone 59 (GenBank™ accession number L26292), was obtained during a differential screening of a cDNA library made from rat Sertoli cells that had been stimulated with follicle-stimulating hormone (Hamil and Hall, 1994). This cDNA is 800 bp long and is 93% identical to the *GKLF* sequence. The high degree of sequence identity in the 3′-untranslated region between *GKLF* and these two partial cDNA clones suggests that the latter two potentially represent the human and rat homologues of *GKLF*, respectively. It is of interest to note that in the mouse, *GKLF* is expressed in the colon and testis (see below).

Characterization of the GKLF Protein—To characterize the protein encoded by *GKLF*, a cDNA fragment containing the ORF was subcloned into two prokaryotic expression vectors, pET3d and pET16b (Studier *et al.*, 1990), the latter creating a fusion protein, which contains an additional 3 kDa of bacterial sequence when expressed. The BL21(DE3) strain of host *E. coli* cells was transformed with pET3d-GKLF and induced with isopropyl-β-D-thiogalactopyranoside to produce GKLF. The protein was resolved by SDS-polyacrylamide gel electrophoresis, purified, and used to generate a rabbit polyclonal antiserum. The same *GKLF* ORF cDNA fragment was also cloned into the mammalian expression vector PMT3 (Swick *et al.*, 1992), and the resultant construct was used to express GKLF in transiently transfected COS-1 cells. Fig. 3*A* is an immunoblot of proteins isolated from pET16b-GKLF-transformed *E. coli* and PMT3-GKLF-transfected COS-1 cells. A single prominent polypeptide band with an apparent molecular mass of 56 kDa from the transformed and isopropyl-β-D-thiogalactopyranoside-induced bacteria was detected by anti-GKLF serum (*lane 1*). Similarly, a polypeptide band of 53 kDa was detected in lysates of COS-1 cells transiently transfected with PMT3-GKLF (*lane 2*). The higher apparent molecular mass of GKLF in *lane 1* was due to the presence of bacterial sequence in the recombinant protein. In contrast, no antigens were detected by anti-GKLF serum in lysates of COS-1 cells transfected with the PMT3 vector only (*lane 3*), indicating that these cells contained little or no endogenous GKLF. The specificity of the antiserum was demonstrated by the ability of purified, bacterially produced GKLF to block the immunoreactivity of the 53-kDa protein band in PMT3-GKLF-transfected COS-1 cells (data not shown).

The intracellular localization of GKLF in mammalian cells was examined by indirect immunofluorescence analysis of COS-1 cells transiently transfected with PMT3-GKLF using anti-GKLF serum. As shown in Fig. 3*B*, GKLF was primarily localized to the cell nucleus in cells that expressed the transfected gene. In contrast, nonexpressing cells showed staining only at background levels (Fig. 3*B*), as did cells transfected with the PMT3 vector alone and immunostained under identical conditions (data not shown).

Expression of GKLF in Response to Serum Stimulation in Cultured Fibroblasts—GKLF was isolated from an NIH 3T3 cDNA library generated with RNA from cells that had been rendered quiescent and then stimulated for 3 h with serum. The serum responsiveness of *GKLF* in NIH 3T3 cells was therefore examined by Northern blot analysis. The mRNA content of *GKLF* from growth-arrested quiescent NIH 3T3 cells (which had been maintained in 0.5% FCS for 5 days) was compared with that from cells induced to enter the cell cycle by the addition of medium containing 15% FCS for various lengths of time between 0 and 24 h. In addition, RNA isolated from proliferating cells in the exponential phase of growth was analyzed. As shown in Fig. 4, it is apparent that a significant level of *GKLF* mRNA was present in quiescent cells (*lane 2*), but was nearly absent in actively proliferating cells (*lane 1*). The addition of 15% FCS not only failed to increase the abundance of *GKLF* mRNA, but a decrease in the message content was detected beginning at 8 h after treatment. By 24 h after serum stimulation, a partial recovery of the *GKLF* mRNA level was observed. Fig. 5 summarizes the results of quantitative densitometric measurements of mRNA band intensities from Northern blot analyses of three independent experiments. The data confirmed that the level of *GKLF* transcript was much higher

[2] K. Okubo, unpublished data.

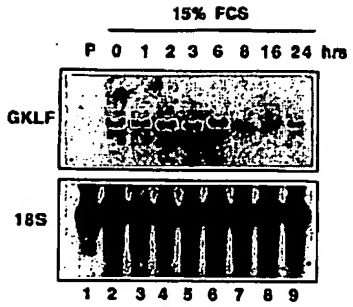

FIG. 4. **Time course of GKLF expression in serum-starved NIH 3T3 cells stimulated with 15% FCS.** NIH 3T3 fibroblasts were rendered quiescent by maintenance in DMEM containing 0.5% FCS for 5 days, at which time they were ~50% confluent (*lane 2* or *time 0*). Cells were stimulated to enter the cell cycle by the addition of fresh DMEM containing 15% FCS for various periods of time between 1 and 24 h. Total RNA was isolated from cells at the times indicated, and 20 μg were examined by Northern blot analysis using a radioactively labeled *GKLF* cDNA probe. RNA from exponentially proliferating, nonsynchronized cells (*lane 1* or *P*), maintained in DMEM supplemented with 10% FCS at ~30% confluency, was also examined for comparison. To control for RNA loading, the blot was subsequently stripped and reprobed with a DNA fragment encoding the 18 S ribosomal RNA gene.

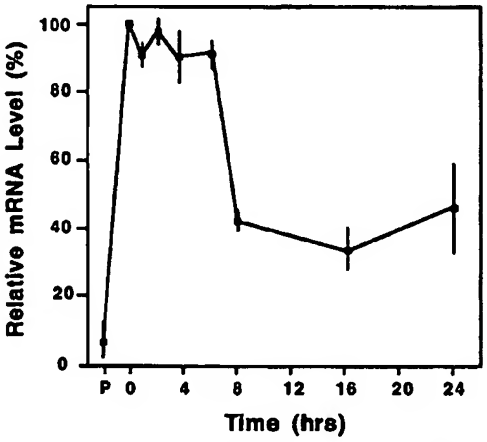

FIG. 5. **Quantification of *GKLF* expression during serum stimulation of quiescent NIH 3T3 cells.** Densitometric tracings of mRNA band intensities at different times following serum stimulation were performed, and the values were standardized to that of the mRNA level observed in quiescent (time 0) cells, taken as 100%. Shown are the mean values of three independent experiments. The *vertical bars* represent standard errors. *P* denotes proliferating cells.

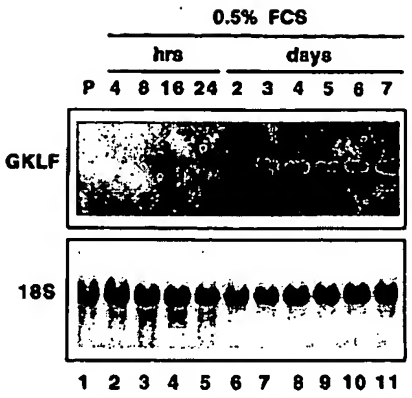

FIG. 6. **Time course of *GKLF* expression during serum starvation.** Proliferating NIH 3T3 cells (*lane 1* or *P*) in DMEM supplemented with 10% FCS were fed DMEM containing 0.5% FCS for various periods of time as indicated. Media were changed every other day. Northern blot analysis of 20 μg of total RNA was performed as described for Fig. 4.

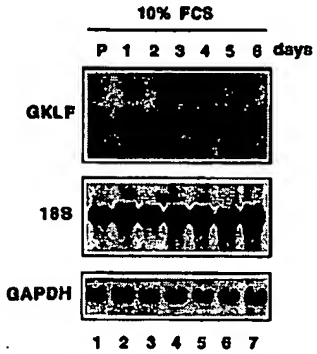

FIG. 7. **Effect of contact inhibition on *GKLF* expression.** Proliferating NIH 3T3 cells (*lane 1* or *P*) were maintained in DMEM containing 10% FCS without any additional feedings for up to 6 days. The initial cell density was ~30%. By day 2, all the dishes were nearly 100% confluent. Northern blot analysis of 20 μg of total RNA was performed as described for Fig. 4. To control for RNA loading, the blot was stripped and sequentially reprobed with the DNA encoding the 18 S ribosomal RNA gene, followed by the cDNA encoding glyceraldehyde-3-phosphate dehydrogenase (*GAPDH*).

in growth-arrested cells compared with proliferating cells and that when cells were induced to enter the cell cycle, a reproducible decrease in the transcript level was observed beginning at a time period that precedes the commencement of DNA synthesis in NIH 3T3 cells (Quelle *et al.*, 1993).

The growth arrest-specific nature of *GKLF* expression was confirmed by a reverse experiment to that of Fig. 4 in which NIH 3T3 cells in the exponential phase of proliferation were induced to enter quiescence by a reduction of the serum content in the medium from 10 to 0.5% for various lengths of time. Fig. 6 shows that the initial *GKLF* transcript was barely detectable, which only became apparent beginning 2 days after the cells were deprived of serum. A further increase in the *GKLF* mRNA level was seen between days 2 and 3, after which nearly equivalent levels of transcript were present up to 7 days. Similarly, when actively proliferating NIH 3T3 cells were left in 10% FCS without any additional feedings, levels of *GKLF* mRNA increased in a time-dependent manner (Fig. 7). This result was in clear contrast to the largely constant levels of the 18 S ribosomal RNA and of the mRNA encoding glyceraldehyde-3-phosphate dehydrogenase (Fig. 7). In this experiment, cell-to-cell contact seemed to play a role in the increased expression of *GKLF* as cells were fully confluent by day 2 of the experiment. Taking the results of Figs. 6 and 7 together, it appears that expression of *GKLF* is correlated with quiescence induced by serum deprivation and withdrawal from the cell cycle due to contact inhibition.

Effect of Constitutive GKLF Expression on DNA Synthesis—The results of the preceding experiments suggest that expression of *GKLF* is temporally associated with growth arrest and that a down-regulation of *GKLF* occurs in cells that are stimulated to enter the cell cycle. To assess the effect of constitutive expression of *GKLF* on cell growth, COS-1 cells were transiently transfected with PMT3-GKLF or PMT3 for 24 h, at which time DNA synthesis was determined by [^{3}H]thymidine incorporation. Table I shows the results of three independent experiments. In each experiment, the percentage of cells expressing GKLF in PMT3-GKLF-transfected cells was determined in parallel dishes by indirect immunofluorescence and found to vary between 25 and 30%. As shown, a statistically significant decrease in the incorporation of [^{3}H]thymidine by

TABLE I
[³H]Thymidine incorporation into PMT3-GKLF- and PMT3-transfected COS-1 cells

All experiments were performed in 3.5-cm culture dishes, and [³H]thymidine incorporation was performed 24 h after transfection.

Construct	[³H]Thymidine incorporation[a]	n[b]	p[c]	Inhibition by GKLF
				%
Exp. 1				
PMT3	588.3 ± 84.9	6	<0.01	31.3
PMT3-GKLF	403.4 ± 66.4	6		
Exp. 2				
PMT3	433.5 ± 90.3	12	<0.001	26.3
PMT3-GKLF	319.7 ± 65.0	12		
Exp. 3				
PMT3	319.3 ± 40.8	12	<0.0001	28.2
PMT3-GKLF	229.0 ± 52.5	12		

[a] [³H]Thymidine incorporated was measured in triplicate over a 3-h period from one-tenth of the entire cell population in each dish. Data represent the mean ± S.D. for each construct.
[b] Number of dishes assayed.
[c] Statistical analysis was performed using the one-tailed *t* test.

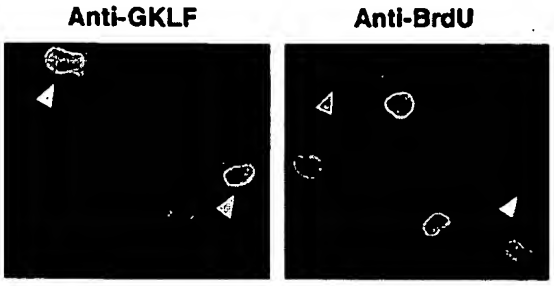

FIG. 8. **Inhibition of DNA synthesis by constitutive expression of GKLF.** COS-1 cells were transiently transfected with PMT3-GKLF as described under "Experimental Procedures." Following transfection, cells were fed DMEM containing 0.5% FCS for 24 h, after which they were refed DMEM containing 10% FCS and 100 μM BrdUrd for an additional 24 h before being processed for immunocytochemical analysis. Cells were immunostained first with a mouse monoclonal BrdUrd antibody, followed by rabbit anti-GKLF serum. The secondary antibodies used were fluorescein isothiocyanate-conjugated goat anti-rabbit IgG (*left panel*) and Texas Red-conjugated sheep anti-mouse IgG (*right panel*). The *arrowheads* point to two GKLF-positive and BrdUrd-negative cells, whereas four other cells in the same field were GKLF-negative and BrdUrd-positive.

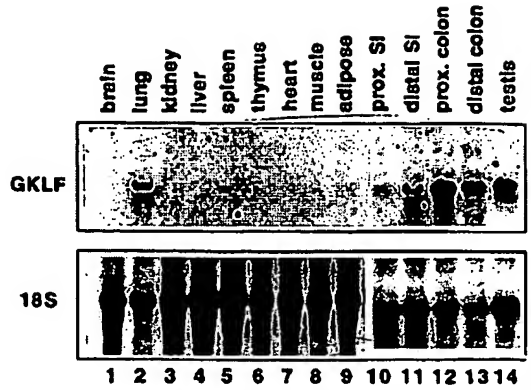

FIG. 9. **Tissue distribution of *GKLF mRNA*.** RNA was extracted from various mouse tissues, and 20 μg were analyzed by Northern blot hybridization as described for Fig. 4. *SI*, small intestine; *prox.*, proximal.

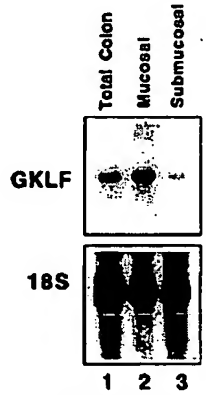

FIG. 10. **Distribution of *GKLF mRNA* in a fractionated mouse colon.** The inner surface of a mouse colon was scraped with a razor blade to give rise to the mucosal fraction of cells from which RNA was extracted (*lane 2*). As a comparison, RNA was also extracted from the remaining tissue (*lane 3*). *Lane 1* represents RNA obtained from an intact colon. Twenty μg of total RNA were analyzed by Northern blot hybridization.

cells transfected with PMT3-GKLF as compared with cells transfected with vector alone was observed in all three experiments. The close correlation between the degree of inhibition of [³H]thymidine incorporation into PMT3-GKLF-transfected cells and the percentage of cells expressing *GKLF* suggests that GKLF, when constitutively expressed, inhibits DNA synthesis.

To demonstrate directly that the cells expressing GKLF do not synthesize DNA, PMT3-GKLF-transfected COS-1 cells were first incubated with BrdUrd and then double-stained for GKLF and BrdUrd by indirect immunofluorescence. As shown in Fig. 8, two cells that expressed GKLF (*arrowheads*) failed to stain for BrdUrd. In contrast, four non-GKLF-expressing cells were positive for BrdUrd. After counting 100 consecutive GKLF-expressing cells, only five were noted to positively stain for BrdUrd, whereas >80% of the non-GKLF-expressing cells were BrdUrd-positive.

Tissue Distribution of GKLF—To determine the tissue distribution of *GKLF*, RNA was isolated from various adult mouse tissues and examined by Northern blot analysis. Of the tissues examined, the colon (both proximal and distal) contained the highest level of *GKLF* transcript (Fig. 9). Moderate levels of transcript were also noted in the distal small intestine (*SI*), testis, and lung. In addition, a small amount of *GKLF* transcript was present in the proximal small intestine. Smaller mRNA species were also noted in the intestinal tissues and testis and could represent other closely related sequences or products of alternative splicing. No appreciable amount of message was detected in the brain, kidney, liver, spleen, thymus, heart, muscle, and fat. These results indicate that the expression of *GKLF* is tissue-selective and is most abundant in the colon.

The mouse colon is composed of a heterogeneous population of cells, ranging from the epithelial cells lining the inner mucosal surface to various other non-epithelial cell types such as lymphocytes, fibroblasts, enteric neurons, and smooth muscle cells. To further localize the cellular origin of *GKLF*, Northern blot analysis was performed on RNA isolated from colonic mucosal scrapings (Fig. 10, *lane 2*), which represent an enrichment of the epithelial cell population as previously demonstrated (Oliva *et al.*, 1993). As a comparison, Northern blot analysis was also performed on RNA isolated from the remaining colonic tissue after scraping (Fig. 10, *lane 3*). As shown, *GKLF* mRNA was highly enriched in the mucosal population of cells, suggesting that *GKLF* is mainly expressed in epithelial cells. The epithelium-specific expression of *GKLF* was confirmed by *in situ* hybridization. Fig. 11*A* shows that the antisense *GKLF* RNA probe hybridized primarily to the middle to

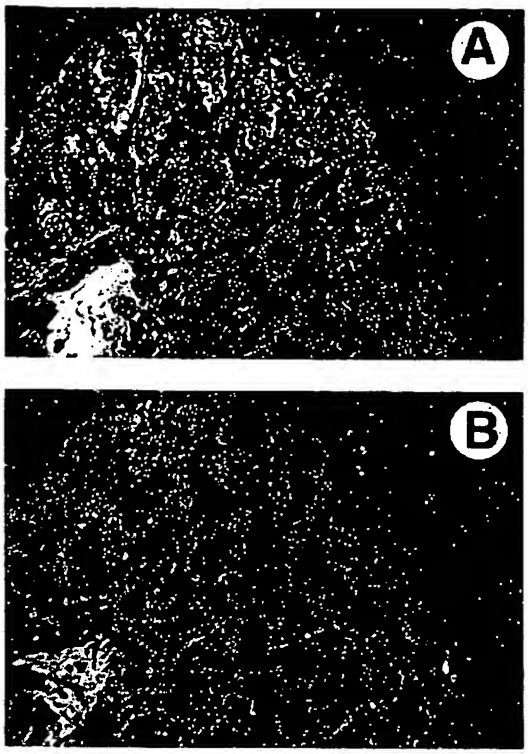

FIG. 11. ***In situ* hybridization analysis of *GKLF* expression in the colon.** An adult mouse colon was fixed, sectioned, and processed for *in situ* hybridization as described under "Experimental Procedures" using ^{35}S-labeled antisense GKLF RNA probe (*A*) or control sense RNA probe (*B*). The sections were counterstained with hematoxylin and eosin and visualized by dark-field microscopy. The *bright areas* in the submucosal fractions of both panels represent a refractory material and are not silver grains.

upper region of the colonic crypt epithelium. In contrast, the control sense *GKLF* RNA probe produced a random background distribution of silver grains (Fig. 11*B*). These results indicate that *GKLF* is epithelium-specific and is expressed primarily in cells that are in the process of migrating from the base toward the top of the crypt.

DISCUSSION

The cDNA encoding GKLF was isolated by low stringency hybridization to a zinc finger-containing transcription factor, zif/268. Although not proven in this study, several features of GKLF strongly suggest that it is a transcription factor. First, the amino acid sequence at the carboxyl terminus containing the zinc fingers is similar to those of a number of proteins, many of which are proven transcription factors, such as LKLF, EKLF, and BTEB2 (Fig. 2). Second, GKLF contains a potential nuclear localization signal between amino acid residues 384 and 390 and is in fact localized to the cell nucleus in transfected cells (Fig. 3). Third, like many transcription factors with short half-lives (Chevaillier, 1993), GKLF contains a PEST sequence with a high PEST score of 5.8 (Rogers *et al.*, 1986). Finally, GKLF contains abundant proline and serine residues, amino acid residues purportedly involved in the transactivation function of many transcription factors (Nakamura *et al.*, 1993). Furthermore, its proline-rich nature is shared by proteins closely related to GKLF, namely LKLF (Anderson *et al.*, 1995), EKLF (Miller and Bieker, 1993), and BTEB2 (Sogawa *et al.*, 1993). Based on the high degree of homology in the Krüppel region of the proteins and their proline-rich characteristics, the latter three transcription factors have recently been assigned

TABLE II

Amino acid sequence and DNA binding sequence comparison of GKLF with other Krüppel-like proteins

TF[a]	Finger[b]	Amino acid sequence[c]	Binding sequence[d]	Ref.
		1		
GKLF	1	KSSHLKA		
	2	RSDELTR		
	3	RSDHLAL		
BTEB2	1	KSSHLKA	GGG-3'	Sogawa *et al.* (1993)
	2	RSDELTR	GCG	
	3	RSDHLAL	5'-GGG	
EKLF	1	KSSHLKA	TGG-3'	Miller and Bieker (1993)
	2	RSDELTR	GTG	
	3	RSDHLAL	5'-AGG	
Sp1	1	KTSHLRA	GGG-3'	Berg (1992)
	2	RSDELQR	GCG	
	3	RSDHLSK	5'-GGG	
zif/268	1	RSDELTR	GCG-3'	Cao *et al.* (1993)
	2	RSDHLTT	GGG	
	3	RSDERKR	5'-GCG	

[a] Transcription factor.
[b] Fingers are numbered from the amino terminus to the carboxyl terminus.
[c] Amino acid sequences shown are those present in the α helical region of each zinc finger. Each helix begins at the position marked 1.
[d] The DNA binding sequences begin at the bottom left corner (5'-) and end at the upper right corner (3').

to a new multigene family (Anderson *et al.*, 1995). GKLF is thus the newest addition to this protein family.

Aside from the proline-rich domain of GKLF, amino acid sequence outside its zinc finger region further defines its phylogenetic origin. For example, absent from the GKLF sequence are the FAX (finger-associated box) (Knochel *et al.*, 1989) and KRAB (Krüppel-associated box) (Bellefroid *et al.*, 1991) motifs, the latter estimated to be present in one-third of zinc finger-containing transcription factors. Genes encoding the FAX- and KRAB-containing zinc finger proteins (called class 1 zinc finger proteins by Pieler and Bellefroid (1994)) are generally organized in large clusters on certain chromosomes and are thought to have appeared late during evolution. Most of these genes are widely expressed in adult tissues and in most stages of embryogenesis. The Krüppel family of transcription factors (called class 2 zinc finger proteins by Pieler and Bellefroid (1994)), in contrast, includes fewer members that are highly conserved and that function in the context of cell differentiation and embryogenesis. The majority of class 2 zinc finger proteins exhibit highly restricted patterns of expression in tissues and during embryogenesis. The tissue-selective nature of *GKLF* and its close relationship with other Krüppel-like factors such as *LKLF* and *EKLF* indicate that it belongs to the class 2 zinc finger protein gene family according to the classification of Pieler and Bellefroid (1994).

Structural analysis of zinc finger-containing proteins indicates that each finger consists of a β-pleated sheet at the amino-terminal half and an α-helix at the carboxyl-terminal half and that the latter makes direct contact with DNA (Berg, 1990). A number of studies examined the relationship between the amino acid sequence in the helical portion of a finger and the DNA sequence to which the finger binds (Berg, 1992; Klug and Schwabe, 1995; Nardelli *et al.*, 1991). These studies revealed a number of important conclusions that enable one to predict the DNA sequence to which a zinc finger protein may bind. Table II compares the amino acid sequences in the α-helical portions of each of the three zinc fingers of GKLF to those of several other Krüppel-like transcription factors along with the DNA sequences with which the fingers interact. It is ap-

parent that amino acid sequences in the helical region of each of the three zinc fingers of GKLF, BTEB2, and EKLF are identical. Moreover, finger 2 of GKLF is identical to finger 1 of zif/268 and nearly identical to finger 2 of Sp1 as well as finger 3 of zif/268. With the exception of EKLF, these amino acid sequences recognize the consensus trinucleotide GCG. In addition, finger 1 of GKLF is highly similar to finger 1 of Sp1, which binds the trinucleotide GGG. Finally, finger 3 of GKLF is very similar to finger 3 of Sp1 and finger 2 of zif/268, both of which bind to the sequence GGG. Based on these comparisons, one can predict a sequence of 5′-GGG GCG GGG-3′ to which GKLF is potentially capable of binding. This sequence is identical to the binding sequences of BTEB2 and Sp1. Of note is that although EKLF recognizes a different DNA sequence despite an overall identity in the zinc finger sequences, it is capable of interacting with an Sp1-binding site (Hartzog and Myers, 1993).

The expression of *GKLF* in cultured fibroblasts is of interest. The cDNA library from which *GKLF* was initially derived was made with RNA from quiescent NIH 3T3 cells that had been stimulated with serum for 3 h. Because the number of positive clones obtained during a repeat screening of the same library with a partial *GKLF* cDNA fragment was quite high (>50 positive plaques out of a total of 1 million), we initially thought that *GKLF*, like *zif/268*, would behave like an immediately-early gene. We were therefore surprised to find from the Northern blot experiment shown in Fig. 4 that *GKLF* behaved quite differently from *zif/268* or other immediate-early genes. The differences include the following. 1) The steady-state *GKLF* transcript level was high in serum-starved quiescent NIH 3T3 cells. 2) The transcript level did not rise appreciably during the first few hours of serum induction. 3) The transcript level began to fall at 8 h of serum treatment. In addition, the *GKLF* transcript was nearly undetectable in RNA harvested from exponentially proliferating cells. Combining the results of serum stimulation (Figs. 4 and 5), serum starvation (Fig. 6), and contact inhibition (Fig. 7) experiments, it becomes apparent that expression of *GKLF* is associated with cessation of cell growth. It is especially of interest to note that in serum-stimulated cells, the *GKLF* transcript level first decreases at a time that immediately precedes the S phase of the cell cycle (Figs. 4 and 5) (Quelle *et al.*, 1993). This observation suggests that GKLF may exhibit a negative effect on cell cycle progression, particularly at the G_1/S transition phase. The diminished [^{3}H]thymidine incorporation by cells in which *GKLF* was constitutively expressed (Table I) and the lack of BrdUrd uptake by cells expressing *GKLF* (Fig. 8) support this hypothesis.

The expression of *GKLF* in response to serum stimulation and deprivation in cultured fibroblasts is reminiscent of that of a group of genes exclusively expressed in the growth arrest state. These genes are divided into two categories: the *gas* (growth arrest-specific) genes (Ciccarelli *et al.*, 1990; Gorski *et al.*, 1993) and the *gadd* (growth arrest- and DNA damage-inducible) genes (Fornance *et al.*, 1989; Zhan *et al.*, 1994). Like *GKLF*, expression of the *gas* genes is highest in quiescent cells and is down-regulated following mitogen stimulation. In particular, the time course of expression of *GKLF* following mitogen addition to quiescent cells (Figs. 4 and 5), serum deprivation (Fig. 6), and cell contact (Fig. 7) is remarkably similar to that for *gas1* (Ciccarelli *et al.*, 1990; Schneider *et al.*, 1988) and *gas5* (Ciccarelli *et al.*, 1990). Similar to the inhibitory effect of *GKLF* on DNA synthesis (Table I), when ectopically expressed, some of the *gas* genes cause growth arrest and are thought to be involved in a negative circuit that governs growth suppression (Del Sal *et al.*, 1992). Nevertheless, despite an overall similarity in the pattern of expression of the *gas* gene family, they encode a diverse group of protein products. For example, *gas1* and *gas3* encode integral membrane proteins (Del Sal *et al.*, 1992; Manfioletti *et al.*, 1990); *gas2* encodes a protein of the microfilament network system (Brancolini *et al.*, 1992); and *gas6* encodes a secreted, vitamin K-dependent protein that is a ligand for the Axl receptor tyrosine kinase (Varnum *et al.*, 1995). The *gax* gene (growth arrest-specific homeobox) is a notable exception of the *gas* gene family in that it encodes a homeobox-containing transcription factor that is highly specific for vascular smooth muscle cells (Gorski *et al.*, 1993). Finally, *gadd153*, the only *gadd* gene with an identified function, is a member of the C/EBP family of transcription factors and is the human homologue of the murine *CHOP-10* gene (Ron and Habener, 1992).

In vivo, the expression of *GKLF* is highly tissue-selective and is enriched in regions of the intestinal tract, testis, and lung (Fig. 9). It is of interest to note that a partial cDNA fragment encoding the putative rat homologue of *GKLF* was identified in Sertoli cells that had been treated with follicle-stimulating hormone (clone 59) (Hamil and Hall, 1994). Other than its induction by follicle-stimulating hormone, little information regarding the expression of clone 59 is available. *In situ* hybridization experiments should help clarify the cellular origin of *GKLF* in the testis. It is clear from Figs. 10 and 11, however, that expression of *GKLF* in the colon is highly enriched in the crypt epithelium. This finding is supported by the cloning of a putative human homologue of *GKLF* from the colonic mucosa (see "Results"). Moreover, results of *in situ* hybridization indicate that the *GKLF* transcript is localized to a population of epithelial cells residing in the middle to upper crypt region. This portion of the colonic crypt is thought to consist of cells that have undergone growth arrest and that have begun to differentiate into mature colonocytes as they emerge from the proliferating compartment at the base of the crypt (Gordon *et al.*, 1992). Thus, GKLF may play two potential physiological roles in this environment. It can act either as a growth-suppressing gene product that is involved in the growth arrest of epithelial cells as they exit the base of the crypt or as a differentiation-promoting gene product that is responsible for activating downstream genes that are required for the differentiated epithelial phenotype. These two functions are not mutually exclusive such that GKLF can potentially serve both, in a manner similar to MyoD, which promotes both myogenic differentiation and terminal withdrawal from the cell cycle (Halevy *et al.*, 1995). Clearly, the exact function of GKLF in the cell cycle and/or in terminal differentiation awaits further examination.

Acknowledgments—We thank Dr. Lanahan for providing the NIH 3T3 cDNA library and the Genetics Institute for the PMT3 plasmid. We also thank Dr. Corey Mjaatvedt for assisting in the *in situ* hybridization.

REFERENCES

Alexandropoulos, K., Cheng, G., and Baltimore, D. (1995) *Proc. Natl. Acad. Sci. U. S. A.* 92, 3110–3114
Anderson, K. P., Kern, C. B., Crable, S. C., and Lingrel, J. B. (1995) *Mol. Cell. Biol.* 15, 5957–5965
Ausubel, F. M., Brent, R., Kingston, R. E., Moore, D. D., Seidman, J. G., Smith, J. A., and Struhl, K. (1991) *Current Protocols in Molecular Biology*, 2nd Ed., John Wiley & Sons, Inc., New York
Bellefroid, E. J., Poncelet, D. A., Lecocq, P. J., Revelant, O., and Martial, J. A. (1991) *Proc. Natl. Acad. Sci. U. S. A.* 88, 3608–3612
Berg, J. M. (1990) *Annu. Rev. Biophys. Biophys. Chem.* 19, 405–421
Berg, J. M. (1992) *Proc. Natl. Acad. Sci. U. S. A.* 89, 11109–11110
Boulikas, T. (1993) *Crit. Rev. Eukaryotic Gene Expression* 3, 193–227
Brancolini, C., Bottega, S., and Schneider, C. (1992) *J. Cell Biol.* 117, 1251–1261
Call, K. M., Glaser, T., Ito, C. Y., Buckler, A. J., Pelletier, J., Haber, D. A., Rose, E. A., Kral, A., Yeger, H., Lewis, W. H., Jones, C., and Housman, D. E. (1990) *Cell* 60, 509–520
Cao, X., Mahendran, R., Guy, G. R., and Tan, Y. H. (1993) *J. Biol. Chem.* 268, 16949–16957
Chevaillier, P. (1993) *Int. J. Biochem.* 25, 479–482

Chirgwin, J. M., Przbyla, A. E., MacDonald, R. J., and Rutter, W. J. (1979) *Biochemistry* **18**, 5294–5299
Chowdhury, K., Deutsch, U., and Gruss, P. (1987) *Cell* **48**, 771–778
Christy, B. A., Lau, L. F., and Nathans, D. (1988) *Proc. Natl. Acad. Sci. U. S. A.* **85**, 7857–7861
Ciccarelli, C., Philipson, L., and Sorrentino, V. (1990) *Mol. Cell. Biol.* **10**, 1525–1529
Del Sal, G., Ruaro, M. E., Philipson, L., and Schneider, C. (1992) *Cell* **70**, 595–607
DuBois, R. N., McLane, M. W., Ryder, K., Lau, L. F., and Nathans, D. (1990) *J. Biol. Chem.* **265**, 19185–19191
Felgner, P. L., Gadek, T. R., Holm, M., Roman, R., Chan, H. W., Wenz, M., Northrop, J. P., Ringold, G. M., and Danielsen, M. (1987) *Proc. Natl. Acad. Sci. U. S. A.* **84**, 7413–7417
Fornance, A. J., Nebert, D. W., Hollander, M. C., Luethy, J. D., Papathanasiou, M., Fargnoli, J., and Holbrook, N. J. (1989) *Mol. Cell. Biol.* **9**, 4196–4203
Fraser, P. D., Linden, H., and Sandmann, G. (1993) *Biochem. J.* **291**, 687–692
Gordon, J. I., Schmidt, G. H., and Roth, K. A. (1992) *FASEB J.* **6**, 3039–3050
Gorski, D. H., LePage, D. F., Patel, C. V., Copeland, N. G., Jenkins, N. A., and Walsh, K. (1993) *Mol. Cell. Biol.* **13**, 3722–3733
Halevy, O., Novitch, B. G., Spicer, D. B., Skapek, S. X., Rhee, J., Hannon, G. J., Beach, D., and Lassar, A. B. (1995) *Science* **267**, 1018–1021
Hamil, K. G., and Hall, S. H. (1994) *Endocrinology* **134**, 1205–1212
Hartwell, L. H., and Kastan, M. B. (1994) *Science* **266**, 1821–1828
Hartwell, L. H., and Weinert, T. A. (1989) *Science* **246**, 629–634
Hartzog, G. A., and Myers, R. M. (1993) *Mol. Cell. Biol.* **13**, 44–56
Hoovers, J. M. N., Mannens, M., John, R., Bliek, J., van Heyningen, V., Porteus, D. J., Leschot, N. J., Westerveld, A., and Little, P. F. R. (1992) *Genomics* **12**, 254–263
Kadonaga, J. T., Carner, K. R., Masiarz, F. R., and Tjian, R. (1987) *Cell* **51**, 1079–1090
Kinzler, K. W., Ruppert, J. M., Bigner, S. H., and Vogelstein, B. (1988) *Nature* **332**, 371–374
Klug, A., and Schwabe, J. W. R. (1995) *FASEB J.* **9**, 597–604
Knochel, W., Poting, A., Koster, M., el Baradi, T., Nietfeld, W., Bouwmeester, T., and Pieler, T. (1989) *Proc. Natl. Acad. Sci. U. S. A.* **6**, 6097–6100
Kozak, M. (1987) *Nucleic Acids Res.* **15**, 8125–8148
Laemmli, U. K. (1970) *Nature* **227**, 680–685
Lanahan, A., Williams J. B., Sanders, L. K., and Nathans, D. (1992) *Mol. Cell. Biol.* **12**, 3919–3929
Lau, L. F., and Nathans, D. (1987) *Proc. Natl. Acad. Sci. U. S. A.* **84**, 1182–1186
Lopata, M. A., Cleveland, D. W., and Sollner-Webb, B. (1984) *Nucleic Acids Res.* **12**, 5707–5717
Manfioletti, G., Ruaro, M. E., Del Sal, G., Philipson, L., and Schneider, C. (1990) *Mol. Cell. Biol.* **10**, 2924–2930
Miller, I. J., and Bieker, J. J. (1993) *Mol. Cell. Biol.* **13**, 2776–2786
Morris, J. F., Hromas, R., and Rauscher, F. J. (1994) *Mol. Cell. Biol.* **14**, 1786–1795
Nakamura, T., Alder, H., Gu, Y., Prasad, R., Canaani, O., Kamada, N., Gale, R. P., Lange, B., Crist, W. M., Nowell, P. C., Croce, C. M., and Canaani, E. (1993) *Proc. Natl. Acad. Sci. U. S. A.* **90**, 4631–4635
Nardelli, J., Gibson, T. J., Vesque, C., and Charnay, P. (1991) *Nature* **349**, 175–178
Oliva, M. M., Wu, T. C., and Yang, V. W. (1993) *Arch. Biochem. Biophys.* **302**, 183–192
Pieler, T., and Bellefroid, E. (1994) *Mol. Biol. Rep.* **20**, 1–8
Proudfoot, N. J., and Brownlee, G. G. (1976) *Nature* **263**, 211–214
Quelle, D. E., Ashmun, R. A., Shurtleff, S. A., Kato, J., Bar-Sagi, D., Roussel, M. F., and Sherr, C. J. (1993) *Genes Dev.* **7**, 1559–1571
Ren, R., Mayer, B. J., Cicchetti, P., and Baltimore, D. (1993) *Science* **259**, 1157–1161
Rogers, S., Wells, R., and Rechsteiner, M. (1986) *Science* **234**, 364–368
Ron, D., and Habener, J. F. (1992) *Genes Dev.* **6**, 439–453
Schneider, C., King, R. M., and Philipson, L. (1988) *Cell* **54**, 787–793
Schuh, R., Aicher, W., Gaul, U., Cote, S., Preiss, A., Maier, D., Seifert, E., Nauber, U., Schroder, C., Kemler, R., and Jackle, H. (1986) *Cell* **47**, 1025–1032
Sherr, C. J. (1993) *Cell* **73**, 1059–1065
Sogawa, K., Imataka, H., Yamasaki, Y., Kusume, H., Abe, H., and Fujii-Kuriyama, Y. (1993) *Nucleic Acids Res.* **21**, 1527–1532
Stanojevic, D., Hoey, T., and Levine, M. (1989) *Nature* **341**, 331–335
Studier, F. W., Rosenberg, A. H., Dunn, J. J., and Dubendorff, J. W. (1990) *Methods Enzymol.* **185**, 60–89
Sukhatme, V. P. (1992) *Kidney Int.* **41**, 550–553
Sukhatme, V. P., Cao, X. M., Chang, L. C., Tsai-Morris, C., Stamenkovich, D., Ferreira, P. C. P., Cohen, D. R., Edwards, S. A., Shows, T. B., Curran, T., LeBeau, M. M., and Adamson, E. D. (1988) *Cell* **53**, 37–43
Swick, A. G., Janicot, M., Cheneval-Kastelic, T., McLenithan, J. C., and Lane, M. D. (1992) *Proc. Natl. Acad. Sci. U. S. A.* **89**, 1812–1816
Tietjen, T. G., Mjaatvedt, C. H., and Yang, V. W. (1994a) *Histochem. J.* **26**, 526–532
Tietjen, T. G., Mjaatvedt, C. H., and Yang, V. W. (1994b) *J. Histochem. Cytochem.* **42**, 745–753
Towbin, H., Staehelin, T., and Gordon, J. (1979) *Proc. Natl. Acad. Sci. U. S. A.* **76**, 4350–4354
Varnum, B. C., Young, C., Elliott, G., Garcia, A., Bartley, T. D., Fridell, Y. W., Hunt, R. W., Trail, G., Clogston, C., Toso, R. J., Yanagihara, D., Bennett, L., Sylber, M., Merewether, L. A., Tseng, A., Escobar, E., Liu, E. T., and Yamane, H. K. (1995) *Nature* **373**, 623–626
Zhan, Q., Lord, K. A., Alamo, I., Hollander, M. C., Carrier, F., Ron, D., Kohn, K. W., Hoffman, B., Liebermann, D. A., and Fornance, A. J. (1994) *Mol. Cell. Biol.* **14**, 2361–2371

ILL Document Delivery

REG-14014372

VAUZGE

NLM -- W1 GA458 (GENCOLL); W1 GA458 (REFCOLL); Film S1100

US PATENT AND TRADEMARK OFFICE
SCIENTIFIC AND TECHNICAL INFO CTR
107 S. WEST STREET, PMB 803
ALEXANDRIA, VA 22314

ATTN:
PHONE: 571-272-2550
FAX: 571-272-0230
E-MAIL: STIC-DOCS@uspto.gov

SUBMITTED: 2007-01-18 10:29:18
PRINTED: 2007-01-18 13:24:12
REQUEST NO.: REG-14014372
SENT VIA: DOCLINE
DOCLINE NO: 21661994

REG **Copy** **Journal**

TITLE:	GASTROENTEROLOGY
PUBLICATION PLACE:	Baltimore.
VOLUME/ISSUE/PAGES:	1998;114(4 pt.2):A616-A617 A616-A617
DATE:	1998
ISSN:	0016-5085
OTHER NUMBERS/LETTERS:	
	NLM Unique ID: 0374630
SOURCE:	Unique Key
MAX COST:	$4.00
COPYRIGHT COMP.:	Guidelines
CALL NUMBER:	W1 GA458 (GENCOLL); W1 GA458 (REFCOLL); Film S1100
REQUESTER INFO:	615295
DELIVERY:	E-mail Post to Web: STIC-DOCS@uspto.gov
REPLY:	Mail:

KEEP THIS RECEIPT TO RECONCILE WITH BILLING STATEMENT

For problems or questions, contact NLM at http://wwwcf.nlm.nih.gov/ill/ill_web_form.cfm or phone 301-496-5511.

Include LIBID and request number.

● G2532

ASSOCIATION BETWEEN MANGANESE - SUPEROXIDE DISMUTASE AND THE HUMAN COLORECTAL CANCER SEQUENCE. A.M.L. Janssen, C.B. Bosman, L. Kruidenier, C.F.M. Sier, M.M. Oostendorp-van de Ruit, G. Griffioen, C.B.H.W. Lamers, H.W. Verspaget. Dept. Gastroenterology-Hepatology, Leiden University Medical Center, The Netherlands

The balance between reactive oxygen metabolites and antioxidants, such as Mn (manganese) - and Cu/Zn (copper/zinc) - superoxide dismutase (SOD), is thought to play a role in gastrointestinal cancer development and treatment response. In the present study the Mn-SOD and Cu/Zn-SOD expression was evaluated at the antigen level by ELISAs using monospecific antibodies, confirmed by Western-blotting and immunohistochemistry, and at the activity level by a spectrophotometric assay, confirmed by electrophoretic NBT-reduction. The complete colorectal neoplasia sequence was assessed, i.e. colorectal adenomas, carcinomas and liver metastases and their corresponding normal tissues (n=35 in each group).

The Mn-SOD content (μg/mg protein), immunohistochemically primarily expressed in the (neoplastic) epithelial cells, increased in the sequence normal mucosa (0.23 ± 0.04) - adenoma (0.63 ± 0.08) - carcinoma (0.93 ± 0.08) (both $p<0.0005$). The activity level (U/mg protein) changed similarly (respectively 3.8 ± 0.6, 4.9 ± 0.4, and 7.3 ± 0.8 ($p<0.0005$), all n=17). Liver metastases expressed Mn-SOD antigen and activity levels comparable to that of the primary carcinomas. The Mn-SOD content was associated ($p<0.05$) with the differentiation grade of the carcinomas and in the adenomas with the diameter. There were no differences in the Cu/Zn-SOD content (mucosa: 0.56 ± 0.03, adenomas: 0.55 ± 0.04, and carcinomas: 0.61 ± 0.04), immunohistochemically expressed ubiquitously, whereas there was a significant decrease in the Cu/Zn-SOD activity [respectively 6.2 ± 0.6, 3.8 ± 0.4 ($p<0.0005$), and 4.1 ± 0.5 ($p \leq 0.01$)], which might be attributable to interference by extracellular-SOD in the activity assay. Liver metastases expressed comparable Cu/Zn-SOD activity levels (5.3 ± 1.1) but significantly ($p<0.02$) higher antigen levels (1.07 ± 0.17) as carcinomas. Normal liver contained 8- to 15-fold higher SOD levels than all other tissues.

In conclusion, colorectal neoplasia is accompanied by major changes in the level of Mn-SOD. These observations, in combination with the previously reported association between colorectal cancer Mn-SOD level and patient survival, might have both clinical and therapeutical implications.

This research was funded by the Dutch Cancer Society (Grant RUL 94-864).

● G2533

PROGNOSTIC RELEVANCE OF SUPEROXIDE DISMUTASES IN GASTRIC CANCER. A.M.L. Janssen, C.B. Bosman, F.J.G.M. Kubben, W. van Duijn, M.M. Oostendorp-van de Ruit, G. Griffioen, C.B.H.W. Lamers, H.W. Verspaget. Dept. Gastroenterology-Hepatology, Leiden University Medical Center, The Netherlands.

The oxidant-antioxidant balance is thought to contribute to the initiation, development and treatment response of cancer. In the present study we evaluated the prognostic significance of the antioxidants Mn- and Cu/Zn-SOD in gastric carcinomas and corresponding normal gastric mucosa obtained from resection specimens (n=81), as determined by ELISAs, in comparison with major clinicopathological parameters.

The Mn-SOD content (ng/mg protein) of carcinomas was significantly higher compared to that of normal mucosa (911 ± 62 vs 493 ± 30, $p<0.0005$). Within the normal mucosa, a high Mn-SOD content (>335) was associated with a good (25.5%) and a low Mn-SOD content with a poor (6.7%) overall survival ($p=0.02$, follow-up ranging from 2.8 to 9.8 years). In contrast, a high Mn-SOD content (>450) of the carcinomas was found to be associated with a poor (14.1%) and a low Mn-SOD content with a good (35.3%) overall survival ($p=0.03$), as previously reported in colorectal cancer. The Cu/Zn-SOD content was significantly lower in carcinomas compared to normal mucosa (606 ± 33 vs 718 ± 25, $p=0.001$). Furthermore, a high Cu/Zn-SOD content (>754) of the normal mucosa was associated with a good (35.3%) and a low Cu/Zn-SOD with a poor (6.4%) overall survival ($p=0.002$). There was no significant association between the Mn- and Cu/Zn-SOD content and nine dichotomized clinicopathological parameters (gender, age, TNM, Laurén, WHO, localization, diameter, eosinophils, and intestinal metaplasia), with the exception of the Mn-SOD and the gender of the patients. Multivariate Cox analyses showed that the SOD variables are independent predictors of survival ($0.002 \leq p \leq 0.03$), in addition to the dichotomized clinicopathological parameters.

In conclusion, human gastric cancer is accompanied by major changes in the Mn-SOD and Cu/Zn-SOD content, which are also important predictors of the clinical outcome of the patients. Particularly, a high SOD content in normal mucosa is associated with a good and, in contrast, a high SOD content in carcinomas is associated with a relatively poor overall survival. The SOD antioxidant status of gastric cancer patients might, therefore, be of relevance for (adjuvant) therapy planning.

This research was funded by the Dutch Cancer Society (Grant RUL 94-864).

● G2534

COOPERATION BETWEEN THE CYCLIN D1 ONCOGENE AND THE CHEMICAL CARCINOGEN N-NITROSOMETHYLBENZYLAMINE IN THE INDUCTION OF ESOPHAGEAL DYSPLASIA IN TRANSGENIC MICE. TD Jenkins[1], A Mueller[1], R Odze[4], A Shahsafaei[4], L Zukerberg[3], G Stoner[5], AK Rustgi[1,2]. [1]Gastrointestinal, [2]Hematology/Oncology, and [3]Pathology Units, Massachusetts General Hospital and [4]Department of Pathology, Brigham and Women's Hospital, Harvard Medical School, Boston, MA 02114 and the [5]Arthur James Cancer Research Institute, Ohio State University, Columbus, OH 43210

INTRODUCTION: The molecular pathogenesis of esophageal squamous dysplasia and squamous cell carcinoma has been hypothesized to involve an interaction between environmental exposures and genetic factors. We proposed to directly test this hypothesis in an animal model of esophageal squamous dysplasia, a precursor to esophageal squamous carcinoma. This was pursued with transgenic mice in which the cyclin D1 oncogene, known to be overexpressed in premalignant and malignant conditions of the esophagus, is targeted to the esophageal squamous epithelium resulting in squamous dysplasia. To determine whether environmental factors exert additive effects on neoplasia, we administered the esophageal specific carcinogen N-nitrosomethylbenzylamine (NMBA) to cyclin D1 transgenic and wild type FVB/N mice. **METHODS:** 80 FVB/N w/t and cyclin D1 transgenic mice were randomized to three treatment arms, to receive in blinded fashion either 1.0 mg NMBA/kg body weight once weekly for 15 weeks, three times weekly for 5 weeks, or no treatment. Subcutaneous injections of NMBA (in 20% DMSO) were given beginning at four weeks of age and mice were monitored for general appearance, activity, and weight. Mice from each group were euthanized at 9, 12, and 15 months of age and tissues examined for the presence of gross pathology. Representative hematoxylin and eosin stained tissue sections of tongue, proximal and distal esophagus, stomach, and liver were examined. Immunohistochemical staining was performed on sections of esophagus with an antibody to proliferating cell nuclear antigen (PCNA). **RESULTS:** Histologic analysis of the esophageal squamous epithelium revealed more severe dyskeratosis, hyperplasia, and dysplasia at all time points in NMBA treated cyclin D1 mice. Cyclin D1 mice treated with both schedules of NMBA developed a greater severity of dysplasia than untreated transgenic mice and NMBA treated wild type mice. Age matched untreated FVB/N mice developed no abnormalities. PCNA staining of cells in the esophageal squamous epithelium was increased in NMBA treated cyclin D1 mice compared with untreated transgenic or treated wild type mice. **CONCLUSIONS:** NMBA administration and overexpression of cyclin D1 in the esophageal squamous epithelium of mice increases the severity of dysplastic change compared with that induced by either factor alone. This lends support to the hypothesis that a combination of genetic and environmental factors increases the risk for esophageal squamous carcinogenesis.

● G2535

***TRANS*-ACTIVATION OF THE ESOPHAGEAL SQUAMOUS EPITHELIAL SPECIFIC HUMAN KERATIN 4 AND EPSTEIN-BARR VIRUS ED-L2 PROMOTERS BY GUT-ENRICHED KRÜPPEL-LIKE FACTOR.** TD Jenkins[1], OG Opitz[1], J Okano[1], AK Rustgi[1,2]. [1]Gastrointestinal and [2]Hematology/Oncology Units, Massachusetts General Hospital, Harvard Medical School, Boston, MA.

INTRODUCTION: Gut-enriched Krüppel-like Factor (GKLF), also referred to as Epithelial Zinc Finger (EZF), may transcriptionally regulate the switch from proliferation to differentiation in the suprabasal layer of the esophageal squamous epithelium based upon its cellular localization and effects on cell proliferation. To determine whether GKLF regulates genes expressed in this zone of the squamous upper gastrointestinal tract, we investigated its effects on two esophageal squamous epithelial-specific promoters, the Epstein-Barr Virus ED-L2 early lytic cycle promoter and the human keratin 4 (K4) promoter. **METHODS:** RT-PCR and Northern blot analysis were used to determine expression of GKLF in the esophageal squamous carcinoma TE-11 cell line, 293, and 3T3 cell lines. Using a DNA probe specific to the zinc finger domain of GKLF, a TE-11 library was screened to obtain the full length GKLF cDNA, which was placed into expression vector pcDNA3.1/HisB 3' to a polyhistidine and epitope tag. The GKLF vector was transfected into 293 cells for Northern and Western blot analysis. Co-transfection experiments were performed with GKLF and reporter gene constructs of the ED-L2 and keratin 4 promoters. Electromobility shift assays (EMSAs) were performed with radiolabeled *cis*-regulatory elements from both promoters, using affinity column and gel filtration purified GKLF-Histidine fusion protein. **RESULTS:** GKLF was expressed in TE-11 and 3T3 but not 293 cells. Transient transfection of the GKLF vector yielded expression of a 3.5 kB transcript and 65 kDa protein. A less abundant 34 kDa tagged protein was also detected. GKLF was found to markedly transactivate both the ED-L2 and keratin 4 promoters. The transactivation was localized to regions -144 to -114 and -340 to -140 of the ED-L2 and K4 promoters, respectively. Both regions contain CACCC-like elements known to bind GKLF in EMSAs. EMSAs revealed that purified GKLF-fusion protein specifically bound CACCC-like elements corresponding to *cis*-regulatory elements of both promoters. Size fractionation of the 65 and 34 kDa proteins revealed that the 65 kDa GKLF-fusion was sufficient to bind CACCC. **CONCLUSIONS:** These experiments demonstrate that GKLF is expressed in the TE-11 cell line in which

esophageal squamous epithelial specific genes are highly active. In the non-GKLF expressing 293 cell line, GKLF powerfully activates transcriptional activity of the ED-L2 and K4 promoters, requiring the presence of a CACCC-like motif. This is the first demonstration that GKLF transactivates genes of the squamous upper gastrointestinal tract active at the point of transition from proliferation to early differentiation. GKLF may thus play an important role in orchestrating this critical pattern of gene expression.

G2536

METASTATIC BREAST CARCINOMA TO THE AMPULLA: A CASE REPORT. C. Jones, N. Tibaldi, J. Shogan, T. Jan Ravi, R. Agrawal, M. Roh, G. Brodmerkel Jr., Allegheny University of the Health Sciences, Pittsburgh, PA.

CASE: A 45 year old white female who had been treated by modified radical mastectomy was found to have a dilated common bile duct but no evident metastatic disease on follow-up staging thoracoabdominal CT. Routine labs at that time were normal. ERCP revealed a mass at the ampulla and a common bile duct measuring 25mm. Biopsy showed histologic similarity to the original breast lesion tissue. Estrogen and progesterone receptors were negative in both breast and ampullary lesions. After 4 cycles of Adriamycin with concurrent Tamoxifen local surgical excision revealed negative margins. High dose chemotherapy and bone marrow transplant are the next stage of therapy.
DISCUSSION: Although metastases may occur in 30 % of breast cancer patients, localization to the pancreas and biliary tree, however, is rare. Titus et al.(1) described 4 cases with only one being confined to the ampulla. All patients were treated by pancreaticoduodenectomy. Controversy exist regarding surgical treatment of primary tumors of the ampulla, there are no controlled studies regarding metastatic disease of the ampulla. In our case, due to tumor free margins on frozen section, we elected to do a local excision. This is a viable option with less morbidity and mortality than pancreaticoduodenectomy.
Conclusion: Consider local excision as an option in patients with the rare metastatic lesion of the ampulla.
[1] Solitary Breast Metastasis to the Ampulla and Distal Bile Duct, Titus et al, The American Surgeon, June 1997 (63) 512-515

G2537

IMMUNOHISTOCHEMICAL ANALYSIS OF TGF β_1 GENE PROTEIN IN SQUAMOUS CELL CARCINOMA OF ESOPHAGUS. Zhang Jun Deng DengHao Luo Jinyan Wang Kangmin. Gastroenterology Section of Internal Medicine, Second Affiliated Hospital, Xian Medical University.

The expression of TGF β_1 protein in normal esophageal mucosa(EM), esophageal epithelial dysplasia (EED) and squamous cell carcinoma of esophagus(SCCE) was examined immunohisto-chemically. In order to show how TGF β_1 would express in EM, EED and SCCE, whether the rate of TGF β_1 postive expression might show any correlation with established histologic grade and the presence of lymph node metastasis in SCCE. The results indicated: There wasn't expression in normal cells of EM; The rates of TGF β_1 positve expression were 62.8% in cells of EED and 77.1% incells of SCCE, which had statistically significant difference compared with EM group. The positive rate of TGF β_1 increased successively in the order of EM→well EED→moderately EED→poorly EED→SCCE. It suggested that early examination of expression of TGF β_1 could help predict the occurrence of esophageal cancer. It can't find any correlation between the positive rate of TGF β_1 and established histological grade as well as the presence of lymph node metastasis in SCCE.

G2538

ADENOVIRUS-MEDIATED TRANSDUCTION OF *ESCHERICHIA COLI* URACIL PHOSPHORIBOSYL-TRANSFERASE GENE SENSITIZES CANCER CELLS TO LOW CONCENTRATION OF 5-FLUOROURACIL: A NEW WAY TO OVERCOME THE RESISTANCE OF CHEMOTHERAPEUTIC AGENT. Fumihiko Kanai, Takayuki Kawakami, Makoto Ohashi, Yasushi Shiratori, and Masao Omata. Second Department of Internal Medicine, Faculty of Medicine, The University of Tokyo, Japan.

Background/Aim: 5-fluorouracil (5-FU), although a widely used chemotherapuetic agent, has a limited effect in the treatment of human solid tumors due to its resistance to the cytotoxic effects of 5-FU. *Escherichia coli* uracil phosphoribosyltransferase is a pyrimidine salvage enzyme which catalyzes the synthesis of uridine monophosphate from uracil and 5-phosphoribosyl-α-1-diphosphate. We hypothesized that tumors can be more sensitive to the cytotoxic effect of 5-FU if the balance is shifted to the activation pathway by E. coli UPRT gene transduction.
Methods: Recombinant adenovirus expressing *E. coli* UPRT gene (AdCA-UPRT) or lacZ gene (AdCA-lacZ) were prepared. Human cancer cell lines, colon (WiDr), gastric (MKN45, 28, and 1), liver (Hep3B, PLC/PRF/5) and pancreas (AsPC-1), were infected with the adenoviruses, cultured in the presence of various concentrations of 5-FU, and determined the 5-FU sensitivity. The expressed UPRT enzymatic activity of cells was determined. Subcutaneous tumors of Hep3B or MKN45 cells were established in nude mice, and the ability of AdCA-UPRT plus systemic 5-FU to suppress tumor growth were evaluated.
Results: After AdCA-UPRT infection, all cell lines became sensitive to low concentration of 5-FU *in vitro*. The ratio of IC_{50} of 5-FU-treated parental/infected cells) was between 6.3 - 100. The *in vitro* bystander effect was observed when only 10 % of Hep3B cells were infected with AdCA-UPRT. In addition, 5-FU treatment of Hep3B or MKN45 xenografts in nude mice transduced with UPRT was demonstrated to result in significant antitumor effects.
Conclusions: Transduction of gastrointestinal and liver cancer cells by recombinant adenovirus expressing the UPRT gene increases cell sensitivity to the cytotoxic effect of 5-FU *in vitro* and *in vivo*. The system is representative of a new chemosensitization strategy for cancer gene therapy.

G2539

MIXED HYPERPLASTIC ADENOMATOUS POLYPS / SERRATED ADENOMAS. NEOPLASTIC TRANSFORMATION OF HYPERPLASTIC COLORECTAL POLYPS. A. Kapsoritakis, S. Potamianos, I. Mouzas, E. Matrella, E. Anagnostopoupou, G. Alexandrakis, M. Tzardi, E. Kouroumalis. University Hospital of Heraklion, Crete, Greece.

Background and aims: Mixed Hyperplastic Adenomatous Polyps (MHAP)/ Serrated adenomas combine histological features of hyperplastic and adenomatous epithelium. It remains controversial whether they represent de novo lesions or they derive from neoplastic transformation of hyperplastic polyps. In order to investigate this subject we compared clinicopathological characteristics of patients with MHAP and patients with hyperplastic, tubular and villous adenomas.
Patients and method. Of 4723 colonoscopies performed in our department during the last 4 years, 22 patients with 23 MHAP were found. These were compared with 61 patients with 86 hyperplastic polyps, 40 with 58 tubular adenomas and 27 with 35 villous adenomas, according the size of the polyps. Patients from other groups had only one histological type. Statistical analysis: Fishers' exact test.
Results. Synchronous lesions of patients with MHAP: 14 hyperplastic polyps, 6 adenomas and 2 carcinomas. Regarding the sex of patients and the anatomical distribution of polyps there were remarkable similarities between the 4 histological groups. The mean age of patients with hyperplastic polyps was 53,7 years, MHAP 63,2, tubular adenomas 65,2 and villous adenomas 69,5. P=0.0093 between MHAP and hyperplastic polyps.Regarding the size, 75 (87,2%) hyperplastic polyps, 4 (17,4%) MHAP, 29 (50%) tubular and 1 (2,9%) villous adenomas were less than 5 mm. 3 (3,5%) hyperplastic polyps, 13 (56,5%) MHAP, 14 (24,1%) tubular and 13 (37,1%) villous adenoma were larger than 10 mm. There were significant differences ($p<0.0001$) between MHAP and hyperplastic polyps in the two size' groups.
Conclusion. Several factors support the hypothesis of neoplastic transformation of hyperplastic polyps: 1) The coexistence of hyperplastic and adenomatous epithelium in the same polyp. 2) Patients with MHAP harbor hyperplastic polyps in a high proportion. 3) The anatomical distribution of all polyps groups is virtually identical. 4) The mean age of patients with MHAP is about 10 years older than those with hyperplastic polyps. 5) As hyperplastic polyps increase in size, they exhibit areas of adenomatous epithelium.

G2540

IMMUNE MECHANISMS OF *HELICOBACTER PYLORI* INVOLVEMENT IN THE PATHOGENESIS OF MALT LYMPHOMAS OF THE STOMACH. A.Karameris, T.Rokkas, C.Liatsos, Ev.Petridou, E.Kalafatis, T.Tsilalis, E.Nanos. Department of Pathology, Gastrointestinal Unit and 1st Surgical Department, 401 Army General Hospital of Athens, Athens, Greece.

In the last few years, several epidemiologic and experimental studies attempt to specify the essential role of Helicobacter pylori (H.pylori) in the pathogenesis of MALT-type low grade lymphomas of the stomach and to correlate them with H.pylori-gastritides. Subepithelial plasma cell differentiation, blast transformation and the specific colonisation of lymphoid follicle centres by neoplastic cells indicate that the tumor is immunologically responsive. **Aim:** To investigate the immunologic mechanisms that trigger the formation of MALT-type lymphomas on the ground of H.pylori gastritis, through the development of anti-idiotypic (AI) monoclonal antibodies (Moabs) that recognise the IgM/λand IgA/λ idiotypes of the neoplastic population of MALT lymphomas. **Methods:** Frozen material of 50 cases of chronic H.pylori- gastritides, 15 MALT lymphomas of the stomach and 20 nodal non-Hodgkin lymphomas, with immunophenotype IgA/λ, CD19+, CD20+, CD5-, CD10-, CD23-, were studied. In order to define/specify Moab 27/165 lymphocyte targets, the idiotypic Moab 21/05 was produced using cell cultures of IgA lymphocytes from a MALT case that excibited the phenotype IgA, CD20+, fused with the heteromyeloma cell line HAB-1. Hybridoma supernatants were screened for Moabs production with an ELISA and subcloned by limiting dilution. Afterwards, the AI Moab 27/165 was produced and its specificity was examined with the idiotypic homologue Moab 21/05 using the ELISA technique. **Results:** The results showed that the Moab 27/165 reacted with lymphocytes and plasmatocytes of the inflammatory population in 45/50 of H.pylori-gastritides, as well as with the neoplastic population of the MALT case used for the production of the idiotypes. None of the 20 nodal and 15 extranodal lymphomas exhibited positive immunosignal. **Conclusions:** The selective specificity of the AI antibody 27/165 to recognise lymphocytes of the inflammatory population in H.pylori-gastritides, give rise to strong suggestions of the involvement of these cells in the development of MALT lymphomas through immune mechanisms rather than direct implication of the microorganisms.

ILL Document Delivery

REG-14014452

VAUZGE

NLM -- W1 GA458 (GENCOLL); W1 GA458 (REFCOLL); Film S1100

US PATENT AND TRADEMARK OFFICE
SCIENTIFIC AND TECHNICAL INFO CTR
107 S. WEST STREET, PMB 803
ALEXANDRIA, VA 22314

ATTN:		SUBMITTED:	2007-01-18 10:30:29
PHONE:	571-272-2550	PRINTED:	2007-01-18 13:24:18
FAX:	571-272-0230	REQUEST NO.:	REG-14014452
E-MAIL:	STIC-DOCS@uspto.gov	SENT VIA:	DOCLINE
		DOCLINE NO:	21662009

REG **Copy** **Journal**

TITLE:	GASTROENTEROLOGY
PUBLICATION PLACE:	Baltimore.
VOLUME/ISSUE/PAGES:	A692;114(4 pt.2):A692 A692
DATE:	692
ISSN:	0016-5085
OTHER NUMBERS/LETTERS:	
	NLM Unique ID: 0374630
SOURCE:	Unique Key
MAX COST:	$4.00
COPYRIGHT COMP.:	Guidelines
CALL NUMBER:	W1 GA458 (GENCOLL); W1 GA458 (REFCOLL); Film S1100
REQUESTER INFO:	615296
DELIVERY:	E-mail Post to Web: STIC-DOCS@uspto.gov
REPLY:	Mail:

KEEP THIS RECEIPT TO RECONCILE WITH BILLING STATEMENT

For problems or questions, contact NLM at http://wwwcf.nlm.nih
.gov/ill/ill_web_form.cfm or phone 301-496-5511.

Include LIBID and request number.

G2861

IMMUNOHISTOCHEMICAL STAINING FOR BCL-2 AND P53 IN GASTRIC ADENOCARCINOMAS. K Triantafyllou[1], M Tzouvala[1], N Kepranos[2], GV Papatheodoridis[1], A Zizi-Serbetzoglou[3], I Elemenoglou[3], DG Karamanolis[1], SJ Hadziyannis[4]. Depts. of [1]Gastroenterology & [3]Pathology, "Tzaneion" Hospital of Piraeus; [2]Dept. of Pathology, "Hygeia" Hospital, [4]Academic Dept. Hippokration Hospital, Athens, Greece.

Apoptosis, an early event during tumorigenesis has been shown to be inhibited by bcl-2 as well as by mutant p53 protein. The aim of the study was to investigate the expression of these proteins in gastric adenocarcinomas (GAC). Forty-eight tumors and tissue from 22 normal consecutive patients (50M/20F, age: 66 ± 12 yrs) were examined. The expression of the proteins was immunohistochemically examined on paraffin-embedded, microwaved sections using the monoclonal antibodies anti-bcl-2, clone 124 (Dako) and anti-p53, clone 1801 (Biogenex). Positive cells were quantified and expressed as the percentage of the total number of cells and assigned to one of 5 categories: 0:≤5%, 1:6-25%, 2:26-50%, 3:51-75%, and 4:>75%. No p53 immunoreactivity was noted in the normal tissue while bcl-2 immunolabeling was located just below the pit/gland junction of the normal mucosa and assigned to category 0. bcl-2 Expression was detected in 29% (14/48) of GAC and it was diffuse (>75% of immunostained cells) in 14% of them. p53 Immunoreactivity was noted in 54% (26/48) of GAC (diffuse in 42% of them). No correlation between bcl-2 and p53 protein expression was observed in GAC (r=0.006, p=0.9). Multivariate analysis revealed that GAC's differentiation was the only significant predictor for bcl-2 protein expression (Odds Ratio: 2.4, 95%CI: 1.1-5.2, p=0.04). No significant predictor was revealed for p53 protein expression. Four patterns of bcl-2/p53 immunoreactivity were observed: bcl-2+/p53+ in 7 (14.6%) GAC, bcl-2-/p53- in 15 (31.3%), bcl-2+/p53- in 7 (14.6%) and bcl-2-/p53+ in 19 (39.6%) of them. bcl-2+/p53 + Immunoreactivity was observed in 7/17 (41%) of the intestinal (according to Lauren's classification) type GAC [relative risk (RR): 2.4, 95%CI: 1.7-3.5] and in none of the other types (p=0.01). The same pattern was also observed in 7/17 (41%) of the well and moderate differentiated GAC (same RR as above) and in none of the poor differentiated ones (p=0.01). bcl-2-/p53- Immunoreactivity was noted significantly more frequently in the diffuse type and in the unclassified GAC than in the intestinal type ones (11/24 or 46% vs 4/24 or 17%, RR: 4.2, 95%CI: 1.1-16.2, p=0.03). The same pattern was noted in all poor differentiated tumors and in 3/24 (12.5%) of the well and moderate differentiated ones (RR: 7, 95%CI: 1.6-30, p=0.005). The bcl-2-/p53+ pattern was observed in all unclassified GAC versus 14/43 (32.5%) of the two Lauren's types GAC (p=0.007). In conclusion, our data suggest that 1. The only significant predictor for bcl-2 protein expression is tumor's differentiation, while no significant predictor was revealed for p53 protein expression. 2. The pattern of bcl-2/p53 immunolabeling depends on the histologic characteristics of the tumors 3. bcl-2+/p53+ Immunoreactivity is detected more frequently in the intestinal type and in the well or moderate differentiated GAC, while bcl-2-/p53- immunoreactivity is expressed more frequently in the diffuse type and in the unclassified GAC as well as, in the poor differentiated tumors. The bcl-2-/p53+ pattern seems to be associated with unclassified GAC.

● G2862

ESOPHAGEAL STENTING FOR MALIGANT ESOPHAGO-RESPIRATORY FISTULA: A COMPARISON BETWEEN SELF-EXPANDING MESH-MEMBRANE STENT VS. PLASTIC STENT. CI Tsai[1,2] WY Lee.[1,2] CH.Chen.[2] YG Chang.[2] TH Yang.[1,2] HY Tsai.[3] JT Lin.[2] TH Wang.[2]. [1]Dept.of Int.Med.Poh-Ai Hosp.Lotung, Taiwan. [2]Dept.of Int.Med.National TaiwanUniversityHosp.Taipei,Taiwan.[3]Union.Chemical Lab.ITRI.Taiwan.

BACKGROUND AND AIM : The development of esophago-respiratory fistula due to cancer (CA) is a devastating complication. Rapid palliation is usually possible with endoscopic placement of either a plastic stent (PS) or a self-expanding mesh-membrane stent (SEMMS). We compared the efficacy and safety between the two methods. **MATERIALS AND METHODS:** From Feb. 1994 to Dec.1997, 16 consecutive patients(p't)with maligant esophago-respiratory fistula (14 esophageal CA.,2 lung CA.) were treated with either PS or a SEMMS..Age ranged from 44 to 77 years (medium ,58.4 years); the rate of male/female was 14:2. The location of fistula included trachea in 10, right bronchus in 3, left bronchus in 1,mediastinum in 1 and pleural cavity in 1. In the PS group, Atkinson type prothesis were used in 6 p'ts,commerical SEMMS were inserted using Wallstent in 9 p'ts and coated-Ultraflex stent in one p't. The p'ts were evaluated every four weeks till death. The effect of palliation was evaluated clinically and roentgenographyically. **RESULTS:** Stent placement was successful in both PS group (6/6) and SEMMS group(10/10). SEMMS obliterated the fistulous tract better than PS (10/10 VS. 4/6). Early complications,including stent migration and airway compression,were significant less frequent with SEMMS than with PS (0 VS. 2/6,0 VS. 5/6,respectively). Common late complications comparing SEMMS with PS were food impaction (3/10 VS. 1/6),tumor overgrowth (3/10 VS. 1/6) and tumor invasion of airway (2/10 VS. 0). Rate of intervention was similar in both treatments.Survivals with SEMMS and PS were 88.8days VS. 71.2 days (P>0.05). **CONCLUSION:** Our preliminary study suggests that SEMMS is superior in completely obliterating the esophago-respiratory fistula with fewer fatal complication and no airway compression.

● G2863

DOWN-REGULATION OF GUT-ENRICHED KRÜPPEL-LIKE FACTOR IN COLONIC NEOPLASM. C-C Tseng J-L Shie, S-F Yet, and M-E Lee. Section of Gastroenterology, Boston University School of Medicine, and Cardiovascular Biology Laboratory, Harvard School of Public Health, Boston, MA.

Gut-enriched Krüppel-like factor (GKLF) belongs to a family of eukaryotic zinc finger transcriptional factors. GKLF possesses a DNA-binding motif and functions as a transcriptional repressor to inhibit DNA synthesis. Although GKLF mRNA is widely distributed in the gastrointestinal tract, its role in the regulation of gastrointestinal mucosal growth is largely unknown. The expression of GKLF mRNA was first examined in human colonic cancerous, adenomatous and hyperplastic tissue in comparison with nearby normal mucosa. Decreases in GKLF mRNA levels were detected in cancerous or adenomatous tissue (42 ± 15 and 64 ± 10 % of control, respectively), whereas GKLF levels remained normal in hyperplastic tissue (n= 5-6 for each group). GKLF mRNA levels were also found to be lower in a human adenocarcinoma cell line (HT-29) than in an embryonic intestinal cell line (I-407). To assess the effect of GKLF expression on cell growth, HT-29 and I-407 cells were transiently transfected with either sense or anti-sense GKLF cDNAs for 48 h, at which time DNA synthesis was determined by [^{3}H]-thymidine incorporation. Overexpression of sense GKLF cDNA in HT-29 and I-407 cells significantly inhibits [^{3}H]-thymidine incorporation by 25 ± 7 %, and 15 ± 5 %, whereas anti-sense GKLF cDNA transfection increases [^{3}H]-thymidine uptake by 76 ± 14 % and 28 ± 10 % respectively. The regulation of GKLF on cell growth was further examined *in vivo* in male Sprague-Dawley rats fasted for 2 days followed by refeeding for 3 h. Colonic GKLF mRNA levels were two-fold higher in fasting than in control rats, and these increases were abolished by refeeding when rapid cell proliferation was detected indicating that GKLF was potentially a negative regulator of mucosal growth. These results demonstrated that expression of GKLF is temporally associated with cell cycle and that repression of GKLF expression stimulates DNA synthesis. Thus, down-regulation of GKLF may facilitate cells to enter the growth cycle and potentially result in tumorgenesis in the gastrointestinal tract.

G2864

CLINICAL FEATURES OF ANORECTAL MALIGNANT MELANOMA IN THE JAPANESE PATIENTS. Y. Tsubosa, T. Akasu, H. Miyake, Y. Moriya, S. Fujita, A. Takada, K. Kubota. National Cancer Center Hospital, Tokyo, Japan.

Anorectal malignant melanoma is a rare tumor that is usually detected late and is associated with poor prognosis. Clinical features of this disease in the Western patients are well known, however, those in the Japanese patients are poorly documented. The purpose of this study is to clarify clinical features of anorectal malignant melanoma in the Japanese patients. **METHODS**: Medical records of 7 patients whom we treated and data of 66 patients, which were reported in the Japanese literature, were reviewed. **RESULTS**: There was a female predominance (50 females, 23 males). The mean age at diagnosis was 62 years (range, 25-84). Treatments included abdominoperineal resection (APR) in 60 patients and local excision (LE) in 9. Overall 5-year survival rate was 19%. The survival distribution of patients with tumors measuring less than 5 cm was significantly better than that of patients with larger tumors (5-year survival rate: 37% vs 0%, P=0.0002). Although there was no significant difference between survival distribution of patients treated with APR and that of patients treated with LE (5-year survival rate: 24% vs 0%, P=0.7), 5-year survival rate of patients who had tumors smaller than 5 cm and underwent APR was acceptable (43%). **CONCLUSION**: The clinical features of the Japanese are generally similar to those of the Westerners. Although prognosis of the Japanese is as poor as that of the Westerners, radical resection of lesions smaller than 5 cm may lead to favorable prognosis in the Japanese patient.

● G2865

FAS LIGAND EXPRESSION DETERMINES LIVER COLONIZATION COMPETENCE OF COLONIC ADENOCARCINOMA. N. Tsuji, A. Tsuji, K. Shiraki, H. Takahashi. Gastrointestinal Unit, Harvard Medical School and Massachusetts General Hospital, Boston, MA.

Background/Purpose: Fas ligand (FasL) plays a pivotal role in lymphocyte cytotoxicity and the maintenance of immunological homeostasis. FasL is also implicated in the existence of immunologically privileged body sites by inducing apoptosis of activated T lymphocytes. We investigated the expression of FasL in human colon cancers and found that human colonic adenocarcinomas metastatic to the liver constitutively express FasL (Proc. Natl. Acad. Sci. USA 94:6420, 1997). Since the FasL expressed in colonic adenocarcinoma was functional, we hypothesized that the FasL expression may determine liver colonization competence of colonic adenocarcinoma through induction of apoptosis in the Fas-expressing hepatocytes at metastatic foci. In this study, we established stable transfectants of murine FasL (mFasL) in MCA-38 colonic adenocarcinoma cell line that was chemically induced by

[CANCER RESEARCH 64, 6002–6009, September 1, 2004]

Identification of Aberrantly Methylated Genes in Association with Adult T-Cell Leukemia

Jun-ichirou Yasunaga,[1] Yuko Taniguchi,[1] Kisato Nosaka,[1] Mika Yoshida,[1] Yorifumi Satou,[1] Tatsunori Sakai,[2] Hiroaki Mitsuya,[2] and Masao Matsuoka[1]

[1]*Laboratory of Virus Immunology, Institute for Virus Research, Kyoto University, Kyoto, Japan; and* [2]*Department of Internal Medicine II, Kumamoto University School of Medicine, Kumamoto, Japan*

ABSTRACT

In this study, we identified 53 aberrantly hypermethylated DNA sequences in adult T-cell leukemia (ATL) cells using methylated CpG island amplification/representational difference analysis method. We also observed a proportionate increase in the methylation density of these regions with disease progression. Seven genes, which were expressed in normal T cells, but suppressed in ATL cells, were identified near the hypermethylated regions. Among these silenced genes, *Kruppel-like factor 4* (*KLF4*) gene is a cell cycle regulator and *early growth response 3* (*EGR3*) gene is a critical transcriptional factor for induction of Fas ligand (FasL) expression. Treatment with 5-aza-2′-deoxycytidine resulted in the recovery of their transcription, indicating that their silencing might be associated with DNA hypermethylation. To study their functions in ATL cells, we transfected recombinant adenovirus vectors expressing *KLF4* and *EGR3* genes. Expression of *KLF4* induced apoptosis of ATL cells whereas enforced expression of *EGR3* induced the expression of *FasL* gene, resulting in apoptosis. Thus, suppressed expression of *EGR3* enabled ATL cells to escape from activation-induced cell death mediated by FasL. Our results showed that the methylated CpG island amplification/representational difference analysis method allowed the isolation of hypermethylated DNA regions specific to leukemic cells and thus shed light on the roles of DNA methylation in leukemogenesis.

INTRODUCTION

Human T-cell leukemia virus type I (HTLV-I) is the causative retrovirus of a neoplastic disease, adult T-cell leukemia (ATL) and an inflammatory disease, HTLV-I-associated myelopathy/tropical spastic paraparesis (1–4). After infection with HTLV-I, a small proportion of carriers (about 2–5%) develop ATL after a long latent period (5). In this virus-induced leukemia, viral proteins encoded by HTLV-I play an important role in the proliferation of infected cells and leukemogenesis. Among them, Tax is considered to play a central role in leukemogenesis because of its pleiotropic actions (6, 7), such as transcriptional activation of cellular genes (8–10), *trans*-repression of cellular genes transcription (11, 12), and functional inactivation of p53 and MAD1 (12, 13). These pleiotropic functions render HTLV-I-infected cells able to proliferate, and confer resistance to apoptotic signals, resulting in clonal expansion.

In the late stage of leukemogenesis, *tax* is frequently inactivated through several mechanisms (14) such as loss of 5′-long terminal repeat (LTR) (15), genetic alterations of *tax* gene (16), and DNA hypermethylation in 5′-LTR (17), indicating that Tax is not always necessary for leukemogenesis. Because Tax is the major target molecule of CTLs *in vivo* (18), the expression of Tax confers a growth advantage to infected cells, but on the other hand, it renders infected cells susceptible to CTLs. Fully transformed ATL cells are considered to acquire the ability to proliferate *in vivo* in the absence of Tax expression. Such a transformation process is thought to include alterations of host genome: genetic and epigenetic changes. Although the genetic changes, such as mutation of *p53* (19) and deletion of *p16* (20, 21), in ATL cells were reported, they are not frequent and are observed predominantly in the late stage of the disease.

In addition to genetic alterations, DNA hypermethylation of promoter region CpG islands has been analyzed in the context of oncogenesis because this process silences gene transcription of tumor-suppressor genes. This epigenetic alteration is observed commonly in various cancer cells. Although methylation "profiling" studies have shown that some genes are frequently methylated in various tumor cells, other genes are methylated in a tumor-type-specific manner (22, 23). To date, several methods have been developed to isolate differentially methylated DNA regions in cancers (24–29). Recently, with methylated CpG island amplification/representational difference analysis (MCA/RDA) method, we isolated hypomethylated DNA regions and demonstrated that *MEL1S* gene was hypomethylated and aberrantly transcribed in ATL cells (30).

The present study was designed to isolate hypermethylated DNA regions in ATL cells compared with cells in the carrier state using the MCA/RDA method and to identify those genes that have an expression associated with DNA hypermethylation. On the basis of our results, we discuss the association between aberrant DNA methylation and leukemogenesis of ATL.

MATERIALS AND METHODS

Cells. Peripheral blood mononuclear cells (PBMCs) were isolated from 10 patients with ATL (five acute type cases and five chronic type cases), five asymptomatic carriers, and five uninfected individuals using Ficoll-Paque density centrifugation method. We also used the cell lines ED, ATL-43T, ATL-48T, ATL-55T, MT-1, and TL-Om1, which were derived from leukemic clones, and MT-2, which is derived from nonleukemic cells. To study the effect of demethylation, ATL-43T was cultured in media supplemented with 10 μmol/l 5-aza-2′-deoxycytidine (5-aza-dC; Sigma, St. Louis, MO) for 3 days, 10 μmol/l 5-aza-dC and 1 μmol/l trichostatin A (TSA; Sigma) for the last 24 hours, or 1 μmol/l TSA for 24 hours alone. The human embryonic kidney cell line, HEK 293, was used for the packaging of recombinant adenovirus vectors.

Viral FLICE-inhibitory protein (FLIP) derived from the equine herpes virus type 2, E8 (31), and the long form of murine cellular FLIP (mCasper$_L$; Ref. 32) expression vectors were transfected into ATL-43T cells by electroporation with a Gene Pulser II (Bio-Rad, Hercules, CA). Stable transfectants were selected and maintained in culture medium containing G418 (500 μg/ml; Nacalai tesque, Kyoto, Japan). The transfected cell lines by each of the vectors were designated as ATL-43T-E8 and ATL-43T-mCas, respectively.

Methylated CpG Island Amplification/Representational Difference Analysis. To identify aberrantly hypermethylated DNA regions in ATL cells, we used the MCA/RDA method, as reported previously (28). Five micrograms of genomic DNA were digested with 100 units of *Sma*I (New England Biolabs, Beverly, MA) twice and then digested once with 20 units of *Xma*I (New England Biolabs). RMCA adaptor was prepared by annealing of the oligonucleotides RMCA24 (5′-CCACCGCCATCCGAGCCTTTCTGC-3′) and

Received 4/26/04; revised 6/15/04; accepted 6/25/04.

Grant support: Grant-in-Aid for Scientific Research from the Ministry of Education, Science, Sports, and Culture of Japan.

The costs of publication of this article were defrayed in part by the payment of page charges. This article must therefore be hereby marked *advertisement* in accordance with 18 U.S.C. Section 1734 solely to indicate this fact.

Note: Supplementary data for this article can be found at Cancer Research Online (http://cancerres.aacrjournals.org).

Requests for reprints: Jun-ichirou Yasunaga, Laboratory of Virus Immunology, Institute of Virus Research, Kyoto University, Kyoto 606-8507, Japan. Phone: 81-75-751-4048; Fax: 81-75-751-4049; E-mail: jyasunag@virus.kyoto-u.ac.jp.

RMCA12 (5′-CCGGGCAGAAAG-3′), and ligated to the digested DNA fragments using T4 DNA ligase (New England Biolabs). To amplify the hypermethylated DNA fragments, which were ligated adaptors in both ends, PCR was performed using the RMCA24 oligonucleotides as primers. The amplicons were synthesized using samples from an ATL patient and a HTLV-I carrier. For detection of ATL cell-specific hypermethylated DNA sequences, MCA products from a carrier were used as a driver of RDA, and those products from an acute ATL patient as a tester. We used GeneFisher Basic Reagent Set (TaKaRa, Shiga, Japan) for RDA. In RDA step, 500 and 100 ng of ligation mixture were used for the first and second selective PCR, respectively. Oligonucleotides used for RDA were JMCA24 (5′-GTGAGGGTCGGATCTGGATGGCTC-3′), JMCA12 (5′CCGGGAGCCAGC-3′), NMCA24 (5′-GTTAGCGGACACAGGGCGGGTCAC-3′), and NMCA12 (5′-CCGGGTGACCCG-3′). Subcloning of the MCA/RDA products was carried out using pCR-XL-TOPO (Invitrogen, Carlsbad, CA) or pGEM-T Easy (Promega, Madison, WI) as vectors, and then the sequences of each fragment were determined by PCR using M13 primers. Sequence homologies and localization in chromosomes were identified using the BLAST program of the National Center for Biotechnology Information.[3]

MCA-Southern Hybridization. To confirm that the isolated DNA regions are specifically hypermethylated in ATL cells, Southern blot method was used. MCA products from an ATL patient and a HTLV-I carrier (500-ng each) were separated by electrophoresis in 1.5% agarose gels and then transferred to Hybond-N + (Amersham Biosciences, Piscataway, NJ). All of the isolated DNA fragments were labeled with ^{32}P, and hybridized to these filters.

Combined Bisulfite Restriction Analysis and Bisulfite Sequencing Analysis. For nine DNA regions identified by MCA/RDA, the methylation status of the DNA regions was determined by Combined Bisulfite Restriction Analysis or bisulfite sequencing as described previously (33). First, genomic DNAs were treated with sodium bisulfite (34) and then amplified by nested PCR using the specific primers listed in Supplementary Table 1. The PCR products of these regions were digested with *Taq*I (New England Biolabs) or *Acc*II (TaKaRa), subjected to electrophoresis in 3% agarose gels, and visualized by ethidium bromide staining. The percentage of DNA methylation was calculated by the intensities of methylation and unmethylation signal determined by ATTO densitometry software (ATTO, Tokyo, Japan).

For detailed analysis of DNA methylation in *Kruppel-like factor 4* (*KLF4*) and *early growth response 3* (*EGR3*) genes, we performed bisulfite sequencing. The PCR products of the isolated regions and promoter regions of these genes were subcloned into pGEM-T Easy, thereafter, the sequences of each of 10 clones were determined. Because the promoter sequence of *KLF4* has not been determined, we predicted its sequence using the program[4] supported by the BioInformatics & Molecular Analysis Section, Computational Bioscience and Engineering Lab, Center for Information Technology, and NIH. Primers for bisulfite sequencing are also listed in Supplementary Table 1.

Semi-quantitative Reverse Transcriptase-PCR. Total RNA was extracted from the PBMCs and cell lines using Trizol reagent (Invitrogen) and then treated DNaseI (Invitrogen). cDNAs were synthesized from 0.5 μg of total RNA with the Superscript First-Strand Synthesis System for reverse transcription (RT)-PCR (Invitrogen) and used for semi-quantitative RT-PCR as template. The primers used for RT-PCR and their annealing temperatures are summarized in Supplementary Table 2. The number of PCR cycles was appropriately determined for each quantification (Supplementary Table 2). We used 1.25 units of ExTaq polymerase (TaKaRa) for each reaction. All experiments were performed including samples of whole brain (Clontech, Palo Alto, CA) and skeletal muscle (Stratagene, La Jolla, CA) as positive control of PCR reaction.

Construction of Adenovirus Vectors. The recombinant adenovirus vectors containing *KLF4* and *EGR3* gene (KLF4-AD and EGR3-AD, respectively) were generated using Adeno-X Expression System (Clontech) according to the manufacturer's protocol. These adenovirus vectors were concentrated and purified by Virakit for adenovirus 5 and recombinant derivatives (Virapur, San Diego, CA), and then the viral titers were determined using Adeno-X Rapid Titer Kit (Clontech). The *lacZ*-containing adenovirus vector (lacZ-AD) was also prepared as a negative control. All adenovirus vectors were used to infect an ATL cell line, ATL-43T, at 1,000 infectious units/cell.

Flow Cytometric Analysis. The flow cytometry (model EPICS XL flow cytometer, Beckman Coulter, Miami Lakes, FL) was used for analyses of apoptosis. Annexin V-FITC/PI double staining and terminal-deoxynucleotidyl transferase-mediated dUTP-FITC nick-end labeling (TUNEL) assay were performed for detection of apoptosis, using MEBCYTO apoptosis kit (MBL, Nagoya, Japan) and MEBSTEIN apoptosis kit direct (MBL), respectively.

RESULTS

Isolation of Hypermethylated DNA Regions in the Genome from ATL Cells. To identify hypermethylated regions in the genome of ATL cells, we carried out MCA/RDA, which was used previously to isolate a number of methylated CpG islands in colon cancer cell line (28). MCA products were generated from the genomic DNA of a carrier (driver) and an acute ATL patient (tester). After the second round of RDA, the PCR products were subcloned, and their sequences were determined. To confirm that identified DNA fragments were amplified in tester amplicon, we examined whether isolated DNA fragment specifically hybridized to the tester amplicon using Southern blot method (MCA-Southern). Specific hybridization to the tester amplicon implied that isolated DNA regions were hypermethylated in ATL cells compared with peripheral blood mononuclear cell (PBMC) from a carrier. Finally, we identified 53 differentially hypermethylated DNA fragments in ATL cells. The chromosomal locations of all of the fragments were analyzed by NCBI BLAST program. We tested whether these identified regions satisfied the criteria for CpG islands proposed by Takai and Jones (35). The results revealed that the majority of clones (48 of 53 clones) were located in CpG islands. Information of isolated sequences is described in Table 1.

Accumulation of Aberrant DNA Hypermethylation during Disease Progression. Chronic ATL is characterized as an indolent form, which later progresses to aggressive forms (*i.e.*, acute or lymphoma-type ATL). To confirm that DNA hypermethylation identified in this study is associated with disease progression, we analyzed the extent of DNA methylation of nine DNA regions at different stages by Combined Bisulfite Restriction Analysis. Fig. 1*A* shows the profiles of the methylation status in these DNA fragments. In cell lines, CpG sites in identified DNA fragments were highly methylated, which was consistent with the finding of DNA methylation in the established cell lines. This confirmed that the isolated DNA regions were hypermethylated in ATL cells and that MCA-Southern could identify the hypermethylated DNA regions. In the carrier state, most DNA fragments were unmethylated. On the other hand, they were frequently methylated in chronic ATL, and the level of methylation increased in acute ATL, indicating that DNA methylation in the isolated DNA regions tends to accumulate according to disease progression. This was also confirmed in the sequential samples from a HTLV-I carrier, who developed acute ATL (Fig. 1*B*).

Identification of Genes near the Hypermethylated DNA Regions. To analyze the influence of identified DNA hypermethylation upon gene transcription, the neighboring genes were searched using NCBI BLAST program as described in Materials and Methods. We found that 31 of 53 (58%) clones were located within the exon or intron of the gene, and 41 of 53 (77%) loci were located within 10 kb from the transcriptional start site of the nearest gene (Table 1). Because the aberrant methylation of some identified genes, such as *PAX5* (clone 10; ref. 36) and *CSPG2* (clone 27; ref. 28), have been reported in various types of cancer cells, it confirmed that MCA/RDA method in this study isolated the hypermethylated DNA regions. Then, we analyzed the transcription of genes in which the transcriptional start sites existed within 2 kb from the identified hypermethylated DNA regions (Fig. 2). On the basis of their expression profiles, we could divide the genes identified into two groups; group I con-

[3] http://www.ncbi.nlm.nih.gov/BLAST/.
[4] http://bimas.dcrt.nih.gov:80/molbio/proscan/.

Table 1 *Characterization of DNA fragments isolated by MCA/RDA*

Clone	Size (bp)	Accession no. (location)	Chromosomal location	Nearest gene	CpG Island	Distance from TSS (bp)
1	733	NT_007592.13 (19499884–19500616)	6p21.31	*No gene**	Yes	
2	511	NT_006713.13 (6324465–6324975)	5q13.3	*OTP*	Yes	2,600
3	377	NT_025741.13 (5075242–5075619)	6q16.3	*SIM1*	Yes	5,800
4	486	NT_079617.1 (40630–41115)	4p16.1	*HMX1*	Yes	200
5	577	NT_016354.16 (9912331–9912907)	4q21.3	*NKX6–1*	Yes	700
6	418	NT_009237.16 (13859103–13859520)	11p15.2	*CALCB*	Yes	50
7	673	NT_011109.15 (19265899–19266571)	19q13.33	*No gene*	Yes	
8	746	NT_022184.13 (23995750–23996496)	2p21	*LOC375201*	Yes	7,600
9	923	NT_026437.10 (32654509–32655429)	14q22.1	*PTGDR*	Yes	40
10	894	NT_008413.16 (37015465–37016356)	9p13	*PAX5*	Yes	8,100
11	533	NT_030059.11 (38044642–38045174)	10q26.1	*EMX2*	Yes	5,300
12	651	NT_010505.14 (1424933–1425583)	16q12.1	*CBLN1*	Yes	680
13	568	NT_007592.13 (1276022–1276589)	6p24	*TFAP2A*	Yes	2,500
14	725	NT_008583.16 (25707371–25708095)	10q22.3	*MGC2555*	Yes	4,500
15	591	NT_079592.1 (49215607–49216197)	7p12.1	*LOC378069*	Yes	190
16	424	NT_023666.16 (1934093–1934516)	8p21.2	*No gene*	Yes	
17	806	NT_009237.16 (30583999–30584804)	11p13	*No gene*	Yes	
18	696	NT_016354.16 (58568060–58568755)	4q28.3	*PCDH10*	Yes	2,500
19	620	NT_079596.1 (7038723–7039342)	7q22	*LAMB1*	Yes	720
20	937	NT_007592.13 (17472263–17473201)	6p21.1	*No gene*	Yes	
21	462	NT_008183.17 (7857852–7858312)	8q11.23	*KIAA1889*	Yes	290
22	487	NT_008470.16 (11911721–11912207)	9q31	*KLF4*	Yes	1,100
23	893	NT_025741.13 (12657384–12658276)	6q21	*NR2E1*	Yes	690
24	750	NT_079592.1 (23721242–23721991)	7p15.1	*NPY*	Yes	370
25	766	NT_077451.3 (1864762–1865527)	5qter	*ADAMTS2*	Yes	1,800
26	607	NT_004610.16 (1272547–1273153)	1p35	*PLA2G2F*	No	2,600
27	404	NT_006713.13 (12160670–12161073)	5q14.3	*CSPG2*	Yes	960
28	521	NT_023666.16 (922959–923479)	8p21.2	*EGR3*	Yes	1,700
29	895	NT_029419.10 (19759986–19760882)	12q13.2	*NXPH4*	No	6,100
30	430	NT_079593.1 (2760886–2761315)	7q11	*No gene*	No	
31	476	NT_011362.8 (4369966–4370441)	20q12	*MAFB*	Yes	350
32	878	NT_033903.6 (11275620–11276497)	11q13.1	*RIN1*	No	550
33	732	NT_009755.16 (3985255–3985983)	12q24.32	*No gene*	Yes	
34	795	NT_026437.10 (16902942–16903736)	14q13	*LOC253970*	Yes	340
35	530	NT_004671.15 (9240059–9240588)	1q31	*LHX9*	Yes	920
36	724	NT_005334.14 (10987626–10988353)	2p24.1	*No gene*	Yes	
37	943	NT_009237.16 (31223373–31224306)	11p13	*WIT-1*	Yes	40
38	587	NT_077921.1 (573714–574300)	1p36.13	*PAX7*	Yes	660
39	273	BX649589.3 (5548–5821)	9q34.3	*AGS3*	Yes	6,100
40	755	NT_022184.13 (8050474–8051228)	2p23.3	*No gene*	No	
41	958	NT_010783.14 (18185717–18186674)	17q22	*TBX4*	Yes	200
42	871	NT_005403.14 (27236075–27236942)	2q31.1	*HOXD3*	Yes	1,300
43	470	NT_030059.11 (21731229–21731698)	10q24	*LBX1*	Yes	5,500
44	406	NT_008818.15 (769699–770104)	10q26.2	*LOC338623*	Yes	230
45	565	NT_023935.16 (8798224–8798788)	9q21	*No gene*	Yes	
46	526	NT_010194.16 (47422212–47422737)	15q23	*ISL2*	Yes	2,700
47	445	NT_029289.10 (9369340–9369784)	5q32	*ADRB2*	Yes	230
48	414	NT_023133.11 (17468804–17469217)	5q34	*NKX2–5*	Yes	2,600
49	583	NT_022792.16 (6841497–6842079)	4q33	*No gene*	Yes	
50	1096	NT_026437.10 (18598721–18599816)	14q13	*SSTR1*	Yes	1,500
51	608	NT_077812.2 (1002922–1003529)	19p13.3	*FLJ46061*	Yes	8,600
52	310	NT_006713.13 (1986840–1987149)	5q13.3	*No gene*	Yes	
53	465	NT_011512.9 (8031349–8031813)	21q21.1	*NCAM2*	Yes	690

Abbreviation: TSS, transcription start site.
* "*No gene*" means TSS of the nearest gene is more than 10 kb away from the isolated region.

tained genes with an expression that was observed in activated T lymphocytes but suppressed in HTLV-I-transformed and ATL cell lines (Fig. 2*A*). On the other hand, the transcription of genes in group II was not detected in activated T cells and HTLV-I-associated cell lines whereas their expression was found in the brain and/or skeletal muscle (Fig. 2*B*). Group II genes were hypermethylated only in ATL cells but not in normal T lymphocytes. These results suggest that the suppressed expression of group I genes is implicated in leukemogenesis.

Relationship between Silencing of Neighboring Genes and DNA Methylation. We studied the detailed DNA methylation status in the promoter and isolated regions of *KLF4* and *EGR3* genes, which belong to group I, using the bisulfite sequencing method. The sequences of each of the 10 clones are summarized in Fig. 3. In both ATL-43T and an acute ATL, the CpGs in the isolated region of *KLF4* gene, which existed in exon 3, were heavily methylated (Fig. 3*A*) whereas there was little methylation in normal PBMCs. In the predicted *KLF4* promoter sequence, there was dense DNA methylation in ATL-43T and mild methylation in fresh ATL cells whereas the CpGs in normal PBMC were little methylated (Fig. 3*A*). DNA methylation in the promoter region of *KLF4* has been studied in primary cells with different stage of ATL to analyze the association with disease progression (Fig. 3*B*). DNA methylation increased according to disease progression from carrier to leukemia although there was little difference between chronic and acute ATL. In the case of the *EGR3* gene, the isolated region, which was in exon 2, was hypermethylated in the ATL cell line and fresh ATL cells but hypomethylated in normal PBMC (Fig. 3*C*). Although the promoter region of *EGR3* was hypermethylated in the ATL cell line, it was not methylated in fresh ATL cells and normal PBMCs.

Next, we analyzed whether the transcriptions of these silenced genes could be recovered by the demethylating agent, 5-aza-dC, and/or a histone deacetylase inhibitor, TSA in ATL cells. The combination of 5-aza-dC and TSA is known to induce a synergistic effect on DNA demethylation (37). As shown in Fig. 2*C*, the transcripts of *KLF4* gene were re-expressed by 5-aza-dC alone or by combination

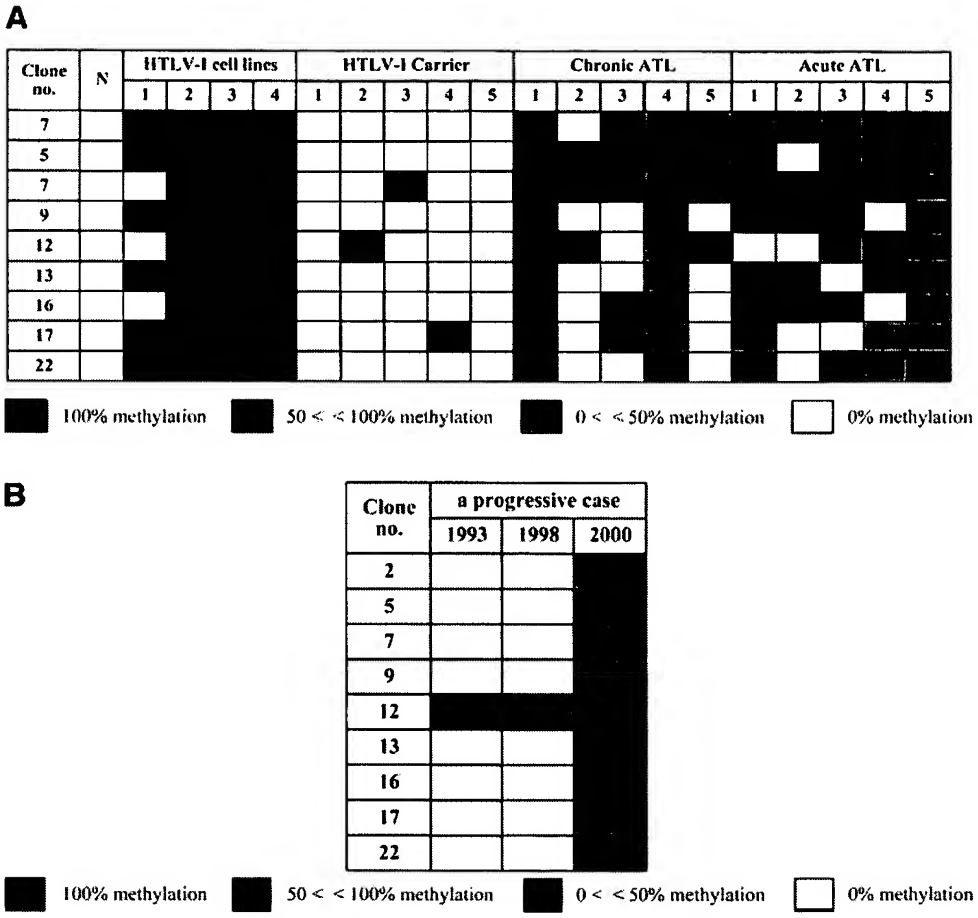

Fig. 1. Frequencies of CpG methylation of the isolated DNA regions in ATL cell lines and clinical samples. The frequencies of CpG methylation in 9 of 53 isolated regions were determined using the Combined Bisulfite Restriction Analysis method. *A*, methylation status in normal PBMCs (N), four ATL cell lines (*1*, MT-1; *2*, ATL-48T; *3*, ATL-43T; *4*, TL-Om1), and PBMCs from five asymptomatic HTLV-I carriers, five chronic ATL, and five acute ATL patients. Densities of methylation are represented by *tones of squares* as presented. *B*, serial changes of methylation status in these regions in a case with progression from carrier state to acute ATL.

treatment but not by TSA alone, suggesting that DNA methylation of *KLF4* gene is associated with its silencing in ATL cells. On the other hand, the transcript of *EGR3* gene was detected more clearly when ATL cells were treated with TSA alone or their combination than with 5-aza-dC alone, indicating that the *EGR3* gene was silenced by histone deacetylation rather than by DNA methylation. However, because demethylation by 5-aza-dC partially recovered *EGR3* gene transcription, we consider that DNA methylation is associated in part with suppressed expression of *EGR3* gene. In addition, the transcriptions of other group I genes, such as *CSPG2*, *MAFB*, and *ADRB2*, were also recovered by 5-aza-dC treatment. Because the transcription of *ADAMTS2* and *PTGDR* could not be recovered by either 5-aza-dC or TSA, the silencing of these genes might be because of other mechanism(s).

Enforced Expression of *KLF4* or *EGR3* Gene in ATL Cells. To investigate the function of *KLF4* and *EGR3* genes in ATL cells, adenovirus vectors expressing *KLF4* (KLF4-AD) or *EGR3* (EGR3-AD), were transfected into ATL-43T, in which the transcription of both genes were completely suppressed. Transfection of *KLF4*-expressing adenovirus vector induced the transcription (Fig. 4*A*) and resulted in accumulation of apoptotic cells as demonstrated by Annexin V-PI staining (Fig. 4*B*). The apoptosis was also confirmed by TUNEL assay (data not shown). The number of apoptotic cells reached maximum 48 hours later (30.1%, Fig. 4*C*). This percentage was similar to that of X-gal-stained cells (49.0%) when lacZ-AD was transfected into ATL-43T. Taken together, these results suggest that *KLF4* expression induced apoptosis in most transduced cells.

Because the *EGR3* gene is reported to be critical for *Fas ligand* (*FasL*) gene transcription (38), we studied whether enforced expression of *EGR3* could induce apoptosis of ATL cells. After transfection, both *EGR3* and *FasL* were transcribed 48 hours later (Fig. 5*A*), which coincided with increased apoptotic cells in ATL-43T infected EGR3-AD, in contrast to control (Fig. 5*B* and *C*). In addition, increased apoptotic cells were also confirmed by TUNEL assay (data not shown). Thus, enforced expression of EGR3 was considered to result in Fas-FasL-mediated apoptosis. To clarify whether this apoptosis is actually mediated by Fas signaling, we transfected vectors expressing $mCasper_L$ or E8. $mCasper_L$ is a mouse c-FLIP that inhibits the activation of procaspase 8 at the death-inducing signaling complex, whereas E8 is a viral FLIP derived from the equine herpes virus type 2. Transfection of EGR3-AD did not increase apoptosis of ATL-43T cells that expressed $mCasper_L$ and E8 (Fig. 5*A* and *C*), confirming that EGR3-induced apoptosis in ATL cell line is mediated by Fas-mediated signal.

DISCUSSION

In the present study, we identified hypermethylated DNA regions by MCA/RDA method. Consistent with the previous study (28), this method could identify hypermethylated CpG islands; 48 of 53 (91%) DNA clones identified in this study satisfied the criteria of CpG islands, and 41 of 53 (77%) DNA clones were located within 10 kb from the transcriptional start site of the nearest gene. Identified genes in the vicinity of isolated hypermethylated DNA regions could be divided into two groups; genes of group II are not expressed and not methylated in normal T lymphocytes, however, are hypermethylated in ATL cells. On the other hand, genes of group I are expressed but not methylated in normal T lymphocytes whereas their expression is suppressed in ATL cells in association with DNA methylation. It is possible that the mechanism of *de novo* methylation is dysregulated,

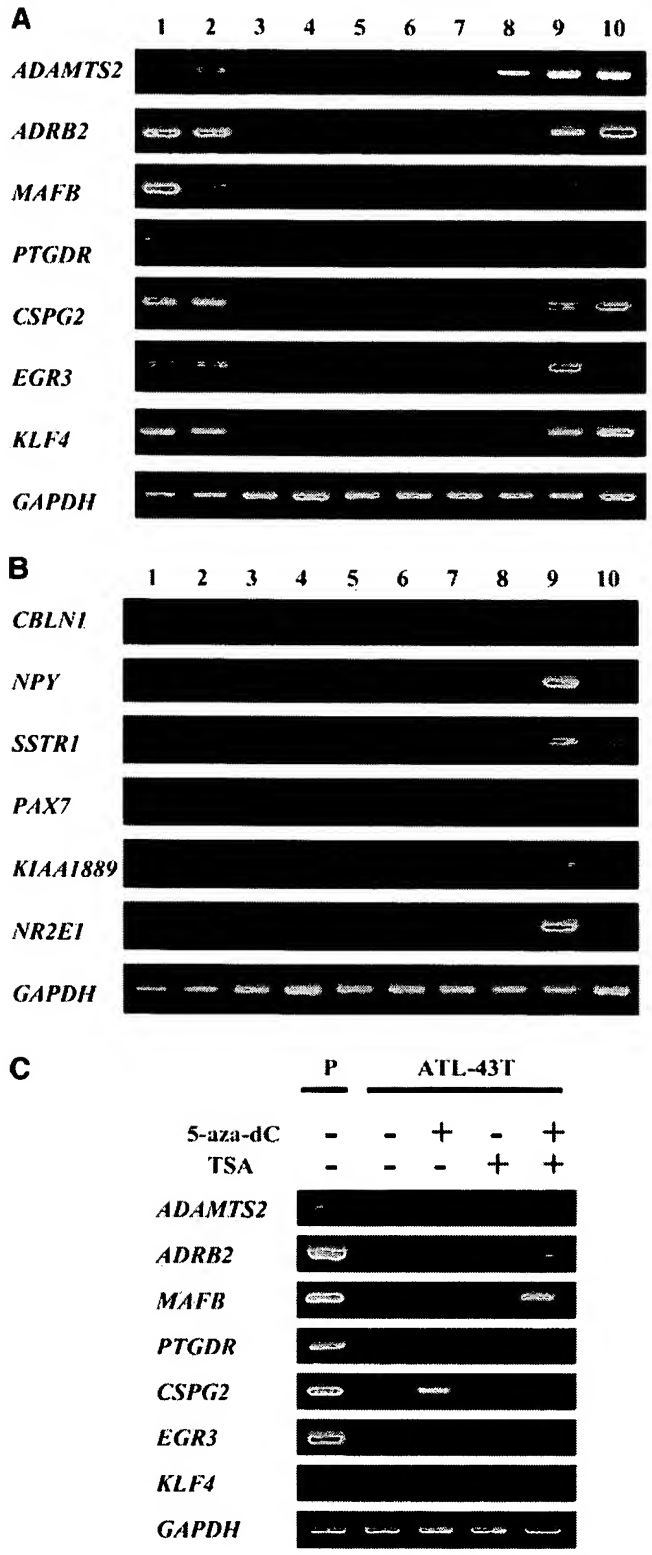

Fig. 2. Expression of genes in the vicinity of hypermethylated regions isolated by MCA/RDA. Expression of the genes near the isolated regions was studied by RT-PCR. Transcripts of the *glyceraldehyde-3-phosphate dehydrogenase* (*GAPDH*) gene were used as a control. *Lane 1*, normal resting PBMC; *Lane 2*, normal activated T cell; *Lane 3*, ED; *Lane 4*, ATL-43T; *Lane 5*, ATL-48T; *Lane 6*, ATL-55T; *Lane 7*, MT-1; *Lane 8*, MT-2; *Lane 9*, normal whole brain; *Lane 10*, normal skeletal muscle. *A*, group I, genes expressed in normal T cells but suppressed in HTLV-I-transformed and ATL cell lines. *B*, group II, genes not expressed in normal T cells and HTLV-I-associated cell lines. *C*, recovered expression of the group I genes after demethylation, ATL-43T was treated with 5-aza-dC only, TSA only, or both. Using cDNAs obtained from the treated and untreated cells, expressions of *KLF4* and *EGR3* were analyzed by RT-PCR. Phytohemagglutinin blast (P) was used as a positive control. RT-PCR of *GAPDH* was also performed to provide a control for initial RNA amounts.

resulting in aberrant methylation of genes despite their transcription as observed in group II genes. In this regard, Toyota *et al.* (28) isolated 33 hypermethylated DNA sequences in a colon cancer cell line using the MCA/RDA method and named these clones MINT1–33. Among DNA regions identified in this study, four clones were identical to MINT clones (Table 1, clone 2, clone 15, clone 30 and clone 48). These findings indicate that such DNA regions in the genome are prone to be methylated in cancer cells, which is consistent with an earlier report (22), although the factors that determine such susceptibility to methylation remain unresolved. In addition to such DNA methylation observed among different types of cancer cells, there are hypermethylated genes specifically observed in ATL cells. Analysis of DNA methylation of such genes in non-ATL T-cell lines showed that they were also methylated (data not shown), suggesting that DNA methylation of such genes is T-cell specific.

In addition to hypermethylation, we also reported hypomethylated genes in ATL cells, which included *MEL1S*, *CACNA1H*, and *Nogo receptor* genes as identified by the MCA/RDA method (30). Among them, the aberrant expression of *MEL1S* was frequently observed in ATL cells and has been shown to confer resistance against transforming growth factor-β. Thus, the MCA/RDA method indicates the involvement of both hyper- and hypomethylation in leukemogenesis of ATL although in a different manner.

In the case of *EGR3* gene, only the coding regions were methylated with little DNA methylation of the promoter region in fresh ATL cells although its expression was suppressed. TSA has more profound effect than 5-aza-dC, suggesting that histone modification, rather than DNA methylation, in the promoter region might silence the transcription of the *EGR3* gene. However, because DNA methylation in the coding region was associated with such silencing, detection of DNA methylation in non-promoter regions is also capable of identifying such silenced genes as observed in the *EGR3* gene.

EGR3 is a transcriptional factor containing zinc finger domain as well as KLF4. It has been reported that enforced expression of *EGR3* gene resulted in expression of *FasL* in HeLa cells (38), indicating that EGR3 is a critical transcriptional factor for *FasL* transcription. In agreement with these results, we also showed that expression of *EGR3* induced *FasL* transcription, resulting in apoptosis of ATL cells. Although ATL cells possess a phenotype of activated T cells and highly express Fas antigens on their surfaces, they do not produce FasL. On the other hand, normal T lymphocytes can express both Fas antigens and FasL after activation, and the number of activated T lymphocytes is regulated by Fas-FasL system-mediated apoptosis, which is designated as activation-induced cell death (39). Activation-induced cell death controls the number of activated T lymphocytes, consequently suppressing the immune response. Suppression of *EGR3* gene in ATL cells could account for lack of expression of FasL, which enables ATL cells to escape from activation-induced cell death. In the present study, we demonstrated that enforced expression of *EGR3* gene-induced FasL expression and apoptosis. Thus, because both KLF4 and EGR3 are accelerators of ATL cell apoptosis, *KLF4* and *EGR3* genes are considered new tumor-suppressor gene candidates in ATL.

KLF4 is a member of the Kruppel-like factor family, which is highly expressed in epithelial tissues such as the gut and skin, especially in the terminally differentiated cells (40, 41). Previous studies reported that KLF4 plays important roles in the regulation of G_1-S and G_2-M cell cycle checkpoint in colon cancer cells and that these functions are likely to be p53-dependent (42–44). According to these findings, KLF4 is thought to be associated with tumorigenicity of colon cancer cells. However, there is no report regarding the functional role of *KLF4* gene in lymphoid cells. Our study demonstrated that KLF4 expression induced apoptosis of ATL cells. Although the

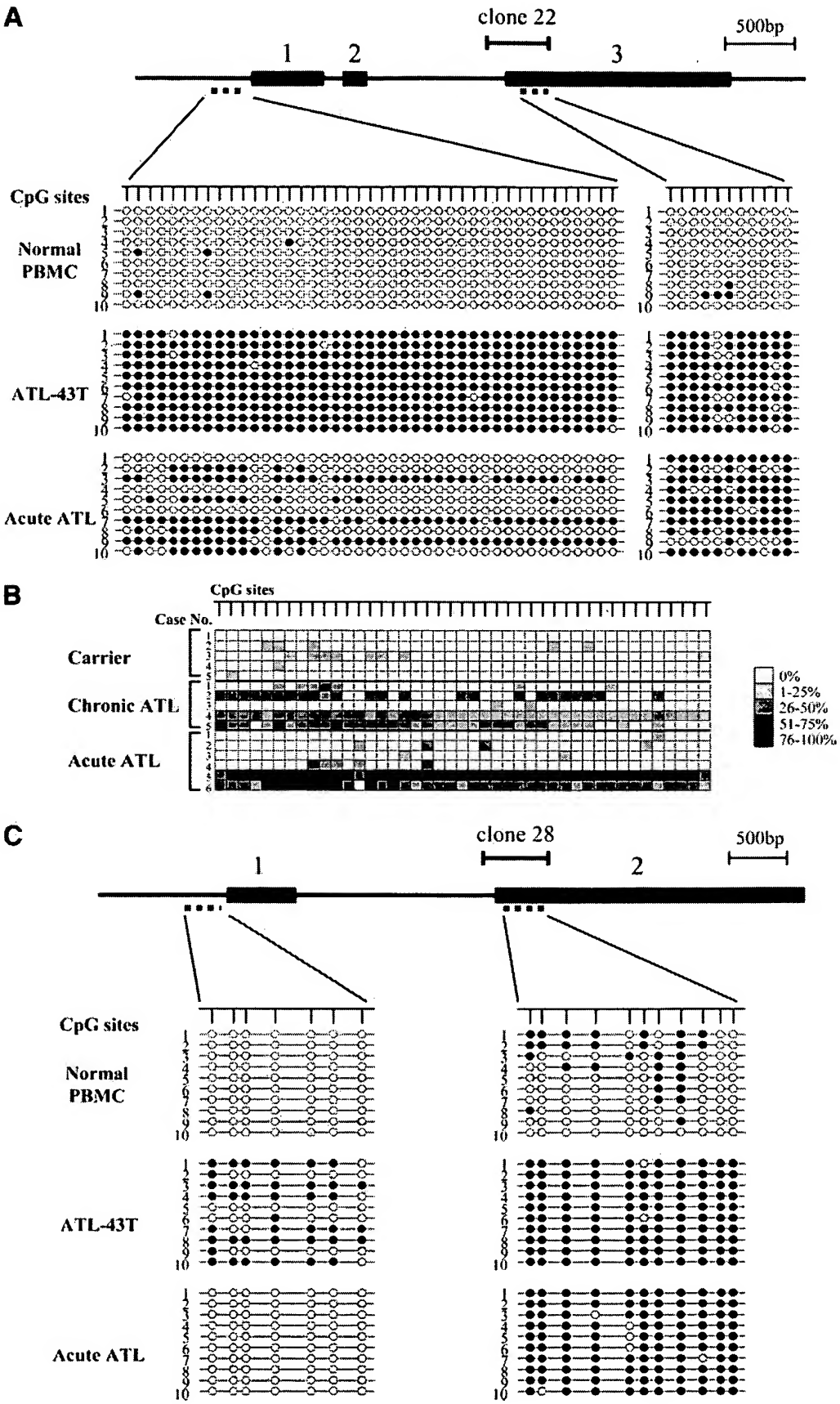

Fig. 3. Methylation status of *KLF4* and *EGR3* genes. Genomic DNAs of normal PBMC, an ATL cell line (ATL-43T), and primary cells of acute ATL were treated by sodium bisulfite and then amplified by primers specific for DNA regions in *KLF4* and *EGR3* genes identified by MCA/RDA and for their promoter regions. Then, PCR products were subcloned into plasmid DNA, and the sequences were determined in 10 clones of each (*A*, *KLF4*; *C*, *EGR3*). ○, unmethylated CpG sites; ●, methylated CpG sites. *B*, methylation status of *KLF4* promoter in primary cells with different stage of ATL; methylation level of each CpG site was calculated based on the results of bisulfite sequencing analysis and represented by *tones of squares*.

mechanism of apoptosis needs additional study, its silencing by DNA methylation facilitates the survival of ATL cells.

The present study showed that the densities of CpG methylation in identified DNA regions tend to increase with disease progression. Moreover, analysis of sequential samples from a patient who was followed from carrier state until the onset of acute ATL revealed that DNA methylation accumulated at the onset of ATL (Fig. 1*B*). These data indicate that serial analysis of the methylation status in identified hypermethylated regions might be a useful tool in the diagnosis and staging of ATL.

HTLV-I-infected clones have been shown to persist over seven years in the same HTLV-I carrier (45), suggesting that HTLV-I-infected cells survive for a long time through the action of viral proteins. On the other hand, it has been reported that aging is closely related to alterations of DNA methylation. Progressive loss of 5-methylcytosine content is observed in normal aging cells, primarily within DNA-repeated sequences. In contrast, some genes show progressive, age-related increases of DNA methylation, resulting in silencing their expressions (46). Taken together, the prolonged life span of HTLV-I-infected T cells might be a predisposing factor for aberrant DNA methylation. During the long latent period, it is possible that HTLV-I-infected cells that are adapted for survival are selected *in vivo*. In such evolution of infected cells, genetic and epigenetic changes are thought to play critical roles by suppressing the transcription of genes with tumor suppressor functions or activating the expression of genes, which exerts positive effects on survival of tumor cells.

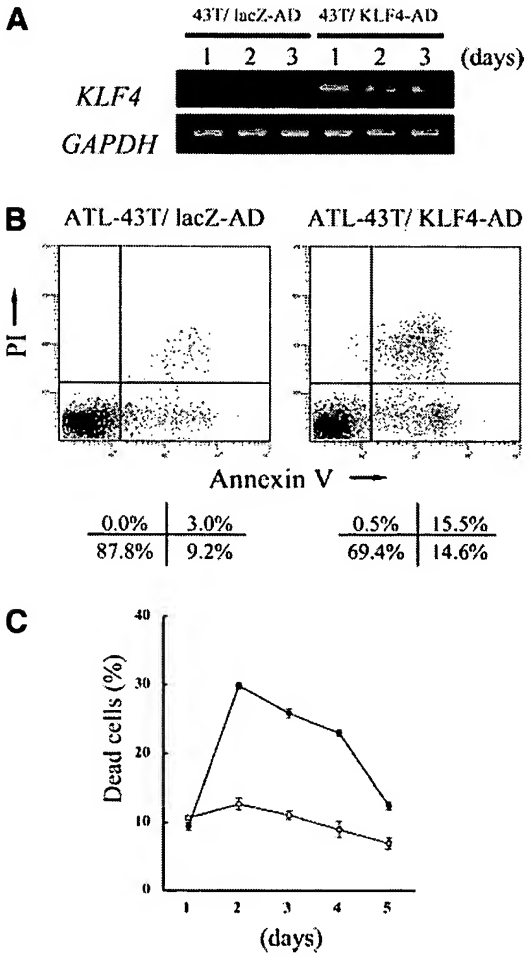

Fig. 4. Induction of apoptosis of ATL-43T by enforced expression of *KLF4*. *A*, expression of *KLF4* gene in ATL-43T transfected with lacZ-AD or KLF4-AD was studied by RT-PCR. *B*, detection of apoptotic cells in ATL-43T by double staining with Annexin V-FITC and PI at day 2 of lacZ-AD and KLF4-AD infection. The percentage of cells in each quadrant is shown at the *bottom of the panels*. *C*, serial changes in the percentages of dead cells detected by Annexin V-PI double staining. ○, ATL-43T infected with lacZ-AD; ●, ATL-43T infected with KLF4-AD. Data are mean ± SE.

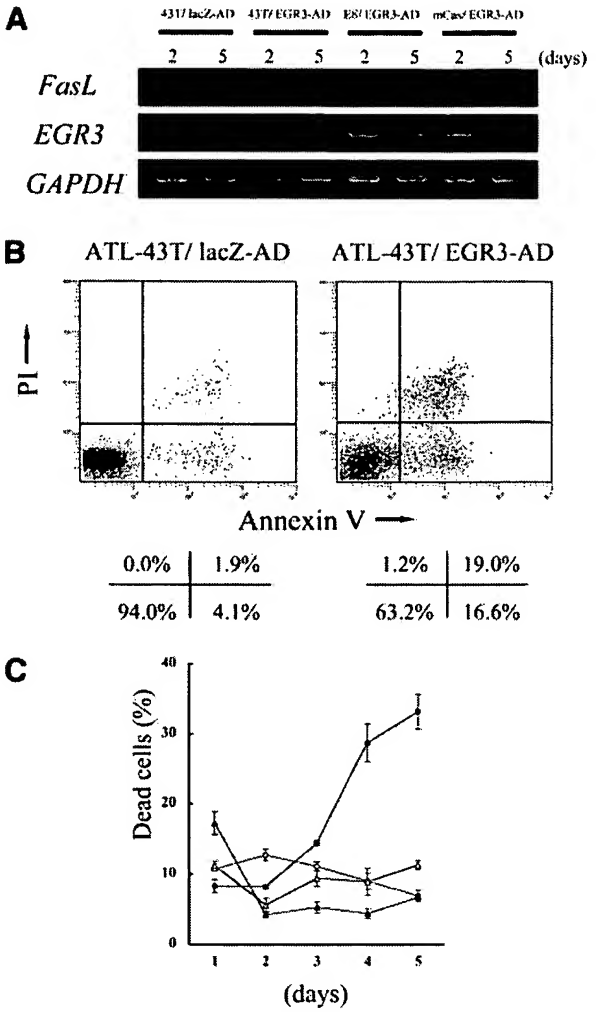

Fig. 5. Induction of *FasL* transcription and apoptosis of ATL-43T by enforced expression of *EGR3*. *A*, expressions of *EGR3* and *FasL* genes in transfected cell lines were studied by RT-PCR. *B*, detection of apoptotic cells in ATL-43T by double staining with Annexin V-FITC and PI at day 5 of lacZ-AD and EGR3-AD infection. The percentage of cells in each quadrant is shown at the *bottom of the panels*. *C*, serial changes in the percentages of dead cells detected by Annexin V-PI double staining. ○, ATL-43T infected with lacZ-AD; ●, ATL-43T infected with EGR3-AD; ∧, ATL-43T-mCas infected with EGR3-AD; and ▲, ATL-43T-E8 infected with EGR3-AD. Data are mean ± SE.

In conclusion, we have demonstrated in the present study that the MCA/RDA method could identify the differentially methylated DNA regions and genes according to disease progression of ATL. Such identification of aberrantly methylated genes allows for the diagnosis and staging of ATL and clarifies the molecular mechanism of leukemogenesis.

ACKNOWLEDGMENTS

We are grateful to Michiyuki Maeda for providing us valuable cell lines and to Yoshihiro Koya for valuable help. The authors also thank Dr. F. G. Issa (word-medex.com.au) for careful reading and editing of the manuscript.

REFERENCES

1. Takatsuki K, Uchiyama T, Sagawa K, Yodoi J. Adult T cell leukemia in Japan. In: Seno S, Takaku F, Irino S, editors. Topic in hematology: proceedings of the 16th international congress of Hematology, Kyoto, September 5–11, 1976. Amsterdam, Oxford: Excerpta Medica; 1977. p. 73–7.

2. Uchiyama T, Yodoi J, Sagawa K, Takatsuki K, Uchino H. Adult T-cell leukemia: clinical and hematologic features of 16 cases. Blood 1977;50:481–92.
3. Poiesz BJ, Ruscetti FW, Gazdar AF, Bunn PA, Minna JD, Gallo RC. Detection and isolation of type C retrovirus particles from fresh and cultured lymphocytes of a patient with cutaneous T-cell lymphoma. Proc Natl Acad Sci USA 1980;77:7415–9.
4. Wong-Staal F, Gallo RC. Human T-lymphotropic retroviruses. Nature (Lond) 1985; 317:395–403.
5. Arisawa K, Soda M, Endo S, et al. Evaluation of adult T-cell leukemia/lymphoma incidence and its impact on non-Hodgkin lymphoma incidence in southwestern Japan. Int J Cancer 2000;85:319–24.
6. Yoshida M. Multiple viral strategies of HTLV-I for dysregulation of cell growth control. Annu Rev Immunol 2001;19 475–96.
7. Franchini G, Fukumoto R, Fullen JR. T-cell control by human T-cell leukemia/ lymphoma virus type 1. Int J Hematol 2003;78:280–96.
8. Jeang KT. Functional activities of the human T-cell leukemia virus type I Tax oncoprotein: cellular signaling through NF-kappa B. Cytokine Growth Factor Rev 2001;12:207–17.
9. Fujii M, Tsuchiya H, Chuhjo T, Akizawa T, Seiki M. Interaction of HTLV-1 Tax1 with p67SRF causes the aberrant induction of cellular immediate early genes through CArG boxes. Genes Dev 1992;6:2066–76.
10. Kwok RP, Laurance ME, Lundblad JR, et al. Control of cAMP-regulated enhancers by the viral transactivator Tax through CREB and the co-activator CBP. Nature (Lond) 1996;380:642–6.
11. Jeang KT, Widen SG, Semmes OJ 4th, Wilson SH. HTLV-I trans-activator protein, tax, is a trans-repressor of the human beta-polymerase gene. Science (Wash D C) 1990;247:1082–4.
12. Suzuki T, Uchida-Toita M, Yoshida M. Tax protein of HTLV-I inhibits CBP/p300-mediated transcription by interfering with recruitment of CBP/p300 onto DNA element of E-box or p53 binding site. Oncogene 1999;18:4137–43.
13. Jin DY, Spencer F, Jeang KT. Human T cell leukemia virus type 1 oncoprotein Tax targets the human mitotic checkpoint protein MAD1. Cell 1998;93:81–91.
14. Takeda S, Maeda M, Morikawa S, et al. Genetic and epigenetic inactivation of tax gene in adult T-cell leukemia cells. Int J Cancer 2004;109:559–67.
15. Tamiya S, Matsuoka M, Etoh K, et al. Two types of defective human T-lymphotropic virus type I provirus in adult T-cell leukemia. Blood 1996;88:3065–73.
16. Furukawa Y, Kubota R, Tara M, Izumo S, Osame M. Existence of escape mutant in HTLV-I tax during the development of adult T-cell leukemia. Blood 2001;97:987–93.
17. Koiwa T, Hamano-Usami A, Ishida T, et al. 5'-long terminal repeat-selective CpG methylation of latent human T-cell leukemia virus type I provirus in vitro and in vivo. J Virol 2002;76:9389–97.
18. Bangham CR. Human T-lymphotropic virus type 1 (HTLV-1): persistence and immune control. Int J Hematol 2003;78:297–303.
19. Sakashita A, Hattori T, Miller CW, et al. Mutations of the p53 gene in adult T-cell leukemia. Blood 1992;79:477–80.
20. Hatta Y, Hirama T, Miller CW, Yamada Y, Tomonaga M, Koeffler HP. Homozygous deletions of the p15 (MTS2) and p16 (CDKN2/MTS1) genes in adult T-cell leukemia. Blood 1995;85:2699–704.
21. Nosaka K, Maeda M, Tamiya S, Sakai T, Mitsuya H, Matsuoka M. Increasing methylation of the CDKN2A gene is associated with the progression of adult T-cell leukemia. Cancer Res 2000;60:1043–8.
22. Costello JF, Fruhwald MC, Smiraglia DJ, et al. Aberrant CpG-island methylation has non-random and tumour-type-specific patterns. Nat Genet 2000;24:132–8.
23. Esteller M, Corn PG, Baylin SB, Herman JG. A gene hypermethylation profile of human cancer. Cancer Res 2001;61:3225–9.
24. Hayashizaki Y, Hirotsune S, Okazaki Y, et al. Restriction landmark genomic scanning method and its various applications. Electrophoresis 1993;14:251–8.
25. Gonzalgo ML, Liang G, Spruck CH, 3rd, Zingg JM, Rideout WM, 3rd, Jones PA. Identification and characterization of differentially methylated regions of genomic DNA by methylation-sensitive arbitrarily primed PCR. Cancer Res 1997;57:594–9.
26. Ushijima T, Morimura K, Hosoya Y, et al. Establishment of methylation-sensitive-representational difference analysis and isolation of hypo- and hypermethylated genomic fragments in mouse liver tumors. Proc Natl Acad Sci USA 1997;94:2284–9.
27. Huang TH, Laux DE, Hamlin BC, Tran P, Tran H, Lubahn DB. Identification of DNA methylation markers for human breast carcinomas using the methylation-sensitive restriction fingerprinting technique. Cancer Res 1997;57:1030–4.
28. Toyota M, Ho C, Ahuja N, et al. Identification of differentially methylated sequences in colorectal cancer by methylated CpG island amplification. Cancer Res 1999;59: 2307–12.
29. Ballestar E, Paz MF, Valle L, et al. Methyl-CpG binding proteins identify novel sites of epigenetic inactivation in human cancer. EMBO J 2003;22:6335–45.
30. Yoshida M, Nosaka K, Yasunaga J, Nishikata I, Morishita K, Matsuoka M. Aberrant expression of the MEL1S gene identified in association with hypomethylation in adult T-cell leukemia cells. Blood 2004;103:2753–60.
31. OhYama T, Tsukumo S, Yajima N, Sakamaki K, Yonehara S. Reduction of thymocyte numbers in transgenic mice expressing viral FLICE-inhibitory protein in a Fas-independent manner. Microbiol Immunol 2000;44:289–97.
32. Krueger A, Schmitz I, Baumann S, Krammer PH, Kirchhoff S. Cellular FLICE-inhibitory protein splice variants inhibit different steps of caspase-8 activation at the CD95 death-inducing signaling complex. J Biol Chem 2001;276:20633–40.
33. Xiong Z, Laird PW. COBRA: a sensitive and quantitative DNA methylation assay. Nucleic Acids Res 1997;25:2532–4.
34. Clark SJ, Harrison J, Paul CL, Frommer M. High sensitivity mapping of methylated cytosines. Nucleic Acids Res 1994;22:2990–7.
35. Takai D, Jones PA. Comprehensive analysis of CpG islands in human chromosomes 21 and 22. Proc Natl Acad Sci USA 2002;99:3740–5.
36. Palmisano WA, Crume KP, Grimes MJ, et al. Aberrant promoter methylation of the transcription factor genes PAX5 alpha and beta in human cancers. Cancer Res 2003;63:4620–5.
37. Cameron EE, Bachman KE, Myohanen S, Herman JG, Baylin SB. Synergy of demethylation and histone deacetylase inhibition in the re-expression of genes silenced in cancer. Nat Genet 1999;21:103–7.
38. Mittelstadt PR, Ashwell JD. Cyclosporin A-sensitive transcription factor Egr-3 regulates Fas ligand expression. Mol Cell Biol 1998;18:3744–51.
39. Krammer PH. CD95's deadly mission in the immune system. Nature (Lond) 2000; 407:789–95.
40. Shields JM, Christy RJ, Yang VW. Identification and characterization of a gene encoding a gut-enriched Kruppel-like factor expressed during growth arrest. J Biol Chem 1996;271:20009–17.
41. Segre JA, Bauer C, Fuchs E. Klf4 is a transcription factor required for establishing the barrier function of the skin. Nat Genet 1999;22:356–60.
42. Zhang W, Geiman DE, Shields JM, et al. The gut-enriched Kruppel-like factor (Kruppel-like factor 4) mediates the transactivating effect of p53 on the p21WAF1/ Cip1 promoter. J Biol Chem 2000;275:18391–8.
43. Yoon HS, Chen X, Yang VW. Kruppel-like factor 4 mediates p53-dependent G1/S cell cycle arrest in response to DNA damage. J Biol Chem 2003;278:2101–5.
44. Yoon HS, Yang VW. Requirement of Kruppel-like factor 4 in preventing entry into mitosis following DNA damage. J Biol Chem 2004;279:5035–41.
45. Etoh K, Tamiya S, Yamaguchi K, et al. Persistent clonal proliferation of human T-lymphotropic virus type I-infected cells in vivo. Cancer Res 1997;57:4862–7.
46. Issa JP. Age-related epigenetic changes and the immune system. Clin Immunol 2003;109:103–8.

Oncogene (2003) 22, 4434–4443
 0950-9232/03 $25.00
www.nature.com/onc

Transcriptional regulation of A33 antigen expression by gut-enriched Krüppel-like factor

Zebin Mao[1,2], Song Shan[1,2], Yunyan Zhu[1], Xia Yi[1], Hua Zhang[1], Yongfeng Shang*[,1] and Tanjun Tong*[,1]

[1]*Depatrtment of Biochemistry and Molecular Biology, Peking University Health Science Center, Beijing 100083, China*

A33 antigen is a membrane-bound protein that is expressed only in intestinal epithelium and in most human colon cancers. Thus, A33 antigen has been explored as a potential therapeutic target for the treatment of colon cancers. However, little is known about the mechanism responsible for the tissue-specific pattern of its expression. In this report, we demonstrate that gut-enriched Krüppel-like factor (GKLF) binds to the promoter region of A33 antigen gene in colonic carcinoma cells and that mutations in the GKLF binding sequence in this region lead to diminished expression of A33 antigen. In addition, the expression of GKLF is linked to the expression of A33 antigen and blocking the expression of GKLF leads to the abolishment of A33 antigen expression. These results suggest that GKLF is a critical regulator in inducing the expression of A33 antigen in intestinal epithelium. While it has been suggested that GKLF is a regulator in inducing cell growth arrest and differentiation of the intestine, our observation that A33 antigen gene is a downstream target for GKLF suggests a more complex and diverse role for GKLF in the gut.
Oncogene (2003) **22**, 4434–4443. doi:10.1038/sj.onc.1206508

Keywords: A33 antigen; GKLF; gene regulation

Introduction

The A33 antigen is a membrane-bound glycoprotein (Catimel *et al.*, 1996; Heath *et al.*, 1997). Like other trans-membrane proteins, A33 antigen possesses three distinct regions: an extracellular region containing two putative immunoglobulin-like domains, a hydrophobic trans-membrane region, and a highly polar intracellular region containing four consecutive cysteine residues. Based on its amino-acid sequence and genomic structure, the A33 antigen is considered to be a member of a growing subfamily within the immunoglobulin superfamily that includes the marker of cortical thymocytes in *Xenopus* (CTX) (Chretien *et al.*, 1996), its putative chicken ortholog ChT1 (Katevuo *et al.*, 1999), mouse and human homologs of CTX (CTM/CTH) (Chretien *et al.*, 1998), and the receptor for group B Coxsackie viruses and adenoviruses types 2 and 5 (CAR) (Bergelson *et al.*, 1997, 1998; Tomko *et al.*, 1997).

The biological function of A33 antigen is not yet understood. It has been suggested that the A33 antigen may be a novel cell surface receptor or cell adhesion molecule in the immunoglobulin superfamily (Heath *et al.*, 1997). Immunohistochemical studies of normal tissues identified the large and small intestinal mucosa as the principal site of A33 antigen expression (Sakamoto *et al.*, 2000). Tests in tumor samples demonstrated that only tumors of the gastrointestinal tract are consistently A33 antigen positive (Sakamoto *et al.*, 2000).

The highly tissue-specific expression of A33 antigen presents a great opportunity for specific tumor targeting in patients with gastrointestinal cancer. Studies using nude mouse models with xenografts of the human colorectal carcinoma cell line SW1222 indicated that an A33 monoclonal antibody (mAb) was capable of inducing tumor regression (Antoniw *et al.*, 1996). In phase I and II trials, ^{131}I- and ^{125}I-labeled murine A33 mAb were shown to have antitumor effects without bowel toxicity (Welt *et al.*, 1994, 1996). A genetically humanized mAb A33 has been generated and phase I trials have been undertaken (Welt *et al.*, 1996). However, the mechanism responsible for the tissue-specific pattern of its expression is not yet understood.

Gut-enriched Krüppel-like factor (GKLF) is a member of the Krüppel-like factor (KLF) family that function as zinc-finger-containing transcription factors. The expression of GKLF is enriched in epithelial cells of the gastrointestinal tract (Ton-That *et al.*, 1997; Behr and Kaestner, 2002) and the skin (Behr and Kaestner, 2002) and in vascular endothelial cells (Yet *et al.*, 1998; McCormick *et al.*, 2001; Gray *et al.*, 2002; Nickenig *et al.*, 2002). Phylogenetically and structurally, KLFs are closely related to Sp1 and Krox transcription factors and they recognize very similar 'GT-box' or 'CACCC element' sites on DNA (Mahatan *et al.*, 1999; Black *et al.*, 2001).

The biological functions of GKLF are not entirely clear. *In vitro* studies have suggested that GKLF plays an important role in cell proliferation and/or differentiation (Shie *et al.*, 2000b). However, gene ablation in mice leads to a specific deficiency in the barrier function of the skin, resulting in postnatal death. Further, the extent of normal development seen in its absence is interesting given the expression pattern and postulated

*Correspondence: Y Shang; E-mail: jason@bjmu.edu.cn; ttjzzy@public.gb.com.cn
[2]These authors contributed equally to the manuscript
Received 3 December 2002; revised 11 February 2003; accepted 14 February 2003

role of GKLF in the intestine and other endodermal tissues (Katz *et al.*, 2002). In addition, although a negative correlation is seen between GKLF level and growth in intestinal and prostatic carcinomas (Foster *et al.*, 2000), GKLF levels are upregulated during progression of human oral/pharyngeal and breast carcinomas (Foster *et al.*, 2000).

Here we demonstrate that GKLF is a critical factor in contributing to the expression of A33 antigen in colonic carcinoma cells. Given the clinical observations that ^{131}I- and ^{125}I-labeled murine A33 mAb lead to the regression of colonic tumors, our results suggest that GKLF plays a more diverse role in the intestine than as a regulator in mediating cell growth arrest and differentiation.

Results

Cloning and analysis of the 5′-flanking region of the human A33 gene

In order to understand the molecular mechanisms involved in the regulation of A33 antigen expression, we first cloned the 5′-flanking region of the A33 antigen gene by PCR using the library provided in the Genome Walker Kit (Clontech). An ~1 kb PCR product was obtained and sequenced in both directions using the automated ABI Prism 370 Sequencer. Analysis of this sequence indicated that it contains a canonical TATA box, two MRE (metal response element), as well as putative binding sites for C/EBP (CCAAT enhancer binding protein), GKLF, and CDX (caudal-related homeobox) (Figure 1a). Primer extension experiments with total RNA from LoVo cells produced a major band of about 248 bp (Figure 1b), indicating that the transcription starting site is 10 nucleotides downstream of the TATA box (Figure 1c). As a control, primer extensions using tRNA did not result in any bands (data not shown).

Identification of cis-elements involved in the regulation of A33 expression in gastrointestinal carcinoma cells

To determine the transcription activation activity of the obtained DNA sequence, we next constructed EGFP

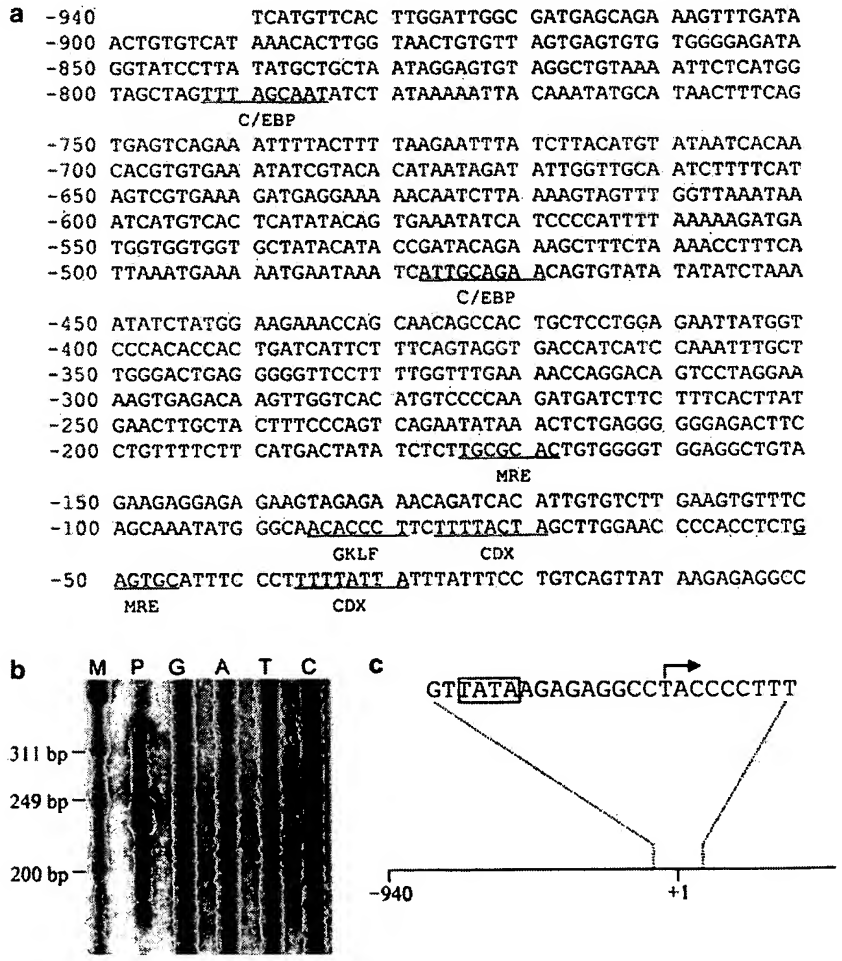

Figure 1 Cloning and analysis of the 5′-flanking region of the human A33 antigen gene. (**a**) The sequence of the 5′-flanking region of the human A33 antigen gene. The numbers represent the position relative to the transcription starting site which is numbered as +1. The putative regulatory elements are indicated by lines underneath the sequence. (**b**) The product of primer extension (lane P) and the sequencing of the product (G, A, T, and C). The analysis was done on 6% denaturing polyacrylamide gels in parallel with a DNA marker (M) (ϕX174 DNA/*Hinf* I, Promega). (**c**) Map of the transcription starting site, which is numbered as +1, of the human A33 gene

reporter constructs with the ~1 kb fragment as well as with the fragments from −759 to +25, −518 to +25, −189 to +25, and −104 to +25 of the cloned sequence by nested PCR reactions. Transient transfections were then carried out to map the *cis*-elements involved in the regulation of A33 antigen gene expression. Cells from LoVo (colonic carcinoma cell line), BGC823 (gastric carcinoma cell line), and 293 (kidney carcinoma cell line) were grown in DMEM supplemented with 10% fetal bovine serum for 24 h and transfected with the A33 antigen gene 5′-flanking region-driven EGFP reporter construct. Cells were then lysed and analysed for EGFP activity. In accordance with the tissue-specific pattern of expression of A33 antigen (Abud *et al.*, 2000; Sakamoto *et al.*, 2000), the A33 antigen promoter fragments were highly active in the human colon carcinoma cell line LoVo (Figure 2), somewhat active in BGC 823 cells, and not active in 293 cells. In addition, the EGFP activation was A33 antigen gene promoter-specific since the promoter-less vector showed low activation of EGFP expression. Serial deletion of the 5′-flanking region of the A33 antigen gene up to position −104 did not affect the transcriptional activation of EGFP expression (Figure 2), suggesting that the *cis*-element(s) for regulating the expression of the A33 antigen in colonic carcinoma cells resides in the region of −104 to +25.

DNase I footprinting analysis of A33 5′-flanking region

To identify the *cis*-elements within the −104 to +25 region, DNase I footprinting analysis was performed using nuclear extracts from LoVo cells. As shown in Figure 3, two DNase I-protected regions, designated as sites A and B, were detected on both strands of this fragment by footprinting. Site A extends from −68 to −86 and covers the sequence 5′-ACACCCTTCTTT-TACTAG-3′. Analysis of this sequence identified a recognition site for GKLF. Site B spans from −40 to −19 and covers the sequence 5′-CCCTTTTTATTATT-TATTTCCT-3′. A CDX-binding sequence was identified and the binding of CDX1 was demonstrated in this site in a recent report by Johnstone *et al.* (2002). DNase I footprinting experiments were also done using nuclear extracts from 293 cells. In agreement with our finding of no transcription activation activity in transient tranfection assays in 293 cells (Figure 2), the sequence from −104 to +25 was not protected by nuclear extracts from 293 cells (data not shown), suggesting that the transcription activity coincides with the binding of transcription factor in this region.

Site-directed mutagenesis in sites A and B

In order to confirm the functional significance of sites A and B to the promoter activity of the A33 antigen, site-directed mutagenesis was carried out to change nucleotides CC at positions −81 and −82 in site A to AG and to change nucleotides TAT at positions −28 to −30 in site B to CGA. Transient transfection experiments were performed to assess the effect of these mutations on the transcription activation activity of the −104 to +25 fragment. As shown in Figure 4, mutation in either site A or site B resulted in a significant decrease in the promoter activity of this fragment, suggesting that both sites are essential for the transcription activation activity of this fragment.

Identification of trans-acting factors

Next, we performed electrophoretic mobility shift assays (EMSA) to determine the binding of protein factors in the fragment −104 to +25. Double-stranded synthetic oligonucleotides named probes A and B (see details under the Materials and methods) encompassing each of the two DNase I footprinted sites were used as probes and incubated with nuclear extracts from LoVo, BGC823, and 293 cells. As shown in Figure 5a (upper

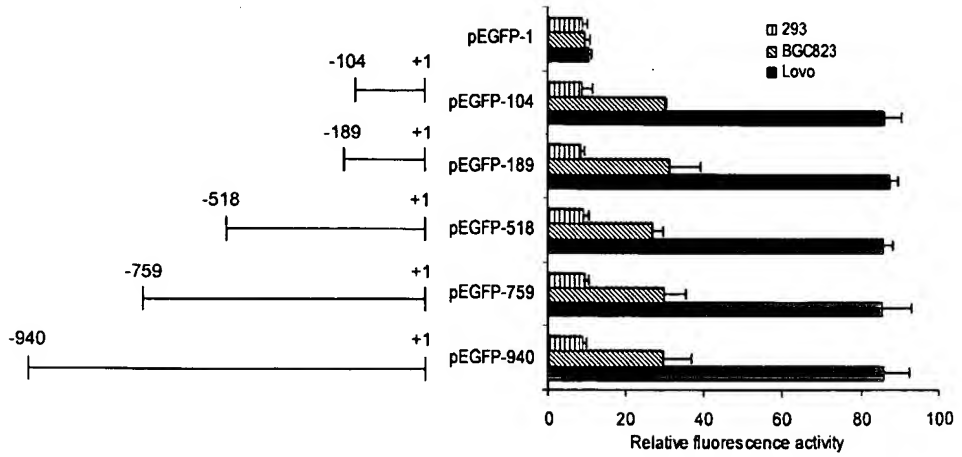

Figure 2 Analysis of the transcriptional activity of the 5′-flanking regions of the human A33 antigen gene. Serial deletions of the 5′-flanking sequence of the human A33 antigen gene were fused to the EGFP gene and transfected into LoVo, BGC823, or 293 cells. EGPF activity was measured according to the description in Materials and methods; the promoter-less vector pEGFP was used as a control. The numbers represent the positions relative to the transcription starting site of the A33 antigen gene. The results were normalized to β-galactosidase activity and represent the mean±s.d. for three independent experiments

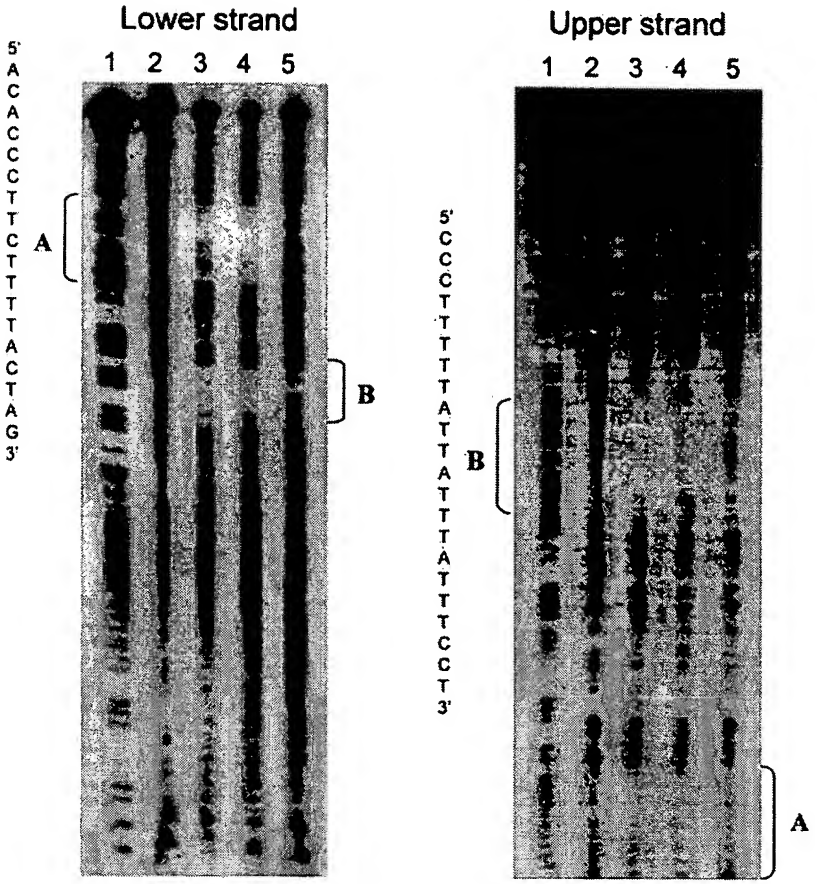

Figure 3 DNase I footprinting analysis of ^{32}P-labeled A33 antigen gene 5′-flanking fragment −104 to +25. Double-stranded fragments labeled with ^{32}P on the lower strand (left) and the upper strand (right) were digested with DNase I in the presence of 30 μg BSA (lane 2), 30 μg (lane 3) or 60 μg (lane 4) of LoVo nuclear extracts, or 60 μg of 293 nuclear extracts (lane 5). Positions of protected regions are indicated as A and B. Lane 1 represents a Maxam–Gilbert sequencing reaction of the same fragment

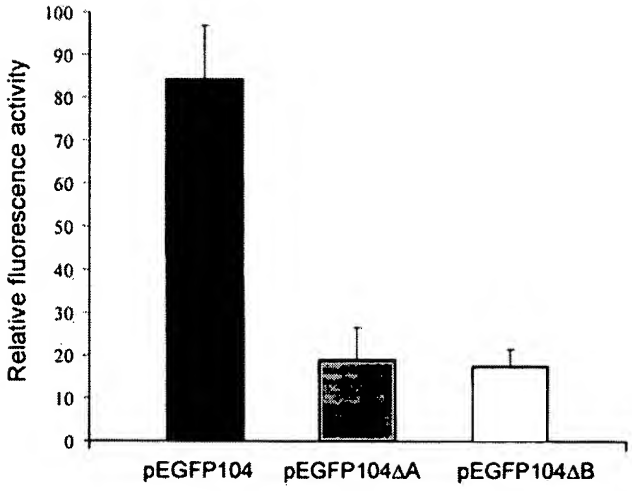

Figure 4 Transcription activity of the A33 gene promoter −104 fragment carrying mutations in either region A or region B in LoVo cells. pEGFP-104 constructs as well as constructs carrying mutations in either region A (pEGFP-104ΔA) or region B (pEGFP-104ΔB) were transfected into LoVo cells and EGPF activity was measured according to the description in Materials and methods. The results are expressed as EGFP fluorescence/β-galactosidase activity and represent the mean ± s.d. for three independent experiments

panel), a DNA–protein complex was formed when ^{32}P-labeled probe A, which contains a GKLF binding site, was incubated with nuclear extracts from LoVo cells (Figure 5a, lane 2) or from BGC823 cells (Figure 5a, lane 5). Addition of a 50-fold molar excess of unlabeled probe A oligonucleotide was able to abrogate the binding of protein factors from the nuclear extracts of both cell lines (Figure 5a, lanes 3 and 6), whereas an unrelated oligonucleotide did not have such an effect (Figure 5a, lanes 4 and 7). Consistent with the transient transfection data and data from DNase I footprinting, no protein binding was observed when probe A was incubated with 293 cell nuclear extracts (Figure 5a, lane 8). Collectively, these data indicate that the formation of the DNA–protein complex is sequence-specific and is related to the tissue-specific activity of the sequence from which the probe was derived. EMSA experiments with probe B from site B show a DNA–protein complex with nuclear extracts from all LoVo, BGC823, and 293 cells (Figure 5a, lower panel), albeit the complex was weaker with nuclear extracts from 293 cells (Figure 5a, lower panel, lane 8) compared with that from LoVo (Figure 5a, lower panel, lane 2) and from BGC8323 (Figure 5a, lower panel, lane 5). Addition of a 50-fold molar excess of unlabeled probe B eliminated the formation of the complex in both LoVo (Figure 5a,

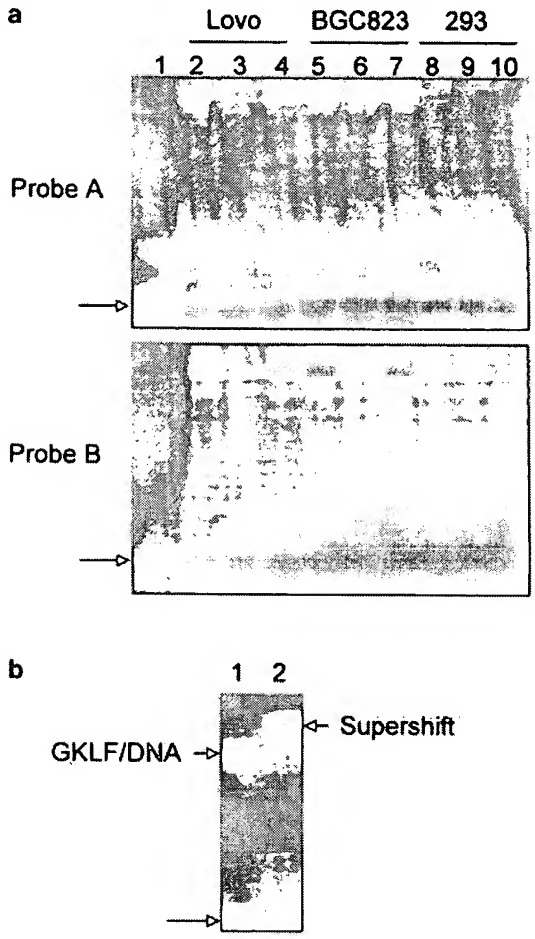

Figure 5 DNA–protein interactions in the two DNase I-protected regions. (**a**) Electrophoretic mobility shift assays were performed using radiolabeled oligonucleotides containing either the footprinted site A (probe A, upper panel) or site B (probe B) and cell nuclear extracts. A total of 1 ng of radiolabeled oligonucleotides and 10 μg of nuclear extracts from LoVo, BGC823, or 293 cells were used in each reaction. Lane 1 contains the free probe only; lanes 2, 5, and 8 contain labeled probe and nuclear extracts; lanes 3, 6, and 9 contain labeled probe, nuclear extract, and unlabeled probe; lane 4, 7, and 10 contain labeled probe, nuclear extracts, and an unrelated DNA fragment. (**b**) Supershift assays were performed with nuclear extracts from LoVo cells and the oligonucleotide probe containing GKLF binding site in the absence (lane 1) or the presence of GKLF antibody (lane 2). The arrows indicate the free probes

lower panel, lane 3) and BGC823 cells (Figure 5a, lower panel, lane 6), whereas no such effect was observed with a nonspecific DNA sequence (Figure 5a, lower panel, lanes 4 and 7).

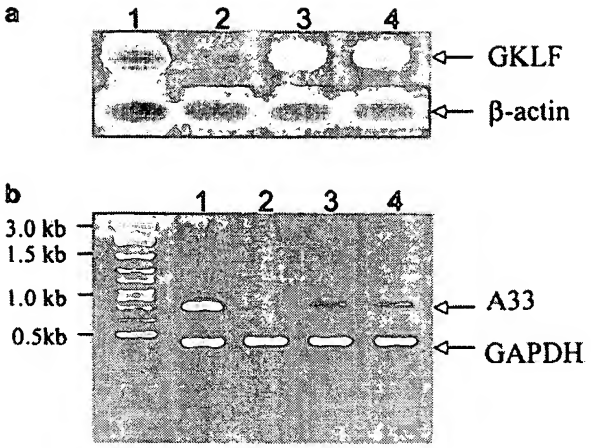

Figure 6 Expression of GKLF and A33 antigen in various cells. (**a**) The expression of GKLF mRNA in LoVo cells (lane 1), 293 cells (lane 2), BGC823 cells (lane 3), and HeLa cells (lane 4) was measured by Northern blotting. β-Actin mRNA expression was used as the control. (**b**) The expression of A33 antigen mRNA in LoVo cells (lane 1), 293 cells (lane 2), BGC823 cells (lane 3), and HeLa cells (lane 4) was measured by RT–PCR experiments. GAPDH mRNA expression was used as the control

To identify the protein factor(s) bound to probe A, a super-shift experiment was performed. Based on the presence of a putative GKLF binding site in this sequence, anti-GKLF antibodies were incubated with LoVo cell nuclear extracts followed by the addition of labeled probe A. As shown in Figure 5b, addition of the GKLF antibody caused a super-shift of the DNA–protein complex (Figure 5b, lane 2), indicating that the probe contains a GKLF binding site. The probe B contains a CDX-binding sequence and was demonstrated to be able to interact with CDX1 in a recent report by Johnstone *et al.* (2002).

Regulation of A33 expression by GKLF

To test the hypothesis that GKLF might contribute to the tissue-specific expression of the A33 antigen, we first examined the expression of GKLF and A33 antigen in LoVo, BGC823, and 293 cells by Northern blotting and RT–PCR. As shown in Figure 6a, the GKLF mRNA expression was high in LoVo cells, low in BGC823 cells, and undetectable in 293 cells. Interestingly, a similar pattern of expression was also observed for A33 antigen (Figure 6b). These data agree well with the data observed in the reporter experiments described in Figure 2, in fingerprinting experiments described in

Figure 7 Sufficiency of GKLF expression in the activation of A33 antigen gene promoter. (**a**) 293 cells were transfected with pEGFP-104 alone (lane 3) or cotransfected with pcDNA3.1 empty vector (lane 2) or with GKLF expression vector, pcDNA3.1-GKLF (lane 1), and the EGFP activity was recorded by photomicrographs. (**b**) LoVo cells were transfected with pEGFP-104 alone or cotransfected with pcDNA3.1 or with pcDNA3.1-AS-GKLF, and the fluorescence was monitored by photomicrographs (upper panel). GKLF expression was measured by Western blotting (middle panel) in transfections with pEGFP-104 alone (C), cotransfection of pEGFP-104 with pcDNA3.1 (V), or cotransfection of pEGFP-104 with pcDNA3.1-AS-GKLF (AS). A β-galactosidase expression construct was also cotransfected and the β-galactosidase expression was measured by Western blotting to show a similar transfection efficiency in all experiments including transfections with β-galactosidase expression construct alone (lane 1), transfection with pEGFP-104 alone (lane 2), cotransfection of pEGFP-104 with pcDNA3.1 (lane 3), or cotransfection of pEGFP-104 with pcDNA3.1-AS-GKLF (lane 4). (**c**) LoVo cells were transfected with pEGFP-104 alone or cotransfected with pcDNA3.1 or with pcDNA3.1-AS-GK.LF and the fluorescence activity was measured according to the procedures described in Materials and methods

Figure 3, and in EMSA experiments described in Figure 5, suggesting an important role for GKLF in regulating the expression of the A33 antigen.

In order to further establish the contribution of GKLF to the regulation of A33 antigen expression, we first ectopically expressed GKLF in 293 cells and assayed the effect of the GKLF expression on the promoter activity of the A33 antigen gene in these cells. The expression of GKLF in 293 cells was undetectable (Figure 7a, lower panel, lane 3; also see Figure 6a, lane

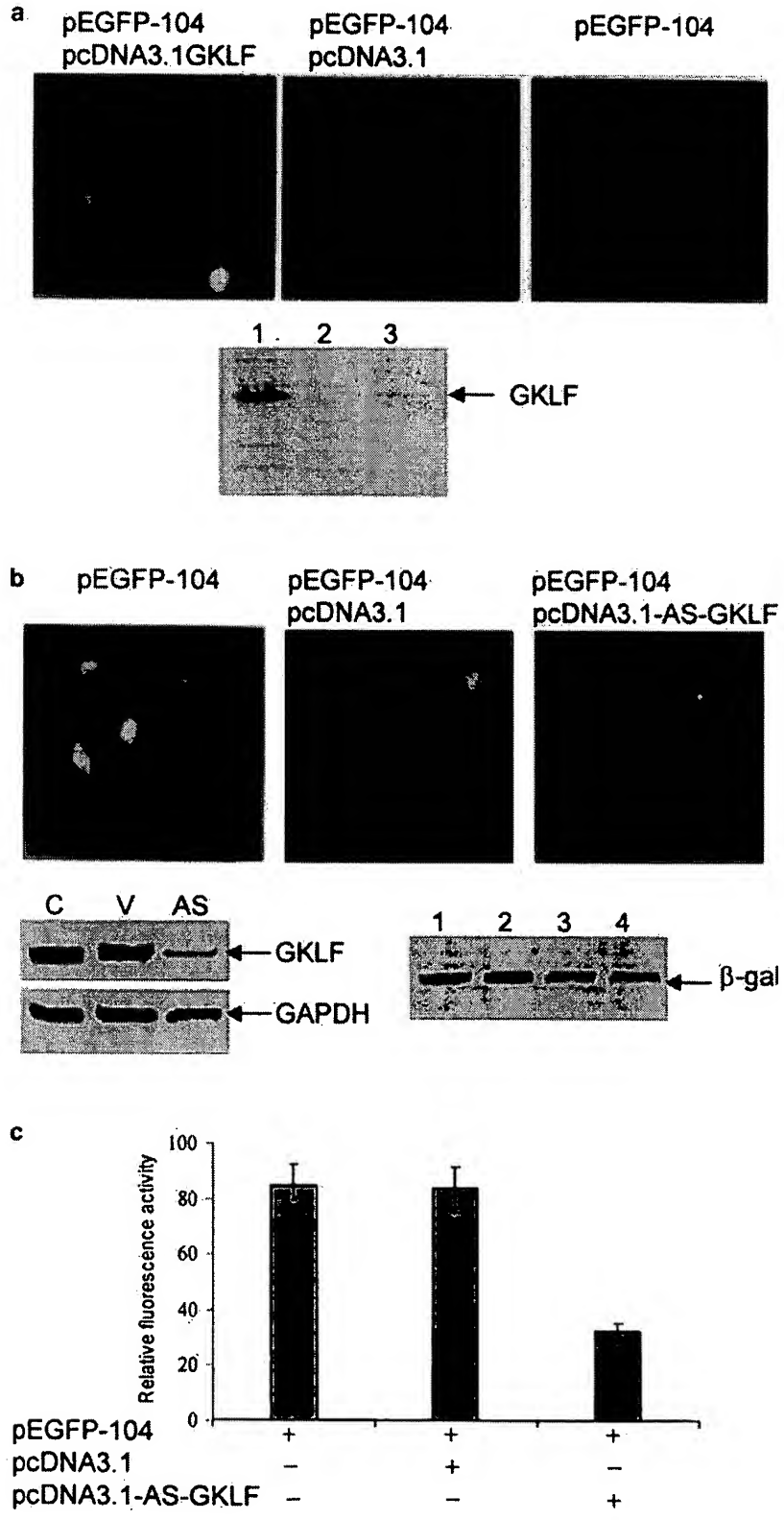

2), so was A33 antigen expression (Figure 6b, lane 2) and A33 antigen gene promoter activation (Figure 2). After transfection of 293 cells with a GKLF expression vector which led to the expression of GKLF (Figure 7a, lower panel, lane 1), however, the A33 antigen gene promoter was activated (Figure 7a, upper panel). Next, we utilized an antisense approach to inhibit the expression of GKLF in LoVo cells and the transcription activation activity of the A33 antigen gene promoter was assessed by transient transfection experiments. As shown in Figure 7b and c, after inhibition of the GKLF expression by its antisense (AS) (Figure 7b, middle panel), the activity of A33 antigen gene promoter was effectively inhibited only in LoVo cells (Figure 7b, upper panel, and Figure 7c). The effects on the A33 antigen promoter were not because of the transfection efficiency as the expression levels of a co-transfected *Lac Z* construct in all the experiments were similar (Figure 7b, lower panel). Collectively, these data indicate that GKLF is an essential transcription factor that contributes to the tissue-specific expression of the A33 antigen.

Discussion

A33 antigen is a highly tissue-specific gene with expression found primarily in gastrointestinal epithelia. Although A33 antigen is being investigated as a potential target for immunotherapy of colon cancer (Welt *et al.*, 1994, 1996; King *et al.*, 1995; Antoniw *et al.*, 1996; Barendswaard *et al.*, 2001), a basic understanding of the mechanisms underlying its tightly regulated tissue-specific expression is lacking. Such knowledge is likely to shed light on the biological functions of A33 antigen and thus its roles in colon cancer carcinogenesis. In this paper, we report on the cloning and characterization of the 5′-flanking region of the human A33 antigen gene. The sequence of the 5′-flanking region of the human A33 gene contains a typical TATA box. The major start site for transcription was determined to be 10 nucleotides downstream of the TATA sequence, which is consistent with the recent finding by Johnstone *et al.* (2002). However, the transcription of the A33 antigen gene might not be TATA-dependent as suggested by Johnstone *et al.* (2002), since most of TATA boxes are located 25–30 bp upstream of the initiation of transcription. Functional analysis by transient transfections showed that the promoter for human A33 antigen gene is most active in intestinal cells, less active in gastric cells, and not active in 293 cells, which is consistent with the expression pattern of the A33 gene in these cells. Serial deletion analysis revealed that the proximal region of the promoter (positions −104 to +25) was sufficient to generate maximal activity of the promoter in LoVo cells. Two protected sites in the proximal promoter region were subsequently identified by using the DNase I footprinting assay. Both sites are required for promoter activity since mutations in either site led to a significant decrease in promoter activity. Electrophoretic mobility shift assays identified one site, site A, which is bound by transcription factor GKLF, and the other site, site B, as recently reported by Johnstone *et al.* (2002) to harbor a CDX-binding site. The biological connection between GKLF binding in the A33 antigen gene promoter and the expression of A33 antigen is evident as blocking the expression of GKLF in GKLF-positive LoVo cells abolished the expression of the A33 antigen. Collectively, these data indicate that GKLF contributes to the tissue-specific expression of A33 antigen. It will be interesting in the future investigation to explore the relation between GKLF and CDX1 transcription factors in the regulation of the A33 antigen expression as CDX1 was also identified as a critical factor in contributing to the tissue-specific expression of the A33 antigen. It could be that both GKLF and CDX1 are necessary but not sufficient in regulating the tissue-specific expression of the A33 antigen, and it is intriguing to speculate that there is another yet unidentified protein factor or protein factors that serve as a coactivator(s) in coordinating the transcription activation of the A33 antigen gene.

GKLF is a Krüppel-type zinc-finger transcription factor (Shields *et al.*, 1996; Yet *et al.*, 1998; Mahatan *et al.*, 1999; Katz *et al.*, 2002). Expression of GKLF is enriched in epithelial cells of the gastrointestinal tract (Ton-That *et al.*, 1997; Behr and Kaestner, 2002) and the skin (Ton-That *et al.*, 1997) and in vascular endothelial cells (Yet *et al.*, 1998; McCormick *et al.*, 2001; Gray *et al.*, 2002). GKLF has been investigated with respect to its role in cellular differentiation, initially within the gastrointestinal tract and in the epidermis where GKLF is critical for late-stage differentiation of skin cells (Ohnishi *et al.*, 2000; Behr and Kaestner, 2002). GKLF has been shown to contain a transcription activation domain as well as a transcription repression domain (Yet *et al.*, 1998; Zhang *et al.*, 1998, 2000; Shie *et al.*, 2000a; Chen *et al.*, 2002). It was observed that the p21 promoter contains CACCC elements, and GKLF was shown to bind and directly transactivate the p21 promoter via these sites (Zhang *et al.*, 2000). The induction of p21 was dependent on p53 and thus also occurred after DNA damage with methyl methanesulfonate. In addition, GKLF physically interacts with p53 (Zhang *et al.*, 2000). The resultant synergistic induction by p53 and GKLF of p21 then leads to its inhibition of cyclin-dependent kinases and subsequent growth arrest. In keratinocytes, GKLF activates the keratin 4 promoter and may be implicated in the transition toward cell differentiation (Jenkins *et al.*, 1998; Okano *et al.*, 2000). GKLF has also been shown to upregulate the expression of keratin 19 (Brembeck and Rustgi, 2000) and laminin α3A (Miller *et al.*, 2001). On the other hand, GKLF has also been found to inhibit gene transcription by competing for the binding site with Sp1 (Zhang *et al.*, 1998; Shie *et al.*, 2000a) or by interacting with/sequestering p300/CBP (Geiman *et al.*, 2000). It was also shown that the minimal cyclin D1 promoter contains multiple CACCC elements that bind GKLF *in vitro* and that GKLF binding results in *in vivo* repression of the promoter, an effect not seen after transfection of Sp1. Together, these data argue that

GKLF plays a critical role in the decision between proliferation and cell cycle arrest/differentiation and they suggest that GKLF is a pleiotropic (activating and repressive) transcription factor. Our studies demonstrated that GKLF upregulates the expression of A33 antigen in colonic carcinoma cells. Although the biological functions of the A33 antigen is currently not understood, targeting A33 antigen by its antibody led to the growth inhibition of colon carcinomas, suggesting that A33 antigen is involved in cell growth and proliferation (Welt *et al.*, 1994, 1996; Antoniw *et al.*, 1996). Hence our results showing that A33 is a downstream target of GKLF suggest that GKLF plays more complex and diverse roles in the intestine.

Materials and methods

Cell lines and reagents

All chemicals were from Sigma (St Louis, MO, USA) unless otherwise noted. The human cell lines LoVo, BGC823, and 293 were from ATCC (Manassas, VA, USA). Dulbecco's modified Eagle's medium (DMEM), fetal bovine serum, and the TOPO2.1 T/A cloning vector were from Invitrogen (Carlsbad, CA, USA). All restriction enzymes were either from New England Biolab (Beverly, MA, USA) or Promega (Madison, WI, USA).

Cloning of the 5′-flanking region of human A33 antigen gene

The 5′-flanking region of the human A33 gene was cloned using a Genome Walker Kit from Clontech (Palo Alto, CA, USA) according to the manufacturer's instructions. PCR primer sequences used for cloning were: forward, 5′-ACCTCCCCTGCCTTCTCCCTACTTA-3′, and reverse, 5′-TCCTAGACTGCTCACAAAGGGGTA-3′. An ~1 kb band from the PCR reaction was extracted and purified with QIAquick Gel Extraction kit (Qiagen, Valencia, CA, USA) and cloned into the TOPO2.1 T/A cloning vector. The cloned product was sequenced in both directions using the automated ABI Prism 370 Sequencer.

Primer extension analysis

Primer extension analyses were done with GeneRacer™ Kit (Invitrogen) according to the manufacturer's instructions. Briefly, an 18-base oligonucleotide complementary to the position of −97 to −114 bp relative to the translation starting site of the human A33 gene was end-labeled with γ^{32}P[ATP] using T4 polynucleotide kinase. A quantity of 100 μg of total RNA from human LoVo cells isolated with the RNeasy Mini kit (Qiagen) was annealed to 10^6 c.p.m. of the primer and extended with 200 U of Superscript II reverse transcriptase. The resultant products were analysed on 7 M urea, 6% polyacrylamide gels in parallel with a DNA marker.

Construction of reporter genes driven by the 5′-flanking region of A33 antigens

DNA fragments representing different lengths of the A33 antigen gene 5′-flanking region were cloned upstream of the EGFP coding sequence in the pEGFP-1 vector (Clontech). The resultant plasmid is designated as pA33-EGFP.

Transient transfection

Human cell lines LoVo, BGC823, and 293 were cultured in DMEM supplemented with 10% fetal bovine serum for 24 h before being transfected with A33 antigen gene 5′-flanking region-driven EGFP reporter gene or the promoter-less pEGFP-1 vector plus a *LacZ* construct (pCMVβ; Clontech) using Effectene Transfection Reagent (Qiagen). At 48 h after transfection, cells were harvested and lysed in 1 ml of reporter lysis buffer and EGFP activity was measured by photomicrographs. The fluorescence activity was normalized to β-galactosidase activity which was measured using the β-galactosidase Enzyme Assay System provided by Promega.

DNase I footprinting

Nuclear extracts were prepared by collecting cells in cold buffer A (10 mM HEPES, pH 7.9, 1.5 mM $MgCl_2$, 10 mM KCl, 0.5 mM dithiothreitol, and 0.2 mM phenylmethylsulfonyl fluoride) and incubating on ice for 10 min. Cells were then frozen and thawed once and vortexed briefly. Nuclei were pelleted by brief centrifugation and resuspended in cold buffer C (20 mM HEPES, pH 7.9, 25% glycerol, 420 mM NaCl, 1.5 mM $MgCl_2$, 0.2 mM EDTA, 0.5 mM dithiothreitol, and 0.2 mM phenylmethylsulfonyl fluoride) followed by incubation on ice for 30 min. The samples were then briefly centrifuged to remove debris and the supernatant was collected and stored at −80°C. DNase I footprinting experiments were performed with a fragment corresponding to −140 to +25 of the A33 gene transcription starting site. This fragment was labeled with α^{32}p[dATP] and incubated with nuclear extracts at room temperature for 30 min in a reaction mixture containing 4% glycerol, 10 mM Tris-HCl, pH 7.5, 50 mM NaCl, 2.5 mM $MgCl_2$, 0.5 mM dithiothreitol, and 2 μg poly(dI:dC). After incubation, 2 U of DNase I was added and incubation was continued for exactly 1 min. Footprinting was done using a SureTrack Footprinting Kit from Amersham Biosciences (Piscataway, NJ, USA) according to the manufacturer's instructions. The samples were analysed on a 6% acrylamide/7 M urea denaturing gel.

Site-directed mutagenesis

Substitution mutations for nucleotides at positions −81 and −82 (CC→AG) and at positions −28, −29, and −30 (TAT→CGA) of the 5′-flanking region of A33 gene were generated using the QuikChange Mutagenesis Kit (Stratagene, La Jolla, CA, USA) according to the manufacturer's instructions. Synthetic oligonucleotides containing the desired bases were used in the mutagenesis and the sequences of these oligonucleotides were (CC→AG mutation: 5′-GCAAAT ATGGGCAACAAGCTTCTTTTACTAGCTTGG-3′ and TAT→CGA mutation: 5′-GCATTTCCCTTTTTATCGATTATTTCCTGTCAGTTA-3′). DNAs that incorporated the desired mutations were transformed into *Epicurian Coli* XL1-blue supercompetent cells. Plasmid DNAs were prepared and the presence of the mutations was confirmed by sequencing.

Electrophoretic mobility shift assays

γ^{32}P end-labeled double-strand oligonucleotide (0.25 pmol) was mixed with 10 μg of nuclear extract in a final volume of 20 μl containing 10 mM Tris-HCl, pH 7.5, 100 mM NaCl, 3 mM $MgCl_2$, 0.5 mM EDTA, 1 mM dithiothreitol, 5% glycerol, 2 μg of poly(dI:dC), 4 mM spermidine, and 1 μg of bovine serum albumin. Samples were incubated at 30°C for 30 min. The reaction was conducted in the absence or presence of specific or nonspecific competitors, both added at a 50-fold molar

excess. Specific competitors were cold probes and nonspecific competitors were an unrelated oligonucleotide. The DNA–protein complexes were analysed by electrophoresis on 6% nondenaturing polyacrylamide gels. The sequences of the oligonucleotides were as follows: probe A: 5′-GCAA-CACCCTTCTTTTACTAGC-3′, corresponding to the −86 to −68 and probe B: 5′-CCCTTTTTATTATTTATTTCCT-3′, corresponding to −40 to −19 region of the A33 antigen gene 5′-flanking region. For supershift assays, nuclear extracts and rabbit polyclonal anti-GKLF antibodies (Santa Cruz Biotechnologies, Santa Cruz, CA, USA) were incubated for 30 min on ice prior to the addition of the radiolabeled probe.

Northern blot analysis and RT–PCR

Total RNA was isolated from cells using an RNeasy total RNA kit (Qiagen). DNA fragments from GKLF cDNA and β-actin cDNA were labeled with α^{32}P[dCTP] using a random-priming kit (Promega). A quantity of 30 μg of total RNA from each sample was electrophoresed on 1% agrose/2.2 M formaldehyde gels. The RNA was then transferred to nylon membranes and crosslinked by UV exposure. Blots were hybridized using Expresshyb™ Hybridization solution (Clontech) and autoradiographed.

RT–PCR was performed by using a Qiagen OneStep RT-PCR Kit (Qiagen). Briefly, 1 μg of total RNA was subjected to reverse transcription at 50°C for 30 min. Reactions were stopped by heating at 95°C for 15 min. PCR products were analysed using 1.2% agarose gel electrophoresis and visualized with ethidium bromide staining. The forward primer was 5′-GCTTCGCAGGGAAAGA-3′ from exon 2 of the A33 antigen gene and the reverse primer was 5′-CGATGCCCA-CATACAGG-3′ from exon 6. GAPDH amplification was performed as an internal control. The primers for GAPDH amplification were: forward, 5′-ACCACAGTCCATGCCAT-CAC-3′ and reverse, 5′-TCCACCACCCTGTTGCTGTA-3′.

Generation of the GKLF sense and anti-sense expression constructs

Full-length cDNA of human GKLF was obtained by RT–PCR and cloned into pcRII-Topo vector (Invitrogen). The sequence of the GKLF cDNA was then confirmed and subcloned in right orientation (for sense construct) or reverse orientation (for antisense construct) into pcDNA3.1(+) vector (Invitrogen). The sequence of the inserts was confirmed by sequencing.

Abbreviations

GKLF, gut-enriched Krüppel-like factor; EGFP, enhanced green fluorescent protein; EMSA, electrophoretic mobility shift assays.

Acknowledgements

This work was supported by grants (30000199 to ZM and 30225043 to YS) from National Natural Science Foundation of China.

References

Abud HE, Johnstone CN, Tebbutt NC and Heath JK. (2000). *Mech. Dev.*, **98**, 111–114.

Antoniw P, Farnsworth AP, Turner A, Haines AM, Mountain A, Mackintosh J, Shochat D, Humm J, Welt S, Old LJ, Yarranton GT and King DJ. (1996). *Br. J. Cancer*, **74**, 513–524.

Barendswaard EC, Humm JL, O'Donoghue JA, Sgouros G, Finn RD, Scott AM, Larson SM and Welt S. (2001). *J. Nucl. Med.*, **42**, 1251–1256.

Behr R and Kaestner KH. (2002). *Mech. Dev.*, **115**, 167–169.

Bergelson JM, Cunningham JA, Droguett G, Kurt-Jones EA, Krithivas A, Hong JS, Horwitz MS, Crowell RL and Finberg RW. (1997). *Science*, **275**, 1320–1323.

Bergelson JM, Krithivas A, Celi L, Droguett G, Horwitz MS, Wickham T, Crowell RL and Finberg RW. (1998). *J. Virol.*, **72**, 415–419.

Black AR, Black JD and Azizkhan-Clifford J. (2001). *J. Cell. Physiol.*, **188**, 143–160.

Brembeck FH and Rustgi AK. (2000). *J. Biol. Chem.*, **275**, 28230–28239.

Catimel B, Ritter G, Welt S, Old LJ, Cohen L, Nerrie MA, White SJ, Heath JK, Demediuk B, Domagala T, Lee FT, Scott AM, Tu GF, Ji H, Moritz RL, Simpson RJ, Burgess AW and Nice BC. (1996). *J. Biol. Chem.*, **271**, 25664–25670.

Chen ZY, Shie JL and Tseng CC. (2002). *J. Biol. Chem.*, **277**, 46831–46839.

Chretien I, Marcuz A, Courtet M, Katevuo K, Vainio O, Heath JK, White SJ and Du Pasquier L. (1998). *Eur. J. Immunol.*, **28**, 4094–4104.

Chretien I, Robert J, Marcuz A, Garcia-Sanz JA, Courtet M and Du Pasquier L. (1996). *Eur. J. Immunol.*, **26**, 780–791.

Foster KW, Frost AR, McKie-Bell P, Lin CY, Engler JA, Grizzle WE and Ruppert JM. (2000). *Cancer Res.*, **60**, 6488–6495.

Geiman DE, Ton-That H, Johnson JM and Yang VW. (2000). *Nucleic Acids Res.*, **28**, 1106–1113.

Gray S, Feinberg MW, Hull S, Kuo CT, Watanabe M, Sen-Banerjee S, DePina A, Haspel R and Jain MK. (2002). *J. Biol. Chem.*, **277**, 34322–34328.

Heath JK, White SJ, Johnstone CN, Catimel B, Simpson RJ, Moritz RL, Tu GF, Ji H, Whitehead RH, Groenen LC, Scott AM, Ritter G, Cohen L, Welt S, Old LJ, Nice EC and Burgess AW. (1997). *Proc. Natl. Acad. Sci. USA*, **94**, 469–474.

Jenkins TD, Opitz OG, Okano J and Rustgi AK. (1998). *J. Biol. Chem.*, **273**, 10747–10754.

Johnstone CN, White SJ, Tebbutt NC, Clay FJ, Ernst M, Biggs WH, Viars CS, Czekay S, Arden KC and Heath JK. (2002). *J. Biol. Chem.*, **277**, 34531–34539.

Katevuo K, Imhof BA, Boyd R, Chidgey A, Bean A, Dunon D, Gobel TW and Vainio O. (1999). *J. Immunol.*, **162**, 5685–5694.

Katz JP, Perreault N, Goldstein BG, Lee CS, Labosky PA, Yang VW and Kaestner KH. (2002). *Development*, **129**, 2619–2628.

King DJ, Antoniw P, Owens RJ, Adair JR, Haines AM, Farnsworth AP, Finney H, Lawson AD, Lyons A and Baker TS (1995). *Br. J. Cancer*, **72**, 1364–1372.

Mahatan CS, Kaestner KH, Geiman DE and Yang VW. (1999). *Nucleic Acids Res.*, **27**, 4562–4459.

McCormick SM, Eskin SG, McIntire LV, Teng CL, Lu CM, Russell CG and Chittur KK. (2001). *Proc. Natl. Acad. Sci. USA*, **98**, 8955–8960.

Miller KA, Eklund EA, Peddinghaus ML, Cao Z, Fernandes N, Turk PW, Thimmapaya B and Weitzman SA. (2001). *J. Biol. Chem.*, **276**, 42863–42868.

Nickenig G, Baudler S, Muller C, Werner C, Werner N, Welzel H, Strehlow K and Bohm M. (2002). *FASEB J.*, **16**, 1077–1086.

Ohnishi S, Laub F, Matsumoto N, Asaka M, Ramirez F, Yoshida T and Terada M. (2000). *Dev. Dyn.*, **217**, 421–429.

Okano J, Opitz OG, Nakagawa H, Jenkins TD, Friedman SL and Rustgi AK. (2000). *FEBS Lett.*, **473**, 95–100.

Sakamoto J, Kojima H, Kato J, Hamashima H and Suzuki H. (2000). *Cancer Chemother. Pharmacol.*, **46**(Suppl), S27–S32.

Shie JL, Chen ZY, Fu M, Pestell RG and Tseng CC. (2000a). *Nucleic Acids Res.*, **28**, 2969–2976.

Shie JL, Chen ZY, O'Brien MJ, Pestell RG, Lee ME and Tseng CC. (2000b). *Am. J. Physiol. Gastrointest. Liver Physiol.*, **279**, G806–G814.

Shields JM, Christy RJ and Yang VW. (1996). *J. Biol. Chem.*, **271**, 20009–20017.

Tomko RP, Xu R and Philipson L. (1997). *Proc. Natl. Acad. Sci. USA*, **94**, 3352–3356.

Ton-That H, Kaestner KH, Shields JM, Mahatanankoon CS and Yang VW. (1997). *FEBS Lett.*, **419**, 239–243.

Welt S, Divgi CR, Kemeny N, Finn RD, Scott AM, Graham M, Germain JS, Richards EC, Larson SM and Oettgen HF (1994). *J. Clin. Oncol.*, **12**, 1561–1571.

Welt S, Scott AM, Divgi CR, Kemeny NE, Finn RD, Daghighian F, Germain JS, Richards EC, Larson SM and Old LJ. (1996). *J. Clin. Oncol.*, **14**, 1787–1797.

Yet SF, McA'Nulty MM, Folta SC, Yen HW, Yoshizumi M, Hsieh CM, Layne MD, Chin MT, Wang H, Perrella MA, Jain MK and Lee ME. (1998). *J. Biol. Chem.*, **273**, 1026–1031.

Zhang W, Geiman DE, Shields JM, Dang DT, Mahatan CS, Kaestner KH, Biggs JR, Kraft AS and Yang VW. (2000). *J. Biol. Chem.*, **275**, 18391–18398.

Zhang W, Shields JM, Sogawa K, Fujii-Kuriyama Y and Yang VW. (1998). *J. Biol. Chem.*, **273**, 17917–17925.

[CANCER RESEARCH 57, 2789–2798, July 1, 1997]

Two Cytodifferentiation Agent-induced Pathways, Differentiation and Apoptosis, Are Distinguished by the Expression of Human Papillomavirus 16 E7 in Human Bladder Carcinoma Cells[1]

Victoria M. Richon,[2] Paul Russo, Gisela Venta-Perez, Carlos Cordon-Cardo, Richard A. Rifkind, and Paul A. Marks

Cell Biology Program [V. M. R., G. V-P., R. A. R., P. A. M], Urology Service, Departments of Surgery [P. R.] and Pathology [C. C-C.], Memorial Sloan-Kettering Cancer Center, New York, New York 10021

ABSTRACT

Many transformed cells have been found to lose the capacity to proliferate and undergo differentiation following exposure to hybrid polar agents. This study investigates the mechanism by which hexamethylene bisacetamide (HMBA) suppresses the proliferation of the human bladder carcinoma line, T24. We found that following a 24-h exposure to HMBA, T24 proliferation was inhibited, and cells arrested in G_1 phase and underwent morphological maturation. HMBA-induced cessation of proliferation was mediated, in part, by effects on cell cycle regulatory proteins. In T24 cells cultured without HMBA, E2F complexes predominantly with p107. In culture with inducer, p107 protein decreased, pRB and p130 were converted to underphosphorylated forms, and E2F was shifted into complexes with pRB and p130. To determine whether the formation of pRB:E2F and p130:E2F complexes was required for the HMBA-induced G_1 arrest, the ability of the pocket proteins to bind E2F was blocked by enforced expression of human papillomavirus 16 E7. Following culture with HMBA, the T24 clones expressing E7 died, whereas vector-alone T24 clones arrested in G_1 phase. T24/E7-1 cells did not form pRB:E2F or p130:E2F complexes upon culture with HMBA; rather, E2F was present in its free form. T24/E7-1 cells cultured with HMBA initially accumulate in G_1. By day 2, they have entered into S phase, and by day 3, over 80% of the cells became apoptotic. Taken together, these studies enlarge the repertoire of demonstrated developmental pathways that may be triggered in transformed cells, depending upon their molecular status, and may provide potential therapeutic opportunities for cancer.

INTRODUCTION

As a part of their disordered development, transformed cells have escaped from the controls exercised by normal cell cycle regulatory signals, but they have not necessarily lost the ability to cease division, given appropriate signals. A variety of transformed cells (including both hematopoietic malignancies and solid tumors) can be induced to enter terminal cell differentiation accompanied by loss of the capacity to proliferate when cultured with hybrid polar differentiation agents (1). Hybrid polar cytodifferentiation agents comprise a group of small molecular weight compounds of which the prototype is HMBA[3] (2). The demonstration that a wide variety of cell types are affected by the hybrid polar differentiation agents suggested that a common basic cellular mechanism mediates drug-induced differentiation. Potential intracellular mediators for the action of these agents include proteins that control cell cycle progression and differentiation, such as the retinoblastoma protein (pRB; Refs. 3–5), and the related proteins p107 (6) and p130 (7–9). pRB, p107, and p130 are members of the pocket protein family based on the shared domain that binds to the E2F family of transcription factors (10–12). The E2F transcription factor is a heterodimer of an E2F protein and a DP protein (13–16). Five *E2F* genes (10–12, 17–21) and two *DP* genes (22, 23) have been characterized. The binding of pRB, p107, and p130 to E2F results in the repression of transcription of E2F target genes (24–30), including genes that encode proteins involved in the control of cell cycle progression and DNA synthesis, such as E2F-1 itself, cyclin E, dihydrofolate reductase, and DNA polymerase α (31–35). Hypophosphorylated forms of pRB, present during G_1, bind to E2F (36–39). Phosphorylation of pRB as cells progress through G_1 is carried out by one or more of the cell cycle-dependent kinases, cyclin D/cdk4, cyclin D/cdk6, cyclin E/cdk2, or cyclin A/cdk2 (40–44). Phosphorylation of pRB releases E2F, resulting in increased expression of genes required for entry into S phase. E2F also forms complexes with p130 and p107 in a cell cycle-specific manner (8, 9, 45–48). The predominant E2F complex in quiescent cells is p130:E2F, whereas p107:E2F is detected in cells as they enter S phase. Exit from the cell cycle upon induction of differentiation is associated with a switch from E2F complexes containing p107 to complexes containing pRB and p130 in myoblasts (49, 50), pheochromocytoma cells (51), and HL-60 cells (52). The role of this shift of E2F from p107 to p130 and pRB is not understood; however, it appears to be essential to achieve terminal differentiation in myoblasts. For example, Schneider *et al.* (53) found that although p107 can substitute for pRB as cofactor for muscle differentiation, p107 cannot maintain the terminally differentiated state in RB−/− myotubes.

In this study, we investigate the role of E2F complexes in the response of the bladder transitional cell carcinoma cell line T24 to culture with HMBA. We found that T24 cells arrest in G_1 phase during culture with HMBA and undergo phenotypic maturation. During induction, the growth-suppressive forms of pRB and p130 proteins accumulated, whereas the level of p107 protein decreased. By 24 h of culture with HMBA, pRB and p130 were found to be in complexes with E2F. To determine whether these pocket protein:E2F complexes play a role in inducer-mediated inhibition of cell proliferation, the E7 oncoprotein from HPV-16 was used to inhibit pocket protein binding to E2F. It is established that the E7 oncoprotein from HPV-16 alters cellular growth and differentiation through its ability to bind to and inactivate pRB, p107, and p130 (54–56). In HMBA-induced T24, expression of HPV-16 E7 protein blocked the formation of pocket protein:E2F complexes and resulted in cell death by apoptosis rather than the G_1 arrest and morphological differentiation observed in parental cells exposed to HMBA. The present study indicates that the pocket protein:E2F complexes may be critical mediators of the HMBA-mediated signals, which lead to induction of differentiation, whereas exposure to HMBA under conditions in which these E2F complexes cannot form leads to apoptosis rather than differentiation of transformed bladder cells.

Received 12/17/96; accepted 4/29/97.

The costs of publication of this article were defrayed in part by the payment of page charges. This article must therefore be hereby marked *advertisement* in accordance with 18 U.S.C. Section 1734 solely to indicate this fact.

[1] These investigations were supported, in part, by Grant CA-0874823 from the National Cancer Institute and grants from the Japan Foundation for the Promotion of Cancer Research Fund, the DeWitt Wallace Fund for Memorial Sloan-Kettering Cancer Center, and the Westbranch Leukemia Research Fund.

[2] To whom requests for reprints should be addressed, at Laboratory of Developmental Cell Biology, Rockefeller Research Laboratory-901, Memorial Sloan-Kettering Cancer Center, 1275 York Avenue, New York, NY 10021. Phone: (212) 639-6568; Fax: (212) 639-2861; E-mail: v-richon@ski.mskcc.org.

[3] The abbreviations used are: HMBA, hexamethylene bisacetamide; pRB, retinoblastoma protein; human papillomavirus 16, HPV-16; BrdUrd, bromodeoxyuridine; TUNEL, terminal deoxynucleotidyl transferase-mediated UTP nick end labeling; MEL, murine erythroleukemia.

MATERIALS AND METHODS

Cell Culture and Transfection. T24 bladder transitional carcinoma cells were obtained from American Type Culture Collection (Rockville, MD) and maintained in α-MEM containing 10% FCS (HyClone). Cell cultures were initiated at 10^5 cells/plate. HMBA (Sigma; Ref. 2) was added 18 to 24 h after initiation of culture. Cells were harvested using trypsin (0.05% in 0.02% EDTA). Cell density was determined using an Epics Coulter counter. Viability was determined by trypan blue exclusion. Cells were routinely maintained by subculturing two times/week. The calcium phosphate precipitation technique (57) was used to introduce the CMV-HPV-16E7 expression vector (generously provided by Debra DeFeo Jones; Merck) into T24 cells. G-418-resistant clones were isolated and analyzed for expression of E7 mRNA.

Cell Cycle Analysis. Cells were pulse labeled with BrdUrd for 1 h as described in the Cell Proliferation kit (Amersham Corp.). Cells were harvested and washed two times with PBS/1% BSA. Cells were resuspended in normal saline (0.9% NaCl) and fixed in 70% ethanol for 30 min, followed by a 30-min incubation in 2 N HCl/0.05% Triton X-100 and neutralization with 0.1 M $Na_2B_4O_7$. Cells were resuspended in 0.5% Tween 20/1% BSA, and BrdUrd incorporation was detected by the addition of anti-BrdUrd-FITC conjugated secondary antibody (Becton Dickinson). Samples were washed two times with PBS/1% BSA and resuspended in propidium iodide (50 μg/ml in 5 mM $MgCl_2$, 10 mM Tris-HCl, pH 7.0). Flow cytometric analysis of DNA content (staining with propidium iodide) and DNA synthesis (staining with FITC-conjugated antibody to BrdUrd) were determined. Cells were analyzed on a FACScan II followed by data analysis using CELLQuest (Becton Dickinson).

Immunocytochemistry. Immunocytochemical studies were performed following standard avidin-biotin-peroxidase techniques (58). Cells were cultured on glass slide chambers. At the times indicated for each experiment, slides were fixed for 10 min in acetone:methanol (1:1). Slides were sequentially washed in PBS, quenched in hydrogen peroxide, and blocked with avidin-biotin and 10% horse serum. The cells were then incubated for 2 h with primary antibodies [anti-actin (C4Mab); ICN]. Horse serum (10%) served as a negative control. Cells were incubated with biotinylated horse anti-mouse secondary antibodies at 1:500 dilution (Vector Laboratories), followed by extensive washes and avidin-biotin peroxidase complexes at 1:25 dilution. Diaminobenzidine (0.06%) was used as the final chromogen.

Apoptosis. Cells were cultured under the conditions described above, harvested, and fixed in 10% formalin. Apoptotic cells were detected via labeling of fragmented DNA by the TUNEL method of Gavrieli *et al.* (59).

Preparation of Nuclear Extracts. Nuclear extracts were prepared as described by Dignam *et al.* (60). Briefly, 10^8 cells were washed two times, and cells were lysed by adding a volume of buffer A [10 mM HEPES (pH 7.5), 10 mM KCl, 1.5 mM $MgCl_2$, 0.5 mM DTT, and 10 mM NaF] equal to the volume of the cell pellet and incubated on ice for 15 min. The cells were lysed by passing the cells through a 26-gauge needle. Nuclei were collected by centrifugation at 14,000 × *g* for 20 s, and proteins were extracted from the nuclei in buffer C [20 mM HEPES (pH 7.5), 1.5 mM $MgCl_2$, 25% glycerol, 420 mM KCl, 0.2 mM EDTA, 1 mM DTT, and 0.5 mM phenylmethylsulfonyl fluoride] for 30 min at 4°C and pelleted by centrifugation at 14,000 rpm for 15 min. The supernatant solution was dialyzed for 1 h against buffer D [20 mM HEPES (pH 7.5), 20% glycerol, 100 mM KCl, 0.2 mM EDTA, 1 mM DTT, and 0.5 mM phenylmethylsulfonyl fluoride] and stored at −80°C. Protein concentrations were determined using the Bio-Rad Protein Assay kit (Bio-Rad).

Gel Mobility Shift Assays. Gel mobility shift assays were performed as follows (47). Reaction mixtures (25 μl) contained 20 μl of binding buffer [buffer A: 50 mM KCl, 20 mM HEPES-KOH (pH 7.5), 10 mM $MgCl_2$, 10% glycerol, 0.5 mM DTT, 1% NP40], 0.5 ng of ^{32}P-labeled oligonucleotide probe, 2 μg of sonicated salmon sperm DNA, 20 μg of BSA, and 5–15 μg of protein extract. Reactions were incubated 10 min at room temperature (20–25°C). The reaction products were separated on a 4% polyacrylamide gel run in 0.25× TBE (22.5 mM Tris-Borate, 0.5 mM EDTA) at 4°C. The gel was dried and exposed to film (Kodak XAR5). For antibody perturbation experiments, 1 μl (0.25 μg) of antibody was added to the incubation 10 min prior to addition of the oligonucleotide probe and incubated at room temperature. The following antibodies were used: C36 (Oncogene Science, New York, NY) and 245 (PharMingen, San Diego, CA) monoclonal antibodies to RB and the negative control antibody (neg, 03301D) obtained from PharMingen. The p107 antibody (SD-15) was generously provided by N. Dyson and E. Harlow (61). The p130 antibody (C20) was obtained from Santa Cruz Biotechnology, Inc. The pRB and p107 antibodies were specific for pRB and p107 proteins, respectively, and did not cross-react with the other pocket protein members (data not shown). The p130 antibody was not specific and did cross-react with p107 protein but not pRB (data not shown). For the oligonucleotide competition experiments, 100-fold excess of the unlabeled competitor oligonucleotide (or titration) was added 10 min prior to addition of the oligonucleotide probe and incubated at room temperature. The following double-stranded oligonucleotides were used in the experiments (the sense strand is shown): E2F/E2, 5′-AGCTTGTTTTCGCGCTTAAATTTGAGAAAGGGCGCGAAACTAGTCA-3′; DRTF 71/50, 5′-TAGTTTTCGCGCTTAAATTTGA-3′; and DRTF 62/60, 5′-TAGTTTTCGATATTAAATTTGA-3′.

Immunoblot Analysis. Cells grown under the conditions described for each experiment were recovered by centrifugation, and total cell extracts were prepared. Cells were lysed in SDS-PAGE sample buffer, boiled 5 min, sheared through a 26-gauge needle, and clarified by centrifugation. Samples were applied to SDS-7.5% polyacrylamide gels. Electrophoretic transfer of proteins from the SDS-polyacrylamide gels to nitrocellulose (Schleicher and Schuell) were carried out as described by Towbin *et al.* (62) and modified by Burnette (63). The membranes were blocked for 30 min at room temperature in 1× TBST [10 mM Tris-HCl (pH 8.0), 150 mM NaCl, and 0.05% Tween 20] containing 4% dry milk. The following antibodies were used: antihuman pRB G-245 (PharMingen); anti-p130 (C-20), anti-p107 (C-18), anti-p21 (H-164), anti-cdk2 (M2), anti-E2F-1 (C20), and anti-cyclin A (BF683) were obtained from Santa Cruz Biotechnology. The binding of antibody was detected using the enhanced chemiluminescence system as described (Amersham).

RNase Protection Assay. The RNase protection assay was carried out as described by Melton *et al.* (64). The probes for RNase protection assays were prepared by recloning each fragment into the pBluescript II KS(+/−) vector (Stratagene) containing promoters for T3 and T7 RNA polymerases. The HPV-16 E7 vector was prepared by subcloning the *Bgl*II-digested E7 320-bp fragment into *Bam*HI-digested pKS vector. A human β-actin probe (Ambion, Austin, TX) was used for normalization and was added to each hybridization. The probes were first tested individually and then combined. The addition of two probes in the hybridization yielded the same results as the individual probes. The antisense strand RNA probes were prepared and mixed (5×10^5 cpm of test probe and 5×10^4 cpm of β-actin probe) with 10 mg of total cellular RNA, hybridized, and digested with a mixture of RNase A and RNase T1. Following ethanol precipitation, the size of the RNase-resistant probe was determined by electrophoresis on a denaturing acrylamide-8 M urea gel. The resulting gels were analyzed using the Fuji phosphoimager Fujix BAS1000 and analyzed using MacBas 2.0 software.

Histone H1 Kinase Assay. Kinase activity was determined as described by Rosenblatt *et al.* (65) and modified by Kiyokawa *et al.* (66). Nuclear extracts were prepared as described above, and 25 μg of protein were immunoprecipitated with anti-cdk2 (M2) and assayed for kinase activity using 1 μg of histone H1 as a substrate for 30 min at 30°C. Reactions were terminated by the addition of SDS sample buffer and boiling. Reaction products were resolved on SDS-polyacrylamide gels (12.5% polyacrylamide), and then gels were dried and autoradiographed.

RESULTS

Effect of HMBA on T24 Bladder Carcinoma Cell Proliferation and Morphology. We first examined the effect of HMBA on T24 cell proliferation and morphology. The effect of HMBA at concentrations of 0, 2.5, 5, 10, and 20 mM was determined (Fig. 1). An antiproliferative effect was observed at 5 mM HMBA, and complete inhibition of proliferation was observed at 10 mM HMBA. Following 24 h of culture with 10 mM HMBA, T24 cells arrested in the G_1 phase of the cell cycle, as determined by DNA content analysis of propidium iodide-stained cells and by inhibition of bromodeoxyuridine incorporation (Fig. 2). With continued culture with HMBA, the cells remained arrested in G_1 for over 21 days. Despite proliferation arrest, HMBA did not affect cell viability (determined by trypan blue exclusion; >90% viability with or without HMBA). The morphology of

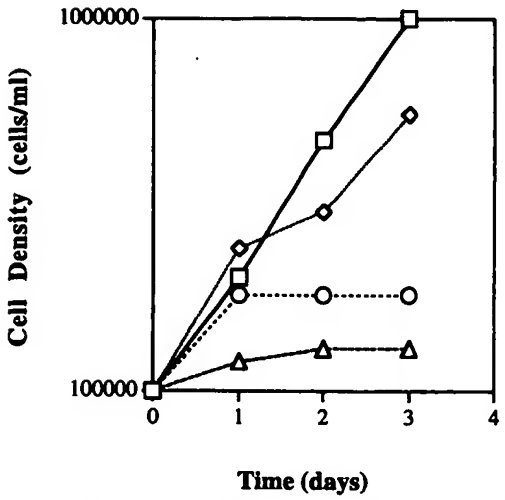

Fig. 1. Effect of HMBA on T24 cell proliferation. T24 were cultured in the presence of 0 (□), 5 (◇), 10 (○), and 20 (△) mM HMBA as indicated, and cell density was determined for each culture following 1, 2, and 3 days of culture. The scale for cell density is logarithmic.

T24 cells during culture with 10 mM HMBA was evaluated by fixing the cells directly on their culture chamber slides, staining with Giemsa, or visualizing the pattern of actin distribution by immunohistochemical staining (Fig. 3). By 3 days of culture with HMBA, the cells were more uniform in shape and size, increased in cytoplasmic volume, spread out on the culture surface forming junctions with surrounding cells, and exhibited less distinct intercellular borders. There was also an increase in the number of cytoplasmic granules. These changes could be detected as early as 1 day following culture with HMBA and became more pronounced by 2 and 3 days. Although not specific, these morphological features are characteristics of the mature superficial (umbrella) cells of the urothelium. Umbrella cells are large, flat cells that make up the bladder lining facing the lumen (67, 68).

Effect of HMBA on pRB, p107, and p130 Proteins and E2F Complexes. We explored the mechanism underlying the antiproliferative effect of HMBA by examining the expression and phosphorylation of pRB and the pRB-related proteins p107 and p130. T24 cells were cultured without or with 10 mM HMBA for 1, 4, 8, 12, and 24 h, extracts were prepared, and immunoblots were performed (Fig. 4, *A* and *B*). During culture with HMBA, a progressive decrease in the phosphorylated form of pRB was detected, as early as 4 h. In addition to conversion to the underphosphorylated form of pRB detected by 4 h, there was a fall in the absolute level of all forms of pRB protein. The level of p107 protein decreased 10-fold by 24 h, and there was a change in p107 to a more rapidly migrating form. p130 protein exists in two forms in untreated proliferating T24 cells. The slowly migrating form is the more abundant. Upon culture with HMBA, the level of both forms of p130 decrease and are replaced by a form of intermediate migration. The intermediate form of p130 has been shown to be the form that binds to E1A protein and is the growth-suppressive form capable of interacting with E2F (69). Thus, HMBA caused the conversion to the growth-suppressive forms of pRB and p130 that accompanied the arrest of T24 cells in G_1 phase.

The antiproliferative effect of the pocket proteins is mediated, at least in part, by binding to the E2F family of transcription factors and inhibiting the transcription of genes for proteins required for G_1 to S phase progression (24–30). Gel mobility assays were performed following culture with HMBA to examine the proteins involved in E2F complexes that are recognized by binding to the E2F consensus DNA sequence (Fig. 4*C*). In preconfluent T24 cells, two specific complexes

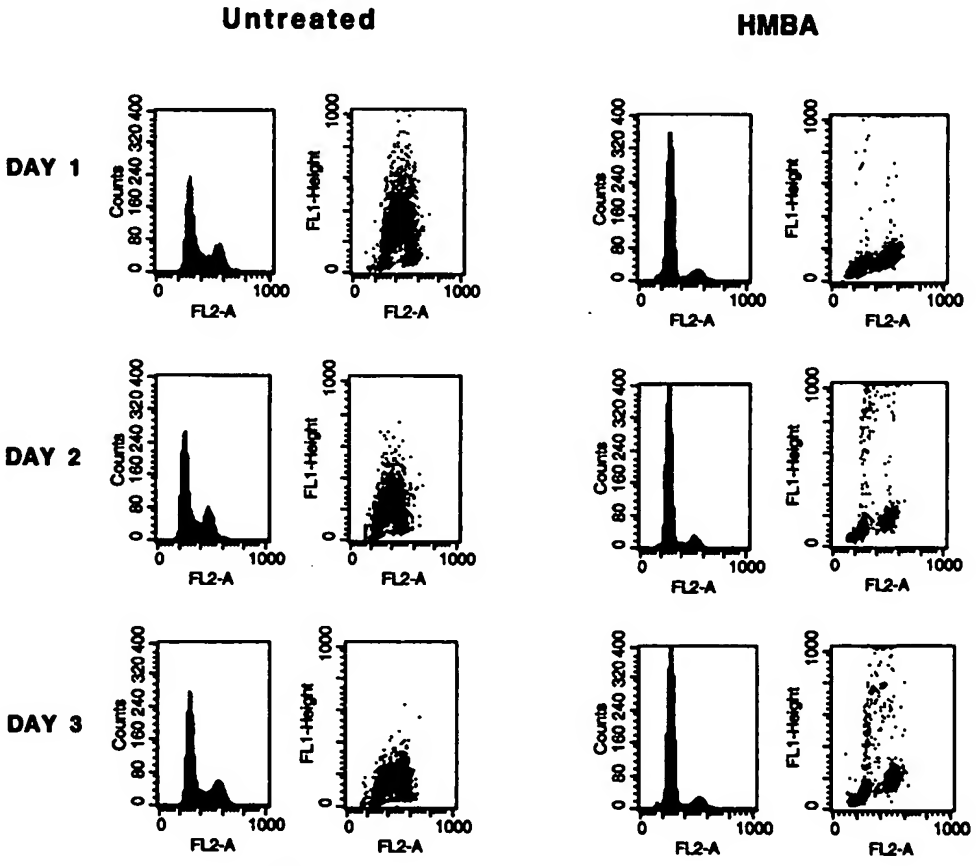

Fig. 2. Effect of HMBA on T24 cell cycle progression. T24 cells were cultured without or with 10 mM HMBA for the indicated times. Cells were labeled with BrdUrd (*FL1-Height*), and DNA content was determined by propidium iodide staining (*FL2-A*) as described.

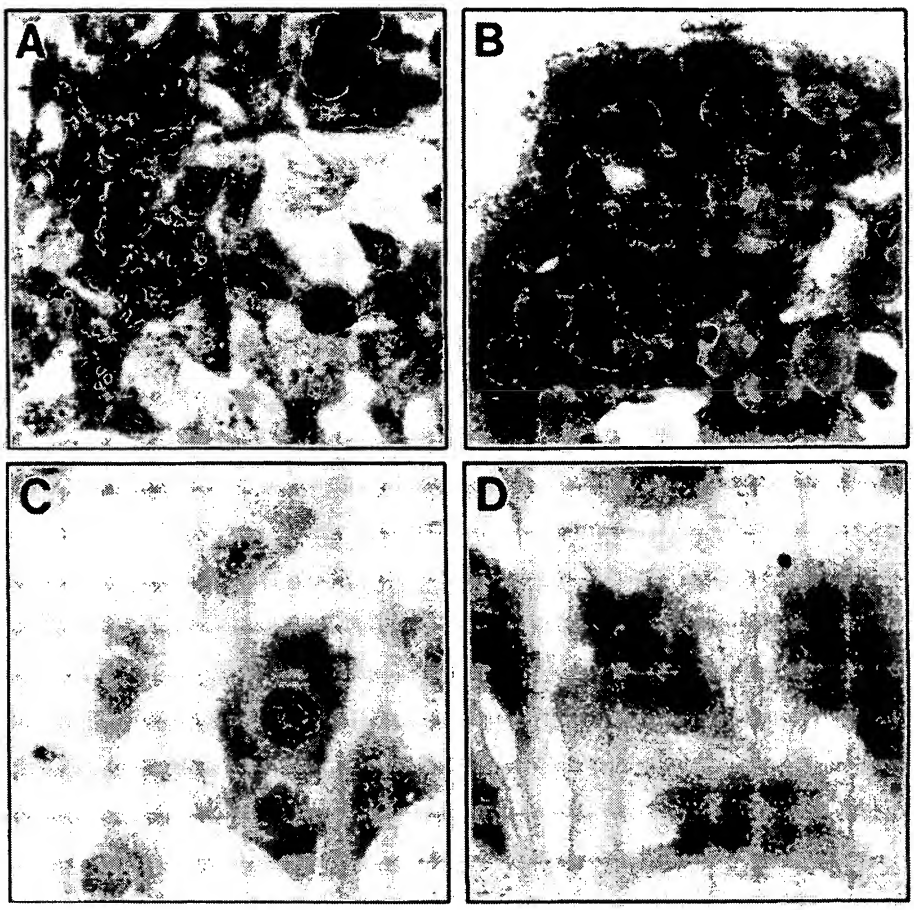

Fig. 3. Effect of HMBA on T24 Morphology. T24 cells were cultured without (*A* and *B*) or with 10 mM HMBA (*C* and *D*) for 3 days on culture slides. Cells were stained with Giemsa (*A* and *C*) or expression of actin using the anti-actin antibody (*B* and *D*).

were present. Antibody supershift experiments revealed that the complex with the slower mobility contains p107 (p107:E2F), whereas the less abundant complex with more rapid mobility contains the pRB protein. The complexes shifted with the p130 antibody in the cultures not treated with HMBA most likely reflects the cross-reaction with p107 protein (see "Materials and Methods"), because the anti-p107 antibody shifts most if not all of the complex, and the p107 antibody does not cross-react with p130 or pRB. However, the presence of a small amount of p130:E2F complex cannot be ruled out. The predominant complex detected in the undifferentiated T24 cells is the p107:E2F complex. The p107:E2F complex is characteristic of S-phase cells (46, 47) and suggests that most of the cells in this culture are cycling. During culture with HMBA, the complex containing p107 decreased in abundance, consistent with the fall in p107 protein level. At the same time, the pRB:E2F complex remains unchanged. A complex migrating with slightly slower mobility than the pRB:E2F complex was shifted by the anti-p130 antibody. A low abundance complex with much slower mobility was also detected and contains the p130 protein as indicated by the loss of the band upon addition of antibody. Induction of proliferative arrest by HMBA in T24 cells resulted in a decrease of the p107:E2F complex, no change in the pRB:E2F, and appearance of p130:E2F complexes.

Effect of HMBA in T24 Cells Expressing HPV-16 E7 Protein. To gain further insight into the role of the pocket proteins in HMBA-induced suppression of proliferation, we next examined the effect of HMBA on T24 cells expressing HPV-16 E7 protein. HPV-16 E7 protein binds to pRB, p107, and p130 and inhibits E2F binding (54, 55). Three E7-expressing clones were selected following transfection with an E7 cDNA on the basis of E7 mRNA expression (Fig. 5*A*); two vector-only clones were also selected, and the responses to HMBA were assayed. The vector controls (T24neo1 and T24neo2) and E7-expressing clones (T24/E7-1, T24/E7-2, and T24/E7-3) proliferated at approximately the same rate, in the absence of HMBA (Fig. 5*B*). In culture with HMBA, the proliferation of each of these clones was inhibited. For T24, T24neo1, or T24neo2 cells, the cell density reached a plateau between day 1 and 2 with little to no further change by day 3. The proliferation of the E7-expressing clones was inhibited by day 2 and remained inhibited at day 3. With respect to cell viability (trypan blue exclusion; Fig. 5*C*), following addition of HMBA to proliferating cultures, T24, T24neo1, and T24neo2 cells showed no change in viability, whereas the E7 clones displayed over 50% nonviable cells by 3 days of exposure to HMBA (Fig. 5*C*).

The extent of loss of viability in response to HMBA appears to correlate with the level of expression of E7 mRNA; T24/E7-1 > T24/E7-2 > T24/E7-3. Moreover, the expression of E7 mRNA in the T24/E7-2 and T24/E7-3 clones was not stable upon continued culture. The level of E7 mRNA decreased after five passages, and the loss of E7 mRNA expression was associated with a loss in HMBA-induced cell death in these clones (data not shown). The expression of E7 protein in T24/E7-1 cells was stable, and additional experiments were performed with this clone. A revertant T24/E7-1 clone (T24/E7-1R) was isolated by continued culture of T24/E7-1 in HMBA. T24/E7-1R was then maintained in the absence of HMBA and responded to culture with HMBA by inhibition of proliferation but without an increase in nonviable cells (Fig. 5*C*). This T24/E7-1R clone was found to have lost expression of E7 protein (data not shown).

Cell cycle progression was examined in T24/E7-1 cells. By 24 h in culture with 10 mM HMBA, proliferation was inhibited, and the cells were arrested in G_1 phase, determined by analysis of DNA content and BrdUrd incorporation (Fig. 6). Unlike T24 cells, which remain

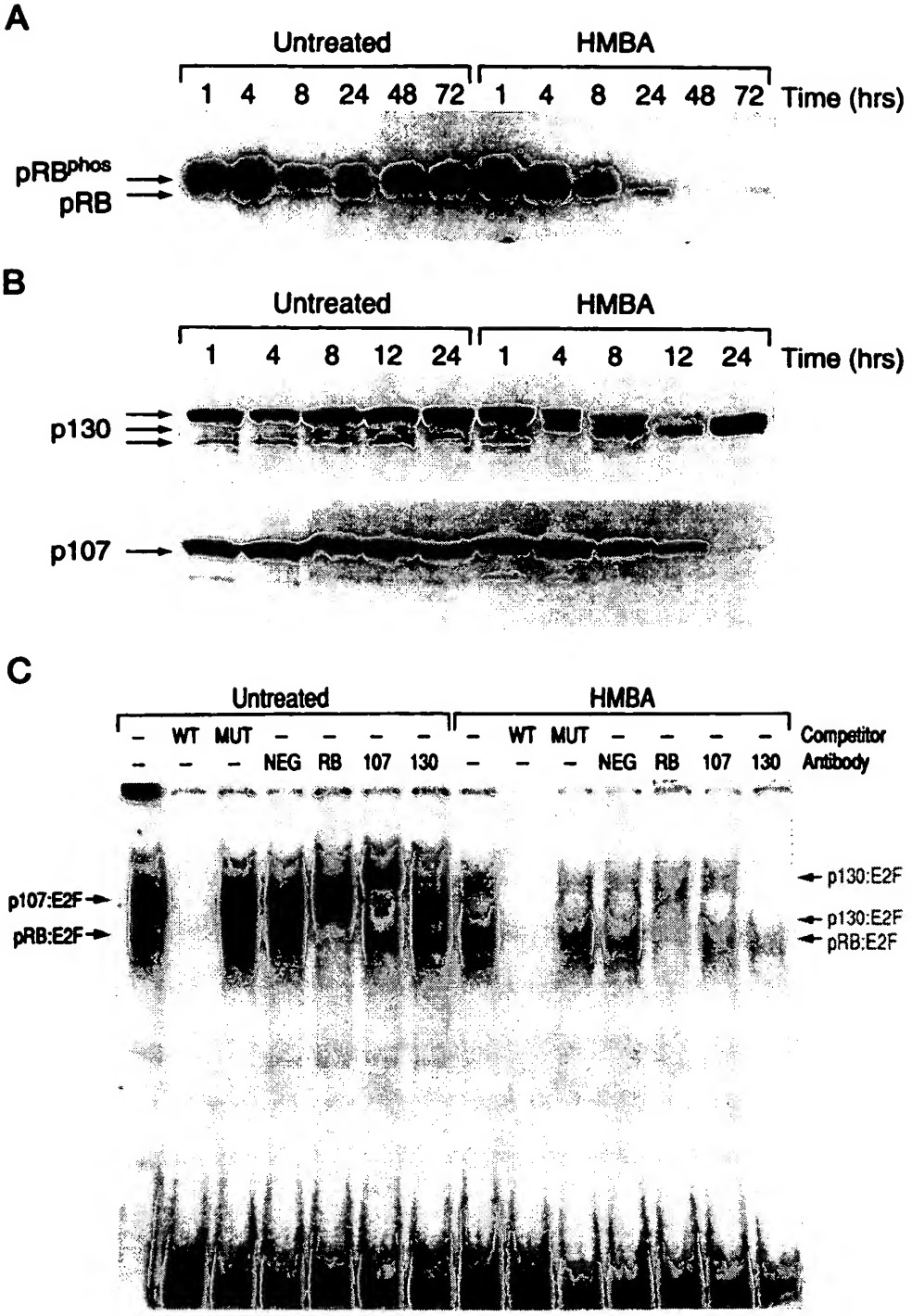

Fig. 4. Effect of HMBA on Expression of pRB, p130, and p107 proteins and E2F complexes. In *A* and *B*, T24 cells were cultured without or with 10 mM HMBA for the indicated times, and total cell lysates were prepared. pRB, p130, and p107 proteins were detected by immunoblotting. Cell equivalents (6×10^5) were loaded on each lane. The filters were probed with 1 μg/ml anti-pRB (PMG-245; PharMingen), 1 μg/ml anti-130 (C20; Santa Cruz Biotechnology) or 0.03 μg/ml anti-p107 (C18; Santa-Cruz Biotechnology). In *C*, E2F DNA-binding complexes were detected by gel mobility shift assay. Nuclear extracts were prepared from cultures treated without or with 10 mM HMBA for 24 h. Competitor or antibody was added 10 min prior to the addition of the E2F-E2 oligonucleotide. *WT*, DRTF71/50 oligonucleotide; *MUT*, DRTF62/60 oligonucleotide; *NEG*, normal rabbit serum. The antibodies are described in "Materials and Methods."

arrested in G_1 (Fig. 2), by day 2 in culture with HMBA a proportion of T24/E7-1 cells entered S phase, as revealed by BrdUrd incorporation. By day 3, although there was an increase in the percentage of cells with S phase DNA content, a portion of these apparently S-phase cells had ceased incorporating BrdUrd, indicating that they were arrested in S phase.

Effect of HMBA on E2F Complexes in T24/E7-1 Cells. We then examined the effect of E7 expression on pocket protein:E2F complexes by gel mobility shift assays. T24/E7-1 cells were cultured without or with HMBA for 24 h, nuclear extracts were prepared, and gel mobility shift analysis was performed (Fig. 7*A*). This analysis detected the presence of three E2F complexes before culture with HMBA. By antibody supershift analysis, pRB:E2F was the most abundant complex, whereas free E2F and p107:E2F were less abundant. Following culture with HMBA, only one complex was detected. This complex was determined to be free E2F by its migration on the gel and lack of supershift with antibodies against pRB, p107, or p130. This complex was shifted following addition of GST-pRB fusion protein to the gel mobility shift assay (data not shown), consistent with it being in the free form.

Effect of HMBA on pRB, p107, and p130 Proteins in T24/E7-1 Cells. We next investigated the effect of E7 on the expression of pRB, p107, and p130 proteins during culture with HMBA (Fig. 7*B*). In the absence of HMBA, the level of pRB protein in T24/E7 cells was

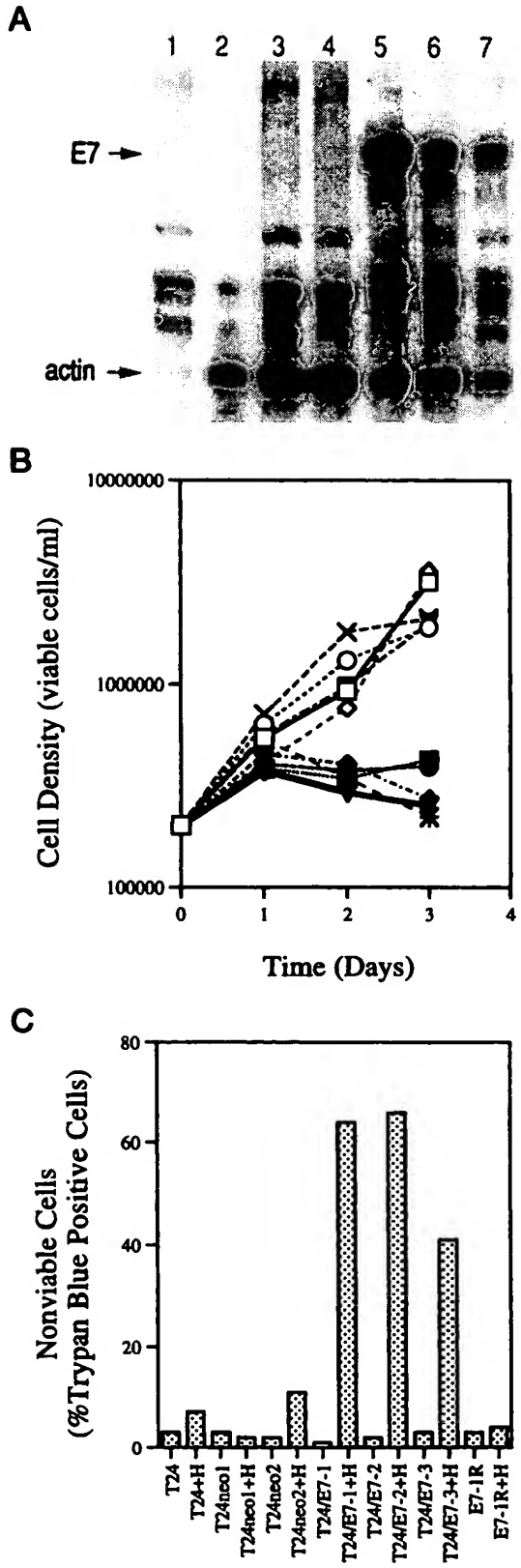

Fig. 5. Characterization of T24/E7 cells. In *A*, T24 clones expressing E7 mRNA were identified by RNase protection assay. RNase protection assays were performed using 10 μg of total RNA. Actin was used as a normalization control for RNA loading. *Lane 1*, tRNA; *Lane 2*, T24; *Lane 3*, T24neo-1; *Lane 4*, T24neo-2; *Lane 5*, T24/E7-1; *Lane 6*, T24/E7-2; *Lane 7*, T24/E7-3. In *B*, cells were cultured without or with 10 mM HMBA (*H*) for 1, 2, and 3 days. Cell density was determined, and cell viability was determined by trypan blue exclusion. □, T24neo-1; ■, T24neo-1 + H; ○, T24neo-2; ●, T24neo-2 + H; ◇, T24/E7-1; ◆, T24/E7-1 + H; ×, T24/E7-2; ✱, T24/E7-2 + H; ▽, T24/E7-3; ▼, T24/E7-3 + H. In *C*, the viability of the cells in culture was determined by trypan blue exclusion following 3 days of exposure to 10 mM HMBA.

similar to that in the T24 cells. Upon culture with HMBA, the changes in pRB phosphorylation occurred over a similar time course, but the level of pRB after 24 h of HMBA culture was lower in T24/E7-1 cells than in T24 parental cells. The baseline level of p130 protein is similar in the T24 and T24/E7 cells, and there are three forms of p130 detected in T24/E7-1. Upon culture with HMBA, there was a fall in the level of the slowest migrating form and an increase in the more rapidly migrating, presumably active, form. No decrease in the total amount of p130 was detected. The amount of p107 protein is lower in the T24/E7-1 cells than in the T24 cells, and as in T24 cells, the amount of p107 protein falls during culture with HMBA.

Effect of HMBA on Induction of Apoptosis in T24 and T24/E7-1 Cells. We next asked whether the HMBA-induced cell death of T24/E7 cells is due to apoptosis. Apoptotic cells were identified by an increase in DNA fragmentation, detected by the TUNEL technique (Fig. 8*A*). Little apoptosis (<5%) was detected in T24 and T24/E7-1 cells cultured in the absence of HMBA. T24 cells cultured with HMBA also showed little (<5%) apoptosis. Although the T24/E7-1 culture contained less than 5% apoptotic cells following 1 day of treatment with HMBA, by day 3 over 80% of the cells were apoptotic.

It has been suggested that induction of apoptosis results from improper S-phase entry (70). We asked whether upon culture with HMBA, E7-transfected cells were generating signals promoting G_1 to S phase progression accompanied by signals for inhibition of G_1 to S phase progression. To answer this question, the levels of p21, cdk2, cyclin A, and E2F-1 proteins and cdk2 histone H1 kinase activity were determined in T24 and T24/E7-1 cells following 24 h culture with HMBA (Fig. 8, *B* and *C*). Under these conditions, the levels of cdk2 and cyclin A protein did not change, but an increase in the level of p21 was detected in both T24 and T24/E7-1 cells, and the histone H1 kinase activity associated with immunoprecipitated cdk2 decreased in both T24 and T24/E7-1 cells. T24 and T24/E7-1 differed, however, in that upon culture with HMBA, E2F-1 protein decreased in T24 cells and increased in T24/E7-1 cells. These data suggest that the induction of apoptosis in the T24/E7-1 cells may result from conflicting cell cycle signals: increased E2F-1 protein promoting S-phase entry; and low cdk2 activity inhibiting S-phase entry.

DISCUSSION

The present study demonstrates: (*a*) that the hybrid polar differentiation agent HMBA inhibits the proliferation of T24 transitional cell bladder carcinoma cells and induces morphological changes consistent with maturation; and (*b*) that the expression of HPV-16 E7 protein blocks pocket protein:E2F interaction and causes T24 cells in culture with HMBA to undergo apoptosis rather than differentiation.

HMBA-induced cessation of proliferation in T24 cells is mediated, at least in part, by effects on the pocket proteins and E2F. HMBA induces the accumulation of underphosphorylated forms of pRB and p130 proteins and a decrease in the level of p107 protein. Following treatment with HMBA, E2F switches from complexes containing predominantly p107 to complexes containing pRB and p130. The molecular specificity of pocket protein binding to E2F upon induction of differentiation supports the current hypothesis that the transcription-modulating effects of E2F-associated pocket proteins serve to regulate different classes of E2F-responsive genes (71). Although all three pocket proteins have been shown to repress E2F transcriptional activity, they do not possess completely redundant functions. For example, both mouse knockout studies and the analysis of certain human tumors demonstrate that pRB is a tumor suppressor protein, but p130 and p107 are not (72–74). Our findings are consistent with this concept that pRB, p130, and p107 have, at least in part, different functions.

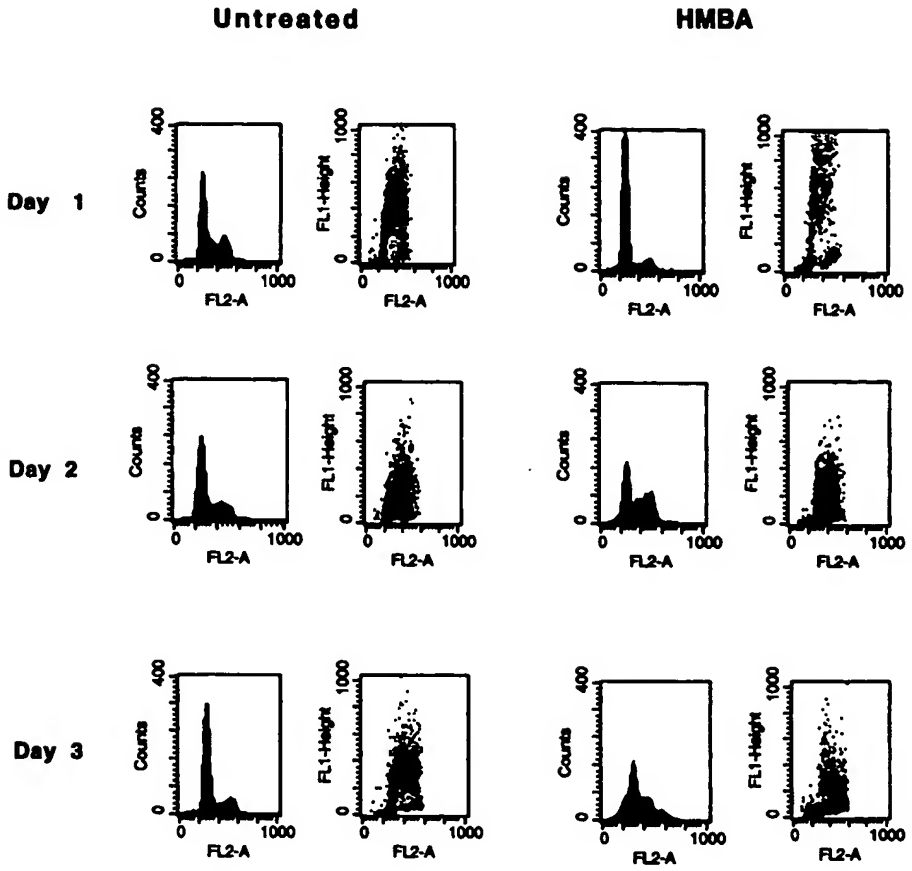

Fig. 6. Effect of HMBA on cell cycle progression in T24/E7-1 cells. T24/E7-1 cells were cultured without or with 10 mM HMBA for the indicated times. Cell cycle analysis was performed as described for Fig. 2.

The pocket proteins are important in controlling the transcriptional activity of E2F, which in turn is critical for cell growth and differentiation decisions (52). A variety of experiments have demonstrated that E2F-1 overexpression can induce S-phase entry (75–78) and that overexpression of dominant-negative E2F mutants inhibits cell cycle progression from G_1 to S phase (79). In some cultured cells, overexpression of E2F-1 has been found to induce p53-dependent apoptosis (76–78, 80). Overexpression of E2F-1 may induce apoptosis by

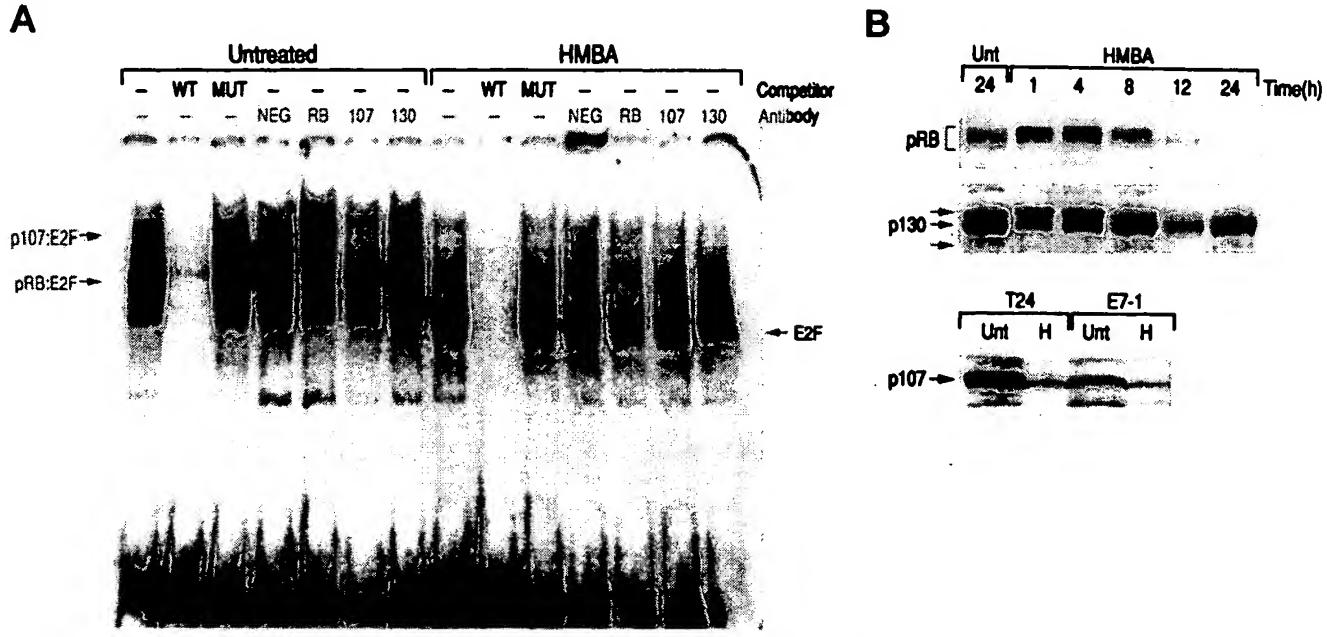

Fig. 7. Effect of E7 protein expression on E2F complexes and pRB, p107, and p130 proteins. In *A*, E2F DNA-binding complexes were detected by gel mobility shift assay. Nuclear extracts were prepared from cultures treated without and with 10 mM HMBA for 24 h. Competitor or antibody was added 10 min prior to the addition of the E2F-E2 oligonucleotide. *WT*, DRTF71/50 oligonucleotide; *MUT*, DRTF62/60 oligonucleotide; *NEG*, normal rabbit serum. The antibodies are described in "Materials and Methods." *B*, immunoblot analysis of pRB, p130, and p107 proteins in T24/E7-1 cells. Cells were cultured with 10 mM HMBA for the indicated times, and total cell extracts were prepared and analysis was performed as described for Fig. 4. p107 protein expression was determined in extracts prepared from T24 and T24/E7-1 cells cultured without or with 10 mM HMBA for 24 h.

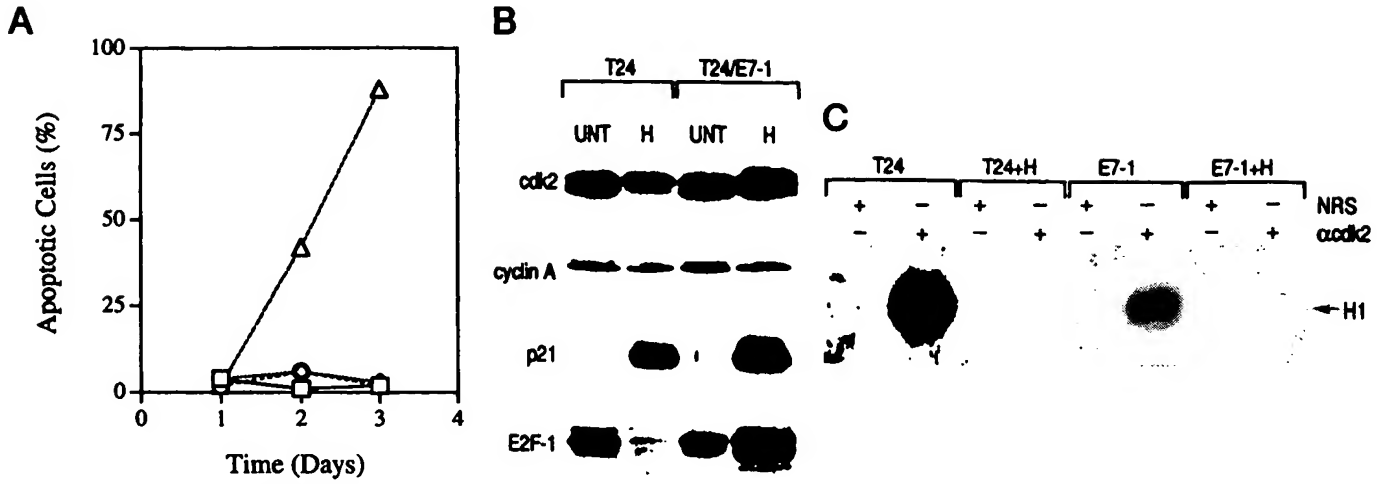

Fig. 8. HMBA induces apoptosis in T24/E7-1 cells cultured with HMBA. In *A*, T24 and T24/E7-1 cells were cultured without or with 10 mM HMBA for 1, 2, and 3 days. □, T24; ◇, T24 + H; ○, T24/E7-1; △, T24/E7-1 + H. Apoptotic cells were detected using the TUNEL method. Over 200 cells were counted for each determination. *B*, effect of HMBA on cdk2, cyclin A, p21, and E2F-1 protein expression in T24 and T24/E7-1 cells. Cells were cultured without or with 10 mM for 1 day, and total cell extracts were prepared. Immunoblots were performed as described for Fig. 2 using the following antibodies (1 μg/ml) obtained from Santa Cruz Biotechnology, Inc.: anti-cdk2 (M2), anti-cyclin A (BF683), anti-p21 (H-164), and anti-E2F-1 (C20). *C*, effect of HMBA on cdk2 kinase activity in T24 and T24/E7-1 cells. Cells were cultured without or with 10 mM HMBA for 1 day. Nuclear extracts were prepared and immunoprecipitated (25 μg) with anti-cdk2 (M2) or with normal rabbit serum (*NRS*). Kinase activity was assayed by using 1 μg of histone H1 as a substrate.

regulating genes important for cell survival or perhaps by driving cells into S phase at an inappropriate time (70).

The finding of the switch from induction of differentiation to induction of apoptosis upon expression of HPV-16 E7 is not specific for culture of T24 bladder carcinoma cells with HMBA. Pan and Griep (81) have found altered regulation of cell cycle in transgenic mice, in which the expression of E7 was directed to the developing lens. The adult E7 transgenic mice revealed inhibition of lens fiber cell differentiation and apoptosis.

This study provides evidence that E2F:pocket protein complex regulation plays an important role in HMBA-induced cessation of proliferation and induction of differentiation in T24 cells. The effects of HMBA are markedly altered when pocket protein:E2F complex formation is blocked or impeded by constitutive expression of HPV-16 E7 protein. T24/E7-1 cells cultured with HMBA do not remain arrested in G_1 phase as do T24 cells. This may reflect the fact that in T24/E7-1 cells cultured with inducer, E2F is present in its free form, and the level of E2F-1 protein increases. Our results are consistent with those of DeGregori *et al.* (82), who show that the E2F-1 overexpression can overcome a G_1 arrest caused by the inhibition of G_1 cyclin-dependent kinase activity. The transient G_1 arrest that occurred in T24/E7-1 cells following 1 day of culture with HMBA may be due, in part, to effects on other cell cycle proteins involved in regulating G_1 to S-phase progression. We have found that HMBA causes a greater than 10-fold increase in p21 protein and inhibition of cdk2 activity in both T24 and T24/E7-1 cells. These changes may be sufficient to transiently suppress S-phase entry, even in the presence of high levels of free E2F. Indeed, our findings indicate that E2F must be in complexes with pocket proteins during culture with HMBA to maintain T24 cells in the G_1-arrested state.

Unlike T24 cells, T24/E7-1 cells cultured with HMBA enter S phase and undergo apoptosis. In T24/E7-1 cells cultured with HMBA, the combination of low cdk2 activity and high levels of active E2F, capable of binding to DNA, may activate an S-phase checkpoint and contribute to the onset of apoptosis. This model is supported by studies of Krek *et al.* (83, 84), who show that in S phase, E2F-1 forms a stable complex with cyclin A-kinase, which in turn causes DP-1 to become phosphorylated and the E2F complex to be released from DNA (85, 86). The release of E2F from DNA by phosphorylation of DP-1 is required for S-phase progression, and failure to release E2F from DNA during S phase results in apoptosis.

These studies demonstrate that T24 transitional cell carcinoma bladder cells provide another and complementary model system to study differentiation agent-mediated proliferation arrest of transformed cells in addition to the well-studied MEL cell system (1). Induction of MEL cell differentiation by hybrid polar compounds also results in the modulation of E2F complexes (87). Following induction of differentiation, the level of the free form of E2F decreases, and E2F is in complex with p107. The finding that in MEL cells E2F complexes with p107, and in T24 cells E2F complexes with pRB and p130, not p107 during HMBA-induced differentiation, indicates that formation of specific pocket protein:E2F complexes during differentiation may be cell lineage specific.

These studies suggest that pocket protein:E2F complex formation is required for HMBA-induced sustained inhibition of proliferation associated with morphological differentiation of bladder carcinoma T24 cells. It appears that under conditions in which pRB and p130 are not available to complex with E2F, HMBA can induce an alternative developmental option, *i.e.*, apoptosis. Taken together, these studies enlarge the repertoire of demonstrated developmental pathways that may be triggered in transformed cells, depending upon their molecular status, and may provide potential therapeutic opportunities for cancer.

ACKNOWLEDGMENTS

We thank Maria Dudas, Lang Ngo, and Tom Tolentino for expert technical assistance; Drs. Ed Harlow and Nick Dyson for p107 antibody SD-15; and Drs. Allen Oliff and Deborah DeFeo-Jones for the HPV-16 E7 expression vector and E7 antibodies.

REFERENCES

1. Marks, P. A., Richon, V. M., and Rifkind, R. A. Cell cycle regulatory proteins are targets for induced differentiation of transformed cells: molecular and clinical studies employing hybrid polar compounds. Int. J. Hematol., *63:* 1–17, 1996.
2. Reuben, R. C., Wife, R. L., Breslow, R., Rifkind, R. A., and Marks, P. A. A new group of potent inducers of differentiation in murine erythroleukemia cells. Proc. Natl. Acad. Sci. USA, *73:* 862–866, 1976.
3. Friend, S. H., Horowitz, J. M., Gerber, M. R., Wang, X. F., Bogenmann, E., Li, F. P.,

and Weinberg, R. A. Deletions of a DNA sequence in retinoblastomas and mesenchymal tumors: organization of the sequence and its encoded protein. Proc. Natl. Acad. Sci. USA, *84:* 9059–9063, 1987.
4. Lee, W-H., Bookstein, R., Hong, F., Young, L., Shew, J., and Lee, E. Y. H. Human retinoblastoma susceptibility gene: cloning, identification, and sequence. Science (Washington DC), *235:* 1394–1399, 1987.
5. Fung, Y. T., Murphree, A. L., T'Ang, A., Qian, J., Hinrichs, S. H., and Benedict, W. F. Structural evidence for the authenticity of the human retinoblastoma gene. Science (Washington DC), *236:* 1657–1659, 1987.
6. Ewen, M. E., Xing, Y., Lawrence, J. B., and Livingston, D. M. Molecular cloning, chromosomal mapping and expression of the cDNA for p107, a retinoblastoma gene product-related protein. Cell, *66:* 1155–1164, 1991.
7. Cobrinik, D., Whyte, P., Pepper, D. S., Jackson, T., and Weinberg, R. A. Cell cycle-specific association of E2F with the p130 E1A-binding domain. Genes Dev., *7:* 2392–2404, 1993.
8. Li, Y., Graham, C., Lacy, S., Duncan, A. M. W., and Whyte, P. The adenovirus E1A-associated 130-kD is encoded by a member of the retinoblastoma gene family and physically interacts with cyclin A and E. Genes Dev., *7:* 2366–2377, 1993.
9. Hannon, G. J., Demetrick, D., and Beach, D. Isolation of the Rb-related p130 through its interaction with CDK2 and cyclins. Genes Dev., *7:* 2378–2391, 1993.
10. Kaelin, W. G., Jr., Krek, W., Sellers, W. R., DeCaprio, J. A., Ajchenbaum-Cymbalista, F., Fuchs, C. S., Chittenden, T., Li, Y., Farnham, P. J., Blanar, M. A., Livingston, D. M., and Flemington, E. K. Expression cloning of a cDNA encoding a retinoblastoma-binding protein with E2F-like properties. Cell, *70:* 351–364, 1992.
11. Helin, K., Lees, J. A., Vidal, M., Dyson, N., Harlow, E., and Fattaey, A. A cDNA encoding a pRB-binding protein with properties of the transcription factor E2F. Cell, *70:* 337–350, 1992.
12. Shan, B., Zhu, X., Chen, P-L., Durfee, T., Yang, Y., Sharp, D., and Lee, W-H. Molecular cloning of cellular genes encoding retinoblastoma-associated proteins: identification of a gene with properties of the transcription factor E2F. Mol. Cell. Biol., *12:* 5620–5631, 1992.
13. Bandara, L. R., Buck, V. M., Zamanian, M., Johnston, L. H., and La Thangue, N. B. Functional synergy between DP-1 and E2F-1 in the cell cycle-regulating transcription factor DRTF1/E2F. EMBO J., *12:* 4317–4324, 1993.
14. Girling, R., Partridge, J. F., Bandara, L. R., Burden, N., Totty, N. F., Hsuan, J. J., and La Thangue, N. B. A new component of the transcription factor DRTF1/E2F. Nature (Lond.), *362:* 83–87, 1993.
15. Helin, K., Wu, C., Fattaey, A. R., Lees, J. A., Dynlacht, B. D., Ngwu, C., and Harlow, E. Heterodimerization of the transcription factors E2F-1 and DP-1 leads to cooperative *trans*-activation. Genes Dev., *7:* 1850–1861, 1993.
16. Krek, W., Livingston, D. M., and Shirodkar, S. Binding to DNA, and the retinoblastoma gene product promoted by complex formation of different E2F family members. Science (Washington DC), *262:* 1557–1560, 1993.
17. Ivey-Hoyle, M., Conroy, R., Huber, H. E., Goodhart, P. J., Oliff, A., and Heimbrook, D. C. Cloning and characterization of E2F-2, a novel protein with the biochemical properties of transcription factor E2F. Mol. Cell. Biol., *13:* 7802–7812, 1993.
18. Lees, J. A., Saito, M., Vidal, M., Valentine, M., Look, T., Harlow, E., Dyson, N., and Helin, K. The retinoblastoma protein binds to a family of E2F transcription factors. Mol. Cell. Biol., *13:* 7813–7825, 1993.
19. Ginsberg, D., Vairo, G., Chittenden, T., Xiao, Z., Xu, G., Wydner, K. L., DeCaprio, J. A., Lawrence, J. B., and Livingston, D. M. E2F-4, a new member of the E2F transcription factor family, interacts with p107. Genes Dev., *8:* 2665–2679, 1994.
20. Beijersbergen, R. L., Kerkhoven, R. M., Zhu, L., Carlee, L., Voorhoeve, P. M., and Bernards, R. E2F-4, a new member of the E2F gene family, has oncogenic activity and associates with p107 *in vivo*. Genes Dev., *8:* 2680–2690, 1994.
21. Sardet, C., Vidal, M., Cobrinik, D., Geng, Y., Onufryk, C., Chen, A., and Weinberg, R. A. E2F-4 and E2F-5, two members of the E2F family, are expressed in the early phases of the cell cycle. Proc. Natl. Acad. Sci. USA, *92:* 2403–2407, 1995.
22. Bandara, L. R., Lam, E. W., Sorensen, M., Zamanian, M., Girling, R., and La Thangue, N. B. DP-1: a cell cycle-regulated and phosphorylated component of transcription factor DRTF1/E2F which is functionally important for recognition by pRB and the adenovirus E4 of 6/7 protein. EMBO J., *13:* 3104–3114, 1994.
23. Wu, C., Zukerberg, L. R., Ngwu, C., Harlow, E., and Lees, J. A. *In vivo* association of E2F and DP family proteins. Mol. Biol. Cell, *15:* 2536–2546, 1995.
24. Hamel, P. A., Gill, R. M., Phillips, R. A., and Gallie, B. L. Transcriptional repression of the E2-containing promoters EIIaE, c-myc, and RB1 by the product of the *RB1* gene. Mol. Cell. Biol., *12:* 3431–3438, 1992.
25. Hiebert, S. W., Chellappan, S. P., Horowitz, J. M., and Nevins, J. R. The interaction of RB with E2F coincides with an inhibition of the transcriptional activity of E2F. Genes Dev., *6:* 177–185, 1992.
26. Weintraub, S. J., Prater, C. A., and Dean, D. C. Retinoblastoma protein switches the E2F site from positive to negative element. Nature (Lond.), *358:* 259–261, 1992.
27. Zamanian, M., and La Thangue, N. B. Adenovirus E1A prevents the retinoblastoma gene product from repressing the activity of a cellular transcription factor. EMBO J., *11:* 2603–2610, 1992.
28. Schwartz, J. K., Devoto, S. H., Smith, E. J., Chellappan, S. P., Jakoi, L., and Nevins, J. R. Interactions of the p107 and Rb proteins with E2F during the cell proliferation response. EMBO J., *12:* 1013–1020, 1993.
29. Zamanian, M., and La Thangue, N. B. Transcriptional repression by the Rb-related protein p107. Mol. Biol. Cell, *4:* 389–396, 1993.
30. Zhu, L., van den Heuvel, S., Helin, K., Fattaey, A., Ewen, M., Livingston, D. M., Dyson, N., and Harlow, E. Inhibition of cell proliferation by p107, a relative of the retinoblastoma protein. Genes Dev., *7:* 1111–1125, 1993.
31. DeGregori, J., Kowalik, T., and Nevins, J. R. Cellular targets for activation by the E2F1 transcriptional factor include DNA synthesis and G_1-S-regulatory genes. Mol. Cell. Biol., *15:* 4215–4224, 1995.
32. Nevins, J. R. E2F: a link between the Rb tumor suppressor protein and viral oncoprotein. Science (Washington DC), *258:* 424–429, 1992.
33. Lam, E. W., and Watson, R. J. An E2F-binding site mediates cell-cycle regulated repression of mouse B-myb transcription. EMBO J., *12:* 2705–2713, 1994.
34. Hsiao, K-M., McMahon, S. L., and Farnham, P. J. Multiple DNA elements are required for the growth regulation of the mouse E2F1 promoter. Genes Dev., *8:* 1526–1537, 1994.
35. Johnson, D. G., Ohtani, K., and Nevins, J. R. Autoregulatory control of E2F1 expression in response to positive and negative regulators of cell cycle progression. Genes Dev., *8:* 1514–1525, 1994.
36. Bagchi, S., Weinmann, R., and Raychaudhuri, P. The retinoblastoma protein copurifies with E2F-I, an E1A-regulated inhibitor of the transcription factor E2F. Cell, *65:* 1063–1072, 1991.
37. Bandara, L. R., and La Thangue, N. B. Adenovirus E1A prevents the retinoblastoma gene product from complexing with a cellular transcription factor. Nature (Lond.), *351:* 494–497, 1991.
38. Chellappan, S. P., Hiebert, S., Mudryj, M., Horowitz, J. M., and Nevins, J. R. The E2F transcription factor is a cellular target for the RB protein. Cell, *65:* 1053–1061, 1991.
39. Chittenden, T., Livingston, D. M., and Kaelin, W. G., Jr. The T/E1 A-binding domain of the retinoblastoma product can interact selectively with a sequence-specific DNA-binding protein. Cell, *65:* 1073–1082, 1991.
40. Ewen, M. E., Sluss, H. K., Sherr, C. J., Matsushime, H., Kato, J., and Livingston, D. M. Functional interactions of the retinoblastoma protein with mammalian D-type cyclins. Cell, *73:* 487–497, 1993.
41. Hinds, P. W., Mittnacht, S., Dulic, V., Arnold, A., Reed, S. I., and Weinberg, R. A. Regulation of retinoblastoma protein functions by ectopic expression of human cyclins. Cell, *70:* 993–1006, 1992.
42. Lees, J. A., Buchkovich, K. J., Marshak, D. R., Anderson, C. W., and Harlow, E. The retinoblastoma protein is phosphorylated on multiple sites by human cdc2. EMBO J., *10:* 4279–4290, 1991.
43. Matsushime, H., Quelle, D. E., Shurtleff, S., Sherr, C. J., and Kato, J. D-type cyclin-dependent kinase activity in mammalian cells. Mol. Cell. Biol., *14:* 2066–2076, 1994.
44. Meyerson, M., and Harlow, E. Identification of G1 kinase activity for cdk6 a novel cyclin D partner. Mol. Cell. Biol., *14:* 2077–2086, 1994.
45. Cao, L., Faha, B., Dembski, M., Tsai, L-H., Harlow, E., and Dyson, N. Independent binding of the retinoblastoma protein and p107 to the transcription factor E2F. Nature (Lond.), *355:* 176–179, 1992.
46. Lees, E., Faha, B., Dulic, V., Reed, S. I., and Harlow, E. Cyclin E/cdk2 and cyclin A/cdk2 kinase associate with p107 and E2F in a temporally distinct manner. Genes Dev., *6:* 1874–1885, 1992.
47. Shirodkar, S., Ewen, M., DeCaprio, J. A., Morgan, J., Livingston, D. M., and Chittenden, T. The transcription factor E2F interacts with the retinoblastoma product and a p107-cyclin A complex in cell cycle-regulated manner. Cell, *68:* 157–166, 1992.
48. Cobrinik, D., Dowdy, S. F., Hinds, P. W., Mittnacht, S., and Weinberg, R. A. The retinoblastoma protein and the regulation of cell cycling. Trends Biochem. Sci., *17:* 312–315, 1992.
49. Shin, E. K., Shin, A., Paulding, C., Schaffhausen, B., and Yee, A. S. Multiple changes in E2F function and regulation occur upon muscle differentiation. Mol. Cell. Biol., *15:* 2252–2262, 1995.
50. Kiess, M., Gill, R. M., and Hamel, P. A. Expression and activity of the retinoblastoma protein (pRB)-family proteins, p107 and p130, during L6 myoblast differentiation. Cell Growth & Differ., *6:* 1287–1298, 1995.
51. Buchkovich, K. J., and Ziff, E. B. Nerve growth factor regulates the expression and activity of p33cdk2 and p34cdc2 kinases in PC12 pheochromocytoma cells. Mol. Biol. Cell, *5:* 1225–1241, 1994.
52. Ikeda, M., Jakoi, L., and Nevins, J. R. A unique role for the Rb protein in controlling E2F accumulation during cell growth and differentiation. Proc. Natl. Acad. Sci. USA, *93:* 3215–3220, 1996.
53. Schneider, J. W., Gu, W., Zhu, L., Mahdavi, V., and Nadal-Ginard, B. Reversal of terminal differentiation mediated by p107 in Rb−/− muscle cells. Science (Washington DC), *264:* 1467–1471, 1994.
54. Dyson, N., Howley, P. M., Munger, K., and Harlow, E. The human papillomavirus-16 E7 oncoprotein is able to bind to the retinoblastoma gene product. Science (Washington DC), *243:* 934–937, 1989.
55. Chellappan, S. P., Kraus, V. B., Kroger, B., Munger, K., Howley, P. M., Phelps, W. C., and Nevins, J. R. Adenovirus E1A, simian virus 40 tumor antigen, and human papillomavirus E7 protein share the capacity to disrupt the interaction between transcription factor E2F and the retinoblastoma gene product. Proc. Natl. Acad. Sci. USA, *89:* 4549–4553, 1992.
56. Dyson, N., Guida, P., Munger, K., and Harlow, E. Homologous sequences in adenovirus E1A and human papillomavirus E7 proteins mediate interaction with the same set of cellular proteins. J. Virol., *66:* 6893–6902, 1992.
57. Wigler, M., Pellicer, A., Silverstein, S., Axel, R., Urlaub, G., and Chasin, L. DNA-mediated transfer of the adenine phosphoribosyltransferase locus into mammalian cells. Proc. Natl. Acad. Sci. USA, *76:* 1373–1376, 1979.
58. Cordon-Cardo, C., and Richon, V. M. Expression of the retinoblastoma protein is regulated in normal human tissues. Am. J. Pathol., *144:* 500–510, 1994.
59. Gavrieli, Y., Sherman, Y., and Ben-Sasson, S. A. Identification of programmed cell death *in situ* via specific labeling of nuclear DNA fragmentation. J. Cell Biol., *119:* 493–501, 1992.
60. Dignam, J. D., Lebovitz, R. M., and Roeder, R. G. Accurate transcription initiation by

RNA polymerase II in a soluble extract from isolated mammalian nuclei. Nucleic Acids Res., *11:* 1475–1489, 1983.
61. Dyson, N., Dembski, M., Fattaey, A., Ngwu, C., Ewen, M., and Helin, K. Analysis of p107-associated proteins: p107 associates with a form of E2F that differs from pRB-associated E2F-1. J. Virol., *67:* 7641–7647, 1993.
62. Towbin, H., Staehelin, T., and Gordon, J. Electrophoretic transfer of protein from polyacrylamide gels to nitrocellulose sheets: procedure and some applications. Proc. Natl. Acad. Sci. USA, *76:* 4350–4354, 1979.
63. Burnette, W. N. Western blotting: electrophoretic transfer of proteins from sodium dodecyl sulfate-polyacrylamide gels to unmodified nitrocellulose and radiographic detection with antibody and radioiodinated protein A. Anal. Biochem., *112:* 195–203, 1981.
64. Melton, D. A., Krief, P. A., Rebagliati, M. R., Maniatis, T., Zinn, K., and Green, M. R. Efficient *in vitro* synthesis of biologically active RNA and RNA hybridization probes from plasmids containing a bacteriophage SP6 promoter. Nucleic Acids Res., *12:* 7035–7056, 1984.
65. Rosenblatt, J., Gun, Y., and Morgan, D. O. Human cyclin-dependent kinase 2 is activated during the S and G2 phases of the cell cycle and associates with cyclin A. Proc. Natl. Acad. Sci. USA, *89:* 2824–2828, 1992.
66. Kiyokawa, H., Richon, V. M., Rifkind, R. A., and Marks, P. A. Suppression of cyclin-dependent kinase 4 during induced differentiation of erythroleukemia cells. Mol. Cell. Biol., *14:* 7195–7203, 1994.
67. Southgate, J., Hutton, K. A. R., Thomas, D. F. M., and Trejdosiewicz, L. K. Normal human urothelial cells *in vitro*: proliferation and induction of stratification. Lab. Invest., *71:* 583–593, 1994.
68. Koss, L. G. Some ultrastructural aspects of experimental and human carcinoma of the bladder. Cancer Res., *37:* 2824–2835, 1977.
69. Mayol, X., Garriga, J., and Grana, X. Cell cycle-dependent phosphorylation of the retinoblastoma-related protein p130. Oncogene, *11:* 801–808, 1995.
70. Yamasaki, L., Jacks, T., Bronson, R., Goillot, E., Harlow, E., and Dyson, N. Tumor induction and tissue atrophy in mice lacking E2F-1. Cell, *85:* 537–548, 1996.
71. Moberg, K., Starz, M. A., and Lees, J. A. E2F-4 switches from p130 to p107 and pRB in response to cell cycle reentry. Mol. Cell. Biol., *16:* 1436–1449, 1996.
72. Jacks, T., Fazeli, A., Schmitt, E. M., Bronson, R. T., Goodell, M. A., and Weinberg, R. A. Effects of an Rb mutation in the mouse. Nature (Lond.), *359:* 295–300, 1992.
73. Clarke, A. R., Maandag, E. R., van Roon, M., van der Lugt, N. M. T., van der Valk, M., Hooper, M. L., Berns, A., and te Riele, H. Requirement for a functional *Rb-1* gene in murine development. Nature (Lond.), *359:* 328–330, 1992.
74. Lee, E. Y. H., Chang, C-Y., Hu, N., Wang, Y-C. J., Lai, C-C., Herrup, K., Lee, W-H., and Bradley, A. Mice deficient for Rb are nonviable and show defects in neurogenesis and haematopoiesis. Nature (Lond.), *359:* 288–294, 1992.
75. Johnson, D. G., Schwarz, J. K., Cress, W. D., and Nevins, J. R. Expression of transcription factor E2F1 induces quiescent cells to enter S phase. Nature (Lond.), *365:* 349–352, 1993.
76. Qin, X., Livingston, D. M., Kaelin, W. G., Jr., and Adams, P. D. Deregulated transcription factor E2F-1 expression leads to S-phase entry and p53-mediated apoptosis. Proc. Natl. Acad. Sci. USA, *91:* 10918–10922, 1994.
77. Shan, B., and Lee, W-H. Deregulated expression of E2F-1 induces S-phase entry and leads to apoptosis. Mol. Cell. Biol., *14:* 8166–8173, 1994.
78. Kowalik, T. F., DeGregori, J., Schwartz, J. K., and Nevins, J. R. E2F1 overexpression in quiescent fibroblasts leads to induction of cellular DNA synthesis and apoptosis. J. Virol., *69:* 2491–2500, 1995.
79. Dobrowolski, S. F., Stacey, D. W., Harter, M. L., Stine, J. T., and Hiebert, S. W. An E2F dominant negative mutant blocks E1A induced cell cycle progression. Oncogene, *9:* 2605–2612, 1994.
80. Wu, X., and Levine, A. J. p53 and E2F-1 cooperate to mediate apoptosis. Proc. Natl. Acad. Sci. USA, *91:* 3602–3606, 1994.
81. Pan, H., and Griep, A. E. Altered cell cycle regulation in the lens of HPV-16 E6 or E7 transgenic mice: implications for tumor suppressor gene function in development. Genes Dev., *8:* 1285–1299, 1994.
82. DeGregori, J., Leone, G., Ohtani, K., Miron, A., and Nevins, J. R. E2F-1 accumulation bypasses a G1 arrest resulting from the inhibition of G1 cyclin-dependent kinase activity. Genes Dev., *9:* 2873–2887, 1995.
83. Krek, W., Ewen, M. E., Shirodkar, S., Arany, Z., Kaelin, W. G., Jr., and Livingston, D. M. Negative regulation of the growth-promoting transcription factor E2F-1 by a stably bound cyclin A-dependent protein kinase. Cell, *78:* 161–172, 1994.
84. Krek, W., Xu, G., and Livingston, D. M. Cyclin A-kinase regulation of E2F-1 DNA binding function underlies suppression of an S phase checkpoint. Cell, *83:* 1149–1158, 1995.
85. Dynlacht, B. D., Flores, O., Lees, J. A., and Harlow, E. Differential regulation of E2F *trans*-activation by cyclin/cdk2 complexes. Genes Dev., *8:* 1772–1786, 1994.
86. Xu, M., Sheppard, K. A., Peng, C-Y., Yee, A. S., and Piwnica-Worms, H. Cyclin A/cdk2 binds directly to E2F-1 and inhibits the DNA-binding activity of E2F-1/Dp-1 by phosphorylation. Mol. Cell. Biol., *14:* 8420–8431, 1994.
87. Richon, V. M., and Venta-Perez, G. Changes in E2F DNA-binding activity during induced erythroid differentiation. Cell Growth & Differ., *7:* 31–42, 1996.

Oncogene Expression Cloning by Retroviral Transduction of Adenovirus E1A-immortalized Rat Kidney RK3E Cells: Transformation of a Host with Epithelial Features by c-MYC and the Zinc Finger Protein GKLF[1]

K. Wade Foster, Songrong Ren,[2] Iuri D. Louro, Susan M. Lobo-Ruppert, Peggy McKie-Bell, William Grizzle, Martha R. Hayes, Thomas R. Broker, Louise T. Chow, and J. Michael Ruppert[3]

Department of Biochemistry and Molecular Genetics [K. W. F., S. R., I. D. L., S. M. L-R., M. R. H., T. R. B., L. T. C., J. M. R.], Division of Hematology/Oncology, Department of Medicine [P. M-B., J. M. R.], Department of Pathology [W. G.], and Oral Cancer Research Center and Comprehensive Cancer Center [W. G., T. R. B., L. T. C., J. M. R.], University of Alabama at Birmingham, Birmingham, Alabama 35294-3300

Abstract

The function of several known oncogenes is restricted to specific host cells *in vitro*, suggesting that new genes may be identified by using alternate hosts. RK3E cells exhibit characteristics of epithelia and are susceptible to transformation by the G protein RAS and the zinc finger protein GLI. Expression cloning identified the major transforming activities in squamous cell carcinoma cell lines as c-MYC and the zinc finger protein gut-enriched Krüppel-like factor (GKLF)/epithelial zinc finger. In oral squamous epithelium, *GKLF* expression was detected in the upper, differentiating cell layers. In dysplastic epithelium, expression was prominently increased and was detected diffusely throughout the entire epithelium, indicating that *GKLF* is misexpressed in the basal compartment early during tumor progression. The results demonstrate transformation of epithelioid cells to be a sensitive and specific assay for oncogenes activated during tumorigenesis *in vivo*, and identify *GKLF* as an oncogene that may function as a regulator of proliferation or differentiation in epithelia.

Received 12/21/98; revised 4/2/99; accepted 4/15/99.
The costs of publication of this article were defrayed in part by the payment of page charges. This article must therefore be hereby marked *advertisement* in accordance with 18 U.S.C. Section 1734 solely to indicate this fact.
[1] Supported by NIH Grant R29 CA65686 (to J. M. R.) and the University of Alabama at Birmingham Oral Cancer Research Center (DE 11910). K. W. F. is a Medical Scientist Training Program trainee (NIGMS T32GM08361-0607). Core Facilities at The University of Alabama at Birmingham are partially supported by the Comprehensive Cancer Center (5P50 CA13148).
[2] Present address: Salk Institute for Biological Studies, La Jolla, CA 92037.
[3] To whom requests for reprints should be addressed, at Department of Medicine, Room 570 WTI, University of Alabama at Birmingham, Birmingham, AL 35294-3300. Phone: (205) 975-0556; Fax: (205) 934-9573; E-mail: mruppert@uab.edu.

Introduction

Cellular oncogenes have been isolated by characterization of transforming retroviruses from animal tumors, by examination of the breakpoints resulting from chromosomal translocation, by expression cloning of tumor DNA molecules using mesenchymal cells such as NIH3T3, and by other methods (1–5). Several human tumor-types exhibit loss-of-function mutations in a tumor suppressor gene that lead to activation of a specific oncogene in a large proportion of tumors. For example, *c-MYC* expression is regulated by the *APC* colorectal tumor suppressor; expression of *GLI* is activated by loss-of-function of *PATCHED1* in human basal cell carcinoma and in animal models; E2F is activated by loss-of-function of the retinoblastoma susceptibility protein $p105^{Rb}$; and RAS GTPase activity is regulated by the familial neurofibromatosis gene *NF1* (6–12). The comparative genomic hybridization assay and related methods have shown that numerous uncharacterized loci in tumors undergo gene amplification (13). These observations, and the infrequent genetic alteration of known oncogenes in certain tumor types, suggest that novel transforming oncogenes remain to be identified.

One limitation to the isolation of oncogenes has been the paucity of *in vitro* assays for functional expression cloning. Whereas most studies have used NIH3T3 or other mesenchymal cells as host for analysis of oncogenes relevant to carcinoma, the potential use of a host cell with epithelial characteristics has been discussed (2). In addition, several known oncogenes exhibit cell-type specificity. *GLI*, *BCR-ABL*, *NOTCH1/TAN1*, and the G protein GIP2 have been found to transform immortalized rat cells (14–18), but not NIHT3 cells, demonstrating the potential use of alternate assays for oncogene expression cloning.

A consistent feature of human tumors is inactivation of the G_1 phase cell cycle regulatory pathway that includes $p105^{Rb}$ (19–22). Loss-of-function mutations affect $p105^{Rb}$ or the cyclin-dependent kinase inhibitors, or gain-of-function mutations occur in cyclin-dependent kinases or associated cyclins. Such alterations are rate-limiting for tumor formation *in vivo* because inheritance of these defects predisposes to retinoblastoma, cutaneous malignant melanoma, and other tumors. During viral infection of normal cells, disruption of the same pathway is critical for successful induction of the cellular DNA replicative machinery to support viral replication. Therefore, viruses express proteins, such as adenovirus E1A, that affect cell cycle progression through direct interaction with cell cycle regulators including $p105^{Rb}$, $p27^{Kip1}$, and others (23–26).

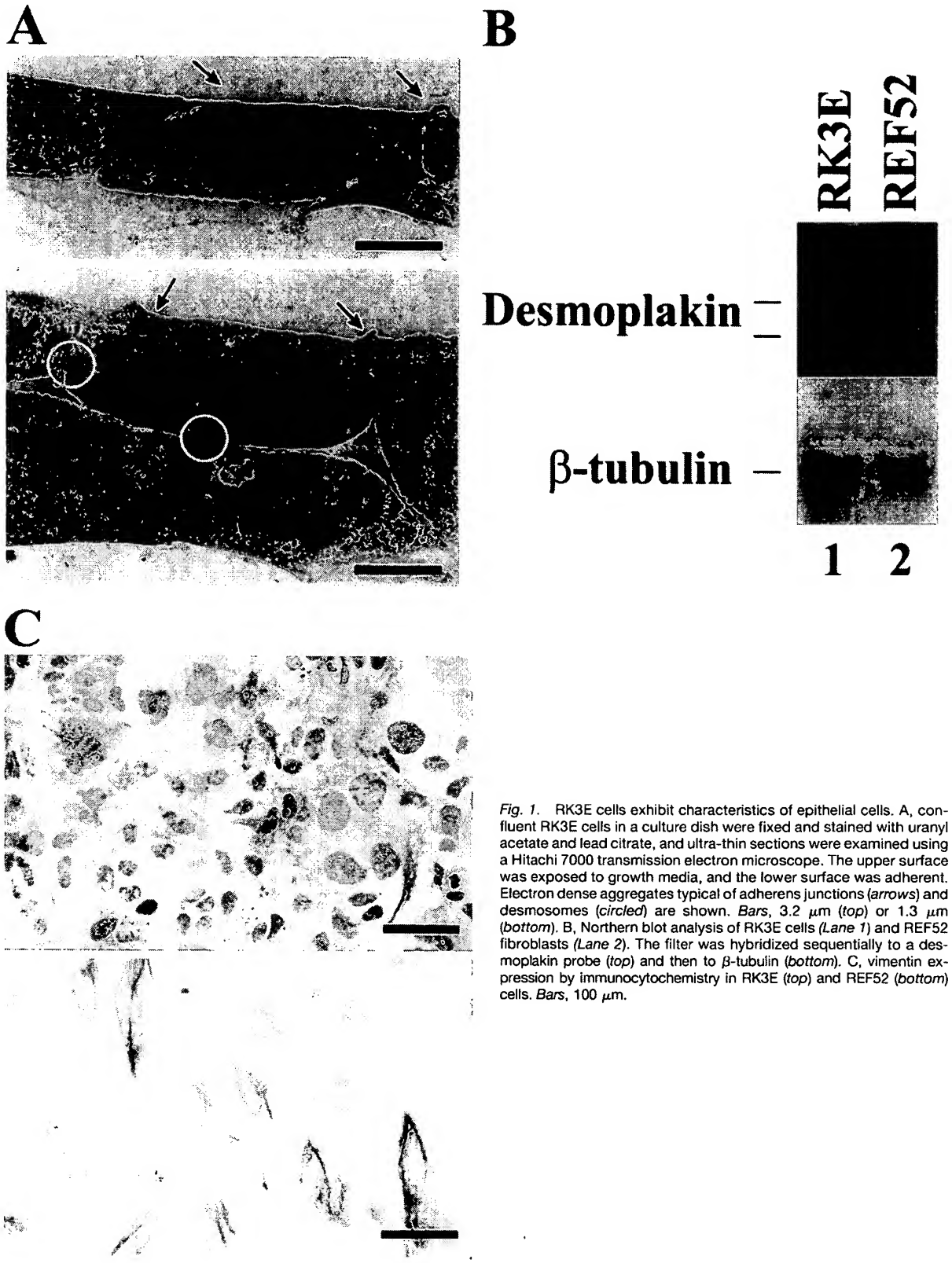

Fig. 1. RK3E cells exhibit characteristics of epithelial cells. A, confluent RK3E cells in a culture dish were fixed and stained with uranyl acetate and lead citrate, and ultra-thin sections were examined using a Hitachi 7000 transmission electron microscope. The upper surface was exposed to growth media, and the lower surface was adherent. Electron dense aggregates typical of adherens junctions (*arrows*) and desmosomes (*circled*) are shown. *Bars*, 3.2 μm (*top*) or 1.3 μm (*bottom*). B, Northern blot analysis of RK3E cells *(Lane 1)* and REF52 fibroblasts *(Lane 2)*. The filter was hybridized sequentially to a desmoplakin probe (*top*) and then to β-tubulin (*bottom*). C, vimentin expression by immunocytochemistry in RK3E (*top*) and REF52 (*bottom*) cells. *Bars*, 100 μm.

Table 1 Assessment of cDNA libraries

Library	λ titer	cDNA size (N,R)[a]	Probe[b]	cDNA clones transduced[c]	Transduced RK3E cells[d]	Foci identified
Squamous cell carcinoma	8.9×10^6	1.69 (10, 1.00–3.60)	NT	$\sim 4 \times 10^6$	$\sim 1.2 \times 10^7$	13
Breast carcinoma	7.4×10^6	1.64 (18, 0.50–2.7)	hBRF	$\sim 4 \times 10^6$	$\sim 1.2 \times 10^7$	1

[a] The mean size of cDNAs in kb pairs; the number of clones sized by gel electrophoresis (N) and the size range (R) are indicated.
[b] Plaques (420,000) were analyzed by hybridization to the 5′ end of the RNA polymerase III transcription factor hBRF cDNA (see "Results"); NT, not tested.
[c] The number of clones processed at each step of library construction was equal to or greater than 4×10^6. The *Bst* XI adapter strategy generates recombinant cDNA expression plasmids in an orientation-independent fashion, such that both sense and antisense vectors result.
[d] The number of RK3E cells transduced was estimated as the product of the transduction frequency (20%), the number of dishes screened (20), and the number of cells/dish (3×10^6).

We previously developed and used RK3E cells, immortalized by *E1A*, to demonstrate the transforming activity of *GLI* (17). We now show that these cells exhibit multiple features of epithelia and detect known and novel transforming activities in tumor cell lines. The epithelial features of the cells and/or the mechanism of immortalization may explain the surprising sensitivity and specificity of the assay compared with previous expression cloning approaches (27). Three of the four genes known to transform RK3E cells are activated by genetic alterations in carcinomas, and, of these genes, only *RAS* exhibits transforming activity in the commonly used host NIH3T3. We identify *GKLF*[4] (3) as an oncogene that is expressed in the differentiating compartment of epithelium and misexpressed in dysplastic epithelium. We also suggest that *GKLF* may regulate the rate of differentiation and maturation and the overall cellular transit time through epithelium. The functional similarities shared with other oncogenes, including *GLI* or *c-MYC*, identify *GKLF* as an attractive candidate gene relevant to tumor pathogenesis.

Results

RK3E Cells Have Characteristics of Epithelia. RK3E cells are a clone of primary rat kidney cells immortalized by transfection with adenovirus *E1A in vitro* (17). The cells exhibit morphological and molecular features that are epithelioid. They are contact-inhibited at confluence and are polarized with apical and basolateral surfaces and electron-dense intercellular junctions typical of adherens junctions and desmosomes (Fig. 1*A*). Northern blot analysis showed that RK3E cells, but not REF52 fibroblasts, expressed desmoplakin, a major component of desmosomes and an epithelial marker (Fig. 1*B*). By immunocytochemical staining, the mesenchymal marker vimentin was low or undetectable in RK3E cells, but was strongly positive in REF52 cells (Fig. 1*C*). Neither line reacted strongly with anticytokeratin or antidesmin antibodies. These results are consistent with the observation that E1A induces multiple epithelial characteristics without inducing cytokeratin expression (28).

Karyotype analysis revealed RK3E cells to be diploid with a slightly elongated chromosome 5q as the only apparent abnormality (17). Importantly, RK3E cells can be transformed by functionally diverse oncogenes such as *RAS* and *GLI*. Four such transformed lines were each homogeneous for DNA content, as determined by fluorescence analysis of propidium iodide-stained cells derived from *RAS*- (one line) or *GLI*- (three lines) induced foci, indicative of a relatively stable genetic constitution (data not shown). These properties suggested that RK3E cells may serve as an *in vitro* model for identification and mechanistic analysis of gene products involved in the progression from normal epithelial tissue to malignancy.

cDNA Library Construction. To identify transforming genes, we used mRNA from human squamous cell carcinoma- or breast tumor-derived cell lines. These tumor types do not exhibit frequent alteration of *RAS* or *GLI*. After pooling mRNAs for each tumor type, oligo dT-primed cDNA libraries were constructed in bacteriophage λ (Table 1). The libraries were high-titer (assessed before amplification on agar plates) with a mean insert size of 1.6–1.7 kb. The amplified breast cDNA library was further assessed by plaque screening for the transcription factor hBRF, using a probe derived from the 5′ end of the protein coding region (bases 315–655, accession U75276). Each of the seven clones identified were derived from independent reverse transcripts, as determined by end sequencing, confirming that complexity of the library was maintained during amplification. The inserts ranged in size from 2.1–3.4 kb and contained the entire 3′ UTR and much or all of the protein coding region intact. Three of the seven clones extended through the predicted initiator methionine codon, whereas four others were truncated further downstream. These results suggested that the library is relatively free of COOH-terminally truncated clones and contains full-length cDNAs even for relatively long mRNAs. The overall abundance of hBRF mRNA has not been determined.

Isolation of c-MYC and GKLF by Expression Cloning. The libraries were cloned into the MMLV retroviral expression plasmid pCTV1B (27), packaged in BOSC23 cells (29), and high-titer virus supernatants were applied to RK3E cells. Fourteen foci, identified at 10–20 days after transduction, were individually expanded into cell lines. Thirteen of these foci contained a single stably integrated cDNA, as indicated by PCR (Fig. 2*A*). Eleven of these PCR products were identified as human *c-MYC* by end-sequencing and restriction enzyme analysis. The *c-MYC* cDNA in *Lane 15* included the coding region and 193 bases of 5′ UTR sequence (accession V00568). As determined by sequencing or restriction mapping, the other *c-MYC* cDNAs extended further 5′ (*Lanes 1, 3, 5–7, 9–7, 13,* and *14*), such that all of the clones contained the entire protein-coding region.

[4] The abbreviations used are: GKLF, gut-enriched Krüppel-like factor; β-gal, β-galactosidase; UTR, untranslated region; MMLV, Moloney murine leukemia virus; GAPDH, glyceraldehyde-3-phosphate dehydrogenase; ISH, *in situ* hybridization.

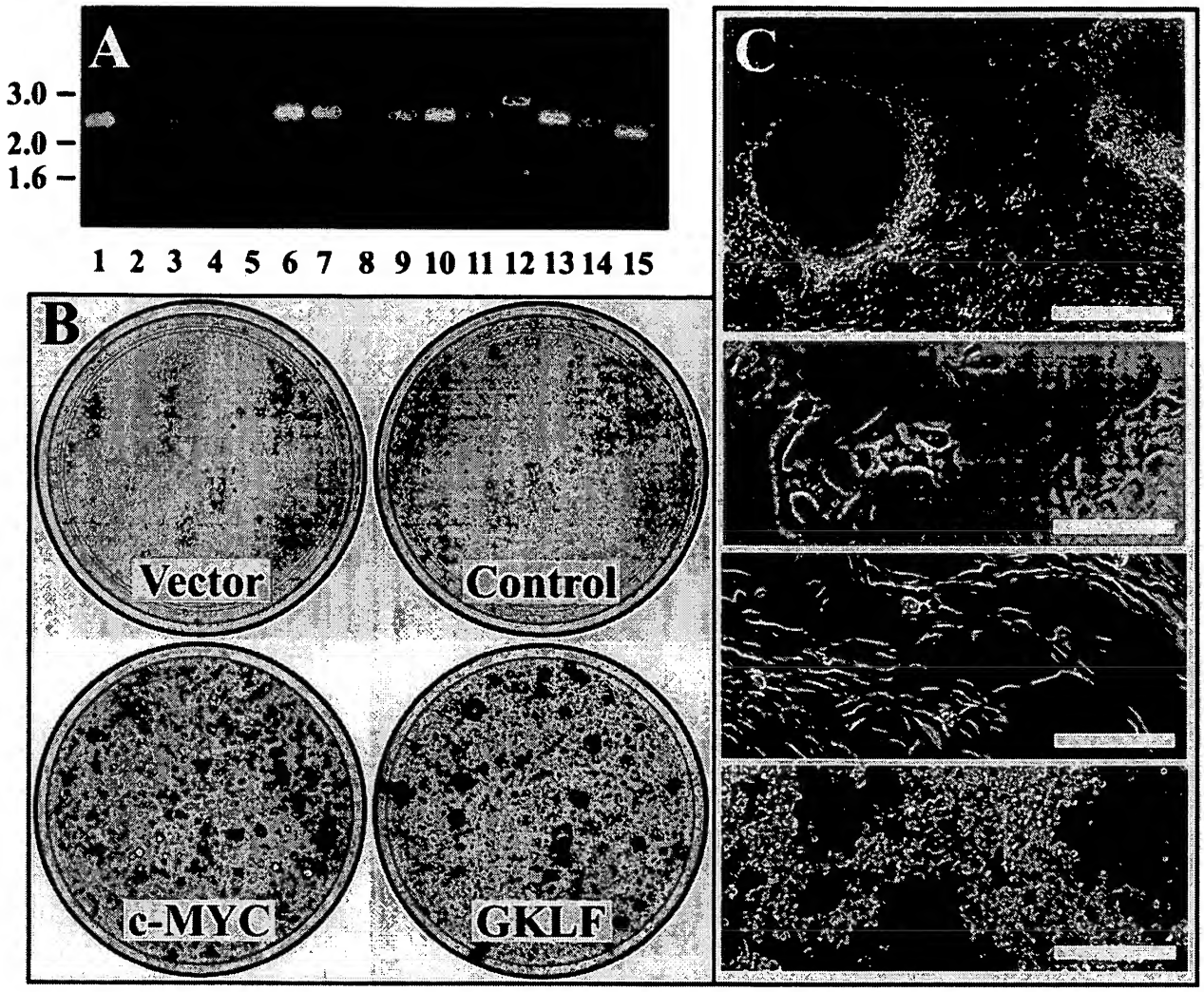

Fig. 2. Expression cloning of *c-MYC* and *GKLF*. A, identification of human cDNAs present in transformed RK3E cell lines SQC1-SQC13 (derived using a squamous cell carcinoma library, *Lanes 1* and *3–14*) and BR1 (derived using a breast carcinoma library, *Lane 15*). PCR was used in combination with vector-derived primers and cell line genomic DNA. RK3E genomic DNA served as a negative control template *(Lane 2)*. No cDNA was retrieved from cell line SQC3 *(Lane 4)*. All foci identified in the screen are represented. Molecular weight markers are indicated on the left in kb pairs. B, reconstitution of transforming activity by cloned PCR products. cDNAs were cloned into a retroviral expression plasmid, packaged into virus using BOSC23 cells, and applied to RK3E cells. Foci were fixed and stained at 3–4 weeks. *Vector*, pCTV3K; *Control*, pCTV3K-SQC1; *c-MYC*, pCTV3K-BR1; *GKLF*, pCTV3K-SQC7. C, morphology of foci and cloned cell lines. *Top to bottom*: *first panel*, low-power phase contrast view of adjacent foci in a dish transduced with retrovirus encoding *GKLF* (*bar*, 900 μm); *second through fourth panels*, high-power phase contrast view (*bar*, 230 μm); *second panel*, RK3E cells at subconfluence; *third panel*, *GKLF*-transformed RK3E cells; *fourth panel*, *c-MYC*-transformed RK3E cells.

In addition, two cell lines (Fig. 2*A*, *Lanes 8* and *12*) contained cDNAs coding for *GKLF*. Mouse and human *GKLF* cDNAs were previously isolated by hybridization with zinc finger consensus probes (30–32), but were not implicated as oncogenes or found to be induced during neoplastic progression. After cloning into plasmid, the sequences of these two cDNAs, termed SQC7 and SQC11, were obtained in total. As determined by comparison with multiple expressed sequence tags and two full-length coding sequence files in the database (accessions U70663 and AFO22184), each contained the predicted GKLF protein coding region bounded by 5′ and 3′ UTRs. An ATG in good context for translation initiation was located at base 330, with the predicted terminator codon at base 1740. Both isolates were artificially truncated at the *Xho*I site in the 5′ UTR during library preparation. Because the transcripts had been processed using distinct AAUAAA polyadenylation signals, the cDNAs were slightly different in length and derived from independent mRNA molecules (Fig. 2*A*).

Sequencing revealed these two *GKLF* isolates to be identical within the residual 5′ UTR and throughout the coding region. A single bp difference in the 3′ UTR represents a PCR-induced error or a rare variant, as determined by comparison with ESTs. Comparison to a placenta-derived sequence (accession U70663) revealed three single bp differences in the coding region. These differences were resolved by alignment with other sequences in the database (accessions AF022184 and AA382289) from normal tissues, indi-

Table 2 Retroviral transduction of reconstituted *GKLF* and *c-MYC* expression vectors

Plasmid	Focus assay (no. foci/10 cm dish)[a]	Colony morphology assay (no. transformed/total)[b]
pCTV3K (vector)	0, 0	0/184
pCTV3K-SQC1[c] (*c-MYC*)	0, 0	0/232
pCTV3K-SQC5 (*c-MYC*)	>1000, >1000	ND[d]
pCTV3K-BR1 (*c-MYC*)	>1000, >1000	81/91 (89%)
pCTV3K-SQC7 (*GKLF*)	>1000, >1000	91/206 (44%)
pCTV3K-SQC11-2[e] (*GKLF*)	>1000, >1000	ND
pCTV3K-SQC11-3 (*GKLF*)	>1000, >1000	ND

[a] RK3E cells were transduced with 4 ml of virus supernatant after calcium phosphate-mediated plasmid transfection of virus packaging cells.
[b] RK3E cells were transduced with 0.4 ml of thawed viral supernatant. Cells were split 1:4 into selective media 30 h later. At 2 weeks, drug-resistant colonies were fixed, stained, and examined visually for morphological transformation. Numbers indicate colonies/10-cm dish. A duplicate transduction experiment yielded similar results (data not shown). No colonies formed in control dishes that were not exposed to virus.
[c] pCTV3K-SQC1 is a *c-MYC* allele obtained by PCR that exhibited greatly reduced transforming activity compared with other alleles.
[d] ND, not determined.
[e] SQC11-2 and -3 are independent plasmid clones derived from the same PCR reaction (Fig 2*A*, *Lane 12*).

cating that the *GKLF* molecules obtained by expression cloning are predicted to encode the wild-type protein.

Reconstitution of Transforming Activity for *c-MYC* and *GKLF*. To demonstrate transforming activity, three independent PCR products each for the *c-MYC* and *GKLF* cDNAs were cloned into the retroviral expression vector pCTV3K (27), packaged into virions, and tested for transformation of RK3E cells *in vitro* (Fig. 2, *B* and *C*; Table 2). One of the *c-MYC* clones (pCTV3K-SQC1) possessed greatly reduced transforming activity in multiple experiments despite similar viral titers, as determined by induction of hygromycin resistance, suggesting that an error may have been introduced during PCR. Each of the other virus supernatants carrying *GKLF* and *c-MYC* transgenes induced >1000 foci/dish compared with no foci for virus controls.

To determine the efficiency of transformation by *GKLF* and *c-MYC*, a colony morphology assay was used, as described previously (27). Virally transduced cells were selected in hygromycin at low confluence, and stable colonies were fixed, stained, and scored for morphological transformation by visual inspection as above for foci (Table 2). The *c-MYC*-transduced cells exhibited loss of contact inhibition and dense growth in 89% of colonies. The *GKLF*-transduced cells exhibited a transformed morphology in 44% of colonies. In comparison, a previous study showed that 70% and 40% of NIH3T3 colonies transduced by viruses carrying *RAS* and *RAF* exhibited a transformed morphology (27). We, likewise, tested virus supernatants for transformation of NIH3T3 cells. Neither *c-MYC* nor *GKLF* induced morphological transformation of NIH3T3 colonies, as previously described for *GLI* and others (data not shown; Ref. 17). These results identify the RK3E assay as not only highly specific, but also sensitive to the activity of a select group of oncogenes.

In lieu of sequencing the *c-MYC* alleles, we confirmed that wild-type *c-MYC* can transform RK3E cells. A human wild-type expression vector (pSRαMSV *c-MYC* tk-neo) induced foci using direct plasmid transfection of RK3E cells in multiple experiments. Foci were observed at a similar frequency using known wild-type or new *c-MYC* isolates when analyzed in parallel (data not shown). In addition, retrovirus encoding the estrogen receptor-c-MYC (wild-type) fusion protein induced morphological transformation of RK3E cells in the presence or absence of 4-hydroxy-tamoxifen (33). No effect was observed for controls (empty vector or a control containing a deletion in c-MYC residues 106–143).

Northern blot analysis of transformed RK3E cell lines demonstrated expression of the *c-MYC* and *GKLF* vector-derived transcripts (Fig. 3*A*). No endogenous transcripts were detected at the stringency used in this experiment. Compared with RK3E cells at subconfluence (*Lane 1*) or confluence (*Lane 2*), no consistent increase of *E1A* transcripts was detected in cells transformed by *RAS*, *GLI*, *c-MYC*, or *GKLF*, suggesting that these genes act upon cellular targets to induce transformation.

To detect the endogenous rat *GKLF* transcript, we used reduced-stringency wash conditions and a *Sma*I fragment from the coding region exclusive of the COOH-terminal zinc fingers and with no sequence similarity to other genes in the database. By this approach, the apparent *GKLF* transcript was identified and migrated at 3.1 kb, similar to the human 3.0-kb transcript, in RK3E and all derivative-transformed cell lines (data not shown). A single transcript with the same mobility was detected by hybridization of the filter to full-length coding region probe. These studies revealed similar *GKLF* expression in RK3E and in derivatives transformed by *RAS*, *GLI*, or *c-MYC*. The results show that *GKLF* mRNA expression is not significantly altered by these other oncogenes and is consistent with function of *GKLF* in an independent pathway.

Cell lines derived from foci induced by *c-MYC* or *GKLF* were further tested for tumorigenicity in athymic mice by s.c. inoculation at four sites for each line (Table 3; Ref. 17). Tumors were >1 cm in diameter and were scored at 2–4 weeks after inoculation. Cells transformed by *c-MYC* induced tumors in 75% or 100% of sites injected (two lines tested). Three lines transformed by *GKLF* each induced tumors in 50–75% of sites injected. No tumors resulted from injection of RK3E cells, whereas a *GLI*-transformed cell line induced tumors in each of the four sites injected. In all, *GKLF* cell lines induced tumors in 8 of 12 injection sites, compared with 7 of 8 injection sites for *c-MYC* and 4 of 4 injection sites for *GLI*. *GKLF*-induced tumors also grew more slowly *in vivo*, reaching 1 cm in diameter by 3.4 weeks, on average, compared with 2.6 weeks for c-MYC and 3 weeks for *GLI*. The

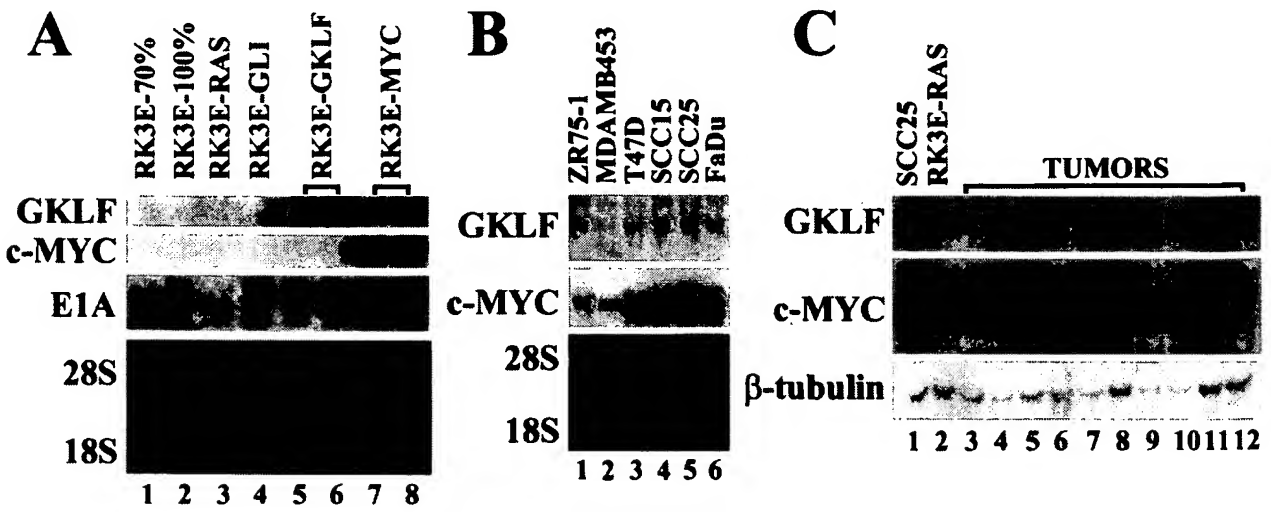

Fig. 3. Northern blot analysis of *c-MYC* and *GKLF* expression. Total RNA (25 μg) was loaded for each sample. *A*, analysis of transgene expression in RK3E cells and derivative cell lines transformed by the indicated oncogene. *Lane 1*, RK3E cells in exponential growth phase; *Lane 2*, RK3E cells incubated at confluence for 5 days. Ethidium bromide-stained RNA is shown below after transfer to the filter. *B*, endogenous *GKLF* (3.0 kb) or *c-MYC* (2.3 kb) expression in tumor cell lines. *Lanes 1–3*, breast cancer lines; *Lanes 4–6*, squamous cell carcinoma lines. *C*, analysis of gene expression in laryngeal squamous cell carcinoma. *Lane 1*, SCC25 cell line; *Lanes 3–6*, *9*, and *12*, primary tumors; *Lanes 7*, *8*, *10*, and *11*, metastatic tumors; *Lanes 3–12* correspond to case numbers 5, 8, 18–20, 6, and 21–24, respectively (see Table 4). RK3E-RAS cell RNA served as a negative control *(Lane 2)*, whereas hybridization to β-tubulin served as a control for loading.

Table 3 Tumorigenicity of RK3E-derived cell lines in athymic mice

Cell line	No. tumors/ no. sites injected	Tumor latency *in vivo* (weeks)[a]	Doubling time *in vitro* (h)
RK3E	0/4	–	12.7
RK3E-c-MYC BR1[b]	3/4	3,3,4	19.1
RK3E-c-MYC B[c]	4/4	2,2,2,2	19.8
RK3E-GKLF E	3/4	3,3,3	33.7
RK3E-GKLF F	2/4	4,4	27.0
RK3E-GKLF G	3/4	3,3,4	ND[d]
RK3E-GLI	4/4	3,3,3,3	18.0

[a] The time required for tumors to reach 1 cm in diameter is indicated.
[b] Cell line derived from a focus identified in the original screen using a breast cancer cDNA library.
[c] Cell line derived by transformation with the reconstituted plasmid pCTV3K-BR1.
[d] ND, not determined.

moderately increased latency and decreased efficiency of tumor formation for *GKLF* cell lines may be attributable to the intrinsic rate of proliferation for these cells (Table 3). Although *c-MYC*, *GLI*, and *GKLF* cell lines all exhibited prolonged doubling times *in vitro* compared with RK3E cells, *GKLF* cells divided more slowly than the other transformed cell lines.

Northern Blot Analysis of Tumors and Tumor-derived Cell Lines. We then examined human tumors and cell lines by Northern blot analysis of total RNA (Fig. 3, *B* and *C*). *GKLF* expression in breast or squamous cell carcinoma cell lines was variable, with increased expression in the breast tumor line ZR75–1 and the squamous cell lines SCC15 and SCC25 (Fig. 3*B*). In human squamous cell carcinomas microdissected to enrich for tumor cells, *GKLF* expression was detected in each of 10 primary or metastatic tumors analyzed, with expression levels comparable with that for the cell line SCC25 (Fig. 3C). The results suggest that *GKLF* represents a potent transforming activity that is consistently expressed in tumors as well as in tumor-derived cell lines. Because *GKLF* was isolated from cell lines that express the gene at a level found in tumors *in vivo*, the results suggest that GKLF may represent a major transforming activity in tumors, as well as in cell lines.

Gene Copy Number of *c-MYC* and *GKLF*. c-MYC was previously shown to be activated by gene amplification in ~10% of oral squamous cancers and may be activated in these or other tumors by genetic alteration of WNT-*APC*-β-catenin pathway components (6, 34–37). To determine whether expression of *GKLF* in cell lines and tumors is, likewise, associated with gene amplification, we performed Southern blot analysis (Fig. 4, *A* and *B*). Filters were sequentially hybridized to *GKLF*, *c-MYC*, and β-tubulin. Increased copies of *c-MYC* were identified in two cell lines used for library construction, FaDu and MCF7. Increased hybridization to *c-MYC* was, likewise, observed for 1 of 11 oral squamous cell carcinomas (Fig. 4*A*, *Lane 10*) and for one of nine breast carcinomas (Fig. 4*B*, *Lane 8*). These results are consistent with the published frequencies of *c-MYC* amplification for these tumor types (34, 35, 38). No copy number gains of *GKLF* were observed, indicating that other mechanisms may contribute to expression of GKLF in tumors. The same may be true for *c-MYC* because gene amplification in FaDu cells was associated with reduced expression compared with other oral cancer cell lines (Fig. 3*B*).

***GKLF* Expression Is Activated Early during Tumor Progression *in Vivo*.** Previously, expression of c-MYC was found to be up-regulated consistently in dysplastic oral mucosa and in squamous cell carcinomas, and tumors with the highest levels of c-MYC expression were associated with the

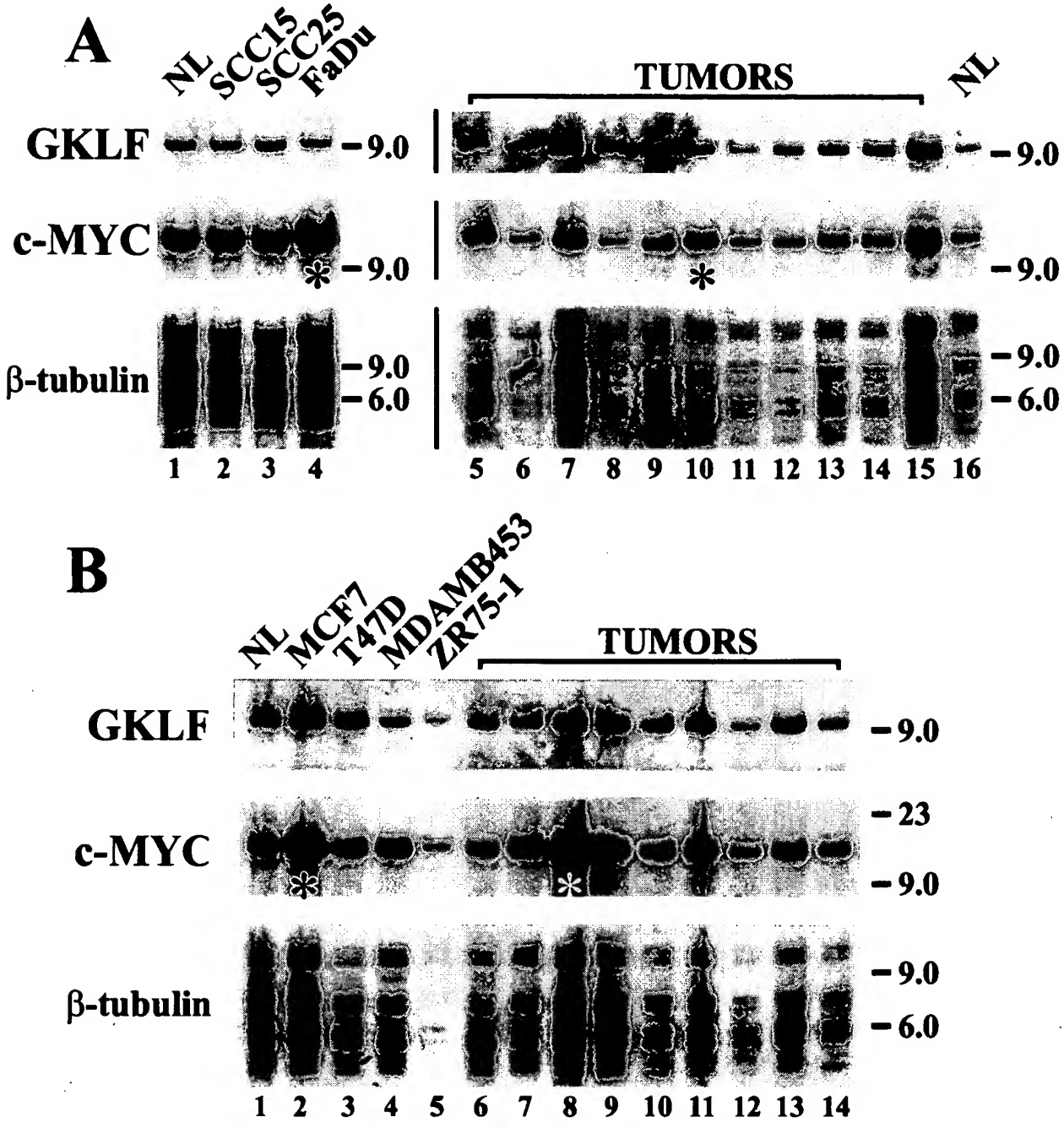

Fig. 4. Southern blot analysis of cell line- and tumor-derived genomic DNA. DNA (5 μg) was digested with *Eco*RI and separated by gel electrophoresis. The filters were hybridized sequentially to GKLF, c-MYC, and β-tubulin probes. *, samples with increased apparent copy number of c-MYC. Molecular weight markers are indicated on the *right*. *NL*, normal human lymphocyte DNA. *A*, oropharyngeal squamous cell carcinoma. Cell lines *(Lanes 2–4)* and tumors *(Lanes 5–15)* are shown. *B*, breast carcinoma. Cell lines *(Lanes* 2–5) and tumors *(Lanes 6–14)* are shown.

poorest clinical outcome (36, 39–41). To determine how *GKLF* mRNA expression is altered during tumor progression, we analyzed squamous cell carcinoma of the larynx and adjacent uninvolved epithelium from the same tissue blocks using ^{35}S-labeled riboprobes by ISH analysis. In apparently normal epithelium, *GKLF* expression was detected in the spinous layer above the basal and parabasal cells (nine specimens analyzed; Fig. 5, *A-C*, *G-I*; Table 4). No specific *GKLF* expression was detected in the basal or parabasal cells or in the underlying dermis. In contrast, a sense control probe produced grains at a much-reduced frequency in a uniform fashion across the epithelium. *GAPDH* expression served as a positive control and was detected diffusely throughout the entire epithelium (data not shown). The ob-

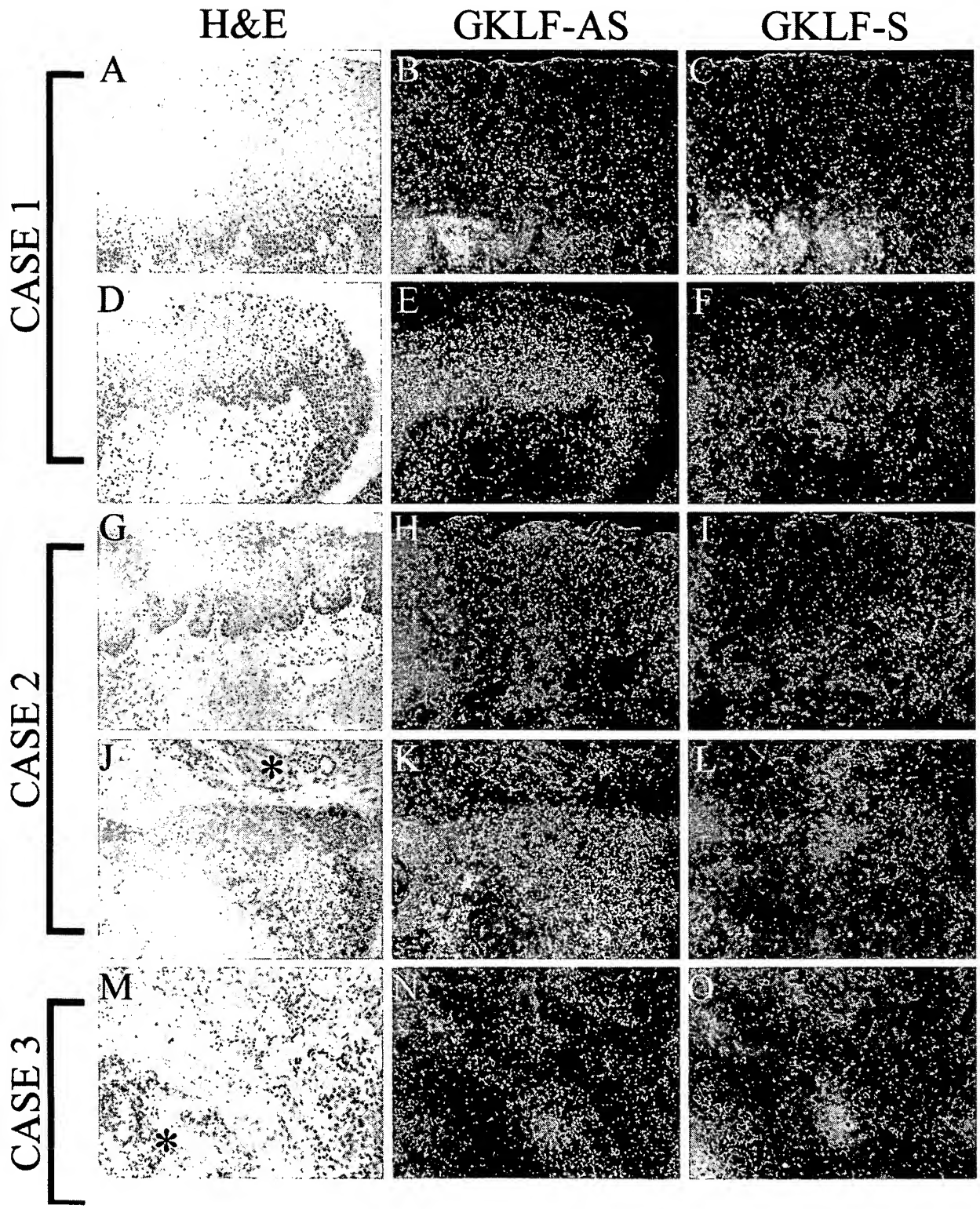

Fig. 5. ISH analysis of *GKLF*. Paraffin-embedded (*A-L*) or fresh-frozen (*M-O*) tissues were analyzed using antisense (*GKLF-AS*) or sense (*GKLF-S*) ^{35}S-labeled RNA probes. Each image (*A-O*) is 650 μm × 530 μm. Sections were stained with H&E. *Case 1*, *A-C*, uninvolved epithelium in a patient with primary laryngeal squamous cell carcinoma; *D-F*, adjacent dysplastic epithelium within the same tissue block. *Case 2*, *G-I*, uninvolved epithelium; *J-L*, adjacent primary tumor nests within stroma in the same tissue block; *, a salivary gland and ducts. *Case 3*, *M-O*, metastatic laryngeal squamous cell carcinoma infiltrating a lymph node; *, lymphocytes.

Table 4 Expression of *GKLF* in oral epithelium and tumors

Case[a]	Histopathology (U,[b]D,P,M)	Tissue source (PE/FF)	Method (N/ISH)	GKLF expression
1	U,D,P	PE	ISH	D,P>U
2	U,D	PE	ISH	D>U
2	U,P	PE	ISH	P>U
3	M	FF	ISH	+
4	U,D	PE	ISH	D>U
5	P	FF	N,ISH	+
6	M	FF	N,ISH	+
7	P	FF	ISH	+
8	P	FF	N,ISH	+
9	D,P	PE	ISH	D,P+
10	M	PE	ISH	+
11	U,D,P	PE	ISH	D,P>U
12	U,D	PE	ISH	D>U
12	U,D,P	PE	ISH	D,P>U
13	U	PE	ISH	+
13	P	PE	ISH	+
14	P	PE	ISH	+
14	M	PE	ISH	+
15	D	PE	ISH	+
15	D	PE	ISH	+
15	D,P	PE	ISH	D,P+
16	U,D,P	PE	ISH	D,P>U
16	M	PE	ISH	+
17	D,P	PE	ISH	D,P+
18	P	FF	N	+
19	P	FF	N	+
20	M	FF	N	+
21	P	FF	N	+
22	M	FF	N	+
23	M	FF	N	+
24	P	FF	N	+

[a] Each row corresponds to a tissue specimen. Levels of gene expression indicate changes identified within, rather than between, single tissue sections. For some cases, multiple specimens isolated during the same surgical procedure were analyzed. ISH results were confirmed by analysis of sections in duplicate.

[b] U, uninvolved or normal-appearing epithelium; D, dysplastic epithelium; P, primary tumor; M, metastatic tumor; PE, paraffin-embedded; FF, fresh-frozen; N, Northern; D,P>U, increased expression in dysplasia and primary tumor compared with uninvolved epithelium in the same section; D,P+, expression in both dysplasia and adjacent primary tumor.

served pattern of *GKLF* expression is identical to the pattern in normal mouse skin (32).

For each of 12 specimens analyzed, dysplastic epithelium exhibited increased *GKLF* expression throughout the epithelium (Fig. 5, *D-F*; Table 4, *Cases 1, 2, 4, 9, 11, 12,* and *15–17*). In contrast to results obtained in normal-appearing epithelium, there was no reduction of expression in the basal and parabasal layers compared with superficial layers. For tissue sections that contained both uninvolved epithelium and adjacent dysplastic epithelium, the overall level of *GKLF* expression in dysplastic epithelium was prominently elevated compared with the *GKLF*-positive cell layers in uninvolved epithelium (Fig. 5, *B, E,* and *H*; Table 4, *Cases 1, 2, 4, 11, 12,* and *16*). These results suggest that *GKLF* expression is qualitatively and quantitatively altered in dysplasia, that exclusion of *GKLF* from the basal and parabasal cell layers is lost early during neoplastic progression, and that *GKLF* exhibits properties of an oncogene not only *in vitro*, but also *in vivo*.

As shown by Northern blot analysis, *GKLF* transcripts are consistently present in tumor-derived mRNA (Fig. 3C; Table 4). To determine whether *GKLF* is expressed in tumor cells, we examined laryngeal squamous cell carcinomas by mRNA ISH. Expression was detected in each primary (13 cases) or metastatic (5 cases) tumor examined (Fig. 5, *J-O*; Table 4), with all or nearly all tumor cells associated with silver grains. The level of expression was somewhat heterogeneous, with higher levels found in the periphery and in nodules of tumor containing centrally necrotic cells or keratin pearls. As for dysplastic epithelium, expression in tumor cells was consistently elevated compared with uninvolved epithelium in the same sections (Fig. 5, *H* and *K*; Table 4, *Cases 1, 2, 11, 12,* and *16*). However, expression in tumor cells was not higher than in dysplastic epithelium (*Cases 1, 9, 11, 12,* and *15–17*). For several cases, expression in the most dysplastic epithelium was higher than in adjacent *GKLF*-positive tumor, suggesting that *GKLF* expression is specifically activated during the transition from normal epithelium to dysplasia, before invasion or metastasis.

Discussion

The results demonstrate that cells with an epithelial phenotype can be used for identification of transforming activities present in carcinoma-derived cell lines. The assay repeatedly identified two genes, and none of the isolated cDNAs were artificially truncated or rearranged within the protein coding region. This indicates that transformation of these cells is unusually specific to a few pathways or genes, including *c-MYC*, *GKLF*, *RAS*, and *GLI*. *c-MYC*, *RAS*, and *GLI* are directly or indirectly activated by genetic alterations in diverse carcinoma types during tumor progression *in vivo* (9, 10, 42–44). For both breast and oral squamous carcinoma, the tumor types analyzed in this study, *c-MYC* gene amplification is one of the more frequent oncogene genetic alterations and is observed in 10–15% of cases. By analogy, novel oncogenes identified by the RK3E assay may be directly activated in neoplasms through gain-of-function mutations or indirectly activated by loss-of-function genetic alterations.

Whitehead *et al.* (27) developed the retroviral vectors that we used in this study for transduction of NIH3T3 cells, in which they isolated 19 different cDNAs encoding 14 different proteins. Known oncogenes were isolated, including *raf-1*, *lck*, and *ect2*. Other known genes included phospholipase C-γ_2, β-catenin, and the thrombin receptor. In addition to the known genes, seven novel cDNAs were isolated, including several members of the CDC24 family of guanine nucleotide exchange factors. Only the thrombin receptor was isolated more than once, and many of the 14 different genes identified were truncated within the protein coding region. The diversity of cDNAs isolated in the NIH3T3 assay is in contrast to results obtained in the current study. The specificity of the RK3E assay may be attributable to the "tumor suppressor" activity of the *E1A* oncogene (28, 45). Although *E1A* antagonizes $p105^{Rb}$ and immortalizes primary cells, it also induces epithelial differentiation in diverse tumor types, including sarcoma, and suppresses the malignant behavior of tumor cells *in vivo*.

GKLF was previously isolated by hybridization to zinc finger probes (30–32). The human gene is located at chromo-

some 9q31 and is closely linked to the autosomal dominant syndrome of multiple self-healing squamous epitheliomata (31, 32, 46, 47). Affected individuals develop recurrent invasive, but well-differentiated, tumors morphologically similar to squamous carcinoma that spontaneously regress. Although *GKLF* has been proposed as a candidate tumor suppressor gene relevant to multiple self-healing squamous epitheliomata (32), our results suggest that activating mutations could account for the syndrome.

GKLF encodes a nuclear protein that functions as a transcription factor when bound to a minimal essential binding site of 5′-$^{G}/_{A}{}^{G}/_{A}$GG$^{C}/_{T}$G$^{C}/_{T}$-3′ (48). The 470 residue polypeptide exhibits modular domains that mediate nuclear localization, DNA binding, and transcriptional activation or repression (31, 32, 49, 50). In mice, *GKLF* expression is found predominately in barrier epithelia, including mucosa of the mouth, pharynx, lung, esophagus, and small and large intestine (30, 32). A role for *GKLF* in differentiation or growth arrest was suggested by the onset of expression at the time of epithelial differentiation (approximately embryonic day 13; Refs. 32 and 51) and by similarity within the zinc finger domain to family members erythroid Krüppel-like factor and lung Krüppel-like factor that were previously associated with growth-arrest or differentiation-specific gene expression (52, 53). Similarity to these other genes is limited to the DNA-binding zinc finger region.

Our results show that *GKLF* can induce proliferation when overexpressed *in vitro*. Analysis of expression in dysplastic cells and tumor cells *in vivo* provides independent evidence that *GKLF* exhibits properties expected of an oncogene. Genetic progression of carcinoma seems to involve genes and pathways important for homeostasis of normal epithelium (6, 7, 9, 54). For example, the zinc finger protein GLI is expressed in normal hair shaft keratinocytes, whereas *c-MYC* is expressed in normal epithelium of the colonic mucosa. In tumors derived from these tissues, *GLI* and *c-MYC* are more frequently activated by recessive genetic changes in upstream components of their respective biochemical pathways than by gain-of-function alterations such as gene amplification. Up-regulation of *GKLF* expression in dysplastic epithelium and tumor cells *in vivo* is particularly interesting as expression seems not to be increased by proliferation *in vitro*. Expression of the endogenous *GKLF* mRNA in RK3E cells was similar in cycling *versus* contact-inhibited cells (data not shown). In contrast, *GKLF* is significantly induced in NIH3T3 cells during growth arrest (30). These different results suggest that cell type-specific mechanisms can regulate *GKLF* expression, and that *GKLF* may play different roles in epithelial *versus* mesenchymal cells.

Squamous epithelium is divided into compartments (55, 56). In the basal cell layer, proliferative reserve or stem cells possess long-term or unlimited self-renewal capacity, whereas the parabasal transit amplifying cells undergo several rounds of mitosis and then withdraw from the cell cycle to differentiate into spinous cells that form the mid strata of the epithelium. These cells then undergo terminal differentiation and programmed cell death at the surface. Proliferation and differentiation are normally balanced such that overall cell number remains constant. In contrast to *GLI* and *c-MYC*, *GKLF* expression in skin seems limited to the differentiating compartment (32). A simple model is that *GKLF* normally regulates the rate of maturation and shedding and the overall transit time for individual cells. The thickness of epithelium, which varies greatly in development and in different adult tissues, may be regulated not only by alterations in the rate of cell division in the basal layer, but also in response to *GKLF* or similarly acting molecules in the suprabasal layers. This model is consistent with the relatively late induction of *GKLF* during mouse development, and is testable by modulating expression of *GKLF* in transgenic animals or using raft epithelial cultures *in vitro*. Activation of *GKLF* in the basal layer of dysplastic epithelium suggests that dysplasia and progression to invasion and metastasis could result from loss of normal compartment-specific patterns of gene expression.

In summary, *GKLF*, *c-MYC*, and *GLI* are potent oncogenes in epithelioid RK3E cells *in vitro*, are analogous with respect to their expression in normal epithelium, and have potentially complex roles in the regulation of epithelial cell proliferation, differentiation, or apoptosis (6, 7, 9, 44, 56–58). How *GKLF* contributes to these processes will require a better understanding of its function and of the pathways that regulate *GKLF* activity in epithelia.

Materials and Methods

Immunocytochemistry. Immunocytochemical assays were performed in the Immunopathology Laboratory at The University of Alabama at Birmingham. Antibodies to vimentin and desmin were from Dako (Carpenteria, CA). A mixture of anticytokeratin included AE1/AE3 (Biogenics, San Ramon, CA), CAM5.2 (Becton Dickinson, San Jose, CA), and MAK-6 (Zymed, South San Francisco, CA). Human tissue served as a positive control for each antibody. No signal was obtained in the absence of primary antibody.

Construction of cDNA Libraries. Two cDNA libraries were constructed using the ZAP-Express cDNA synthesis kit (Stratagene, La Jolla, CA). A library was prepared from human squamous cell carcinoma cells derived from tumors of the oro-pharynx. Equal quantities of total mRNA from cell lines SCC15, SCC25, and FaDu (American Type Culture Collection, Manassas, VA) were pooled. Similarly, equal quantities of mRNA from the breast cancer cell lines MCF-7, ZR75–1, MDAMB-453, and T47D (American Type Culture Collection) were pooled. For each pool, poly(A)+ mRNA was selected by two cycles of oligo-dT cellulose affinity chromatography, and 5 μg were reverse transcribed using an oligo-dT linker primer and MMLV reverse transcriptase. Double-stranded cDNA was synthesized using *Escherichia coli* RNase H and DNA polymerase I. cDNA was ligated to λZAP EXPRESS bacteriophage arms and packaged into virions. The λ titer and the frequency of nonrecombinants were determined before amplification of the library on bacterial plates (Table 1). The frequency of nonrecombinant clones was estimated to be <2% by complementation of β-gal activity (blue/white assay). Phage were converted to pBKCMV plasmids by autoexcision in bacteria. Insert sizes in randomly selected clones were determined at this step by gel electrophoresis of plasmid DNA digested with *Sal*I and *Not*I (Table 1). The pBKCMV plasmid libraries were amplified in soft agar at 4×10^4 colony forming units/ml (27). After incubation at 37°C for 15 h, bacterial cells within the agar bed were isolated by centrifugation, amplified for 3–4 doublings in culture, and plasmid DNA was purified using a Qiagen column (Qiagen, Inc., Chatsworth, CA).

To generate libraries in a retroviral expression vector, cDNA inserts were excised from 10 μg of plasmid using *Sal*I and *Xho*I. After treatment with Klenow and dNTPs and extraction with phenol, the DNA was ligated to 5′ phosphorylated *Bst*XI adapters (5′-TCAGTTACTCAGG-3′ and 5′-CCTGAGTAACTGACACA-3′), as described (27). After treatment with *Not*I, excess adapters were removed by gel filtration, and the residual vector was converted to a 9.0-kb dimer using the *Not*I site and T4 DNA

ligase. The cDNA was size-fractionated by electrophoresis in Sea Plaque agarose (FMC BioProducts, Rockland, ME) and fragments 0.6–8.5 kb were isolated and ligated to the *Bst*XI- and alkaline phosphatase-treated MMLV retroviral vector pCTV1B (27). *E. coli* MC1061/p3 were transformed by electroporation and selected in soft agar as above.

Retroviral Transduction. The libraries were analyzed in two transfection experiments performed on consecutive days. For each library, ten 10-cm dishes of BOSC23 ecotropic packaging cells at 80%–90% confluence were transfected using 30 μg of plasmid DNA/dish (29). The transfection efficiency for these cells was ~60%, as determined using a β-gal control plasmid. Viruses were collected in a volume of 9.0 ml/dish at 36–72 h after transfection, filtered, and the 9.0 ml was expressed into a 10 cm dish containing RK3E cells at ~30% confluence. Polybrene was added to a final concentration of 10 μg/ml. After 15 h, and every 3 days thereafter, the cells were fed with growth media (17). A total of 20 RK3E dishes were transduced for each library. A β-gal retroviral plasmid transduced at least 20–30% of RK3E cells in control dishes. For colony assays, hygromycin was used at 100 μg/ml. Cell proliferation rates for transformed cell lines was measured by plating 2×10^5 cells in duplicate and counting cells 96 h later using a hemacytometer (Table 3).

PCR Recovery of Proviral Inserts. PCR reactions used 200 ng of cell line genomic DNA, 20 mM Tris-HCl (pH 8.8), 87 mM potassium acetate, 1.0 mM $MgCl_2$, 8% glycerol, 2% DMSO, 0.2 mM of each dNTP, 32 pmol of each primer (5′-CCTCACTCCTTCTCTAGCTC-3′; 5′-AACAAATTGGACTAATCGATACG-3′; Ref. 27), 5 units of Taq polymerase (Life Technologies, Inc., Gaithersburg, MD), and 0.3 units of *Pfu* polymerase (Stratagene, La Jolla, CA) in a volume of 0.05 ml. Cycling profiles were: 95°C for 1 min; then 95°C for 10 s, 59°C for 40 s, 68°C for 8 min (35 cycles).

RNA Extraction and Northern Blot Analysis. Tumor samples were obtained through the Tissue Procurement Facility of the University of Alabama at Birmingham Comprehensive Cancer Center and the Southern Division of the Cooperative Human Tissue Network. Microdissection was used to isolate tissue composed of >70% tumor cells. Total RNA was isolated as described (59), then denatured and separated on a 1.5% formaldehyde agarose gel and transferred to nitrocellulose (Schleicher and Schuell, Keene, NH). Prehybridization was at 42°C for 3 h in 50% formamide, 4 × SSC [SSC is 150 mM NaCl, 15 mM sodium citrate (pH 7.5)], 0.1 M sodium phosphate (pH 6.8), 0.1% sodium PP_i, 0.1% SDS, 5 × Denhardt's, and 25 μg/ml denatured salmon sperm DNA. Hybridization was at 42°C for 16–20 h. The hybridization mixture contained 45% formamide, 4 × SSC, 0.1 M sodium phosphate (pH 6.8), 0.075% sodium PP_i, 0.1% SDS, 10% dextran sulfate, and 100 μg/ml denatured salmon sperm DNA. After hybridization, the filter was washed twice in 2 × SSC, 0.1% SDS for 20 min at room temperature, then washed in 0.3 × SSC, 0.3% SDS for 30 min at 59°C (for detection of rat transcripts) or 65°C. For stripping of hybridized probes, the filter was placed in a solution of 2 × SSC, 25 mM Tris-HCl (pH 7.5), 0.1% SDS at initial temperature of 95°C, and shaken for 10 min at room temperature.

ISH. ISHs were conducted as described (60), using sense and antisense ^{35}S-labeled riboprobes generated from a 301-bp *Eco*RI fragment derived from the *GKLF* 3′ UTR positioned 40 bases from the stop codon. A *GAPDH* antisense probe corresponding to bases 366–680 (accession M33197) was synthesized using a commercially available template (Ambion, Inc., Austin, TX). All results were obtained in duplicate. High stringency washes were in 0.1 × SSC and 0.1% (v/v) 2-mercaptoethanol at 58°C for *GKLF* or 68°C for *GAPDH*. Slides were coated with emulsion and exposed for 14 days.

Nucleotide Sequencing. Automated sequence analysis was performed for the two independent *GKLF* isolates using vector-derived primers and sense or antisense primers spaced at 400-bp intervals within the inserts. The complete sequence was obtained for both clones, with one of the clones analyzed for both strands. Primer sequences are available upon request. *GKLF* sequence was submitted to GenBank (accession AF105036).

Acknowledgments

We thank Robert Kay for the gift of excellent retroviral vectors and detailed protocols; Martine Roussel and Trevor Littlewood for c-MYC expression vectors; and William May, Jeffrey Engler, and Tim Townes for critically reviewing the manuscript.

References

1. Weinberg, R. A. Oncogenes, antioncogenes, and the molecular bases of multistep carcinogenesis. Cancer Res., *49:* 3713–3721, 1989.

2. Hunter, T. Cooperation between oncogenes. Cell, *64:* 249–270, 1991.

3. Bishop, J. M. Molecular themes in oncogenesis. Cell, *64:* 235–248, 1991.

4. Miki, T., and Aaronson, S. A. Isolation of oncogenes by expression cDNA cloning. Methods Enzymol., *254:* 196–206, 1995.

5. Look, A. T. Oncogenic transcription factors in the human acute leukemias. Science (Washington DC), *278:* 1059–1064, 1997.

6. He, T. C., Sparks, A. B., Rago, C., Hermeking, H., Zawel, L., da Costa, L. T., Morin, P. J., Vogelstein, B., and Kinzler, K. W. Identification of c-MYC as a target of the APC pathway. Science (Washington DC), *281:* 1509–1512, 1998.

7. Korinek, V., Barker, N., Moerer, P., van Donselaar, E., Huls, G., Peters, P. J., and Clevers, H. Depletion of epithelial stem-cell compartments in the small intestine of mice lacking TCF-4. Nat. Genet., *19:* 379–383, 1998.

8. Goodrich, L. V., Milenkovic, L., Higgins, K. M., and Scott, M. P. Altered neural cell fates and medulloblastoma in mouse patched mutants. Science (Washington DC), *277:* 1109–1113, 1997.

9. Dahmane, N., Lee, J., Robins, P., Heller, P., and Ruiz i Altaba, A. Activation of the transcription factor GLI1 and the sonic hedgehog signaling pathway in skin tumours. Nature (Lond.), *389:* 876–881, 1997.

10. Hahn, H., Wojnowski, L., Zimmer, A. M., Hall, J., Miller, G., and Zimmer, A. Rhabdomyosarcomas and radiation hypersensitivity in a mouse model of Gorlin Syndrome. Nat. Med., *4:* 619–622, 1998.

11. Xu, G. F., O'Connell, P., Viskochil, D., Cawthon, R., Robertson, M., Culver, M., Dunn, D., Stevens, J., Gesteland, R., White, R., Weiss, R. The neurofibromatosis type 1 gene encodes a protein related to GAP. Cell, *62:* 599–608, 1990.

12. Chellappan, S. P., Hiebert, S., Mudryj, M., Horowitz, J. M., and Nevins, J. R. The E2F transcription factor is a cellular target for the RB protein. Cell, *65:* 1053–1061, 1991.

13. Kallioniemi, O. P., Kallioniemi, A., Sudar, D., Rutovitz, D., Gray, J. W., Waldman, F., and Pinkel, D. Comparative genomic hybridization: a rapid new method for detecting and mapping DNA amplification in tumors. Semin. Cancer Biol., *4:* 41–46, 1993.

14. Iftner, T. G., Bierfelder, S., Csapo, Z., and Pfister, H. Involvement of human papillomavirus type 8 genes E6 and E7 in transformation and replication. J. Virol., *62:* 3655–3661, 1988.

15. Lugo, T. G., and Witte, O. N. The *BCR-ABL* oncogene transforms Rat-1 cells and cooperates with v-*myc*. Mol. Cell. Biol., *9:* 1263–1270, 1989.

16. Pace, A. M., Wong, Y. H., and Bourne, H. R. A mutant α subunit of GIP2 induces neoplastic transformation of RAT1 cells. Proc. Natl. Acad. Sci. USA, *88:* 7031–7035, 1991.

17. Ruppert, J. M., Vogelstein, B., and Kinzler, K. W. The zinc finger protein GLI transforms rodent cells in cooperation with adenovirus E1A. Mol. Cell. Biol., *11:* 1724–1728, 1991.

18. Capobianco, A. J., Zagouras, P., Blaumueller, C. M., Artavanis-Tsakonas, S., and Bishop, J. M. Neoplastic transformation by truncated alleles of human NOTCH1/TAN1 and NOTCH2. Mol. Cell. Biol., *17:* 6265–6273, 1997.

19. Draetta, G. F. Mammalian G1 cyclins. Curr. Opin. Cell Biol., *6:* 842–846, 1994.

20. Hussussian, C. J., Struewing, J. P., Goldstein, A. P., Higgins, P. A., Ally, D. S., Sheahan, M. D., Clark, W. H. J., Tucker, M. A., and Dracopoli, N. C. Germline p16 mutations in familial melanoma. Nat. Genet., *8:* 15–21, 1994.

21. Sherr, C. J., and Roberts, J. M. Inhibitors of mammalian G(1) cyclin-dependent kinases. Genes Dev., *9:* 1149–1163, 1995.

22. Weinberg, R. A. The retinoblastoma protein and cell cycle control. Cell, *81:* 323–330, 1995.

23. Bishop, J. M. Viral oncogenes. Cell, *42:* 23–38, 1985.

24. Harlow, E., and Dyson, N. Adenovirus E1a targets key regulators of cell proliferation. Cancer Surv., *12:* 161–195, 1992.

25. Nevins, J. R. Adenovirus E1a: transcription regulation and alteration of cell growth control. Curr. Top. Microbiol. Immunol., *199:* 25–32, 1995.

26. Mal, A., Poon, R. Y. C., Howe, P. H., Toyoshima, H., Hunter, T., and Harter, M. L. Inactivation of $p27^{Kip1}$ by the viral E1a oncoprotein in TGFβ-treated cells. Nature (Lond.), *380:* 262–265, 1996.

27. Whitehead, I., Kirk, H., and Kay, R. Expression cloning of oncogenes by retroviral transfer of cDNA libraries. Mol. Cell. Biol., *15:* 704–710, 1995.

28. Frisch, S. M. E1a induces the expression of epithelial characteristics. J. Cell Biol., *127:* 1085–1096, 1994.

29. Pear, W. S., Nolan, G. P., Scott, M. L., and Baltimore, D. Production of high-titer helper-free retroviruses by transient transfection. Proc. Natl. Acad. Sci. USA, *90:* 8392–8396, 1993.

30. Shields, J. M., Christy, R. J., and Yang, V. W. Identification and characterization of a gene encoding a gut-enriched Krüppel-like factor expressed during growth arrest. J. Biol. Chem., *271:* 20009–20017, 1996.

31. Yet, S. F., Mcanulty, M. M., Folta, S. C., Yen, H. W., Yoshizumi, M., Hsieh, C. M., Layne, M. D., Chin, M. T., Wang, H., Perrella, M. A., Jain, M. K., and Lee, M. E. Human EZF, a Krüppel-like zinc finger protein, is expressed in vascular endothelial cells and contains transcriptional activation and repression domains. J. Biol. Chem., *273:* 1026–1031, 1998.

32. Garrett-Sinha, L. A., Eberspaecher, H., Seldin, M. F., and de Crombrugghe, B. A gene for a novel zinc-finger protein expressed in differentiated epithelial cells and transiently in certain mesenchymal cells. J. Biol. Chem., *271:* 31384–31390, 1996.

33. Littlewood, T. D., Hancock, D. C., Danielian, P. S., Parker, M. G., and Evan, G. I. A modified oestrogen receptor ligand-binding domain as an improved switch for the regulation of heterologous proteins. Nucleic Acids Res., *23:* 1686–1690, 1995.

34. Merritt, W. D., Weissler, M. C., Turk, B. F., and Gilmer, T. M. Oncogene amplification in squamous cell carcinoma of the head and neck. Arch. Otolaryngol. Head Neck Surg., *116:* 1394–1398, 1990.

35. Leonard, J. H., Kearsley, J. H., Chenevix-Trench, G., and Hayward, N. K. Analysis of gene amplification in head-and-neck squamous-cell carcinoma. Int. J. Cancer, *48:* 511–515, 1991.

36. Garte, S. J. The c-*myc* oncogene in tumor progression. Crit. Rev. Oncog., *4:* 435–449, 1993.

37. Fracchiolla, N. S., Pignataro, L., Capaccio, P., Trecca, D., Boletini, A., Ottaviani, A., Polli, E., Maiolo, A. T., and Neri, A. Multiple genetic lesions in laryngeal squamous cell carcinomas. Cancer (Phila.), *75:* 1292–1301, 1995.

38. Courjal, F., Cuny, M., Simonylafontaine, J., Louason, G., Speiser, P., Zeillinger, R., Rodriguez, C., and Theillet, C. Mapping of DNA amplifications at 15 chromosomal localizations in 1875 breast tumors—definition of phenotypic groups. Cancer Res., *57:* 4360–4367, 1997.

39. Field, J. K., Spandidos, D. A., Stell, P. M., Vaughan, E. D., Evan, G. I., and Moore, J. P. Elevated expression of the c-MYC oncoprotein correlates with poor prognosis in head and neck squamous cell carcinoma. Oncogene, *4:* 1463–1468, 1989.

40. Eversole, L. R., and Sapp, J. P. c-MYC oncoprotein expression in oral precancerous and early cancerous lesions. Eur. J. Cancer, *29B:* 131–135, 1993.

41. Porter, M. J., Field, J. K., Leung, S. F., Lo, D., Lee, J. C., Spandidos, D. A., and van Hasselt, C. A. The detection of the c-*myc* and *ras* oncogenes in nasopharyngeal carcinoma by immunohistochemistry. Acta Otolaryngol., *114:* 105–109, 1994.

42. Bos, J. L. RAS oncogenes in human cancer: a review. Cancer Res., *49:* 4682–4689, 1989.

43. Grandori, C., and Eisenman, R. N. *Myc* target genes. Trends Biochem. Sci., *22:* 177–181, 1997.

44. Shim, H., Lewis, B. C., Dolde, C., Li, Q., Wu, C. S., Chun, Y. S., and Dang, C. V. *Myc* target genes in neoplastic transformation. Curr. Top. Microbiol. Immunol., *224:* 181–190, 1997.

45. Fischer, R. S., and Quinlan, M. P. Identification of a novel mechanism of regulation of the adherens junction by E1A, RAC1, and cortical actin filaments that contributes to tumor progression. Cell Growth Differ., *9:* 905–918, 1998.

46. Goudie, D. R., Yuille, M. A., Leversha, M. A., Furlong, R. A., Carter, N. P., Lush, M. J., Affara, N. A., and Ferguson-Smith, M. A. Multiple self-healing squamous epitheliomata (ESS1) mapped to chromosome 9q22–q31 in families with common ancestry. Nat. Genet., *3:* 165–169, 1993.

47. Richards, F. M., Goudie, D. R., Cooper, W. N., Jene, Q., Barroso, I., Wicking, C., Wainwright, B. J., and Ferguson-Smith, M. A. Mapping the multiple self-healing squamous epithelioma (*MSSE*) gene and investigation of xeroderma pigmentosum group a (*XPA*) and patched (*PTCH*) as candidate genes. Hum. Genet., *101:* 317–322, 1997.

48. Shields, J. M., and Yang, V. W. Identification of the DNA sequence that interacts with the gut-enriched Krüppel-like factor. Nucleic Acids Res., *26:* 796–802, 1998.

49. Shields, J. M., and Yang, V. W. Two potent nuclear localization signals in the gut-enriched Krüppel-like factor define a subfamily of closely related Krüppel proteins. J. Biol. Chem., *272:* 18504–18507, 1997.

50. Jenkins, T. D., Opitz, O. G., Okano, J., and Rustgi, A. K. Transactivation of the human keratin 4 and Epstein-Barr virus ED-L2 promoters by gut-enriched Krüppel-like factor. J. Biol. Chem., *273:* 10747–10754, 1998.

51. Tonthat, H., Kaestner, K. H., Shields, J. M., Mahatanankoon, C. S., and Yang, V. W. Expression of the gut-enriched Krüppel-like factor gene during development and intestinal tumorigenesis. FEBS Lett., *419:* 239–243, 1997.

52. Miller, I. J., and Bieker, J. J. A novel, erythroid cell-specific murine transcription factor that binds to the CACCC element and is related to the Krüppel family of nuclear proteins. Mol. Cell. Biol., *13:* 2776–2786, 1993.

53. Kuo, C. T., Veselits, M. L., and Leiden, J. M. LKLF: a transcriptional regulator of single-positive T cell quiescence and survival. Science (Washington DC), *277:* 1986–1990, 1997.

54. Johnson, R. L., Rothman, A. L., Xie, J., Goodrich, L. V., Bare, J. W., Bonifas, J. M., Quinn, A. G., Myers, R. M., Cox, D. R., Epstein, E. H., Jr., and Scott, M. P. Human homolog of patched, a candidate gene for the basal cell nevus syndrome. Science (Washington DC), *272:* 1668–1671, 1996.

55. Fuchs, E., and Byrne, C. The epidermis: rising to the surface. Curr. Opin. Genet. Dev., *4:* 725–736, 1994.

56. Gandarillas, A., and Watt, F. M. c-Myc promotes differentiation of human epidermal stem cells. Genes Dev., *11:* 2869–2882, 1997.

57. Hueber, A. O., Zornig, M., Lyon, D., Suda, T., Nagata, S., and Evan, G. I. Requirement for the CD95 receptor-ligand pathway in c-MYC-induced apoptosis. Science (Washington DC), *278:* 1305–1309, 1997.

58. Brewster, R., Lee, J., and Ruiz i Altaba, A. Gli/zic factors pattern the neural plate by defining domains of cell differentiation. Nature (Lond.), *393:* 579–583, 1998.

59. Chomczynski, P., and Sacchi, N. Single-step method of RNA isolation by acid guanidinium thiocyanate-phenol-chloroform extraction. Anal. Biochem., *162:* 156–159, 1987.

60. Cheng, S., Schmidt-Grimminger, D. C., Murant, T., Broker, T. R., and Chow, L. T. Differentiation-dependent up-regulation of the human papillomavirus E7 gene reactivates cellular DNA replication in suprabasal differentiated keratinocytes. Genes Dev., *9:* 2335–2349, 1995.

[CANCER RESEARCH 60, 6488–6495, November 15, 2000]

Increase of GKLF Messenger RNA and Protein Expression during Progression of Breast Cancer[1]

K. Wade Foster, Andra R. Frost, Peggy McKie-Bell, Chin-Yu Lin, Jeffrey A. Engler, William E. Grizzle, and J. Michael Ruppert[2]

Department of Biochemistry and Molecular Genetics [K. W. F., J. A. E., J. M. R.], Department of Pathology [A. R. F., W. E. G.], Division of Hematology/Oncology, Department of Medicine [P. M-B., J. M. R.], Medical Statistics Section, Department of Medicine [C-Y. L.], and Oral Cancer Research Center and Comprehensive Cancer Center [J. A. E., W. E. G., J. M. R.], University of Alabama at Birmingham School of Medicine, Birmingham, Alabama 35294-3300

ABSTRACT

Genetic alterations found in carcinomas can alter specific regulatory pathways and provide a selective growth advantage by activation of transforming oncogenes. A subset of these genes, including wild-type alleles of *GLI* or *c-MYC*, and activated alleles of *RAS* or *β-catenin*, exhibit transforming activity when expressed in diploid epithelial RK3E cells *in vitro*. By *in vitro* transformation of these cells, the zinc finger protein GKLF/KLF-4 was recently identified as a novel oncogene. Although GKLF is normally expressed in superficial, differentiating epithelial cells of the skin, oral mucosa, and gut, expression is consistently up-regulated in dysplastic epithelium and in squamous cell carcinoma of the oral cavity. In the current study, we used *in situ* hybridization, Northern blot analysis, and immunohistochemistry to detect GKLF at various stages of tumor progression in the breast, prostate, and colon. Overall, expression of GKLF mRNA was detected by *in situ* hybridization in 21 of 31 cases (68%) of carcinoma of the breast. Low-level expression of GKLF mRNA was observed in morphologically normal (uninvolved) breast epithelium adjacent to tumor cells. Increased expression was observed in neoplastic cells compared with adjacent uninvolved epithelium for 14 of 19 cases examined (74%). Ductal carcinoma *in situ* exhibited similar expression as invasive carcinoma, suggesting that GKLF is activated prior to invasion through the basement membrane. Expression as determined by Northern blot was increased in most breast tumor cell lines and in immortalized human mammary epithelial cells when these were compared with finite-life span human mammary epithelial cells. Alteration of GKLF expression was confirmed by the use of a novel monoclonal antibody that detected the protein in normal and neoplastic tissues in a distribution consistent with localization of the mRNA. In contrast to most breast tumors, expression of GKLF in tumor cells of colorectal or prostatic carcinomas was reduced or unaltered compared with normal epithelium. The results demonstrate that GKLF expression in epithelial compartments is altered in a tissue-type specific fashion during tumor progression, and suggest that increased expression of GKLF mRNA and protein may contribute to the malignant phenotype of breast tumors.

INTRODUCTION

Multiple physiological changes lead to acquisition of the malignant phenotype. These include self-sufficiency in growth signaling, insensitivity to growth-inhibitory signals, inhibition of apoptosis, immortalization, induction of angiogenesis, and the ability to invade and metastasize (1, 2). Genetic analyses of inherited predispositions to develop specific carcinomas enabled isolation of tumor suppressor genes important in both inherited and sporadic disease (3), and subsequent functional studies identified certain of these genes as regulators of classical transforming oncogenes. Thus, alterations in the tumor suppressor patched (PTC1), or in other molecules that transduce the hedgehog signal, result in activation of GLI mRNA expression in virtually all basal cell carcinomas of the skin (4–7). In contrast, alterations in the adenomatous polyposis coli (APC) pathway activate the β-catenin/TCF-4 complex and transcription of *c-MYC* and *cyclin D1* during colorectal tumor progression (8, 9). Modulation of the PTC1 and APC pathways by alteration of the mouse genome provides additional support of a role for these gene products in specific tumor types (10–14). Therefore, these pathways exhibit properties of a gatekeeper, indicating that alteration of the pathway in a specific tissue is rate-limiting for tumor progression, and that alterations are found in a large proportion of inherited as well as sporadic tumors (15, 16).

By expression cloning we recently identified the zinc finger protein GKLF[3] as a novel transforming oncogene when expressed in RK3E cells, a diploid epithelial cell line derived from primary rat kidney cells and immortalized with adenovirus E1A (17). cDNA libraries were prepared using mRNA from human oral squamous cell or breast carcinoma cell lines, tumor-types not reported to exhibit frequent genetic alterations that activate well-characterized oncogenes such as *RAS*, *GLI*, or *β-catenin* (18). Retroviral transduction of these libraries into RK3E cells induced morphologically transformed foci, 11 of which were subsequently attributed to enforced expression of wild-type human *c-MYC*. Two other transformed foci contained independently derived, wild-type alleles of *GKLF*. No other genes were identified in the screen, suggesting that only a select subset of all oncogenes are able to transform these cells.

Whereas enforced expression of a human wild-type *GKLF* transgene in RK3E cells induces morphological transformation *in vitro* and tumorigenicity in athymic mice, the doubling time of GKLF-expressing cells was considerably longer than for RK3E cells (27 h *versus* 12 h, respectively; Refs. 17, 19). Similar results were obtained for other oncogenes, including *GLI* and *c-MYC*, as cells expressing these genes exhibited doubling times of 18 and 19 h, respectively. These oncogenes may therefore function in epithelial cells by interfering specifically with contact inhibition rather than by inducing a more general increase in the rate of cell division.

In support of a role for *GKLF* as an oncogene, we observed increased expression of GKLF mRNA during progression of squamous cell carcinomas of the oropharynx. As demonstrated by mRNA ISH analysis of surgical specimens, expression in normal epithelial cells is limited to the differentiating compartment. Expression in dysplastic oral epithelium is increased overall and is found in all cell layers, and GKLF is expressed at similar levels in dysplasia and in invasive carcinoma. These results identified loss of the compartment-specific pattern of GKLF mRNA expression in epithelium as a candidate mechanism of tumor progression in oral cancer (17).

GKLF encodes a DNA-binding transcription factor with functional

Received 4/12/00; accepted 9/12/00.

The costs of publication of this article were defrayed in part by the payment of page charges. This article must therefore be hereby marked *advertisement* in accordance with 18 U.S.C. Section 1734 solely to indicate this fact.

[1] Supported by USPHS Grant R29CA65686-05 (to J. M. R.), the University of Alabama at Birmingham Oral Cancer Research Center P50 DE11910-04 (to J. M. R., W. E. G., and J. A. E.), Grants P50 DE08228-10S3 (to J. A. E.) and NIGMS 5T32 GM08361-08 (to K. W. F.), and a gift to the Comprehensive Cancer Center from the Avon Products Foundation Breast Cancer Research and Care Program.

[2] To whom requests for reprints should be addressed, at Department of Medicine, Room 570 Wallace Tumor Institute, University of Alabama at Birmingham School of Medicine, Birmingham, AL 35294-3300. Phone: (205) 975-0556; Fax: (205) 934-9573; E-mail: mruppert@uab.edu.

[3] The abbreviations used are: GKLF, gut-enriched Krüppel-like factor; DCIS, ductal carcinoma *in situ*; GAPDH, glyceraldehyde-3-phosphate dehydrogenase; HMEC, human mammary epithelial cell; IDC, internal ductal carcinoma; ISH, mRNA *in situ* hybridization; SAGE, serial analysis of gene expression.

domains that mediate activation or repression of transcription (20–22). GKLF is essential for the barrier function of skin, because homozygous knockout mice exhibit morphologically normal skin but die postpartum due to dehydration (23). Transcriptional targets of GKLF that may be relevant to epithelial differentiation have been preliminarily identified (23–25). As shown by analysis of normal mouse or human tissues, GKLF is preferentially expressed in differentiating epithelial cells of the skin, gut, oral cavity, and thymus (17, 20, 23, 26, 27). In contrast to human oral squamous cell carcinoma, expression of GKLF mRNA was found to be reduced in mouse models of intestinal tumorigenesis or hyperproliferation (28, 29). Independently, analysis of human colorectal mucosa and tumors by SAGE confirmed the earlier studies in mice (30, 31). Specifically, mRNA from specimens of normal colonic mucosa generated GKLF tags at frequencies of 138 or 99 per million SAGE tags, whereas mRNA from a microdissected tumor generated only 20 tags per million. These results suggested that GKLF expression is regulated during neoplastic progression in a tumor type-specific fashion.

Increased expression of specific oncogenes in tumors can result from genetic alterations and play a causal role in tumor progression. Alternatively, expression of some oncogenes is cell cycle dependent, and increased expression can occur as a consequence of increased proliferation or altered cell cycle occupancy of tumor cells. In multiple normal tissues as well as in certain cell lines, GKLF expression is reduced in actively cycling cells compared with terminally differentiated or growth-arrested cells, and enforced expression of GKLF in cultured cell lines can retard cell cycle progression (26, 32). These properties predicted that GKLF expression might be reduced in tumors, as observed in colorectal carcinoma. Increased expression in other tumor-types is therefore somewhat unexpected and may result from specific alterations in the pathways that regulate GKLF transcription in normal cells.

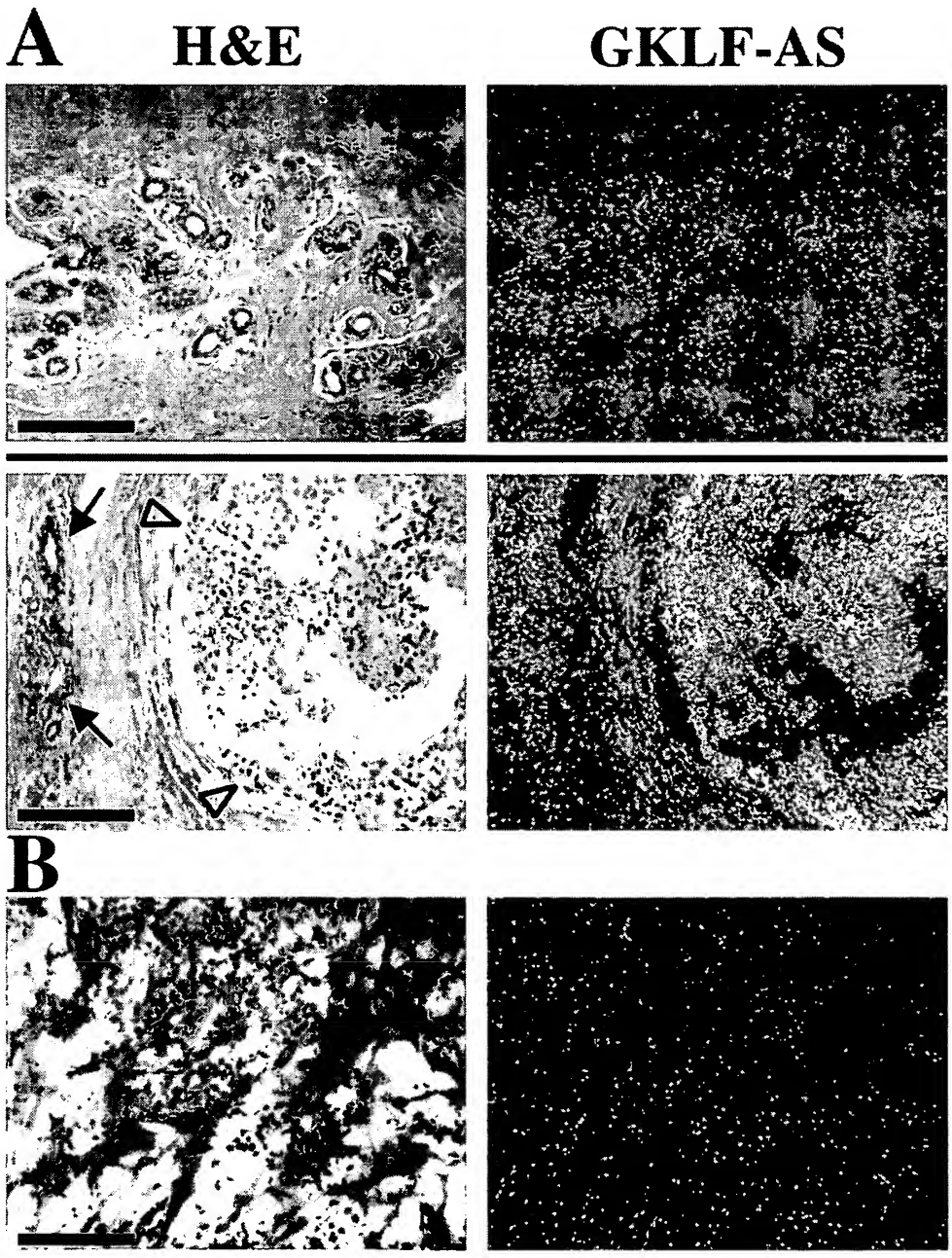

Fig. 1. ISH analysis of GKLF mRNA in carcinoma of the breast. Two distinct cases were analyzed by applying an antisense (*GKLF-AS*) [^{35}S]-labeled RNA probe to sections of paraffin-embedded (*A*) or fresh-frozen (*B*) surgical material. Brightfield (*left*) and darkfield (*right*) views are shown. Sections were stained with H&E. Hybridization to a sense control probe resulted in an average of 0.4 grains/nucleus (not shown). *A*, two areas of the same slide are shown, with uninvolved (*i.e.*, morphologically normal) breast epithelium (*upper plate*) adjacent to an area (*lower plate*) containing DCIS (*arrowheads*) and additional uninvolved tissue (*arrows*). *B*, IDC admixed with cords of stroma. Scale bars = 160 μm.

To better understand the spectrum of tumor-types that exhibit GKLF activation, we obtained samples of breast carcinoma, colorectal carcinoma, and prostatic carcinoma and analyzed expression of GKLF in malignant cells and in adjacent normal-appearing epithelium (*i.e.*, uninvolved epithelium). The results show that levels of GKLF mRNA and protein are each up-regulated before invasion in a majority of cases of breast cancer, but not in tumors of the colorectum or prostate. In neoplastic lesions of the breast as well as in cultured mammary epithelial cells *in vitro*, increased GKLF expression appears to precede overtly malignant behavior. The potent transforming activity of GKLF *in vitro*, the tumor type-specific activation of expression *in vivo*, and activation early during tumor progression identify this oncogene as a potential effector of tumor progression in the breast.

MATERIALS AND METHODS

Tissue Procurement. Fresh-frozen and paraffin-embedded samples were obtained through the Tissue Procurement Core Facility of the University of Alabama at Birmingham Comprehensive Cancer Center and through the Southern Division of the Cooperative Human Tissue Network.

Table 1 *mRNA ISH analysis of GKLF in tumors*[a]

Carcinoma of the breast						
		GKLF-AS				
Case	PE/FF	U	D	T	GKLF-S	GAPDH-AS
1	FF	0.5	2.5	–	0.0	+
2	FF	–	–	2.0	0.0	+
3	FF	0.0	–	1.0	0.0	+
4	FF	–	–	0.0	0.0	+
5	FF	–	–	0.0	0.0	NT
6	FF	–	–	0.0	0.0	NT
7	FF	–	2.0	2.0	0.0	NT
8	FF	0.0	1.0	1.0	0.0	NT
9	FF	–	–	0.0	0.0	NT
10	FF	–	–	0.0	0.0	NT
11	FF	–	–	0.0	0.0	NT
12	FF	–	–	0.5	0.0	NT
13	FF	0.0	–	0.5	0.0	NT
14	FF	–	–	0.5	0.0	NT
15	PE	–	–	1.5	NT	+
16	PE	0.0	–	1.0	NT	+
17	PE	0.0	–	1.0	NT	+
18	PE	0.0	–	2.0	NT	+
19	PE	–	–	0.0	NT	+
20	PE	1.0	2.0	1.0	NT	+
21	PE	0.5	–	1.5	NT	+
22	PE	0.5	2.0	2.0	NT	+
23	PE	1.0	–	1.0	0.0	+
24	PE	0.5	1.0	1.2	0.0	+
25	PE	0.3	1.2	1.2	0.0	+
26	PE	0.5	1.5	1.5	0.0	+
27	PE	0.0	0.0	0.0	0.0	+
28	PE	0.0	0.0	0.0	0.0	+
29	PE	0.0	0.0	0.0	0.0	+
30	PE	0.5	1.0	1.0	0.0	+
31	PE	0.0	1.0	1.5	0.0	0.0

Carcinoma of the prostate						
		GKLF-AS				
Case	PE/FF	U	PIN	T	GKLF-S	GAPDH-AS
1	PE	1.0	–	0.0	NT	+
2	PE	–	–	0.0	NT	+
3	PE	1.0	–	1.0	NT	+
4	PE	1.0	1.0	0.0	NT	0.0

[a] Results obtained for sense (*S*) or antisense (*AS*) probes are presented. Scoring of GKLF used a scale of 0.0–4.0 as described in "Materials and Methods," whereas GAPDH was scored as detected (+) or undetected (0.0). Numbers indicate the level of gene expression for histologically distinct tissue within the same section. A dash (–) indicates that no tissue in the section exhibited the specific histopathologic feature. *PE*, paraffin-embedded; *FF*, fresh-frozen; *U*, uninvolved or morphologically normal epithelium; *D*, ductal carcinoma *in situ*; *PIN*, prostatic intraepithelial neoplasia; *T*, invasive tumor cells; *NT*, not tested.

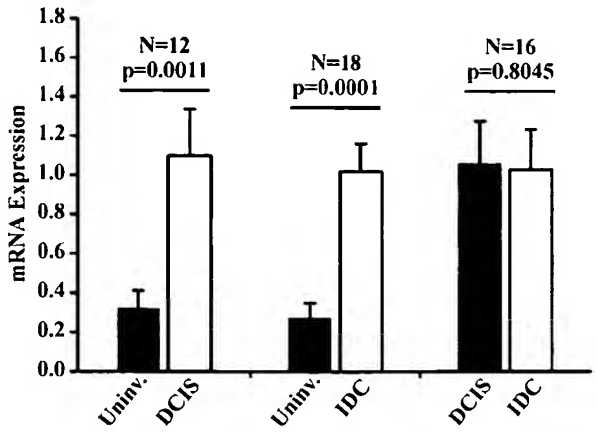

Fig. 2. GKLF mRNA expression in normal and neoplastic breast tissue. The data in Table 1 was analyzed using a paired *t* test. Sample size (*N*), statistical significance (*p*), and SE are indicated for each comparison. *Uninv.*, uninvolved ducts.

mRNA Expression. ISH was conducted as described (17) using sense and antisense [^{35}S]-labeled riboprobes prepared by *in vitro* transcription of a cDNA fragment corresponding to the 3′ untranslated region of human *GKLF*. A *GAPDH* antisense probe corresponding to bases 366–680 (GenBank accession no. M33197) was synthesized using a commercially available template (Ambion, Inc., Austin, TX). High stringency washes were in 0.1 × SSC and 0.1% (v/v) 2-mercaptoethanol at 58°C for *GKLF* or 68°C for *GAPDH*. Slides were coated with emulsion and exposed for 14 days. The number of silver grains/nucleus were counted within representative areas by two individuals, and a score from 0.0 to 4.0 was recorded. A score of 0.0 indicated only nonspecific background, as determined using the sense control, and 1.0 corresponded to an average of four grains/nucleus.

Breast adenocarcinoma cell lines were obtained from the American Type Culture Collection (Manassus, MD). HMECs were described previously and were cultured in mammary epithelial basal media (Clonetics Corp., Walkersville, MD; Ref. 33). Extracts were prepared from exponentially growing cells at 70% confluence, and total RNA isolation and Northern blot analysis were performed as described (17).

Isolation of an Anti-GKLF Monoclonal Antibody. The region of the human GKLF cDNA encoding bases 479-1197 (GenBank accession no. AF105036) was cloned into plasmid pET-32a and expressed in *Escherichia coli* BL21(DE3) bacteria as a histidine-tagged protein. Protein was purified from the bacteria after induction with isopropyl-1-thio-β-D-galactopyranoside using a His-Trap Ni-agarose column (Amersham Pharmacia Biotech, Piscataway, NJ) and eluted with 500 mM imidazole. Purified protein was used to immunize two mice, and lymphocytes were fused with murine myeloma cells (PX63-Ag8.653) as described previously (34). Hybridomas that were immunoreactive in an ELISA assay for the purified antigen were cloned and recloned by limiting dilution. Positive clones were identified by ELISA, and an IgG1 antibody (αGKLF) was purified from ascites on a protein A affinity column.

Immunohistochemistry. Tissues were fixed in neutral buffered formalin and embedded in paraffin. Deparaffinized tissue sections were incubated with αGKLF at a concentration of 1.0 μg/ml for 1 h at room temperature, and processed as described (35). Immunodetection was performed using a biotinylated secondary antibody, streptavidin-horseradish peroxidase detection system (Signet Laboratories, Dedham, MA), and the chromogenic substrate diaminobenzidine (Biogenex, San Ramon, CA). Sections were counterstained with hematoxylin. Results were scored by using a 0.0 to 4.0 scoring system where 4.0 corresponds to a saturated signal (36).

Statistical Analyses. Paired *t* tests were used to compare the differences in expression in breast epithelial cells at various stages of tumor progression (37). Pearson correlation coefficients were used to compare results obtained by ISH to those obtained for the same cases using immunohistochemistry.

RESULTS

GKLF mRNA Expression Is Up-Regulated during Breast Tumor Progression. Previously, SAGE analysis of purified normal breast epithelial cells detected GKLF transcripts at an abundance of

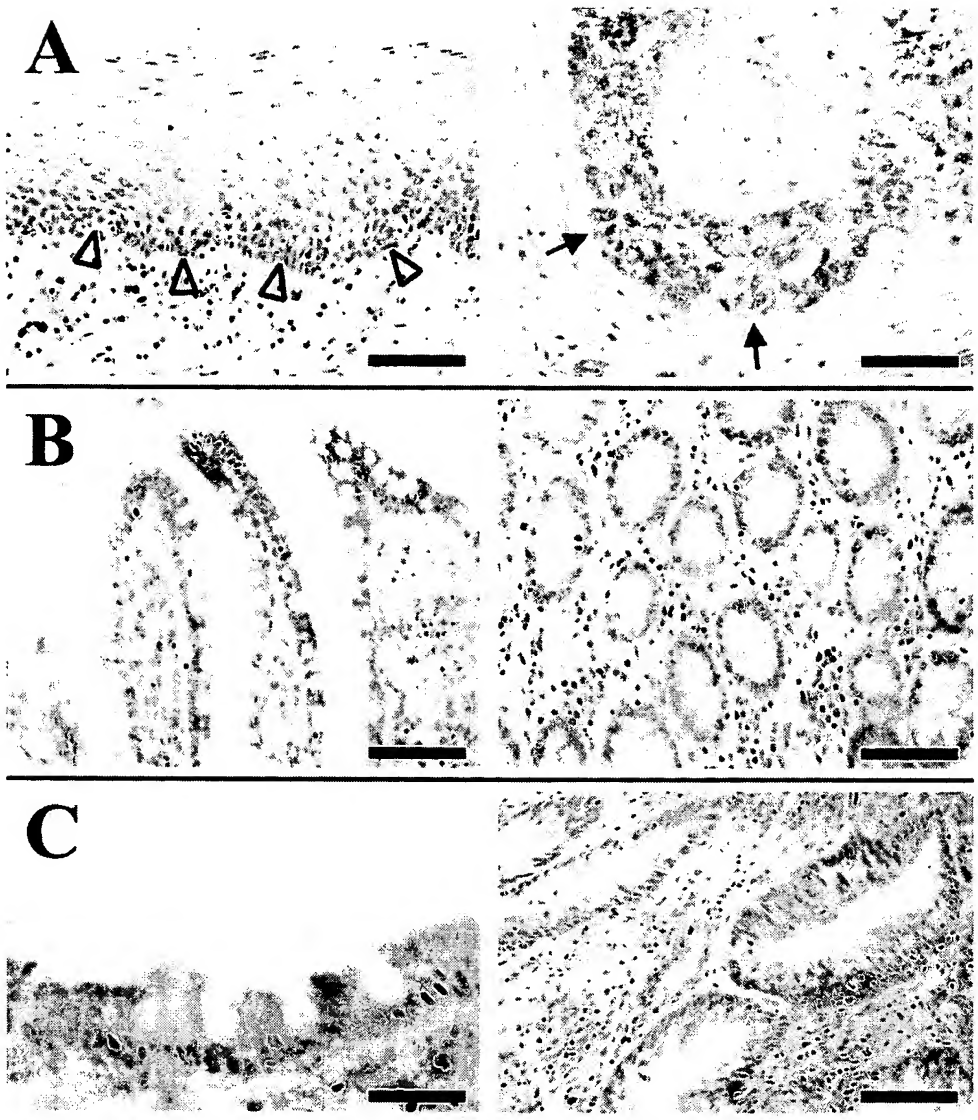

Fig. 3. Immunostaining of human tissues with αGKLF monoclonal antibody. Each panel (*A-C*) illustrates adjacent areas of a tissue section. *A*, uninvolved oral epithelium (*left*) and invasive oral squamous cell carcinoma (*right*). *Arrowheads* indicate the basal cell layer, whereas *arrows* indicate invasive carcinoma. Staining of tumor cells and of superficial epithelial cells is indicated by a *brown* precipitate. *B*, a section of small bowel illustrating increased staining of superficial epithelium (*left*) compared with cells deeper within crypts (*right*). *C*, a case of colorectal carcinoma, with increased staining of uninvolved superficial mucosa (*left*) compared with adjacent tumor cells (*right*). Scale bar for *C* (*left panel*) = 45 μm; other scale bars = 140 μm.

40 tags per million (31, 38), and Northern blot analysis of breast tumor cell lines revealed the presence of GKLF transcripts (17). Using sense and antisense [^{35}S]-labeled riboprobes, we examined the expression of GKLF mRNA in 31 cases of carcinoma of the breast. Specificity of hybridization was determined by using the sense probe as a negative control or by hybridization of the antisense probe to human foreskin, in which GKLF was specifically detected in suprabasal epithelial cells (not shown).

Expression of GKLF was detected in malignant cells in 21 of 31 cases of ductal adenocarcinoma (68%, Fig. 1, Table 1). For several cases that exhibited no detectable expression of GKLF, prominent expression of the housekeeping gene *GAPDH* was observed, indicating that overall mRNA integrity was maintained and that failure to identify GKLF transcripts may reflect reduced levels of expression. GKLF expression was increased in malignant cells of 14 of 19 cases that contained adjacent uninvolved epithelium (Fig. 1*A*). For 7 of these 14 cases, no specific signal was detected in adjacent uninvolved epithelium. In the other seven cases, expression was detected in both uninvolved and malignant cells, with expression of GKLF in malignant cells increased by 3- to 5-fold compared with uninvolved epithelium. Within tumors, expression of GKLF was specific to malignant cells, with little or no expression detected in stromal components (Fig. 1*B*).

GKLF expression in DCIS was not significantly different from invasive carcinoma, but expression in both lesions was higher than for uninvolved breast epithelium (Table 1, Fig. 2). In contrast to results obtained in breast tumors, examination of several cases of prostatic carcinoma revealed equal or reduced expression in tumor cells compared with adjacent uninvolved glandular epithelial cells (Table 1). In summary, the results suggest that GKLF mRNA expression is activated in approximately two-thirds of breast carcinomas, and that expression in positive cases is consistently induced in DCIS before invasion.

Characterization of a GKLF-specific Monoclonal Antibody. An IgG1 isotype antibody raised against bacterially expressed GKLF was subsequently referred to as αGKLF. Immunoblot analysis of GKLF-transformed RK3E cells and control cell lines detected a single protein species of 55 kDa consistent with the predicted size of the full-length polypeptide (data not shown). Compared with RK3E cells or control cell lines transformed by other oncogenes, apparent GKLF abundance was increased by several-fold in each of two cell lines transformed by the human expression vector. The epitope recognized by the antibody may be denaturation-sensitive, as a signal was obtained only after overnight exposure of autoradiographic film using a standard chemiluminescence protocol. The antibody was not sufficiently sensitive

Table 2 *Immunohistochemical analysis of GKLF in tumors*[a]

Carcinoma of the breast						
	Uninvolved		DCIS		Invasive tumor cells	
Case	Nucleus	Cytoplasm	Nucleus	Cytoplasm	Nucleus	Cytoplasm
23	0.25	0.45	–	–	0.35	0.55
24	0.50	1.30	1.00	1.30	1.00	1.30
25	0.65	0.95	0.45	1.40	0.38	1.35
26	0.18	0.75	0.03	1.20	0.12	1.05
27	0.10	1.30	0.00	1.10	0.05	0.50
28	0.10	0.30	–	–	0.35	0.20
29	0.00	0.00	0.10	0.75	0.05	0.75
30	0.00	0.20	0.10	1.05	–	–
31	0.00	0.10	0.65	0.65	0.70	1.15
32	0.25	0.55	0.55	0.75	0.42	0.85
33	0.80	0.45	–	–	0.50	1.25
34	0.18	0.50	–	–	0.45	1.15
35	0.30	0.35	0.60	1.60	0.65	1.50
36	0.00	0.05	0.55	1.70	0.75	1.00
37	0.70	0.60	–	–	1.65	1.80
38	–	–	0.00	0.90	0.00	1.50
39	0.55	0.70	0.75	0.85	1.75	1.75
40	0.35	0.50	0.75	0.90	0.75	0.85

Colorectal carcinoma						
	Normal Superficial[b]		Normal Deep[c]		Tumor[d]	
Case	Nucleus	Cytoplasm	Nucleus	Cytoplasm	Nucleus	Cytoplasm
1	0.45	1.00	0.25	0.05	0.00	0.85
2	0.40	0.60	0.40	0.25	0.20	0.35
3	0.15	1.15	0.30	0.80	0.25	0.85
4	0.00	1.30	0.00	0.15	0.00	0.80
5	–	–	–	–	0.00	0.65

[a] Immunohistochemical scores indicate the intensity of staining of histologically distinct tissue within the same section. A dash (–) indicates that no tissue in the section exhibited the specific histopathologic feature. All samples were paraffin-embedded.
[b] Differentiating epithelial cells located in the superficial portion of intestinal mucosa.
[c] Epithelial cells deep within intestinal mucosa.
[d] Analysis included both adenomas and adenocarcinomas.

to detect GKLF by immunoblot analysis of extracts of human tumor cell lines that express the endogenous GKLF mRNA.

The cell type- and tumor type-specific patterns of GKLF mRNA expression were used to examine the specificity of αGKLF in immunohistochemical assays. These patterns can be summarized as follows. Human GKLF mRNA is detected by ISH in differentiating cells of oral epithelium, and is markedly elevated in oral tumors (17). The mRNA is not detected in morphologically normal basal or parabasal cells, particularly within epidermal pegs that extend further into the submucosa. Mouse GKLF mRNA is similarly found to be more highly expressed in superficial, differentiating cells of the skin and gut, and is reduced or absent in basal epithelial cells in both tissues (20, 23, 26). In contrast to human oral and breast cancer, GKLF mRNA expression is reduced in mouse colorectal tumors compared with normal epithelium (29), and is similarly reduced in human colorectal cancer as indicated by SAGE (31).

The staining pattern of αGKLF exhibited a strict concordance with detection of GKLF mRNA (Figs. 3 and 4, Table 2). In positive tissues, αGKLF exhibited a mixed nuclear and cytoplasmic staining pattern. For uninvolved epithelium, DCIS, and invasive breast carcinoma alike, the average cytoplasmic staining was 1.8- to 2.5-fold greater than nuclear staining, suggesting that subcellular localization was not altered during breast tumor progression in any consistent fashion. Cytoplasmic staining was subsequently used as a more sensitive indicator of overall expression.

In several samples of skin or oral squamous epithelium, αGKLF bound specifically to differentiating suprabasal epithelial cells (Fig. 3*A*). Compared with adjacent uninvolved epithelium, staining was markedly increased in malignant cells for each of several cases of squamous cell carcinoma with little or no staining of stromal components of the tumor, as shown previously for the mRNA (17). Likewise, staining was increased in superficial cells compared with cells deeper within epithelial crypts of the small bowel (Fig. 3*B*) or the large bowel (Table 2; $P = 0.043$). In contrast to oral and breast tumors, staining was reduced in tumor cells compared with adjacent superficial epithelial cells for each of four cases of human colorectal adenoma or carcinoma examined (Fig. 3*C*, Table 2; $P = 0.027$).

Expression of GKLF Protein Is Increased during Neoplastic Progression in the Breast. Eighteen cases were tested for GKLF expression by immunohistochemistry (Table 2, Fig. 4). Nuclear and cytoplasmic staining of normal breast epithelium, DCIS, and invasive carcinoma were semiquantitatively assessed. Low-level staining of tumor cells was observed for 6 cases (*e.g.*, cytoplasmic staining ranging from 0.20 to 0.85), with 11 cases exhibiting higher-level staining (*e.g.*, cytoplasmic staining ranging from 1.00 to 1.75). These results are consistent with detection of the mRNA in approximately two-thirds of tumors by ISH. For cases 23–31, which were analyzed by both ISH and immunohistochemical staining, results of the two methods exhibited a close correlation that reached statistical significance for invasive carcinoma cells ($N = 8$; coefficient = 0.77; $P = 0.024$). In DCIS, the correlation was moderate, although the sample number was small ($N = 7$; coefficient = 0.43). Perhaps because of the overall lower level of expression in uninvolved tissue, the correlation was weakest in uninvolved ducts. Minor differences observed for the two methods may be attributed to differences in sensitivity and specificity, to false negative results attributable to partial degradation of mRNA in some surgical samples, or to analysis of nonserial sections of the same tissue block. As observed in uninvolved tissue adjacent to

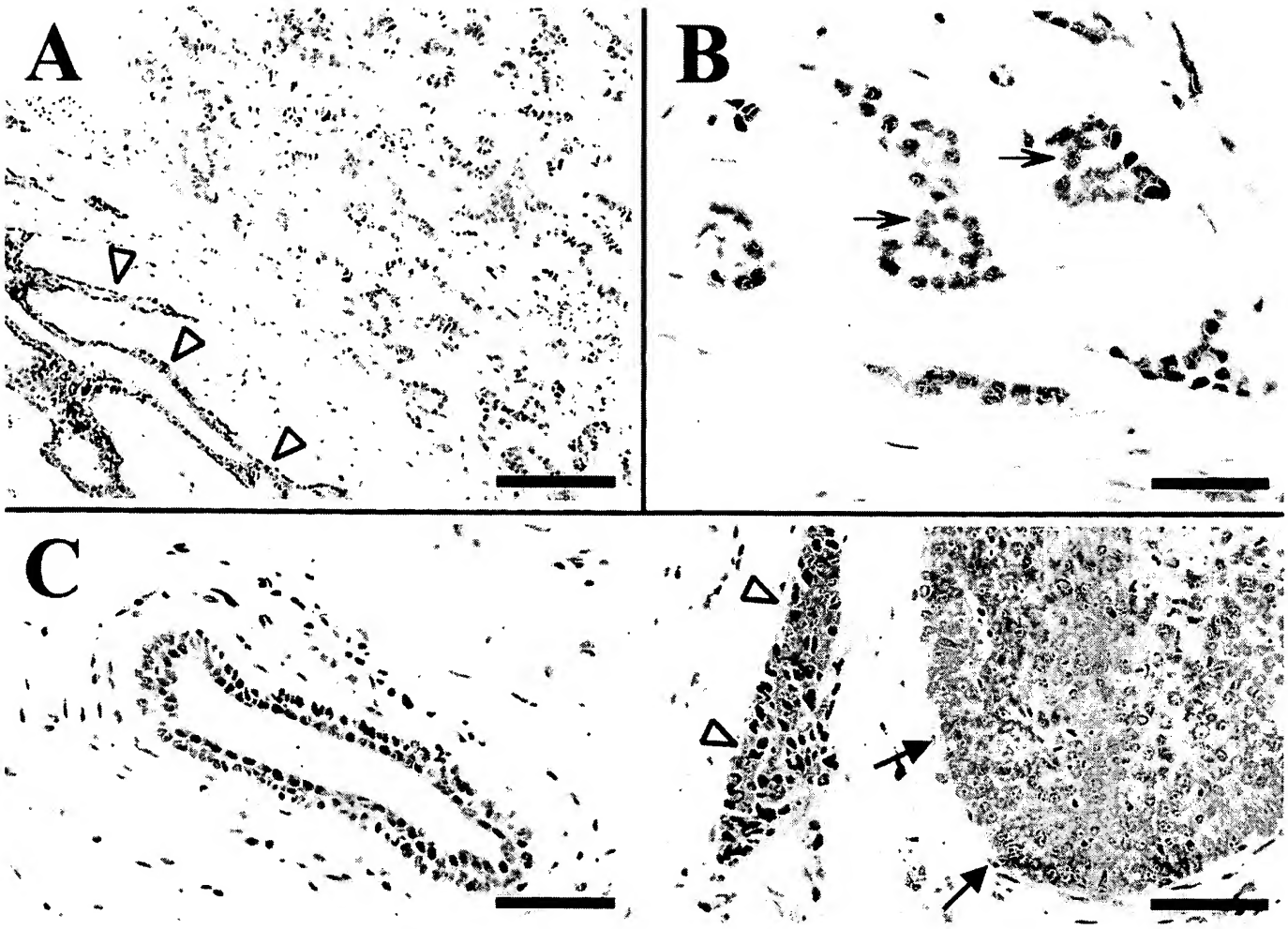

Fig. 4. Immunostaining of breast tissue with αGKLF. *A*, a tissue section containing uninvolved epithelium (*left, arrowheads*) adjacent to invasive carcinoma (*right*). *B*, a different case showing invasive carcinoma cells with a mixed nuclear and cytoplasmic staining pattern. *C*, a tissue section containing an uninvolved duct (*left panel*) adjacent to both DCIS (*right panel, arrows*) and invasive carcinoma (*right panel, arrowheads*). Scale bars: A = 120 μm; B = 30 μm; C = 60 μm.

tumors, staining was low or undetectable for each of five cases of reduction mammoplasty (data not shown).

Apparent GKLF expression as determined by nuclear or cytoplasmic immunostaining was increased in both DCIS and invasive carcinoma compared with uninvolved ducts (Table 2, Fig. 5). For morphologically normal ducts, staining of myoepithelial cells was not significantly different from that of luminal epithelial cells ($P = 0.303$, data not shown). However, staining of neoplastic cells in DCIS was significantly increased compared with myoepithelial cells within the same ducts ($P = 0.0001$), which was consistent with other studies indicating similarities between tumor cells and luminal epithelial cells (39).

Analysis of GKLF in Cultured Breast Epithelial Cells. Northern blot analysis of breast tumor cell lines revealed variable levels of GKLF expression relative to a tubulin control (Fig. 6). GKLF expression was high in MCF7 and ZR75-1; intermediate in BT474, BT20, MDAMB361, and SKBR3; and reduced in MDAMB453 and MDAMB231. Thus, expression in six of eight breast tumor-derived cell lines was increased relative to 184 cells, an HMEC population of finite life span derived from normal breast tissue after reduction mammoplasty (*Lane 1*). Expression was similarly increased in 184A1 cells (33). These immortalized cells were derived from 184 cells by treatment with benzo(*a*)pyrene. They are wild-type for p53 and $p105^{Rb}$ and are anchorage-dependent and nontumorigenic in animals. The results obtained for breast tumor cell lines support the conclusion that GKLF expression is up-regulated at the mRNA level in most breast tumors, whereas activation in 184A1 cells is consistent with identification of GKLF induction as an early event.

DISCUSSION

Oncogenes such as *c-MYC*, *GLI*, and *GKLF* function in a regulated fashion in normal epithelium to control cellular proliferation and differentiation (5, 6, 8, 23, 40, 41). Analysis of well-characterized tumor types such as colorectal carcinoma and basal cell carcinoma of the skin suggests that genetic alterations cluster within specific pathways, rather than within any specific gene, and that these pathways can function as regulators of oncogene transcription (42, 43). An activity common to several oncogenes implicated in carcinoma is the ability to induce transformed foci in the RK3E assay (17, 44, 45). This assay is highly specific, as foci result from expression of tumor-derived mutant (but not wild-type) alleles of *RAS* or *β-catenin* (Ref. 45 and data not shown), and only *GKLF* and *c-MYC* were identified in a large screen (17). The assay also detects a distinct subset of oncogenes compared with other host cell lines. With the exception of *RAS*, the oncogenes that transform RK3E cells do not induce foci in NIH3T3 cells (17, 44, 45).

GKLF encodes a zinc finger transcription factor of the GLI-Krüppel family (46) and is distinct from many other oncogenes in that expression in normal tissue is observed in terminally differentiating epithe-

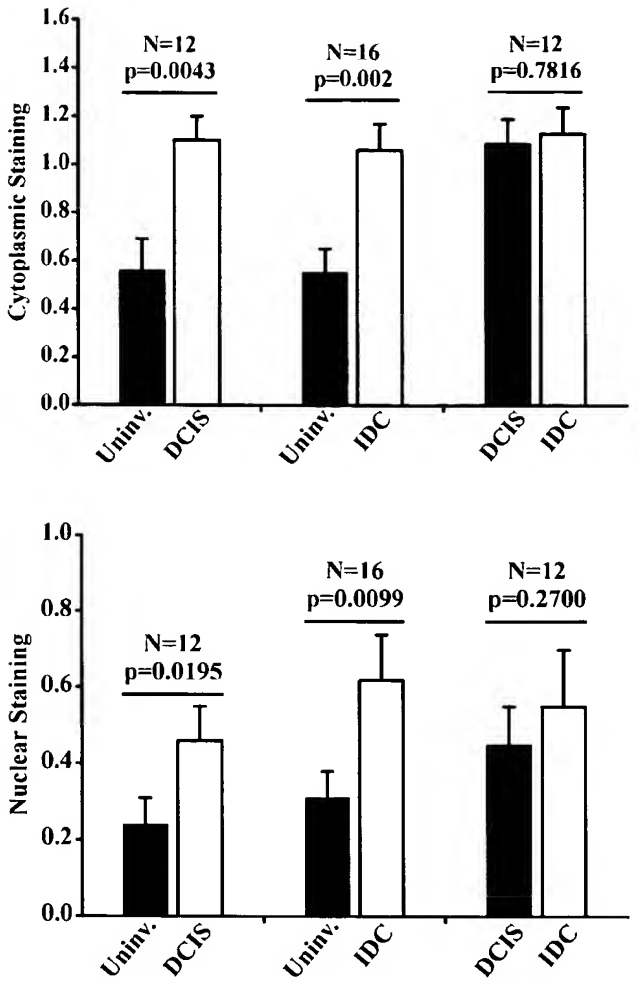

Fig. 5. Staining of uninvolved and neoplastic breast tissue by αGKLF. The data in Table 2 were analyzed using a paired *t* test. Sample size (*N*), statistical significance (*p*), and SE are indicated for each comparison. *Uninv.*, uninvolved ducts.

lial cells. In addition, expression is induced in association with cell growth-arrest *in vitro* (26). As predicted by these observations, expression in certain tumor-types is reduced compared with the relevant normal epithelia. Thus, GKLF expression is reduced in colorectal tumors, a result supported by multiple approaches including analysis of RNA extracted from tissues (29), SAGE (31), and immunohistochemical analysis of human tissues (this work). ISH analysis of several prostatic tumors likewise indicates that GKLF is expressed in normal prostatic epithelium, and that expression can be lost during tumor progression.

In contrast to colorectal and prostatic carcinoma, GKLF expression is activated in both invasive carcinoma and preinvasive neoplastic lesions during progression of most breast carcinomas and virtually all oropharyngeal squamous cell carcinomas. Breast and oral cancers share a number of additional molecular alterations. Loss-of-function mutations frequently affect p53 and p16/CDKN2, whereas a smaller proportion of tumors (5–20%) exhibit gene amplification of *c-MYC*, *cyclin D1*, erbB-family members including the EGF receptor and *erb*B-2/HER-2/*neu*, or others (47–51). Unlike carcinomas of the GI tract or skin, neither breast nor oral carcinoma is reported to exhibit frequent genetic alterations that activate known transforming oncogenes such as *RAS*, *β-catenin*, *c-MYC*, or *GLI*. By analogy with oncogenes in other tumor types, disruption of the pathways that control GKLF mRNA expression in breast epithelial cells and in oral mucosa represents a potential mechanism of tumor initiation or progression *in vivo*.

The pattern of GKLF expression in normal epithelia may provide clues as to how GKLF functions in tumor progression. Stratified squamous epithelium contains at least four functionally distinct compartments (52, 53). The stem cell compartment is composed of cells within the basal cell layer that exhibit a capacity for self-renewal, but which rarely divide. The transit-amplifying compartment is composed of cells within the basal or parabasal cell layers that exhibit rapid cell division but a reduced capacity for self-renewal. Differentiation occurs within the prickle cell layer that contains identifiable desmosomes, leading to the outermost, keratinized superficial layer. Whereas mechanisms regulating transitions from one compartment to the next remain poorly understood, c-MYC activation can induce stem cells to enter the highly proliferative transit-amplifying compartment (40). Because self-renewal and rapid cell division occur in distinct cell types, the organization of compartments enables the rapid turnover of epithelial cells while minimizing the possibility of sustaining permanent genetic damage in stem cells.

The observation that GKLF functions normally in the prickle cell layer suggests that each of the three compartments (stem cell, transit-amplifying, and prickle layer) expresses a transforming activity or a critical function (*e.g.*, self-renewal or proliferation) that may contribute to the progression of carcinoma. These compartments appear to be intermingled in dysplastic stratified squamous epithelium, with prickle layer markers including GKLF misexpressed in the basal layers, whereas other basal or parabasal markers are misexpressed in superficial layers. Loss of compartment-specific patterns of gene expression may result in coexpression of the properties of several compartments in a single cell. For example, specific properties of the prickle cell layer, such as reduced cellular adhesion to basement membranes, altered adhesion to other cells, and/or loss of the cellular mechanisms that mediate contact inhibition could confer invasive or metastatic properties to oral carcinomas.

To better understand the mechanism of transformation, we are characterizing transcriptional alterations induced by GKLF when expressed in epithelial cells *in vitro*. In the future, identification of upstream regulators of GKLF transcription in epithelial cells may elucidate the pathways that regulate GKLF and the mechanism of deregulation of GKLF in specific tumor-types.

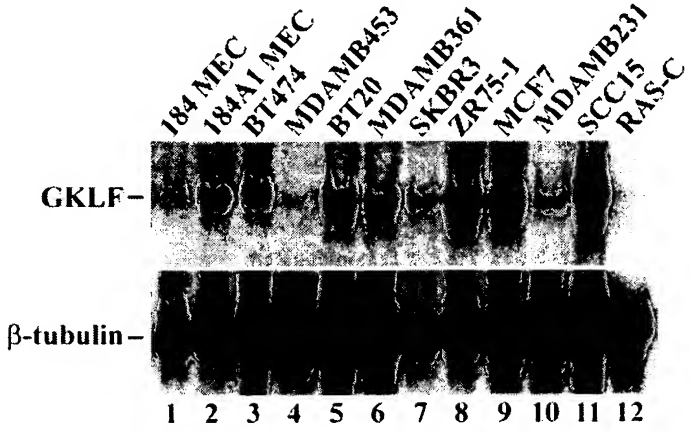

Fig. 6. Northern blot analysis of GKLF expression in human breast tumor cell lines. Total RNA from the indicated cell lines was analyzed. *Lane 1*, finite-life span HMECs. *Lane 2*, benzo(*a*)pyrene-treated, immortalized HMECs. *Lanes 3-10*, breast carcinoma-derived cell lines. *Lane 11*, SCC15, a human oral squamous cell carcinoma-derived cell line. *Lane 12*, a RAS-transformed rat cell line. The filter was stripped and hybridized to a β-tubulin probe.

ACKNOWLEDGMENTS

We gratefully acknowledge Tom Broker and Louise Chow for assistance with ISH, Martha Stampfer for the gift of mammary epithelial cells, and Iuri D. Louro and Pintusorn Hansakul for critical reading of the manuscript.

REFERENCES

1. Hanahan, D., and Weinberg, R. A. The hallmarks of cancer. Cell, *100:* 57–70, 2000.
2. Cahill, D. P., Kinzler, K. W., Vogelstein, B., and Lengauer, C. Genetic instability and darwinian selection in tumours. Trends Cell Biol., *9:* M57–60, 1999.
3. Fearon, E. R. Human cancer syndromes: clues to the origin and nature of cancer. Science (Washington DC), *278:* 1043–1050, 1997.
4. Johnson, R. L., Rothman, A. L., Xie, J., Goodrich, L. V., Bare, J. W., Bonifas, J. M., Quinn, A. G., Myers, R. M., Cox, D. R., Epstein, E. H., Jr., and Scott, M. P. Human homolog of patched, a candidate gene for the basal cell nevus syndrome. Science (Washington DC), *272:* 1668–1671, 1996.
5. Dominguez, M., Brunner, M., Hafen, E., and Basler, K. Sending and receiving the hedgehog signal: control by the Drosophila gli protein cubitus interruptus. Science (Washington DC), *272:* 1621–1625, 1996.
6. Dahmane, N., Lee, J., Robins, P., Heller, P., and Ruiz i Altaba, A. Activation of the transcription factor GLI1 and the sonic hedgehog signalling pathway in skin tumours. Nature (Lond.), *389:* 876–881, 1997.
7. Green, J., Leigh, I. M., Poulsom, R., and Quinn, A. G. Basal cell carcinoma development is associated with induction of the expression of the transcription factor GLI-1. Br. J. Dermatol., *139:* 911–915, 1998.
8. He, T. C., Sparks, A. B., Rago, C., Hermeking, H., Zawel, L., da Costa, L. T., Morin, P. J., Vogelstein, B., and Kinzler, K. W. Identification of c-MYC as a target of the APC pathway. Science (Washington DC), *281:* 1509–1512, 1998.
9. Tetsu, O., and McCormick, F. β-catenin regulates expression of cyclin D1 in colon carcinoma cells. Nature (Lond.), *398:* 422–426, 1999.
10. Oro, A. E., Higgins, K. M., Hu, Z. L., Bonifas, J. M., Epstein, E. H., and Scott, M. P. Basal cell carcinomas in mice overexpressing sonic hedgehog. Science (Washington DC), *276:* 817–821, 1997.
11. Goodrich, L. V., Milenkovic, L., Higgins, K. M., and Scott, M. P. Altered neural cell fates and medulloblastoma in mouse patched mutants. Science (Washington DC), *277:* 1109–1113, 1997.
12. Hahn, H., Wojnowski, L., Zimmer, A. M., Hall, J., Miller, G., and Zimmer, A. Rhabdomyosarcomas and radiation hypersensitivity in a mouse model of Gorlin Syndrome. Nat. Med., *4:* 619–622, 1998.
13. Aszterbaum, M., Epstein, J., Oro, A., Douglas, V., LeBoit, P. E., Scott, M. P., and Epstein, E. H., Jr. Ultraviolet and ionizing radiation enhance the growth of BCCs and trichoblastomas in patched heterozygous knockout mice. Nat. Med., *5:* 1285–1291, 1999.
14. Heyer, J., Yang, K., Lipkin, M., Edelmann, W., and Kucherlapati, R. Mouse models for colorectal cancer. Oncogene, *20:* 5325–5333, 1999.
15. Kinzler, K. W., and Vogelstein, B. Cancer-susceptibility genes: gatekeepers and caretakers. Nature (Lond.), *386:* 761–761, 1997.
16. Vogelstein, B. and Kinzler, K. W. Familial cancer syndromes: caretakers and gatekeepers. *In:* B. Vogelstein and K. W. Kinzler (eds.), The Genetic Basis of Human Cancer. New York: McGraw-Hill, Inc., 1998.
17. Foster, K. W., Ren, S., Louro, I. D., Lobo-Ruppert, S. M., McKie-Bell, P., Grizzle, W., Hayes, M. R., Broker, T. R., Chow, L. T., and Ruppert, J. M. Oncogene expression cloning by retroviral transduction of adenovirus E1a-immortalized rat kidney RK3E cells: transformation of a host with epithelial features by c-MYC and the zinc finger protein GKLF. Cell Growth Differ., *10:* 423–434, 1999.
18. Couch, F. J., and B. L. Weber. Breast cancer. *In:* B. Vogelstein and K. W. Kinzler (eds.), The Genetic Basis of Human Cancer, pp. 537–563. New York: McGraw-Hill, Inc., 1998.
19. Louro, I. D., McKie-Bell, P., Gosnell, H., Brindley, B. C., Bucy, R. P., and Ruppert, J. M. The zinc finger protein GLI induces cellular sensitivity to the mTOR inhibitor rapamycin. Cell Growth Differ., *10:* 503–516, 1999.
20. Garrett-Sinha, L. A., Eberspaecher, H., Seldin, M. F., and de Crombrugghe, B. A gene for a novel zinc-finger protein expressed in differentiated epithelial cells and transiently in certain mesenchymal cells. J. Biol. Chem., *271:* 31384–31390, 1996.
21. Yet, S. F., McA'nulty, M. M., Folta, S. C., Yen, H. W., Yoshizumi, M., Hsieh, C. M., Layne, M. D., Chin, M. T., Wang, H., Perrella, M. A., Jain, M. K., and Lee, M. E. Human EZF, a Krüppel-like zinc finger protein, is expressed in vascular endothelial cells and contains transcriptional activation and repression domains. J. Biol. Chem., *273:* 1026–1031, 1998.
22. Shields, J. M., and Yang, V. W. Identification of the DNA sequence that interacts with the gut-enriched Krüppel-like factor. Nucleic Acids Res., *26:* 796–802, 1998.
23. Segre, J. A., Bauer, C., and Fuchs, E. Klf4 is a transcription factor required for establishing the barrier function of the skin. Nat. Genet., *22:* 356–360, 1999.
24. Jenkins, T. D., Opitz, O. G., Okano, J., and Rustgi, A. K. Transactivation of the human keratin 4 and Epstein-Barr virus ED-L2 promoters by gut-enriched Krüppel-like factor. J. Biol. Chem., *273:* 10747–10754, 1998.
25. Zhang, W., Shields, J. M., Sogawa, K., Fujii-Kuriyama, Y., and Yang, V. W. The gut-enriched Krüppel-like factor suppresses the activity of the CYP1A1 promoter in an Sp1-dependent fashion. J. Biol. Chem., *273:* 17917–17925, 1998.
26. Shields, J. M., Christy, R. J., and Yang, V. W. Identification and characterization of a gene encoding a gut-enriched Krüppel-like factor expressed during growth arrest. J. Biol. Chem., *271:* 20009–20017, 1996.
27. Panigada, M., Porcellini, S., Sutti, F., Doneda, L., Pozzoli, O., Consalez, G. G., Guttinger, M., and Grassi, F. GKLF in thymus epithelium as a developmentally regulated element of thymocyte-stroma cross-talk. Mech. Dev., *81:* 103–113, 1999.
28. Kaestner, K. H., Silberg, D. G., Traber, P. G., and Schutz, G. The mesenchymal winged helix transcription factor fkh6 is required for the control of gastrointestinal proliferation and differentiation. Genes Dev., *11:* 1583–1595, 1997.
29. Tonthat, H., Kaestner, K. H., Shields, J. M., Mahatanankoon, C. S., and Yang, V. W. Expression of the gut-enriched Krüppel-like factor gene during development and intestinal tumorigenesis. FEBS Lett., *419:* 239–243, 1997.
30. Velculescu, V. E., Zhang, L., Vogelstein, B., and Kinzler, K. W. Serial analysis of gene expression. Science (Washington DC), *270:* 484–487, 1995.
31. Lal, A., Lash, A. E., Altschul, S. F., Velculescu, V., Zhang, L., McLendon, R. E., Marra, M. A., Prange, C., Morin, P. J., Polyak, K., Papadopoulos, N., Vogelstein, B., Kinzler, K. W., Strausberg, R. L., and Riggins, G. J. A public database for gene expression in human cancers. Cancer Res., *59:* 5403–5407, 1999.
32. Geiman, D. E., Han, T. T., Johnson, J. M., and Yang, V. W. Transactivation and growth suppression by the gut-enriched Krüppel-like factor (Krüppel-like factor 4) are dependent on acidic amino acid residues and protein-protein interaction. Nucleic Acids Res., *28:* 1106–1113, 2000.
33. Nijjar, T., Wigington, D., Garbe, J. C., Waha, A., Stampfer, M. R., and Yaswen, P. p57KIP2 expression and loss of heterozygosity during immortal conversion of cultured human mammary epithelial cells. Cancer Res., *59:* 5112–5118, 1999.
34. Birkedal-Hansen, B., Moore, W. G., Taylor, R. E., Bhown, A. S., and Birkedal-Hansen, H. Monoclonal antibodies to human fibroblast procollagenase. Inhibition of enzymatic activity, affinity purification of the enzyme, and evidence for clustering of epitopes in the NH2-terminal end of the activated enzyme. Biochemistry, *27:* 6751–6758, 1988.
35. Grizzle, W. E., Myers, R. B., Manne, U., Stockard, C. R., Harkin, L. E., and Srivastava, S. Factors affecting immunohistochemical evaluation of biomarker expression in neoplasia. *In:* M. Hanausek and Z. Walaszek (eds.), John Walker's Methods in Molecular Medicine: Tumor Marker Protocols, pp. 161–179. Totowa, NJ: Humana Press, Inc., 1998.
36. Grizzle, W. E., Myers, R. B., Manne, U., and Srivastava, S. Immunohistochemical evaluation of biomarkers in prostatic and colorectal neoplasia. *In:* M. Hanausek and Z. Walaszek (eds.), John Walker's Methods in Molecular Medicine: Tumor Marker Protocols, pp. 143–160. Totowa, NJ: Humana Press, Inc., 1998.
37. Snedecor, G. W., and Cochran, W. G. Statistical Methods. Ames, Iowa: Iowa State University Press, 1980.
38. Velculescu, V. E., Madden, S. L., Zhang, L., Lash, A. E., Yu, J., Rago, C., Lal, A., Wang, C. J., Beaudry, G. A., Ciriello, K. M., Cook, B. P., Dufault, M. R., Ferguson, A. T., Gao, Y., He, T. C., Hermeking, H., Hiraldo, S. K., Hwang, P. M., Lopez, M. A., Luderer, H. F., Mathews, B., Petroziello, J. M., Polyak, K., Zawel, L., and Kinzler, K. W. Analysis of human transcriptomes. Nat. Genet., *23:* 387–388, 1999.
39. Alford, D., Pitha-Rowe, P., and Taylor-Papadimitriou, J. Adhesion molecules in breast cancer: role of α 2 β 1 integrin. Biochem. Soc. Symp., *63:* 245–259, 1998.
40. Gandarillas, A., and Watt, F. M. c-Myc promotes differentiation of human epidermal stem cells. Genes Dev., *11:* 2869–2882, 1997.
41. Korinek, V., Barker, N., Moerer, P., van Donselaar, E., Huls, G., Peters, P. J., and Clevers, H. Depletion of epithelial stem-cell compartments in the small intestine of mice lacking TCF-4. Nat. Genet., *19:* 379–383, 1998.
42. Sparks, A. B., Morin, P. J., Vogelstein, B., and Kinzler, K. W. Mutational analysis of the APC/β-catenin/TCF pathway in colorectal cancer. Cancer Res., *58:* 1130–1134, 1998.
43. Xie, J. W., Murone, M., Luoh, S. M., Ryan, A., Gu, Q. M., Zhang, C. H., Bonifas, J. M., Lam, C. W., Hynes, M., Goddard, A., Rosenthal, A., Epstein, E. H., and de Sauvage, F. J. Activating smoothened mutations in sporadic basal-cell carcinoma. Nature (Lond.), *391:* 90–92, 1998.
44. Ruppert, J. M., Vogelstein, B., and Kinzler, K. W. The zinc finger protein GLI transforms rodent cells in cooperation with adenovirus E1A. Mol. Cell. Biol., *11:* 1724–1728, 1991.
45. Kolligs, F. T., Hu, G., Dang, C. V., and Fearon, E. R. Neoplastic transformation of RK3E by mutant β-catenin requires deregulation of Tcf/Lef transcription but not activation of c-myc expression. Mol. Cell. Biol., *19:* 5696–5706, 1999.
46. Ruppert, J. M., Kinzler, K. W., Wong, A. J., Bigner, S. H., Kao, F.-T., Law, M. L., Seuanez, H. N., O'Brien, S. J., and Vogelstein, B. The GLI-Krüppel family of human genes. Mol. Cell. Biol., *8:* 3104–3113, 1988.
47. Cairns, P., Polascik, T. J., Eby, Y., Tokino, K., Califano, J., Merlo, A., Mao, L., Herath, J., Jenkins, R., Westra, W., Rutter, J. L., Buckler, A., Gabrielson, E., Tockman, M., Cho, K. R., Hedrick, L., Bova, G. S., Isaacs, W., Koch, W., Schwab, D., and Sidransky, D. Frequency of homozygous deletion at p16/CDKN2 in primary human tumours. Nat. Genet., *11:* 210–212, 1995.
48. Reed, A. L., Califano, J., Cairns, P., Westra, W. H., Jones, R. M., Koch, W., Ahrendt, S., Eby, Y., Sewell, D., Nawroz, H., Bartek, J., and Sidransky, D. High frequency of *p16 (CDKN2/MTS-1/INK4a)* inactivation in head and neck squamous cell carcinoma. Cancer Res., *56:* 3630–3633, 1996.
49. Ruppert, J. M., Wright, M., Rosenfeld, M., Grushcow, J., Bilbao, G., Curiel, D. T., and Strong, T. V. Gene therapy strategies for carcinoma of the breast. Breast Cancer Res. Treat., *44:* 93–114, 1997.
50. Ingvarsson, S. Molecular genetics of breast cancer progression. Sem. Cancer Biol., *9:* 277–288, 1999.
51. Nass, S. J., and Davidson, N. E. The biology of breast cancer. Hematol. Oncol. Clin. North Am., *13:* 311–332, 1999.
52. Fuchs, E., and Segre, J. A. Stem cells: a new lease on life. Cell, *100:* 143–155, 2000.
53. Watt, F. M. Epidermal stem cells: markers, patterning and the control of stem cell fate. Philos. Trans. R. Soc. Lond. B Biol. Sci., *353:* 831–837, 1998.